UNIVERSITY OF CALIFORNIA,
IRVINE

Application of triangular trimers derived from Aβ to create antibodies for immunohistochemical studies and as vaccines against Alzheimer's disease

DISSERTATION

submitted in partial satisfaction of the requirements
for the degree of

DOCTOR OF PHILOSOPHY

in Pharmaceutical Science

by

Chelsea Marie T. Parrocha

Dissertation Committee:
Professor James S. Nowick, Chair
Professor Brian M. Paegel
Professor Frederick J. Ehlert
Professor Elizabeth Head

2023

DEDICATION

To

my sweet father,

Manuel B. Parrocha

in recognition of the hardships you faced
and the sacrifices you made for me to fulfill my dreams.
I promise we will be all together soon.

a realization

Humility is not thinking less of yourself
But thinking of yourself less.

C.S. Lewis

an experience

You must never give into despair.
Allow yourself to slip down that road and you surrender to your lowest instincts.
In the darkest times, hope is something you give to yourself.
This is the meaning of inner strength.

Uncle Iroh
Avatar The Last Airbender

TABLE OF CONTENTS

LIST OF FIGURES

LIST OF TABLES

LIST OF SCHEMES

ACKNOWLEDGEMENTS

Thank you James for giving me the freedom to cultivate who I want to be as a scientist and pushing me to pursue excellence. My vigorous training in your group, your keen attention to detail, patience, and mentorship has prepared me very well for my transition into my next role in the pharmaceutical industry. Thank you for teaching me how to appreciate the quality of food and how to bake that amazing rustic bread—it definitely saved me during the 3-month lockdown in the pandemic.

Thank you so much to my committee members for their guidance. Brian, the pharmaceutical science department is very fortunate to have you. The standards you set for your students and your drive astound me and I aspire to become an innovative and savvy scientist like you. Prof. Ehlert, you have played an instrumental part of my being here at UCI. You were the professor who interviewed me for our department's graduate program, my first professor during my first year graduate classes, a member of my advancement committee, a current a member of my dissertation committee, and my connection to your previous students in industry who have influenced my path post graduate school. Thank you so much for your guidance throughout my graduate journey. Liz, thank you for welcoming me into your lab and for being such a powerful woman scientist. Through spending time in your lab, I was able to enrich my PhD training not only as a scientist, but as a professional woman. I will never forget your kindness, and like you, I will lead by example and spread kindness, coolness, and grace as I move forward in my career.

To my current and previous colleagues in the Nowick Group, we have been through so much together. From months of failed experiments, to BBQ's in the park, from headaches and heart aches, watching equipment and glass fall apart, from a double date to Disneyland, wondering if this graduate experience will ever end, sharing souvenirs and treats from our

hometowns, a pandemic, reminding each other to not live on candy, to remembering how to breathe we've been through it all. Thank you for the fun, mischief, support to survive through the marathon that is graduate school. To the new and future members of the group, pull a Dory and "just keep swimming" and think like Scarlett O'Hara, " for tomorrow is another day."

Thank you so much to my pharmaceutical sciences cohort. It is incredible to see how much we've grown from being students in the same classes, to colleagues specializing in different fields. I can't wait to see where we go from here as we move towards our post-graduate school careers.

Thank you to the Stern, Carlson, and Zitman families your support, family dinners, and random phone calls to check on my wellbeing. Thank you to the Altamirano, Tolentino, and Parrocha families for providing me a strong sense of self that empowered me to succeed in graduate school.

Thank you to my support sisters, Mindetta Vogel and Adeline Schlabaugh, for your care packages, wisdom, and guidance. Thank you to my brothers from other mothers, Andres R. Antuna (soon to be esquire) and Kenyon K. Wright (soon to be M.D.) for our monthly phone calls and group chats making sure we're alive in well as we endured our doctoral journeys.

Lastly, thank you my love, my husband, Ryan Stern. Thank you for the sacrifices you made and helping me achieve my dream of becoming the person a strive to be. Here's to building a future where we live our lives to the fullest and with each other.

CHELSEA MARIE T. PARROCHA

Irvine, CA 92617 |cparroch@uci.edu| http://linkedin.com/in/cmtp-uci2023/

EXECUTIVE SUMMARY

Highly-motivated researcher with strong skills in strategy and tactical development. Proven track record of establishing, fostering, cultivating, and maintaining collaborations. SME in the therapeutic potential of immunotherapies for Alzheimer's disease (AD). Elegantly designs and executes preclinical research. Diligent in acquiring, processing, and working with donated human tissue. Passionate to bring basic research to clinical applications.

EDUCATION

Doctor of Philosophy—Pharmacological Sciences
Concentration— Pharmacology
University of California, Irvine
Start Date: September 2018
Advancement to Candidacy: August 26th, 2021
GPA: 3.993/4.0
Defense date: May 18th, 2023

Bachelor of Science—Biological Sciences
Bachelor of Science—Chemistry, concentration in Biochemistry
Minor—Music
Concentration—University Honors College
University of Alaska Anchorage
Departmental Honors: Biological Sciences
Institutional Honors: Cum Laude, Leadership Honors, University Honors Scholar, Leadership Distinction
GPA: 3.66/4.0
Graduated: May 06, 2018

PROFESSIONAL EXPERIENCE

Ph.D. Candidate in Prof. James Nowick's Research Group
Irvine, CA
April 2019-May 18th, 2023

- Subject matter expert in research group on peptide vaccines and immunotherapies against AD. Presents the current landscape of clinical trials and competing therapies to identify novel vaccine development (**publ. 1**).
- Led vaccine formulation and design of preclinical trials for a novel amyloid β-derived oligomer peptide vaccine against two AD mouse models (**publ. 2**).
- Developed tactful approach to the characterization and discovery of antibodies generated against toxic amyloid β oligomers resulting in 3 manuscripts in preparation and contributing to R01-funded research (**publ. 3–5**).
- Pioneered mouse projects which required communicating to chemists with different technical expertise unfamiliar with animal studies, and development of mouse biomethodology in a traditional organic chemistry laboratory.
- Built upon a preexisting project by developing new information and collaborations with researchers from the University of California, Irvine (UCI) and other institutions across the United States in order to further the understanding of the molecular basis of people with sporadic AD (**publ. 3 and 5)**.

- Collaborated on design parameters establishing SOPs on a tutorial for structure-based design on a COVID-19 inhibitor and synthesis peptide inhibitor candidates during the 2020 COVID-19 pandemic (**publ. 6 and 7**).
- Optimized SOP for gram-scale solid phase peptide synthesis HPLC purification, and chemical analysis of numerous macrocyclic peptides as models of toxic amyloid β oligomers resulting in 4X the production leading to expedited investigation of novel peptides.
- Optimized mammalian cell assays to study modes of toxicity elicited by amyloid β oligomers which resulted in progressing R01 funded research and future graduate student projects.

Rotating Graduate Research Assistant in Prof. Amal Alachkar's Laboratory
Irvine, CA
December 2018-March 2019

- Led the mouse behavior assays and associated histology in a three-month rotation setting the foundation a publication and area of research for future graduate student projects (**publ. 8**).

Rotating Graduate Research Assistant in Prof. Claudia Benevente's Laboratory
Irvine, CA
October 2018-December 2018

- Designed, managed, and extracted plasmids from bacteria cultures to transfected mammalian cell culture yielding a plasmid library in a 3 months which set the foundation for the publication of graduate student projects to better understand the molecular basis of pediatric cancers, retinoblastoma, and osteosarcoma.

Undergraduate Researcher in lab of Professor Frank von Hippel
Anchorage, AK
June 2014-May 2018

- Optimized SOPs for two NIH R01 funded projects to efficiently analyze histomorphological changes of targeted organs in response to acute to chronic exposure of environmental contaminants. Targeted organs include the thyroid, kidney, and gonads of stickleback fish. Efforts expedited data analysis of 10+ year ecotoxicology and public health studies, provided the foundation of graduate student dissertation projects, and manuscripts in preparation (**publ. 9**).

PRESENTATIONS

- **Clinical Trials on Alzheimer's Disease.** San Francisco, CA. *Poster Presentation.* November 26th – December 3rd, 2022.
- **Gordon Research Seminar and Conference.** Ventura, CA. *Oral Presentation*. March 28th – April 1st, 2022.
- **Peptide Therapeutics Symposium.** San Diego, CA. *Poster Presentation and Lightning Talk*. October, 2021 and 2022.
- **UCI Pharmaceutical Sciences Vertex Day.** Irvine, CA. *Poster Presentation*. February, 2020.
- **UAA Undergraduate Chemistry Seminar Alumni Feature.** Anchorage, AK. *Oral Presentation.* August, 2020.
- **UCI Society of Chemical Biology and Chemistry Meeting.** Irvine, CA. *Oral Presentation*. November, 2019.
- **UCI Department of Pharmaceutical Sciences Student Visitation Day.** Irvine, CA. *Poster Presentation*. January, 2020; February, 2021; January 2023.

PUBLICATIONS

1) **Chelsea Marie T. Parrocha** and James S. Nowick. Current peptide vaccine approaches and immunotherapies against Alzheimer's disease. *Manuscript published June 24th 2022.* https://doi.org/10.1002/pep2.24289

2) **Chelsea Marie T. Parrocha**, Adam G. Kreutzer, Lindsey Lueptow, Irina Zhuravka, Jesse Pascual, Jennifer T. Nguyen, Elizabeth Head, and James S. Nowick. A peptide vaccine made with a triangular trimer derived from Aβ may reverse anxiety-like and fear-based memory in 5xFAD mice but does not decrease Aβ plaques. *Manuscript in preparation to ACS Chemical Neuroscience.*

3) **Chelsea Marie T. Parrocha**, Adam G. Kreutzer, Jesse Pascual, Cherie Stringer, Jennifer T. Nguyen, Ashley L. Ith, Elizabeth Head, and James S. Nowick. Antibodies generated from a triangular trimer of Aβ recognize cored and neuritic plaques in brain sections of people who lived with Late-Onset Alzheimer's Disease. *Manuscript in preparation to Acta Neuropathologica.*

4) Adam G. Kreutzer, **Chelsea Marie T. Parrocha**, Sepehr Haerianardakani, Gretchen Guaglianone, Jennifer T. Nguyen, Michelle N. Diab, and James S. Nowick. Antibodies Raised Against an Aβ Oligomer Mimic Recognize Pathological Features in Alzheimer's Disease and Associated Amyloid-Disease Brain Tissue. *Manuscript submitted to ACS Central Science.*

5) Adam G. Kreutzer*, Gretchen Guaglianone*, **Chelsea Marie T. Parrocha**†, Ryan J. Malonis†, Karen Tong, Stan Yoo, Jennifer T. Nguyen, William J. Howitz, Michelle N. Diab, Imane L. Hamza, Jonathan R. Lai, and James S. Nowick. Probing Differences Among Aβ Oligomers: Two Triangular Trimers Derived from Aβ Exhibit Different Biophysical and Biological Properties. *Manuscript accepted to PNAS, April 18th, 2023.*

6) Adam G. Kreutzer, Maj Krumberger, Elizabeth M. Diessner, **Chelsea Marie T. Parrocha**, Michael A. Morris, Gretchen Guaglianone, Carter T. Butts, and James S. Nowick. A cyclic peptide inhibitor of the SARS-CoV-2 main protease. *Euro. J. Med. Chem*. **2021**, *221*, 113530. https://doi.org/10.1016/j.ejmech.2021.113530

7) Sheng Zheng, Maj Krumberger, Michael A. Morris, **Chelsea Marie T. Parrocha**, Adam G. Kreutzer, and James S. Nowick. Structure-based drug design of an inhibitor of the SARS-CoV-2 (COVID-19) main protease using free software: A tutorial for students and scientists. *Euro. J. Med. Chem*. 2021, *218*, 11390. https://doi.org/10.1016/j.ejmech.2021.113390

8) Sammy Alhassen, Siwei Chen, Lamees Alhassen, Alvin Phan, Mohammad Khoudari, Angele De Silva, Huda Barhoosh, Zitong Wang, **Chelsea Marie T. Parrocha**, Charity Henrich, Zicheng Wang, Leon Mutesa, Pierre Baldi, Geoffrey W Abbott, Amal Alachkar. Intergenerational trauma transmission is associated with brain metabotranscriptome remodeling and mitochondrial dysfunction. *Communications Biology*. **2021**, *4*, 1-5. https://doi.org/10.1038/s42003-021-02255-2

9) Renee Jordan-Ward, Frank A. von Hippel , Catherine Wilson, Zyled Rodriguez Maldonado, Alison Gardell, Danielle Dillon, Tom Titus, John H. Postlethwait, Amina Salamova, Staci L. Capozzi, Parinya Panuwet Elise Contreras, **Chelsea Marie T. Parrocha**, Ruth Bremiller, Yann Guiguen, Jesse Gologergen, Tiffany Immingan, Pamela Miller, David Carpenter, and C. Loren Buck. Transcriptomic and developmental effects of persistent organic pollutants in sentinel fishes collected near an arctic formerly used defense site. *Manuscript in submission to Environmental Pollution.*

* and † signifies that the authors contributed equally

SELECTED AWARDS AND ACKNOWLEDGEMENT

- 17th Peptide Therapeutics Symposium Poster Award Winner **($750)**. September 1st, 2022.
- Gordon Research Conference Travel Award (**Total $1,898.21**). March 30th, 2022.
- Honorable Mention in 2020 National Science Foundation Graduate Research Fellowship Program competition. March 2020
- Chancellor's List honoree at the University of Alaska Anchorage. Fall 2013- Spring 2014, Fall 2017, Spring 2018.
- Dean's List honoree at the University of Alaska Anchorage. Fall 2014, Fall 2016, Spring 2017.
- Awarded the 2016 AHAINA's Woman of Excellence for demonstrating a balance between academics, social and community engagement are selected by the AHAINA (African American, Hispanic, Asian, International, and Native American) Multicultural Center of the University of Alaska Anchorage. (**Total award received, $2,656)**. April 2016.

SKILLS

- Mouse biomethodology
- Mouse behavioral assays
- Curation and histology preparation of mouse and human samples
- Enzyme-linked immunoassay (ELISA)
- Immunohistochemistry and immunofluorescent staining
- Immunoblots (western blots and dot blots)
- Vaccine preparation and formulation
- Mammalian cell culture, induced pluripotent stem cell (IPSC) and related techniques and assays
- Solid-phase peptide synthesis
- Maintenance and troubleshooting of automated peptide synthesizer (Liberty Blue CEM)
- Preparative and analytical HPLC
- Mass spectrometry (LC-MS, MALDI, QDA)
- Molecular visualization software

TRAININGS AND CERTIFICATIONS

- Clinical Observer with Dr. Brian Hitt, MD/PhD at UCI Health Laguna Hills (February–May 2023)
- Trainee in Clinical Trials Series at University Lab Partners (March – June 2022)
    - Includes overview of IRB, key elements of a study protocol, informed consent, and best practices when interacting with the FDA.
- Trainee for Industry Insights for STEM scientist, a business class for STEM PhD students (May 2022)
- CITI Training in topics related to preclinical and clinical research
- Human Pluripotent Stem Cell Course (August 2021)
- Mentoring in Excellence by UCI Graduate Division (Summer 2019)

SELECTED LEADERSHIP, MENTORSHIP, AND TEACHING

Leadership

- Liaison for BioRender to report unmet user needs, connect associates with university leaders, and organize events.
- Elected co-chair for the 2024 Gordon Research Seminar on Biotherapeutics and Vaccine Development.
- Led and co-developed COVID-19 guidelines and requirements that were adopted by the School of Physical Sciences and eventually campus-wide to safely continue research in the COVID-19 pandemic.

Mentorship

- Provided scientific onboarding and training for 2 undergraduate research assistants.
- Served as a resource and mentor to 10 international graduate students acclimating to graduate school in the United States.
- Teach, coach and mentor new or less experienced graduate student mentors as the Co-founder and leader of Pharmaceutical Sciences Graduate Student Peer Mentor Program.

Teaching

- Laboratory teaching assistant for upper class undergraduates and PharmD students in Medicinal Chemistry (PHARM SCI 177/L and PHARM 277/L)**,** April-June 2023.

- Summer instructor teaching highschool students basic neuroscience and these concepts are applied to research (California State Summer School for Mathematics and Science, COSMOS, July 2022).
- Distilled concepts of Medicinal Chemistry to PharmD students as a department-hired tutor (Spring 2022).
- Performed chemistry demonstrations teaching K-12 students about how science is in their everyday lives through the UCI Chemistry Outreach Program (September 2019-Present).
- Laboratory and lecture teaching assistant for pre-pharmacy and pre-medical undergraduates Human Anatomy and Physiology (PHARM SCI 120/L)**,** October 2018-December 2018.

REFERENCES

James S. Nowick, Ph.D.
Distinguished Professor, Department of Chemistry
Department of Pharmaceutical Sciences
University of California, Irvine, CA 92697-4625
Email: jsnowick@uci.edu
Research Group Web Page:
http://tinyurl.com/nowickgroup/
Relationship to candidate: Ph.D. Advisor

Elizabeth Head, M.A., Ph.D.
Professor, Vice Chair for Research
Department of Pathology Laboratory Medicine Director, Experimental Pathology Program
University of California, Irvine, CA 92697-4625
Email: heade@uci.edu
Research Group Web Page:
https://sites.mind.uci.edu/headlab/
Relationship to candidate: Ph.D. Committee Member

Brian M. Paegel, Ph.D.
Professor, Department of Pharmaceutical Sciences, School of Pharmacy & Pharmaceutical Sciences
Professor, Chemistry, School of Physical Sciences
Professor, Biomedical Engineering, The Henry Samueli School of Engineering
University of California, Irvine, CA 92697-4625
Email: bpaegel@uci.edu
https://faculty.sites.uci.edu/paegel/
Relationship to candidate: Ph.D. Committee Member

Frederick J. Ehlert, Ph.D.
Professor, Emeritus, Department of Pharmaceutical Sciences, School of Pharmacy & Pharmaceutical Sciences
University of California, Irvine, CA 92697-4625
Professor, Pharmacology, School of Medicine
Email: fjehlert@hs.uci.edu
Relationship to candidate: Ph.D. Committee Member

ABSTRACT OF THE DISSERTATION

Application of triangular trimers derived from Aβ to create antibodies for immunohistochemical studies and as vaccines against Alzheimer's disease

by

Chelsea Marie T. Parrocha

Doctor of Philosophy in Pharmaceutical Sciences

University of California, Irvine, 2023

Professor James S. Nowick, Chair

To understand and treat Alzheimer's disease (AD), we need to understand the structures of the Aβ peptide aggregates that cause neurodegeneration. In this dissertation, I address this need by applying triangular trimers derived from Aβ to create antibodies for immunohistochemical studies and as vaccines against AD. Chapter 1 outlines the exponential growth of people who will live with AD and current therapies to alleviate symptoms or slow down the progression of AD. Here, Chapter 2 demonstrates the application of a conformationally defined Aβ-derived peptide (the 4AT-L trimer) to better understand the composition of Aβ pathology in people who lived with Late-Onset Alzheimer's disease (LOAD). Chapter 3 expands on the subject of current peptide vaccines and immunotherapies against AD by discussing the composition of each therapy, the current state of clinical trials, and the possible future of these therapies. Chapter 4 demonstrates how a structurally defined Aβ antigen may be useful in treating AD-like symptoms in mice. Chapter 5 shows preliminary work demonstrating the recognition of pathology in people who lived with Down Syndrome and Alzheimer's disease

(DSAD). Lastly, Chapter 6 discusses the conclusions collected from the previous chapters and lists future directions that can be pursued by junior members of the Nowick Group.

This body of work is one of the earliest collections of studies in the Nowick Group which provides a biological and therapeutic application to structurally defined triangular trimers derived from Aβ. Additional studies exploring the biological and therapeutic application of trimers of Aβ and associated antibodies will continue to address the need to understand the structures of the Aβ peptide aggregates that cause neurodegeneration. These efforts will contribute to a better understanding of neurodegeneration and develop therapies to slow down the progression of AD.

Chapter 1

INTRODUCTION

A therapy to slow down the on-set and progression of Alzheimer's disease (AD) is an unmet need of our time.

Alzheimer's disease (AD) is the 7th leading cause of death in the United States; it is predicted that by 2060, 13.8 million people will be diagnosed with AD in the United States alone.[1,2] This is a 122.8% increase from the estimated 6.5 million people with AD in 2021.[1] AD is a disease that not only impacts the person living with the disease but also their loved ones and society. The total cost of caring for people with AD was expected to reach 321 billion USD in 2022 and does not account for the 272 billion USD in unpaid caregiving.[1]

Due to an aging population and increased lifespan, AD is an exponentially growing disease and it is imperative that we invest time and resources to slowing disease progression and if not curing the disease. Recent data suggest that within the year of serving as a caregiver 60% of individuals were employed with 18% of them reducing their hours due to caregiving, averaging 35 hours of non-caregiving per week.[1,3] 41% of caregivers have an income of $50,000 or less which does not cover the total lifetime cost of ca. $412,936 to care for a person living with AD in 2022.[4]

Current therapeutic approaches alleviate symptoms with traditional pharmacology.

Behavioral and psychological symptoms of AD greatly impact the quality of life of people who live with AD and include memory and cognitive impairment, apathy, delusions, anxiety, depression, and hostile agitation.[5–11] The first FDA-approved therapies approved in the mid-to-late 1990s to alleviate these symptoms of AD were small molecule neurotransmitter inhibitors.

Cholinesterase inhibitors (donepezil, galantamine, and rivastigmine), as well as the N-methyl-D-Aspartate (NMDA) receptor antagonist (memantine), make up the standard of care for AD over the last 30 years.[12,11] Other small molecules have been designed to treat symptoms of AD. In 2022, suvorexant (Merck) an orexin receptor antagonist, was FDA-approved for treating sleep disorders of people with AD.[13] Blarcamesine, an intracellular sigma-1 chaperone protein agonist, is in Phase 2/3 clinical trials and has demonstrated memory-preserving effects in preclinical trials[14,15]. The approach of repurposing of small molecules for other psychiatric and neurological diseases has been a focus of clinical trials to alleviate AD symptoms. In a phase 3 clinical trial, Ritaline, typically used to treat ADHD, was shown to be a safe and effective treatment for apathy in people with AD.[16] Clinical trials have also been focused on disease-modifying small molecules. Such molecules have been targeting mechanisms of action involved in the progression of AD such as oxidative stress, proteostasis, inflammation/immunity, and metabolic/bioenergetics.[17] There have also been small molecules targeting proteins and peptides, namely beta-amyloid (Aβ) and tau, that contribute to AD disease progression. Below is a Table 1.1 shows current Phase 3 small molecule candidates targeting Aβ and Phase 2 and 3 clinical trial candidates targeting tau .

Table 1.1

Current small molecule clinical candidates targeting Aβ and tau

Name	Sponsor	Purpose	Mechanism of Action	Clinical Trial Status
ALZT-OP1	AZTherapies, Inc.	Decrease amyloid production and inflammation	Promotes microglia recruitment and phagocytosis of Aβ[18]	Phase 3[19]
Simufilam	Cassava Sciences	Decrease amyloid accumulation, tau phosphorylation and neuroprotective	Binds to filamin which interacts with soluble Aβ and triggers tau phosphorylation and synaptic dysfunction[20–22]	Phase 3[23]
ALZ-801	Alzheon Inc.	Inhibits $A\beta_{42}$ aggregation[24,25]	Aβ inhibitor	Phase 3[26]
LY3372689	Eli Lilly and Company	Inhibitor of the O-GlcNAcase (OGA) enzyme to prevent formation of nonpathological form of tau[27,28]	Interferes with post translational modification of tau	Phase 2[29]
AGB101	AgeneBio, Inc.	Inhibition of the synaptic protein SV2A[30]	Attenuates hippocampal overactivity	Phase 3[31]
LMTM	TauRx Therapeutics Ltd.	Blocks and disrupts tau-tau interactions[32]	Tau inhibitor	Phase 3[33]

While there are promising small molecule candidates in clinical trials, 5 and 22 candidates (against tau and Aβ, respectively) have already been discontinued.[34] Failure of these clinical candidates may be due to the lack of understanding of the structure and function of the peptides and proteins responsible for the pathogenesis and progression of AD.

The molecular basis of AD still remains unknown.

AD is one of the five major forms of dementia.[35] A common trait of these different forms of dementia is their association with peptide or protein accumulation, which are suspected to impact disease progression—these diseases are called proteinopathies.[36] Due to mixed pathologies, behavior and psychiatric symptoms tend to overlap; this makes identifying different causes of

dementia. Although the heterogeneous nature of pathology has made establishing a concrete diagnosis and drug targets for specific forms of dementia challenging, studying the structural and physical properties of these pathologies has allowed us to insight into the molecular basis of these neurological proteinopathies.

Two important peptides and proteins in the pathogenesis and progression of AD are Aβ and tau; these have served as clinical markers to distinguish AD from other forms of dementia.[37] The Aβ hypothesis, a driving force in AD research, posits that the accumulation of extracellular Aβ monomers self-assemble to form β-sheet fibrils that aggregate to form plaques.[38,39] Aβ is a cleavage product of the single-pass transmembrane protein amyloid precursor protein (APP). The membrane-bound enzyme, β-secretase cleaves APP creating a 99 amino acid *C*-terminal fragment of APP called C99. γ -secretase then processes C99 at cleavage sites yielding isoforms of Aβ with fragments 40 to 42 amino acids long as the most common isoform ($A\beta_{40}$, and $A\beta_{42}$).[11,38–40] Aβ can be further processed yielding peptides such as pyroglutamate and isoaspartate modified Aβ contributing to the heterogeneous peptide pool contributing to AD progression.[41] The Aβ cascade hypothesis further states that the accumulation of Aβ can drive tau hyperphosphorylation and thus increase the spread of pathology leading to death.[42,43] Tau is a microtubule-associated protein (MAP) essential for stabilizing microtubules for cell processes.[43,44] Unlike Aβ, tau is a significantly larger molecule ranging from 352-441 amino acids and six isoforms.[45] When hyperphosphorylated, tau is liberated from the microtubules, which disassembles, and the tau aggregates into paired helical filaments (PHF) and then neurofibrillary tangles (NFT).[44,46] Similar to Aβ, tau can be further processed by glycosylation and ubiquitination, contributing to the peptide and protein heterogeneity of AD.[27]

Inflammation of the brain, caused by the accumulation of Aβ and tau, is a central

mechanism in AD and there has been considerable discussion of defining AD as an innate autoimmune disease.[47–49] Inflammation is the result of a disturbance (i.e. an injury or infection) in the balance between pro-inflammatory and anti-inflammatory signaling. In the case of AD, brain inflammation is triggered by the presence of Aβ which activates microglia as microgliosis occurs, more cytokines are released thus inflammation continues to perpetuate.

Accumulation of Aβ in the cerebral vasculature of people living with AD exacerbates inflammation and compromises the structural integrity of blood vessels in the brain. This form of Aβ accumulation in cerebral blood vessels is called Cerebral Amyloid Angiopathy (CAA). The resulting collection of Aβ in the blood vessels of the brain reduces Aβ clearance, diminishes the structural integrity of the blood vessels, and ultimately exacerbates AD pathology. In the context of immunotherapies, CAA is especially problematic as pre-existing CAA is exacerbated. This results in Amyloid Related Imaging Abnormalities (ARIA) which can be classified as cerebral **e**dema (ARIA-**E**) or cerebrovascular **h**emorrhages (ARIA-**H**).[50]

By understanding the molecular underpinnings of the physiological symptoms of AD and the causative peptides and proteins, we can better design tools and therapies to understand the disease and help treat people living with AD. Efforts towards developing diagnostic tools have been built upon the field's current understanding of AD and have yielded promising tools to better diagnose and treat AD.

Histology is the workhorse of studying AD.

Post-mortem histology studies on the brains of people who lived with AD were the original experiments that built the foundation of AD research. In 1906, Alois Alzheimer reported his observations on the behavior and post-mortem histology of his former patient Auguste D.[51,52] By staining brain sections of Auguste D. with Bielschowsky's silver stain, Alzheimer observed

the presence of plaques and neurofibrillary tangles, which we know today as Aβ plaques and tau tangles. [51,52] Histology techniques used during Alzheimer's life, modern histology techniques, biochemical assays, and brain donations of people who lived with AD have elucidated the composition of these pathologies and enhanced our understanding of the pathogenesis and progression of AD.

Aβ and tau pathologies are the accumulation of causative peptides and proteins that can appear before cognitive symptoms, which makes them intriguing to better understand their role in AD.[37] Aβ deposits can be seen in the brains of people who lived with AD as diffuse plaques, cored plaques, and neuritic plaques. Aβ plaque accumulation is extracellular with $A\beta_{42}$ as the dominant isoform in plaques which may be due to the additional two amino acids increasing the peptide's propensity to self-assemble.[53–55]

Diffuse plaques (also referred to as senile or nonfibrillar plaques) are defined as non-fibrillar (**Figure 1.1 A**). They are particularly large with a cross section of 10-100 microns[56] or sometimes 50 to several hundred;[57] no fibral center (dense core) or dystrophic neurites but rather have intact neurons;[45] tend to lack margins or have structural boundaries[58] (some have referred to this as "amorphous").[53] Diffuse plaques are not recognized by Thioflavin-S and not associated with glial responses such as microglia and astrocytes;[53]they are present in people that are cognitively normal at the time of death[56], therefore, not used clinically for pathological diagnosis of AD;[53] and is typically the first step in graduate deposits, but can also appear during any stage of Aβ deposition.[59,60]

Neuritic plaques are defined as containing abnormal tau deposits and dystrophic neurites with or without a dense core (**Figure 1.1 B**).[56,59,61] Any other plaque without tau deposits can be considered standard plaques defined by their morphology (**Figure 1.1C**). The presence of tau in

this accumulation of Aβ is one of the many pieces of evidence that supports the synergistic interaction between tau and Aβ.[58] A semiquantitative analysis of the presence of these plaques is associated with cognitive impairment, consequently these plaques are significant to AD diagnosis. Typically, neuritic plaques can appear in two forms, dense deposits of Aβ or cored plaques.

Cored plaques (also known as dense-core plaques or corona plaques) are well defined by the presence of a fibrillar, β-sheet-pleated dense core comprised of $A\beta_{42}$[56] surrounded by Aβ oligomeric halos[45,57] and swollen axons and synaptic terminals otherwise known as dystrophic neurites [45,57,62]. Unlike diffuse plaques, cored plaques are recognized by Thioflavin-S, have defined structural boundaries, and tend to be 30 to 100 microns cross-sectionally.[56] Cored plaques are also defined by the presence of activated microglia and reactive astrocytes surrounding the core of the plaque[56–58,62]. This anatomical feature of the cored plaque may indicate the cellular Aβ clearance of this plaque (**Figure 1.1 D**).[59] Aβ also accumulates in vessels in the brain and forms CAA. As Aβ (mostly $A\beta_{40}$) is secreted by cells during Aβ clearance, it is collected in the fluid-filled space surrounding cerebral blood vessels (also known as the perivascular space) of the brain (**Figure 1.1 E**).[61,63] Aβ then aggregates in cerebral vessels, which may be a result of $A\beta_{40}$ binding to fibrinogen in the walls of the vessels and inducing the accumulation of $A\beta_{40}$.[56,58] As Aβ continues to be cleared by the flow of interstitial fluids, the peptide accumulates in the lining of blood vessels and clearance of Aβ slows down.[64] Severe cases of CAA exacerbate AD progression by activating oxidative stress, inflammatory factors, cell toxicity, the structural integrity of the blood-brain barrier, and ultimately life-threatening hemorrhages.[62,63]

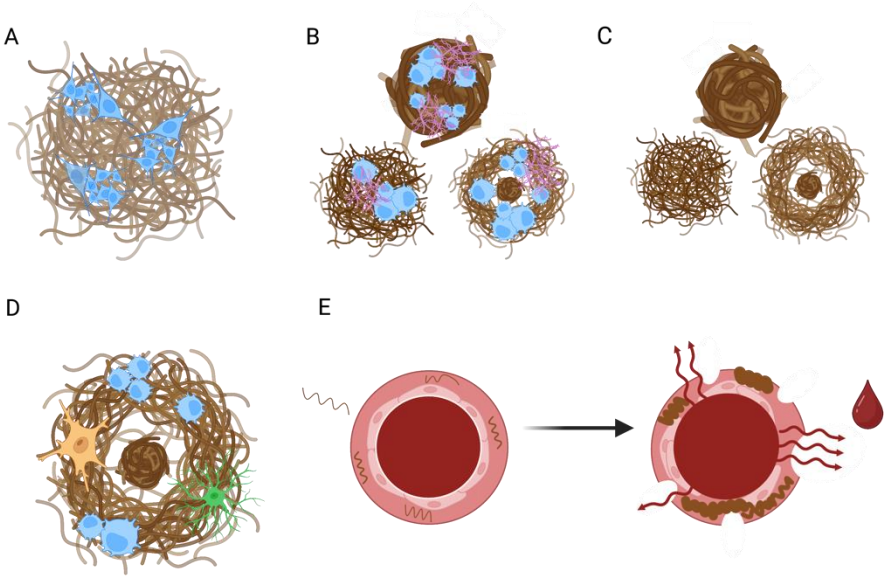

Figure 1.1. Artistic representations of Aβ pathology. All plaques and Aβ are shown in brown. (**A**) Shows a diffuse plaque containing intact neurons (blue). (**B**) Shows three kinds of neuritic plaques including a dense plaque (top), plaque without a dense core (bottom left), and dense core plaque (bottom right) all containing dystrophic neurites (blue) and tau (pink). (**C**) shows standard plaque morphologies such as a standard dense plaque (top), a standard plaque without a dense core or a standard diffuse plaque (bottom left), and a dense core plaque (bottom right). (**D**) shows a cored plaque with dystrophic neurites (blue), microglia (orange), and astrocytes (green). (**E**) shows a cerebral blood vessel slowly accumulating Aβ between the vessel wall and smooth cells (left) and the resulting compromised blood vessel leading to hemorrhages upon continued accumulation of Aβ (right). The figure was designed by Chelsea Marie T. Parrocha and created with BioRender.com.

Tau NFTs can be seen in the brains of people who lived with AD as paired helical filaments, ghost tangles, and neuropil threads.[45,62,65] Tau accumulation is typically intracellular and the pathology is defined by the accumulation of the hyperphosphorylated protein in the cytoplasm of the neuron.[57,46]

Neuropil threads are defined as phosphorylated tau, that form paired helical filaments (PHF) and accumulate in the dendrites of neurons and intermix within cell bodies (**Figure 1.2 A**). They are one of the earliest forms of tau accumulation and interact with the accumulation of Aβ neuritic plaques.[57] Dystrophic neurites are early accumulations of intracellular PHF in the

cell body of neurons (**Figure 1.2 B**).[53,57]

Ghost tangles occur in the latest stages of AD, extracellular accumulations of tau NFTs and are the result of neuronal death. Once the cell dies, the NFTs maintain the shape of the neuron (**Figure 1.2 C**). They are characterized by loss of the *C*-terminal of tau and a cluster of neurites.[57] Unlike Aβ, tau accumulation is closely associated with cognitive impairment and can be used as a more accurate biomarker for diagnosing AD.[45]

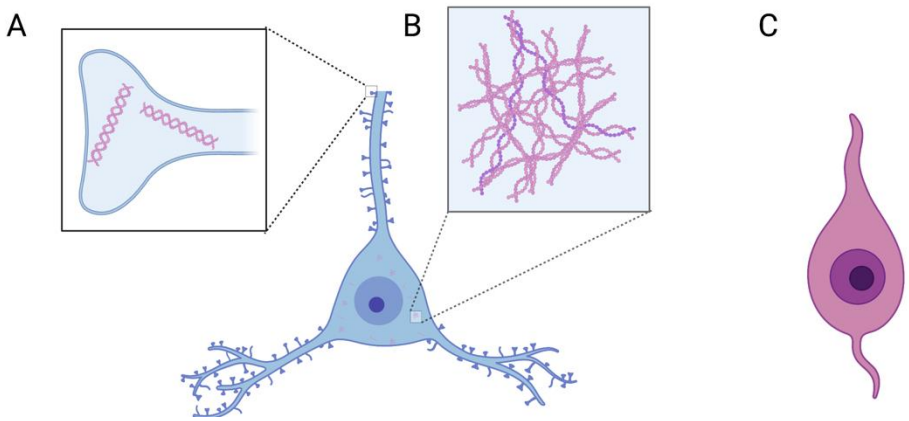

Figure 1.2. Artistic representations of tau pathology. All tau pathologies are shown in shades of pink or purple. (**A**) Shows neuropil threads in the dendrite of a neuron. (**B**) Shows dystrophic neurites in the body of a neuron. (**C**) Shows the product of ghost tangles. The figure was designed by Chelsea Marie T. Parrocha and created with BioRender.com.

The presence of Aβ and tau pathology is and continues to be an essential biomarker for AD research and diagnosis. The ATN model uses Amyloid Tau and Neurodegeneration pathology as a guideline to better define and diagnose people with AD and provide personalized treatment plans.[37] The majority of neuropathological investigations rely on stains and dyes that were used since the time of Alois Alzheimer and have continued to build the knowledge of AD pathology and how they impact the molecular basis of AD. Innovations of additional histochemical and fluorescent techniques have been applied to further characterize the pathologies observed in AD to support what has been established by stains and dyes.

Antibodies have become an essential tool to understand the molecular basis of AD.

Antibodies as a tool have greatly enhanced the understanding of AD. Since the time of Alois Alzheimer, traditional stains such as Thioflavin-S and Congo Red have been the workhorse of identifying pathology in the brains of people who lived with AD.[66] Staining brains of people who lived with AD anti-Aβ antibodies have been developed as additional tools in neuropathology to gain a greater molecular understanding of Aβ pathology.

Antibodies used for immunostaining provide high specificity for tissue targets and provide insight into structure-function relationships and protein-protein interactions within tissues.[67] Polyclonal antibodies are from sera extracted from the blood of immunizing animals with an antigen; this serum is produced from different B-cells that produce individual antibodies that have an affinity for several different regions on similar targets, or epitopes.[67,68] Polyclonal antibodies were primarily used for immunostaining until advances in recombinant DNA technology yielded the discovery of the hybridoma technique and therefore monoclonal antibodies.[69,70] Monoclonal antibodies are produced from a single B-cell and recognize a specific epitope.[70] After animals are immunized the B-cells are isolated by splenocyte extraction followed by fusion with an immortal myeloma cell line. These hybridomas are then cultured and undergo multiple selection processes to isolate monoclonal antibodies[70].

Generating antibodies against conformations of pathologic Aβ is an active area of research in the AD field. Although current conformation-defined Aβ antibodies, such as the A11 polyclonal antibody, are generated with structurally undefined Aβ and this tool has provided the AD research community with a deeper understanding of the molecular basis of Aβ plaques. My efforts in developing a polyclonal antibody against a structurally defined Aβ will be covered in Chapter 2.

Further development of antibodies not only enhances the tools used to research AD, but also holds the promise to develop immunotherapies against AD.

There are few successes and many failures of monoclonal immunotherapies and peptide vaccines.

The last two years of AD research have been called a "renaissance for Alzheimer's disease" which is attributed to the recent positive developments in AD immunotherapies.[71] Inspired by the design of vaccines against infectious disease and cancer immunotherapies, research on designing AD immunotherapies rose as a dominant therapeutic area against AD since the late 90s and early 2000s.[36] AD immunotherapies have focused on either creating a peptide vaccine (active immunotherapy) or monoclonal antibody infusions (passive immunotherapies). Ultimately, this clearing of AD pathology by these immunotherapies is suspected to slow down the progression of AD—a result that was announced November 29th, 2022.[72] In Chapter 3, I will discuss the current peptide vaccine and immunotherapy approaches against AD.

Current AD immunotherapies have a limited approach to designing antigens for the development of peptide vaccines and immunotherapies. One of the most limited scopes of research includes the fragment of Aβ and tau in peptide vaccines. Because of the propensity for these amyloidogenic peptides to aggregate, the conformation of the peptide is unknown which could explain the failed clinical trials of peptide vaccines against AD. In Chapter 4, I discuss efforts toward a novel peptide vaccine testing four conformationally defined Aβ-derived peptides in transgenic AD mice demonstrating the significance of creating an AD peptide vaccine with a well-characterized peptide.

Researching with people with Down Syndrome and AD (DSAD) may help design better therapies.

AD is neurodegenerative proteinopathy that develops with aging and can be genetically inherited. The apolipoprotein gene (*APOE*) is a genetic risk factor that is associated with the onset of AD.[11] Other genetic mutations that are predictors of AD include familial AD mutations (FAD). These autosomal dominant mutations, namely mutations in the genes for the amyloid precursor protein (*APP*), and presenilin 1 and 2 (*PSEN1, PSEN2*) are associated with early onset AD in people being diagnosed from as early as 30 years old to having AD by 40 years old.[73] Another genetic form of AD is developed in people who live with Down Syndrome.

Down Syndrome (DS) is a genetic disease that includes an extra chromosome 21 (hence, Trisomy 21), and therefore people with DS gain an extra copy of the *APP* gene. This addition of APP increases the deposition of AD in people with DS (DSAD), including advanced Aβ accumulation in their teens, microgliosis, astrocytosis, and tau tangles.[42] Although people with DSAD share disease, they have many pathological differences with people with sAD including the accumulation of Aβ pathology.

By 40 years old, people living with DS dramatically accumulate Aβ which contributes to unique pathology.[74] Aβ plaque density is much higher in people with DSAD. Soluble Aβ, which is suspected to be the toxic species of Aβ in AD, is elevated in people with DSAD as well as incidences of CAA.[75,76] Recent reports on new pathology, namely bird's-nest plaques and coarse-grained plaques, are associated with DSAD and are also tied with early onset AD (EOAD).[56,77] The authors hypothesize that the presence of these plaques in sulcal depths and associated with CAA demonstrates unique plaque pathogenesis in DSAD and EOAD.[77] Because people living

with DS have a set temporal onset and progression of AD, learning from this population of people can enrich the understanding of AD in the general population.

Characterizing unique pathology in people who lived with DSAD with $pAb_{4AT\text{-}L}$ may provide further insight into the molecular composition of plaques. In Chapter 5, I discuss my preliminary work toward characterizing the polyclonal antibody created in Chapter 2 ($pAb_{4AT\text{-}L}$) on brain slices from people who lived with DSAD. Asides from my preliminary work, I describe the additional experiments needed to complete this body of work.

Connecting the structural basis of causative peptides and proteins in proteinopathies like AD is an unmet need.

The brain and the molecular basis of AD remain an enigma. Investigating the structural properties of a causative species of AD could lead to a better understanding of the function of these species and ultimately the molecular basis of AD. Having a better understanding of AD allows more insight into how to care for people living with the disease. Further research into causative peptides and proteins of AD may lead to the development of better therapies to alleviate symptoms, slow disease progression, and possibly prevent AD for the predicted 13.8 million people by 2060 who might suffer from this neurological proteinopathy. In this body of work, I describe my efforts in establishing the biological relevance and application of four of the Nowick Groups' biophysically characterized model systems for studying Aβ oligomers. I have shown that $pAb_{4AT\text{-}L}$ is a tool that supports the model of cored plaques serving as reservoirs for Aβ oligomers to elicit neurotoxicity. I have also shown that a peptide vaccine made from 2AT-L demonstrates that in a mouse model system for Aβ oligomers appears to rescue anxiety-like and fear-based memory but does not reduce pathology. These studies are examples of the Nowick Groups' efforts to address the unmet need to connect structural biology to AD's progression and pathogenesis.

References

(1) 2022 Alzheimer's Disease Facts and Figures. *Alzheimer's & Dementia* **2022**, *18* (4), 700–789. https://doi.org/10.1002/alz.12638.

(2) Rajan, K. B.; Weuve, J.; Barnes, L. L.; McAninch, E. A.; Wilson, R. S.; Evans, D. A. Population Estimate of People with Clinical Alzheimer's Disease and Mild Cognitive Impairment in the United States (2020-2060). *Alzheimers Dement* **2021**, *17* (12), 1966–1975. https://doi.org/10.1002/alz.12362.

(3) Dementia-Caregiving-in-the-US_February-2017.Pdf.

(4) Skaria, A. The Economic and Societal Burden of Alzheimer Disease: Managed Care Considerations. **2022**, *28*.

(5) Ismail, Z.; Agüera-Ortiz, L.; Brodaty, H.; Cieslak, A.; Cummings, J.; Fischer, C. E.; Gauthier, S.; Geda, Y. E.; Herrmann, N.; Kanji, J.; Lanctôt, K. L.; Miller, D. S.; Mortby, M. E.; Onyike, C. U.; Rosenberg, P. B.; Smith, E. E.; Smith, G. S.; Sultzer, D. L.; Lyketsos, C.; NPS Professional Interest Area of the International Society of to Advance Alzheimer's Research and Treatment (NPS-PIA of ISTAART). The Mild Behavioral Impairment Checklist (MBI-C): A Rating Scale for Neuropsychiatric Symptoms in Pre-Dementia Populations. *J Alzheimers Dis* **2017**, *56* (3), 929–938. https://doi.org/10.3233/JAD-160979.

(6) Lanctôt, K. L.; Agüera-Ortiz, L.; Brodaty, H.; Francis, P. T.; Geda, Y. E.; Ismail, Z.; Marshall, G. A.; Mortby, M. E.; Onyike, C. U.; Padala, P. R.; Politis, A. M.; Rosenberg, P. B.; Siegel, E.; Sultzer, D. L.; Abraham, E. H. Apathy Associated with Neurocognitive Disorders: Recent Progress and Future Directions. *Alzheimers Dement* **2017**, *13* (1), 84–100. https://doi.org/10.1016/j.jalz.2016.05.008.

(7) Sultzer, D. L.; Leskin, L. P.; Melrose, R. J.; Harwood, D. G.; Narvaez, T. A.; Ando, T. K.; Mandelkern, M. A. Neurobiology of Delusions, Memory, and Insight in Alzheimer Disease. *Am J Geriatr Psychiatry* **2014**, *22* (11), 1346–1355. https://doi.org/10.1016/j.jagp.2013.06.005.

(8) Weissberger, G. H.; Melrose, R. J.; Narvaez, T. A.; Harwood, D.; Mandelkern, M. A.; Sultzer, D. L. 18F-Fluorodeoxyglucose Positron Emission Tomography Cortical Metabolic Activity Associated with Distinct Agitation Behaviors in Alzheimer Disease. *Am J Geriatr Psychiatry* **2017**, *25* (6), 569–579. https://doi.org/10.1016/j.jagp.2017.01.017.

(9) Lozupone, M.; La Montagna, M.; Sardone, R.; Seripa, D.; Daniele, A.; Panza, F. Can Pharmacotherapy Effectively Reduce Alzheimer's Related Agitation? *Expert Opinion on Pharmacotherapy* **2020**, *21* (13), 1517–1522. https://doi.org/10.1080/14656566.2020.1770730.

(10) Agüera-Ortiz, L.; García-Ramos, R.; Grandas Pérez, F. J.; López-Álvarez, J.; Montes Rodríguez, J. M.; Olazarán Rodríguez, F. J.; Olivera Pueyo, J.; Pelegrin Valero, C.; Porta-Etessam, J. Depression in Alzheimer's Disease: A Delphi Consensus on Etiology, Risk Factors, and Clinical Management. *Frontiers in Psychiatry* **2021**, *12*.

(11) Masters, C. L.; Bateman, R.; Blennow, K.; Rowe, C. C.; Sperling, R. A.; Cummings, J. L. Alzheimer's Disease. *Nat Rev Dis Primers* **2015**, *1* (1), 1–18. https://doi.org/10.1038/nrdp.2015.56.

(12) Richter, N.; Beckers, N.; Onur, O. A.; Dietlein, M.; Tittgemeyer, M.; Kracht, L.; Neumaier, B.; Fink, G. R.; Kukolja, J. Effect of Cholinergic Treatment Depends on Cholinergic Integrity in Early Alzheimer's Disease. *Brain* **2018**, *141* (3), 903–915. https://doi.org/10.1093/brain/awx356.

(13) *Merck Receives Approval for BELSOMRA® (suvorexant) C-IV Label Update to Include Findings from Study of Insomnia in Patients with Mild-to-Moderate Alzheimer's Disease*. Merck.com. https://www.merck.com/news/merck-receives-approval-for-belsomra-suvorexant-c-iv-label-update-to-include-findings-from-study-of-insomnia-in-patients-with-mild-to-moderate-alzheimers-disease/ (accessed 2023-01-29).

(14) Villard, V.; Espallergues, J.; Keller, E.; Vamvakides, A.; Maurice, T. Anti-Amnesic and Neuroprotective Potentials of the Mixed Muscarinic Receptor/Sigma 1 (Σ1) Ligand ANAVEX2-73, a Novel Aminotetrahydrofuran Derivative. *J Psychopharmacol* **2011**, *25* (8), 1101–1117. https://doi.org/10.1177/0269881110379286.

(15) Hampel, H.; Williams, C.; Etcheto, A.; Goodsaid, F.; Parmentier, F.; Sallantin, J.; Kaufmann, W. E.; Missling, C. U.; Afshar, M. A Precision Medicine Framework Using Artificial Intelligence for the Identification and Confirmation of Genomic Biomarkers of Response to an Alzheimer's Disease Therapy: Analysis of the Blarcamesine (ANAVEX2-73) Phase 2a Clinical Study. *Alzheimers Dement (N Y)* **2020**, *6* (1), e12013. https://doi.org/10.1002/trc2.12013.

(16) Mintzer, J.; Lanctôt, K. L.; Scherer, R. W.; Rosenberg, P. B.; Herrmann, N.; van Dyck, C. H.; Padala, P. R.; Brawman-Mintzer, O.; Porsteinsson, A. P.; Lerner, A. J.; Craft, S.; Levey, A. I.; Burke, W.; Perin, J.; Shade, D.; ADMET 2 Research Group. Effect of Methylphenidate on Apathy in Patients With Alzheimer Disease: The ADMET 2 Randomized Clinical Trial. *JAMA Neurology* **2021**, *78* (11), 1324–1332. https://doi.org/10.1001/jamaneurol.2021.3356.

(17) Cummings, J.; Lee, G.; Nahed, P.; Kambar, M. E. Z. N.; Zhong, K.; Fonseca, J.; Taghva, K. Alzheimer's Disease Drug Development Pipeline: 2022. *Alzheimer's & Dementia:*

Translational Research & Clinical Interventions **2022**, *8* (1), e12295. https://doi.org/10.1002/trc2.12295.

(18) Zhang, C.; Griciuc, A.; Hudry, E.; Wan, Y.; Quinti, L.; Ward, J.; Forte, A. M.; Shen, X.; Ran, C.; Elmaleh, D. R.; Tanzi, R. E. Cromolyn Reduces Levels of the Alzheimer's Disease-Associated Amyloid β-Protein by Promoting Microglial Phagocytosis. *Sci Rep* **2018**, *8* (1), 1144. https://doi.org/10.1038/s41598-018-19641-2.

(19) Brazier, D.; Perry, R.; Keane, J.; Barrett, K.; Elmaleh, D. R. Pharmacokinetics of Cromolyn and Ibuprofen in Healthy Elderly Volunteers. *Clin Drug Investig* **2017**, *37* (11), 1025–1034. https://doi.org/10.1007/s40261-017-0549-5.

(20) Wang, H. Y.; Lee, D. H.; D'Andrea, M. R.; Peterson, P. A.; Shank, R. P.; Reitz, A. B. Beta-Amyloid(1-42) Binds to Alpha7 Nicotinic Acetylcholine Receptor with High Affinity. Implications for Alzheimer's Disease Pathology. *J Biol Chem* **2000**, *275* (8), 5626–5632. https://doi.org/10.1074/jbc.275.8.5626.

(21) Wang, H.-Y.; Li, W.; Benedetti, N. J.; Lee, D. H. S. Alpha 7 Nicotinic Acetylcholine Receptors Mediate Beta-Amyloid Peptide-Induced Tau Protein Phosphorylation. *J Biol Chem* **2003**, *278* (34), 31547–31553. https://doi.org/10.1074/jbc.M212532200.

(22) Snyder, E. M.; Nong, Y.; Almeida, C. G.; Paul, S.; Moran, T.; Choi, E. Y.; Nairn, A. C.; Salter, M. W.; Lombroso, P. J.; Gouras, G. K.; Greengard, P. Regulation of NMDA Receptor Trafficking by Amyloid-Beta. *Nat Neurosci* **2005**, *8* (8), 1051–1058. https://doi.org/10.1038/nn1503.

(23) *Cassava Sciences Reports Second Quarter Financial Results for 2022, Mid-year Corporate Update and Interim Analysis of Open-label Study | Cassava Sciences, Inc.*

https://www.cassavasciences.com/news-releases/news-release-details/cassava-sciences-reports-second-quarter-financial-results-2022 (accessed 2023-01-30).

(24) Gervais, F.; Paquette, J.; Morissette, C.; Krzywkowski, P.; Yu, M.; Azzi, M.; Lacombe, D.; Kong, X.; Aman, A.; Laurin, J.; Szarek, W. A.; Tremblay, P. Targeting Soluble Abeta Peptide with Tramiprosate for the Treatment of Brain Amyloidosis. *Neurobiol Aging* **2007**, *28* (4), 537–547. https://doi.org/10.1016/j.neurobiolaging.2006.02.015.

(25) Kocis, P.; Tolar, M.; Yu, J.; Sinko, W.; Ray, S.; Blennow, K.; Fillit, H.; Hey, J. A. Elucidating the Aβ42 Anti-Aggregation Mechanism of Action of Tramiprosate in Alzheimer's Disease: Integrating Molecular Analytical Methods, Pharmacokinetic and Clinical Data. *CNS Drugs* **2017**, *31* (6), 495–509. https://doi.org/10.1007/s40263-017-0434-z.

(26) alzheon. *Alzheon Announces First Patient Dosed in APOLLOE4 Phase 3 Trial of Oral ALZ 801 in Patients with Early Alzheimer's Disease*. Alzheon | Preserving Future Memories. https://alzheon.com/alzheon-announces-first-patient-dosed-in-apolloe4-phase-3-trial-of-oral-alz-801-in-patients-with-early-alzheimers-disease/ (accessed 2023-01-30).

(27) Gong, C.-X.; Liu, F.; Grundke-Iqbal, I.; Iqbal, K. Post-Translational Modifications of Tau Protein in Alzheimer's Disease. *J Neural Transm (Vienna)* **2005**, *112* (6), 813–838. https://doi.org/10.1007/s00702-004-0221-0.

(28) Liu, F.; Iqbal, K.; Grundke-Iqbal, I.; Hart, G. W.; Gong, C.-X. O-GlcNAcylation Regulates Phosphorylation of Tau: A Mechanism Involved in Alzheimer's Disease. *Proc Natl Acad Sci U S A* **2004**, *101* (29), 10804–10809. https://doi.org/10.1073/pnas.0400348101.

(29) Eli Lilly and Company. *Assessment of Safety, Tolerability, and Efficacy of LY3372689 in Early Symptomatic Alzheimer's Disease*; Clinical trial registration NCT05063539;

clinicaltrials.gov, 2023. https://clinicaltrials.gov/ct2/show/NCT05063539 (accessed 2023-01-29).

(30) AGENEBIO-AGB101-Deck-AUG2017.Pdf.

(31) Rosenzweig-Lipson, S.; Barton, R.; Gallagher, M.; Edgar, C. J.; Maruff, P. T.; Mohs, R. HOPE4MCI Trial: First Trial Targeting Reduction of Hippocampal Overactivity to Treat Mild Cognitive Impairment Due to Alzheimer's Disease with AGB101. *Alzheimer's & Dementia* **2020**, *16* (S9), e045331. https://doi.org/10.1002/alz.045331.

(32) Wischik, C. M.; Edwards, P. C.; Lai, R. Y.; Roth, M.; Harrington, C. R. Selective Inhibition of Alzheimer Disease-like Tau Aggregation by Phenothiazines. *Proc Natl Acad Sci U S A* **1996**, *93* (20), 11213–11218. https://doi.org/10.1073/pnas.93.20.11213.

(33) TauRx Therapeutics Ltd. *Randomized, Double-Blind, Placebo-Controlled, Three-Arm, 12-Month, Safety and Efficacy Study of TRx0237 Monotherapy in Subjects With Alzheimer's Disease Followed by a 12-Month Open-Label Treatment*; Clinical trial registration NCT03446001; clinicaltrials.gov, 2022. https://clinicaltrials.gov/ct2/show/NCT03446001 (accessed 2023-01-29).

(34) *Therapeutics Search | ALZFORUM*. https://www.alzforum.org/therapeutics/search?fda_statuses%5B%5D=182&target_types%5B%5D=177&therapy_types%5B%5D=166&conditions%5B%5D=145&keywords-entry=&keywords= (accessed 2023-01-30).

(35) *Dementia - Symptoms and causes*. Mayo Clinic. https://www.mayoclinic.org/diseases-conditions/dementia/symptoms-causes/syc-20352013 (accessed 2023-01-29).

(36) Marciani, D. J. A Retrospective Analysis of the Alzheimer's Disease Vaccine Progress – The Critical Need for New Development Strategies. *Journal of Neurochemistry* **2016**, *137* (5), 687–700. https://doi.org/10.1111/jnc.13608.

(37) Jack Jr., C. R.; Bennett, D. A.; Blennow, K.; Carrillo, M. C.; Dunn, B.; Haeberlein, S. B.; Holtzman, D. M.; Jagust, W.; Jessen, F.; Karlawish, J.; Liu, E.; Molinuevo, J. L.; Montine, T.; Phelps, C.; Rankin, K. P.; Rowe, C. C.; Scheltens, P.; Siemers, E.; Snyder, H. M.; Sperling, R.; Contributors; Elliott, C.; Masliah, E.; Ryan, L.; Silverberg, N. NIA-AA Research Framework: Toward a Biological Definition of Alzheimer's Disease. *Alzheimer's & Dementia* **2018**, *14* (4), 535–562. https://doi.org/10.1016/j.jalz.2018.02.018.

(38) Chen, G.-F.; Xu, T.-H.; Yan, Y.; Zhou, Y.-R.; Jiang, Y.; Melcher, K.; Xu, H. E. Amyloid Beta: Structure, Biology and Structure-Based Therapeutic Development. *Acta Pharmacol Sin* **2017**, *38* (9), 1205–1235. https://doi.org/10.1038/aps.2017.28.

(39) O'Brien, R. J.; Wong, P. C. Amyloid Precursor Protein Processing and Alzheimer's Disease. *Annu Rev Neurosci* **2011**, *34*, 185–204. https://doi.org/10.1146/annurev-neuro-061010-113613.

(40) Wang, J.; Gu, B. J.; Masters, C. L.; Wang, Y.-J. A Systemic View of Alzheimer Disease - Insights from Amyloid-β Metabolism beyond the Brain. *Nat Rev Neurol* **2017**, *13* (10), 612–623. https://doi.org/10.1038/nrneurol.2017.111.

(41) Moro, M. L.; Phillips, A. S.; Gaimster, K.; Paul, C.; Mudher, A.; Nicoll, J. A. R.; Boche, D. Pyroglutamate and Isoaspartate Modified Amyloid-Beta in Ageing and Alzheimer's Disease. *Acta Neuropathologica Communications* **2018**, *6* (1), 3. https://doi.org/10.1186/s40478-017-0505-x.

(42) Selkoe, D. J.; Hardy, J. The Amyloid Hypothesis of Alzheimer's Disease at 25 Years. *EMBO Molecular Medicine* **2016**, *8* (6), 595–608. https://doi.org/10.15252/emmm.201606210.

(43) Muralidar, S.; Ambi, S. V.; Sekaran, S.; Thirumalai, D.; Palaniappan, B. Role of Tau Protein in Alzheimer's Disease: The Prime Pathological Player. *International Journal of Biological Macromolecules* **2020**, *163*, 1599–1617. https://doi.org/10.1016/j.ijbiomac.2020.07.327.

(44) Medeiros, R.; Baglietto-Vargas, D.; LaFerla, F. M. The Role of Tau in Alzheimer's Disease and Related Disorders. *CNS Neurosci Ther* **2010**, *17* (5), 514–524. https://doi.org/10.1111/j.1755-5949.2010.00177.x.

(45) Sanchez-Varo, R.; Mejias-Ortega, M.; Fernandez-Valenzuela, J. J.; Nuñez-Diaz, C.; Caceres-Palomo, L.; Vegas-Gomez, L.; Sanchez-Mejias, E.; Trujillo-Estrada, L.; Garcia-Leon, J. A.; Moreno-Gonzalez, I.; Vizuete, M.; Vitorica, J.; Baglietto-Vargas, D.; Gutierrez, A. Transgenic Mouse Models of Alzheimer's Disease: An Integrative Analysis. *International Journal of Molecular Sciences* **2022**, *23* (10), 5404. https://doi.org/10.3390/ijms23105404.

(46) Querfurth, H. W.; LaFerla, F. M. Alzheimer's Disease. *N Engl J Med* **2010**, *362* (4), 329–344. https://doi.org/10.1056/NEJMra0909142.

(47) Meier-Stephenson, F. S.; Meier-Stephenson, V. C.; Carter, M. D.; Meek, A. R.; Wang, Y.; Pan, L.; Chen, Q.; Jacobo, S.; Wu, F.; Lu, E.; Simms, G. A.; Fisher, L.; McGrath, A. J.; Fermo, V.; Barden, C. J.; Clair, H. D. S.; Galloway, T. N.; Yadav, A.; Campágna-Slater, V.; Hadden, M.; Reed, M.; Taylor, M.; Kelly, B.; Diez-Cecilia, E.; Kolaj, I.; Santos, C.; Liyanage, I.; Sweeting, B.; Stafford, P.; Boudreau, R.; Reid, G. A.; Noyce, R. S.; Stevens,

L.; Staniszewski, A.; Zhang, H.; Murty, M. R. V. S.; Lemaire, P.; Chardonnet, S.; Richardson, C. D.; Gabelica, V.; DePauw, E.; Brown, R.; Darvesh, S.; Arancio, O.; Weaver, D. F. Alzheimer's Disease as an Autoimmune Disorder of Innate Immunity Endogenously Modulated by Tryptophan Metabolites. *Alzheimer's & Dementia: Translational Research & Clinical Interventions* **2022**, *8* (1), e12283. https://doi.org/10.1002/trc2.12283.

(48) Weaver, D. F. Alzheimer's Disease as an Innate Autoimmune Disease (AD2): A New Molecular Paradigm. *Alzheimers Dement* **2022**. https://doi.org/10.1002/alz.12789.

(49) Xie, J.; Van Hoecke, L.; Vandenbroucke, R. E. The Impact of Systemic Inflammation on Alzheimer's Disease Pathology. *Frontiers in Immunology* **2022**, *12*.

(50) Sperling, R. A.; Jack, C. R.; Black, S. E.; Frosch, M. P.; Greenberg, S. M.; Hyman, B. T.; Scheltens, P.; Carrillo, M. C.; Thies, W.; Bednar, M. M.; Black, R. S.; Brashear, H. R.; Grundman, M.; Siemers, E. R.; Feldman, H. H.; Schindler, R. J. Amyloid Related Imaging Abnormalities (ARIA) in Amyloid Modifying Therapeutic Trials: Recommendations from the Alzheimer's Association Research Roundtable Workgroup. *Alzheimers Dement* **2011**, *7* (4), 367–385. https://doi.org/10.1016/j.jalz.2011.05.2351.

(51) Hippius, H.; Neundörfer, G. The Discovery of Alzheimer's Disease. *Dialogues Clin Neurosci* **2003**, *5* (1), 101–108.

(52) Dahm, R. Alzheimer's Discovery. *Current Biology* **2006**, *16* (21), R906–R910. https://doi.org/10.1016/j.cub.2006.09.056.

(53) Serrano-Pozo, A.; Frosch, M. P.; Masliah, E.; Hyman, B. T. Neuropathological Alterations in Alzheimer Disease. *Cold Spring Harb Perspect Med* **2011**, *1* (1), a006189. https://doi.org/10.1101/cshperspect.a006189.

(54) Findeis, M. A. The Role of Amyloid β Peptide 42 in Alzheimer's Disease. *Pharmacology & Therapeutics* **2007**, *116* (2), 266–286. https://doi.org/10.1016/j.pharmthera.2007.06.006.

(55) *Initiation and propagation of neurodegeneration | Nature Medicine*. https://www.nature.com/articles/nm.2223 (accessed 2023-02-13).

(56) Boon, B. D. C.; Bulk, M.; Jonker, A. J.; Morrema, T. H. J.; van den Berg, E.; Popovic, M.; Walter, J.; Kumar, S.; van der Lee, S. J.; Holstege, H.; Zhu, X.; Van Nostrand, W. E.; Natté, R.; van der Weerd, L.; Bouwman, F. H.; van de Berg, W. D. J.; Rozemuller, A. J. M.; Hoozemans, J. J. M. The Coarse-Grained Plaque: A Divergent Aβ Plaque-Type in Early-Onset Alzheimer's Disease. *Acta Neuropathol* **2020**, *140* (6), 811–830. https://doi.org/10.1007/s00401-020-02198-8.

(57) Duyckaerts, C.; Delatour, B.; Potier, M.-C. Classification and Basic Pathology of Alzheimer Disease. *Acta Neuropathol* **2009**, *118* (1), 5–36. https://doi.org/10.1007/s00401-009-0532-1.

(58) Rahman, M. M.; Lendel, C. Extracellular Protein Components of Amyloid Plaques and Their Roles in Alzheimer's Disease Pathology. *Molecular Neurodegeneration* **2021**, *16* (1), 59. https://doi.org/10.1186/s13024-021-00465-0.

(59) Thal, D. R.; Capetillo-Zarate, E.; Del Tredici, K.; Braak, H. The Development of Amyloid β Protein Deposits in the Aged Brain. *Science of Aging Knowledge Environment* **2006**, *2006* (6), re1–re1. https://doi.org/10.1126/sageke.2006.6.re1.

(60) Liscic, R. Immunological Aspects and Anti-Amyloid Strategy for Alzheimer's Dementia. *Arhiv za higijenu rada i toksikologiju* **2013**, *64*, 603–608. https://doi.org/10.2478/10004-1254-64-2013-2414.

(61) Jellinger, K. A. Understanding Conflicting Neuropathological Findings. *JAMA Neurology* **2016**, *73* (4), 479–480. https://doi.org/10.1001/jamaneurol.2015.4879.

(62) Serrano-Pozo, A.; Frosch, M. P.; Masliah, E.; Hyman, B. T. Neuropathological Alterations in Alzheimer Disease. *Cold Spring Harb Perspect Med* **2011**, *1* (1), a006189. https://doi.org/10.1101/cshperspect.a006189.

(63) Biffi, A.; Greenberg, S. M. Cerebral Amyloid Angiopathy: A Systematic Review. *J Clin Neurol* **2011**, *7* (1), 1–9. https://doi.org/10.3988/jcn.2011.7.1.1.

(64) Greenberg, S. M.; Bacskai, B. J.; Hernandez-Guillamon, M.; Pruzin, J.; Sperling, R.; van Veluw, S. J. Cerebral Amyloid Angiopathy and Alzheimer Disease — One Peptide, Two Pathways. *Nat Rev Neurol* **2020**, *16* (1), 30–42. https://doi.org/10.1038/s41582-019-0281-2.

(65) Selkoe, D. J. Alzheimer's Disease. *Cold Spring Harb Perspect Biol* **2011**, *3* (7), a004457. https://doi.org/10.1101/cshperspect.a004457.

(66) Yakupova, E. I.; Bobyleva, L. G.; Vikhlyantsev, I. M.; Bobylev, A. G. Congo Red and Amyloids: History and Relationship. *Biosci Rep* **2019**, *39* (1), BSR20181415. https://doi.org/10.1042/BSR20181415.

(67) Goldman, R. D. Antibodies: Indispensable Tools for Biomedical Research. *Trends in Biochemical Sciences* **2000**, *25* (12), 593–595. https://doi.org/10.1016/S0968-0004(00)01725-4.

(68) Ansar, W.; Ghosh, S. Monoclonal Antibodies: A Tool in Clinical Research. *Indian Journal of Clinical Medicine* **2013**, *4*, IJCM.S11968. https://doi.org/10.4137/IJCM.S11968.

(69) Trimmer, J. S. RECOMBINANT ANTIBODIES IN BASIC NEUROSCIENCE RESEARCH. *Curr Protoc Neurosci* **2020**, *94* (1), e106. https://doi.org/10.1002/cpns.106.

(70) Liu, J. K. H. The History of Monoclonal Antibody Development – Progress, Remaining Challenges and Future Innovations. *Ann Med Surg (Lond)* **2014**, *3* (4), 113–116. https://doi.org/10.1016/j.amsu.2014.09.001.

(71) *A Renaissance for Alzheimer's and Dementia Science Brings Vigorous Debate*. Alzheimer's Disease and Dementia. https://www.alz.org/blog/alz/july-2022/a-renaissance-for-alzheimers-and-dementia-science (accessed 2023-04-26).

(72) *EISAI and Biogen Inc. Announce U.S. FDA Grants Breakthrough Therapy Designation for LECANEMAB (BAN2401), an Anti-Amyloid Beta Protofibril Antibody for the Treatment of Alzheimer's Disease | Biogen*. https://investors.biogen.com/news-releases/news-release-details/eisai-and-biogen-inc-announce-us-fda-grants-breakthrough-therapy (accessed 2022-02-23).

(73) Bekris, L. M.; Yu, C.-E.; Bird, T. D.; Tsuang, D. W. Genetics of Alzheimer Disease. *J Geriatr Psychiatry Neurol* **2010**, *23* (4), 213–227. https://doi.org/10.1177/0891988710383571.

(74) Lott, I. T.; Head, E. Dementia in Down Syndrome: Unique Insights for Alzheimer Disease Research. *Nat Rev Neurol* **2019**, *15* (3), 135–147. https://doi.org/10.1038/s41582-018-0132-6.

(75) Johannesson, M.; Sahlin, C.; Söderberg, L.; Basun, H.; Fälting, J.; Möller, C.; Zachrisson, O.; Sunnemark, D.; Svensson, A.; Odergren, T.; Lannfelt, L. Elevated Soluble Amyloid Beta Protofibrils in Down Syndrome and Alzheimer's Disease. *Molecular and Cellular Neuroscience* **2021**, *114*, 103641. https://doi.org/10.1016/j.mcn.2021.103641.

(76) Helman, A. M.; Siever, M.; McCarty, K. L.; Lott, I. T.; Doran, E.; Abner, E. L.; Schmitt, F. A.; Head, E. Microbleeds and Cerebral Amyloid Angiopathy in the Brains of People with

Down Syndrome with Alzheimer's Disease. *J Alzheimers Dis* **2019**, *67* (1), 103–112. https://doi.org/10.3233/JAD-180589.

(77) Ichimata, S.; Martinez-Valbuena, I.; Forrest, S. L.; Kovacs, G. G. Expanding the Spectrum of Amyloid-β Plaque Pathology: The Down Syndrome Associated 'Bird-Nest Plaque.' *Acta Neuropathol* **2022**, *144* (6), 1171–1174. https://doi.org/10.1007/s00401-022-02500-w.

Chapter 2[a]

Antibodies generated from a triangular trimer from Aβ recognize cored and neuritic plaques in brain sections of people who lived with late-onset Alzheimer's disease

Abstract

Oligomers formed by the beta-amyloid peptide (Aβ) are involved in the neurodegeneration of Alzheimer's disease (AD). Although valuable as tools to identify Aβ oligomers, conformation-specific antibodies have thus far been generated against less well characterized heterogenous Aβ oligomer preparations, leading to uncertainty in their precise epitopes. Our laboratory recently reported a structurally defined stable trimer derived from residues 17–36 of Aβ consisting of three covalently linked $A\beta_{17-36}$ β-hairpin peptides that are constrained in a triangular arrangement (4AT-L trimer). The current investigation reports the generation of a rabbit polyclonal antibody against the trimer (pAb_{4AT-L}) and describes its application in the immunostaining of transgenic mouse and human brain tissue. Immunofluorescent staining of sections of 5xFAD mouse brain slices reveals that pAb_{4AT-L} recognizes cored plaques. Immunohistochemical staining with pAb_{4AT-L} shows that more plaques were labeled in brain sections from people with Late Onset Alzheimer's Disease (LOAD) than from people who were cognitively normal. Immunofluorescent staining of brain sections from LOAD shows that pAb_{4AT-L} recognizes dense core plaques, neuritic plaques, and cerebral amyloid angiopathy (CAA). Features of plaques recognized by pAb_{4AT-L} may represent residues 17–36 from the central and *C*-terminal regions of Aβ in an arrangement or conformation

[a] This chapter will be submitted to Acta Neuropathologica.

that resembles the 4AT-L trimer. The staining of cored plaques by $pAb_{4AT\text{-}L}$ suggests that the cores of cored plaques are surrounded by Aβ oligomers and supports a model in which the dense cores of amyloid plaques are surrounded by a halo of Aβ oligomers. We envision $pAb_{4AT\text{-}L}$ will be a valuable tool for identifying Aβ plaque composition and providing functional insights into Aβ plaque morphology.

Introduction

Probes for specific conformations of the beta-amyloid peptide (Aβ) can provide insight into the structure and thus the function of Aβ in Alzheimer's disease (AD). Traditional stains such as Thioflavin-S and Congo Red are used to identify Aβ plaques in people with AD, however, they do not distinguish between conformations of Aβ.[1] Antibodies provide an alternative technique for identifying Aβ plaques and other pathologies in the post-mortem AD brain and provide additional insights into structure-function relationships and protein-protein interactions relevant to Aβ pathology.[2–6]

Conformation-specific antibodies targeting specific Aβ pathology have been generated against preparations of Aβ oligomers and have proven useful as tools to better understand conformations of Aβ and to identify features of plaques in AD brain tissue.[7,8] The A11 and OC polyclonal antibodies and OC monoclonal antibodies are examples of conformation-specific antibodies that recognize Aβ oligomers or soluble fibrils.[9–12] The A11 polyclonal antibody was generated against a heterogenous and less well characterized preparation of Aβ oligomers, making it difficult to understand the precise Aβ oligomer antigen and also led to challenges in antibody production.

Uniform Aβ oligomers are difficult to prepare *in vitro*, as Aβ oligomers are generally

heterogeneous and can further aggregate to form higher-order assemblies. Conventional preparations result in mixtures of different species, and it is difficult or impossible to obtain reproducible and homogeneous preparations of Aβ oligomers.[8,13] A number of conformation-specific antibodies have been developed against Aβ oligomers that have been characterized by a variety of biophysical techniques.[7,8,13] Although a number of conformation-specific antibodies have been developed against Aβ oligomers that have been characterized by a variety of biophysical techniques.[7,8,13] conformation-specific antibodies generated against high-resolution structurally defined Aβ oligomers are needed.[14]

Our laboratory recently reported the structure and assembly of 4AT-L, a stable trimer derived from residues 17–36 of Aβ, (**Figure 2.1A and 2.1B**).[15] The trimer consists of three covalently linked β-hairpins of $A\beta_{17-36}$ in a triangular arrangement. X-ray crystallographic studies of 4AT-L reveal the structure and conformation of the trimer at atomic resolution (PDB 7JXO). Although our laboratory has previously generated trimers and other peptide models derived from Aβ,[16] the 4AT-L trimer is especially easy to generate and includes much of the central and *C*-terminal regions of Aβ. X-ray crystallography, SDS-PAGE, SEC, and cytotoxicity assays demonstrate that the 4AT-L trimer behaves in a similar fashion as Aβ oligomers, in that it self-assembles and is toxic to SH-SY5Y human neuronal blastoma cells.[15] In the current investigation, we report the generation and characterization of a rabbit polyclonal antibody (pAb_{4AT-L}) against the 4AT-L trimer. The pAb_{4AT-L} antibody recognizes cored plaques in brain tissue isolated from 5xFAD transgenic mice and people with Late Onset Alzheimer's Disease (LOAD). We envision pAb_{4AT-L} as a valuable tool for better understanding Aβ plaque composition and thus the role of Aβ in AD.

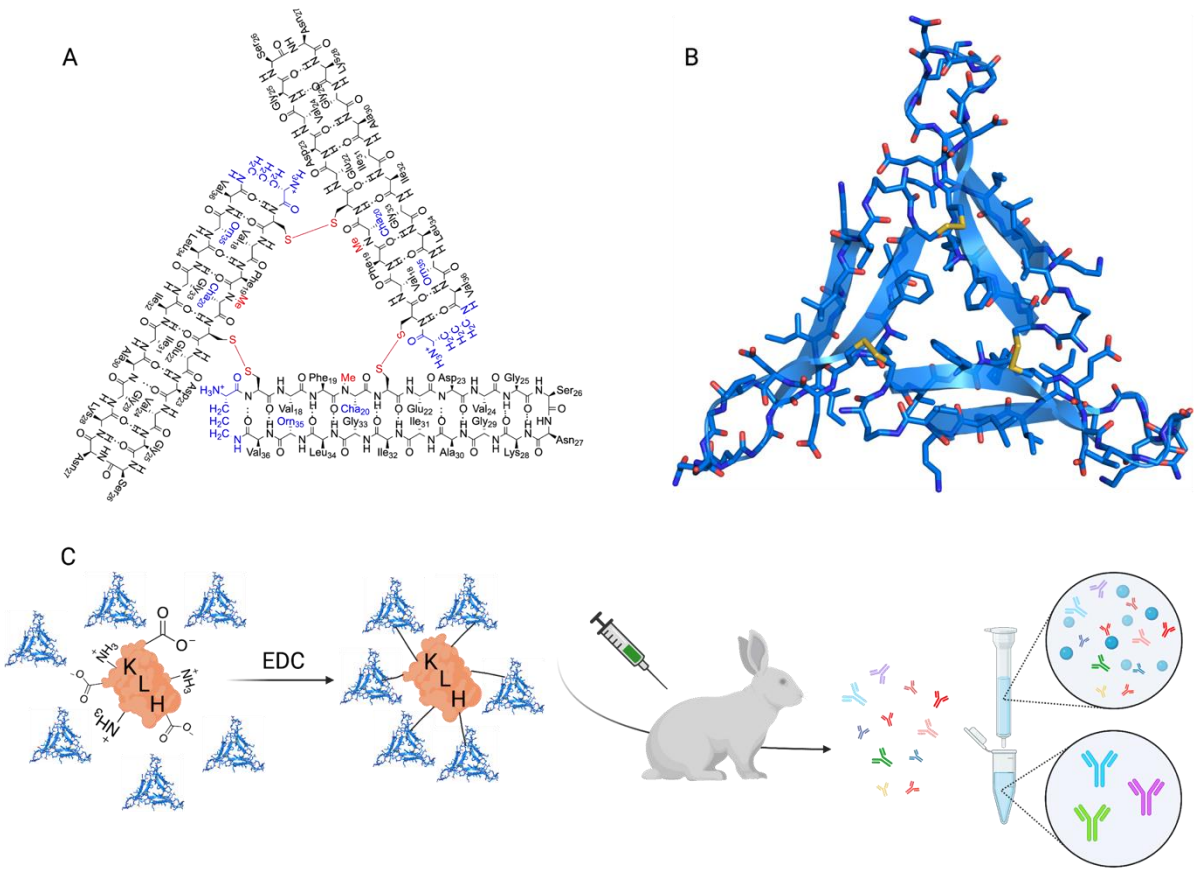

Figure 2.1 (**A)** X-ray crystallographic structure of the 4AT-L trimer (PDB 7JXO). (**B)** Cartoon of the 4AT-L trimer. (**C)** Generation of polyclonal antibodies against 4AT-L: Conjugation of 4AT-L with KLH (keyhole limpet hemocyanin) immunization of rabbits with the KLH-4AT-L conjugate, and affinity purification of rabbit serum to afford $pAb_{4AT\text{-}L}$. The figure was designed by Chelsea Marie T. Parrocha and created with BioRender.com.

RESULTS

Generation of the polyclonal antibody $pAb_{4AT\text{-}L}$ against the 4AT-L trimer.

Antibodies against the 4AT-L trimer were generated by standard procedures by Pacific Immunology in two New Zealand white rabbits. (**Figure 2.1 C**, (**Supplemental Figure S2.1**). Briefly, 4AT-L was conjugated to KLH (keyhole limpet hemocyanin) by EDC coupling. The resulting conjugate produced a robust immune response (titers of >1:500,000). The polyclonal antibody was then isolated by affinity purification of serum on NHS-activated agarose that had

been conjugated to the 4AT-L trimer. From 50 mL of serum, we were typically able to isolate 4 mg of $pAb_{4AT\text{-}L}$. To ensure that we were able to deplete serum of $pAb_{4AT\text{-}L}$, an ELISA was performed with the depleted serum against the 4AT-L trimer (**Supplemental Figure S2.2**).

$pAb_{4AT\text{-}L}$ recognizes pathology in the brains of the 5xFAD mouse model.

To determine if $pAb_{4AT\text{-}L}$ recognizes Aβ in tissue, we used brain slices from the AD transgenic mouse model 5xFAD for immunofluorescence microscopy. The 5xFAD mouse model contains five familial AD mutations with three Aβ precursor protein mutations including the Swedish (K670N/M671L), Florida (I716V), and London mutation (V717I) as well as two mutations in presenilin I including M146L and L286V.[18] 5xFAD mice develop aggressive Aβ pathology by four months of age, and the pathology continues to develop as the mice age. The rapid increase in pathology and relative homogeneity in Aβ pathology across the brain make the 5xFAD mouse model ideal for the initial evaluation of $pAb_{4AT\text{-}L}$.[19]

Brain sections from a 13-month-old 5xFAD mouse show prominent staining of plaques when treated with $pAb_{4AT\text{-}L}$ and then with a fluorescent goat anti-rabbit secondary antibody (**Figure 2.2 A** and **2.2 B**). In contrast, brain sections from wild-type (WT) littermates show no plaques and only weak background fluorescence (**Figure 2.2 C**). As an additional control, we stained an adjacent slice of the 5xFAD mouse brain with only the fluorescent goat anti-rabbit secondary antibody and observed no staining (**Figure 2.2 D**). In the 5xFAD mouse brain, cored plaques appear to be recognized with $pAb_{4AT\text{-}L}$ rather than diffuse plaques. Cored plaques are composed of a fibrillar, β-pleated-sheet dense core composed of $Aβ_{42}$ surrounded by a halo of Aβ and contain swollen axons and synaptic terminals (dystrophic neurites).[20–23] In contrast, diffuse plaques contain non-fibrillar Aβ, but lack a fibral center and dystrophic neurites, and are amorphous with a lack of structural margins or boundaries.[20,22–24] $pAb_{4AT\text{-}L}$ strongly stains the

cores of cored plaques, strikingly staining the periphery of the cores and showing weaker staining around the halo of Aβ (**Figure 2.2 B**).

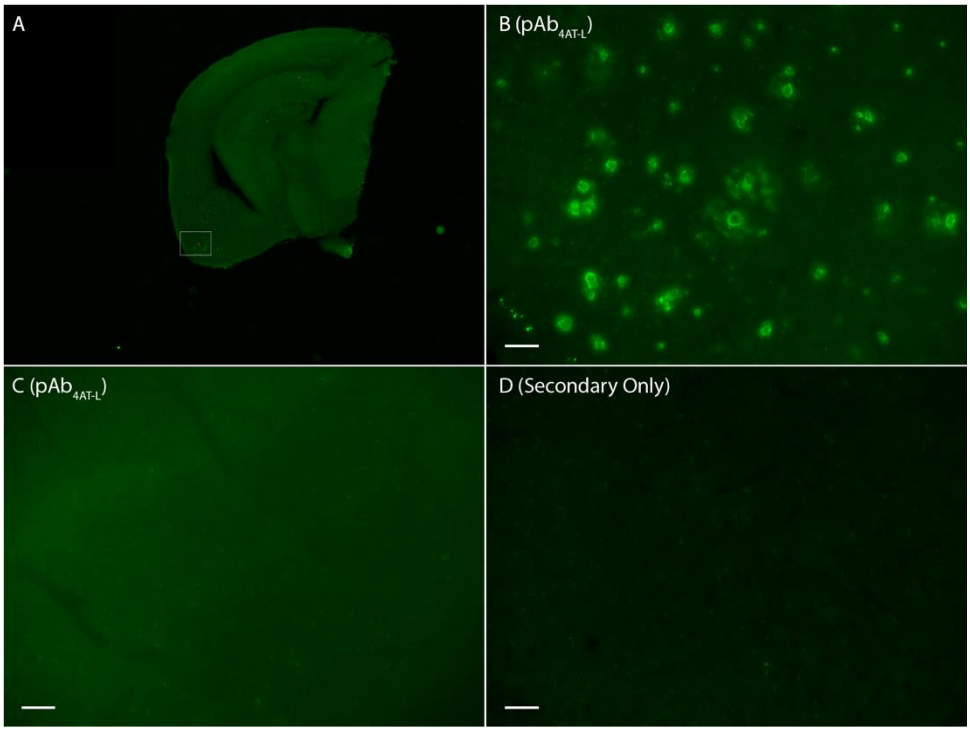

Figure 2.2 Immunofluorescence micrographs comparing staining of pAb_{4AT-L} in brain slices from a 5xFAD mouse and a wild-type littermate. **(A)** Stitched micrograph acquired at 4X magnification of a 5xFAD mouse brain hemisphere stained with pAb_{4AT-L}. The white box shows the region of the brain used for micrographs B-D. The red dots on the image are associated with image acquisition and are not features of the image itself. **(B)** Micrograph of a 5xFAD mouse brain slice stained with pAb_{4AT-L}. **(C)** Micrograph of a wild-type littermate mouse brain slice stained with pAb_{4AT-L}. **(D)** Micrograph of a 5xFAD mouse brain slice stained with secondary antibody only (goat anti-rabbit Alexa Fluor 488). Images B-D were acquired at 20X magnification; the scale bar is 50 μm.

To further characterize the features recognized by pAb_{4AT-L}, we co-stained with the 6E10 monoclonal antibody, which recognizes residues from the *N*-terminus of Aβ ($Aβ_{4-10}$) and broadly identifies standard features associated with Aβ pathology (**Figure 2.3**). Although many similar features are recognized by both antibodies, there are some noteworthy differences. 6E10 recognizes diffuse plaques, while pAb_{4AT-L} does not (shown by the > symbol in **Figure 2.3**). 6E10

also more strongly recognizes halos of Aβ than pAb_{4AT-L} (shown by the # symbol in **Figure 2.3**). Interestingly, 6E10 does not strongly recognize the periphery of cores of the cored plaques as robustly as pAb_{4AT-L} (* symbol in **Figure 2.3**).

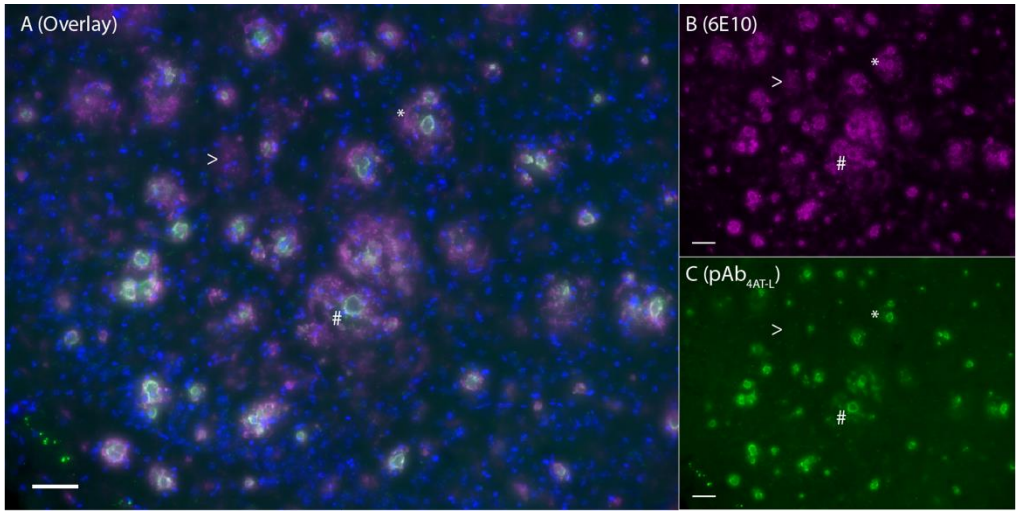

Figure 2.3 Immunofluorescence micrographs comparing staining of pAb_{4AT-L} to the commercially available anti-Aβ antibody 6E10 in a brain slice from a 5xFAD mouse. **(A)** Micrograph of a brain slice from a 5xFAD mouse stained with pAb_{4AT-L} (green), 6E10 (magenta), and DAPI (blue). **(B)** Micrograph of a brain slice from a 5xFAD mouse shown in the magenta channel (6E10). **(C)** Micrograph of a brain slice from a 5xFAD mouse shown in the green channel (pAb_{4AT-L}). The > symbol shows a diffuse plaque recognized only with 6E10. The * symbol shows a halo of Aβ strongly recognized with 6E10. The # symbol shows the periphery of the core of cored plaques strongly recognized by pAb_{4AT-L}. Images were acquired at 20X magnification; the scale bar is 50 μm.

pAb_{4AT-L} recognizes pathology in the brains of people who lived with LOAD.

The robust staining of the 5xFAD mouse plaques and differences from 6E10 prompted us to characterize the features recognized by pAb_{4AT-L} in brain slices of LOAD. For these studies, we obtained post-mortem brain samples from LOAD and those who were cognitively normal. We used the occipital cortex for these studies because this region develops diverse pathology during AD progression.[25] **Table 2.1** displays the demographics of people in this study who were selected based on balancing sex, age, PMI (post-mortem interval), and plaque staging.

Table 1

Case Demographics

Group	Age	Sex	PMI	APoE	NPDx1	Tangle Stage	Plaque Stage
LOAD	86	F	10.1	N/A	AD	Stage 5	Stage C
LOAD	81	M	1.9	3/3	AD	Stage 5	Stage B
LOAD	86	M	4.2	3/4	AD	Stage 5	Stage C
LOAD	90	M	3.75	3/4	AD	Stage 6	Stage B
LOAD	96	F	4.3	3/3	AD	Stage 5	Stage B
LOAD	89	F	4.08	3/3	AD	Stage 6	Stage C
Mean	88.0 $\pm$ 5.0		4.7 $\pm$ 2.8				
Ctrl	88	F	5.17	2/3	Normal (MBC)	Stage 2	Stage A
Ctrl	90	F	3.8	3/3	Normal (MBC)	Stage 4	Stage B
Ctrl	89	F	3.58	3/3	Normal (MBC)	Stage 3	Stage B
Ctrl	92	M	8.75	N/A	Normal (MBC)	Stage 3	Stage A
Ctrl	89	F	5.95	2/3	Normal (MBC)	Stage 3	None
Mean	89.6 $\pm$ 1.5		5.4$\pm$ 2.0				

LOAD, Late Onset Alzheimer's Disease; Ctrl, control; PMI, postmortem interval prior to brain collection in hours; NPDx1, primary neuropathology diagnosis; AD, Alzheimer's disease; APoE, Apolipoprotein E allele, MBC, Mild Braak Changes.

Immunohistochemical staining with DAB reveals that $pAb_{4AT\text{-}L}$ preferentially recognizes plaques in LOAD (**Figure 2.4 A**). Although immunohistochemical staining also shows lesions in the brains of people with mild Braak changes who were not diagnosed with LOAD, plaques are more abundant in the brains of individuals with LOAD (**Figure 2.4 B**). Quantitative digital neuropathology confirms that brain slices from people with LOAD contain more plaques recognized by $pAb_{4AT\text{-}L}$ than from people with mild Braak changes who were not diagnosed with LOAD (**Figure 2.4 C**).

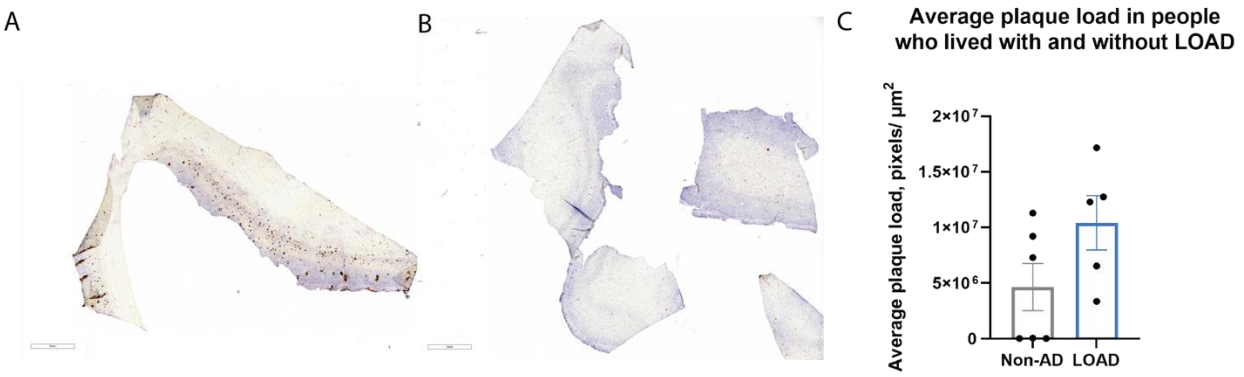

Figure 2.4. Immunohistochemistry staining of brain sections from people who lived with and without LOAD stained with $pAb_{4AT\text{-}L}$ was used to perform quantitative digital neuropathology to quantify average plaque loads detected by $pAb_{4AT\text{-}L}$. **(A)** Micrograph of a section of occipital cortex from a person who lived with LOAD stained with $pAb_{4AT\text{-}L}$. **(B)** Micrograph of a section of occipital cortex from a person who lived without LOAD stained with $pAb_{4AT\text{-}L}$. **(C)** Bar graph representing the average plaque load (pixels/μm^2) detected by $pAb_{4AT\text{-}L}$ in the occipital cortex stained of people who lived with and without LOAD. Images were acquired at 20X and were viewed at 1X using Aperio ImageScope; the scale bar is 2 mm.

We performed a pre-adsorption experiment to further confirm that $pAb_{4AT\text{-}L}$ is indeed recognizing Aβ pathology. In this experiment, $pAb_{4AT\text{-}L}$ was incubated with the 4AT-L trimer prior to staining brain sections from a person who lived with LOAD. As a control, we stained a sequential brain section with $pAb_{4AT\text{-}L}$. When the two sections were imaged, the section stained with the pre-absorbed $pAb_{4AT\text{-}L}$ showed no staining of pathology, while the section stained with $pAb_{4AT\text{-}L}$ did. These observations confirm that $pAb_{4AT\text{-}L}$ specifically recognizes Aβ pathology in human brain tissue (**Supplemental Figure 2.3 C**).

We further characterized the recognition of $pAb_{4AT\text{-}L}$ in human brain tissue by comparing its immunofluorescent staining to that of the commercially available anti-Aβ antibodies 6E10, 4G8, 11A50-B10, and 12F4. We selected these antibodies for these experiments, because of their wide variety of Aβ epitope recognition and published precedents of detecting conformations of Aβ in the brains of people who lived with LOAD (**Table 2**).

Table 2

Commercially available anti-Aβ antibodies

Antibody	Epitope	Vendor	Cat. Number	IF Dilution	References
6E10	$A\beta_{4\text{-}10}$	BioLegend	803015	1:1000	[3]
4G8	$A\beta_{18\text{-}23}$	BioLegend	800708	1:1000	[3]
11A50-B10	$A\beta_{1\text{-}40}$, *C*-terminus	BioLegend	805404	1:1000	[31]
12F4	$A\beta_{1\text{-}42}$, *C*-terminus	BioLegend	805509	1:1000	[26, 42]

$pAb_{4AT\text{-}L}$ recognizes cores of cored plaques in people with LOAD.

To determine if $pAb_{4AT\text{-}L}$ recognizes unique Aβ pathology in LOAD, we compared $pAb_{4AT\text{-}L}$ to four commercially available anti-Aβ antibodies by immunofluorescent staining experiments on sections of the occipital cortex from LOAD. Thus, we stained a series of LOAD brain slices with $pAb_{4AT\text{-}L}$ and 6E10, 4G8, 11A50-B10, or 12F4 and respective fluorescent secondary antibodies and visualized the plaques identified by each antibody (**Figure 2.5**). Shared epitope recognition was determined by the presence or lack thereof of immunofluorescent staining overlap between antibodies on Aβ plaques.

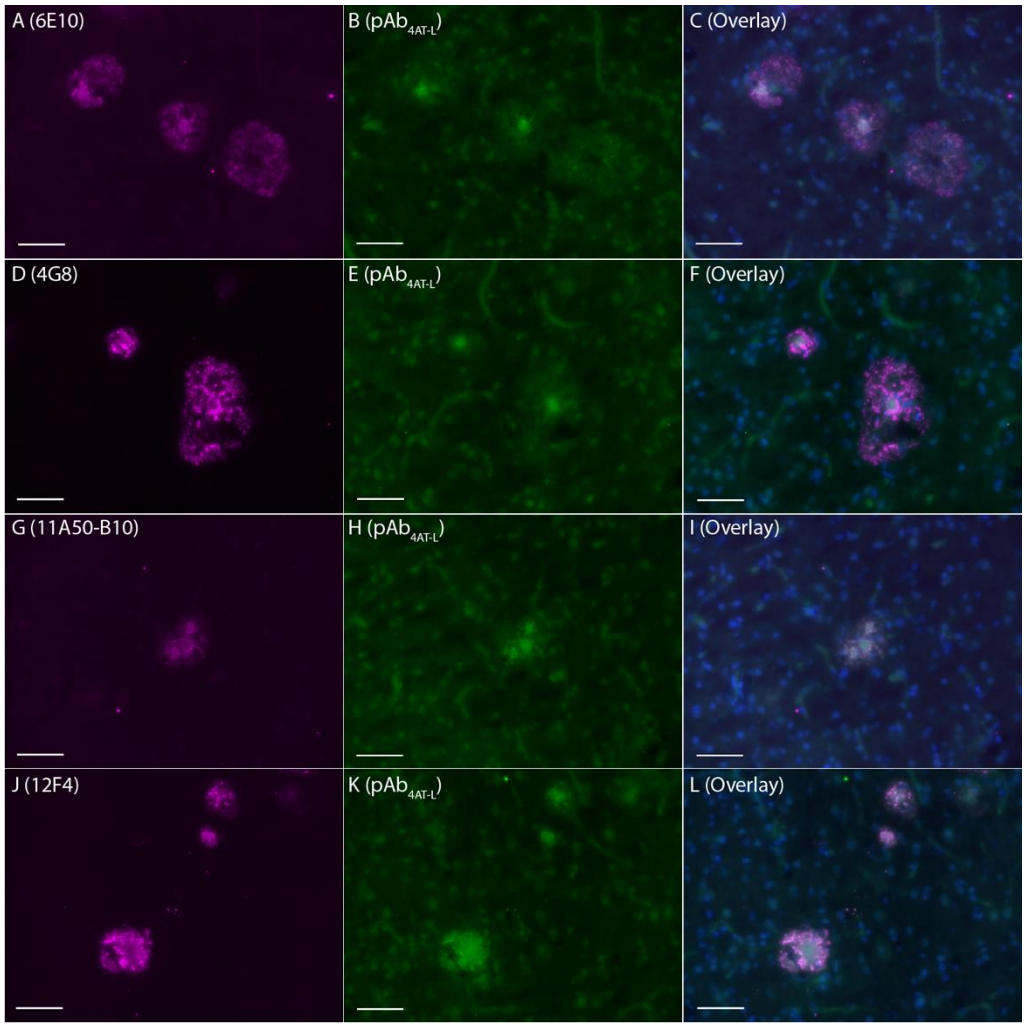

Figure 2.5 Immunofluorescence micrographs comparing Aβ plaque staining of $pAb_{4AT\text{-}L}$ to four commercially available anti-Aβ antibodies in brain slices from a person who lived with LOAD. The left column shows the staining of each commercially available antibody (magenta); the middle column shows the staining of $pAb_{4AT\text{-}L}$ (green); the right column shows the corresponding overlay, as well as the staining of cell nuclei by DAPI (blue). **(A-C)** Images from coincubation with 6E10 and $pAb_{4AT\text{-}L}$; **(D-F)** are images from coincubation with 4G8 and $pAb_{4AT\text{-}L}$; **(G-I)** are images from coincubation with 11A50-B10 and $pAb_{4AT\text{-}L}$; **(J-L)** are images from coincubation with 12F4 and $pAb_{4AT\text{-}L}$. Images were acquired at 40X; the scale bar is 50 μm.

$pAb_{4AT\text{-}L}$ recognizes the cores of cored plaques but shows little or no recognition of the halos (**Figure 2.5**), recognizing the cores of cored plaques more strongly than 6E10 (**Figure 2.5 A-C)**, 4G8 (**Figure 2.5 D-E**), 11A50-B10 (**Figure 2.5 G-I**), and 12F4 (**Figure 2.5 J-L**). These antibodies recognize different epitopes, and the differences in staining by 6E10 and $pAb_{4AT\text{-}L}$ may

reflect the binding of the antibodies to the different epitopes. 6E10 recognizes $A\beta_{4-10}$, whereas pAb_{4AT-L} was generated against a trimer derived from $A\beta_{17-36}$. The strong staining of the cores by pAb_{4AT-L} may reflect that the cores present regions of $A\beta_{17-36}$ in a conformation or arrangement that resembles the 4AT-L trimer.

In contrast to 6E10, 4G8 recognizes $A\beta_{18-23}$, which overlaps with the epitope recognized by pAb_{4AT-L}. When a brain slice was stained with both pAb_{4AT-L} and 4G8, pAb_{4AT-L} strongly recognized the cores of cored plaques (**Figure 2.5 F**), while 4G8 distinctively stained the halo of Aβ around cored plaques in contrast to pAb_{4AT-L} (**Figure 2.5 D** and **2.5E**). The strong recognition of the cores of cored plaques does not appear to simply result from pAb_{4AT-L} out-competing 4G8 for similar epitopes, as strong staining by pAb_{4AT-L} occurs regardless of the order of staining. When a sequential brain slice was stained first with 4G8 and then with pAb_{4AT-L}, similar strong staining of the cores by pAb_{4AT-L} was also observed (**Supplemental Figure 2.4 D-F**). Similar staining was also observed when a sequential brain slice was stained first with pAb_{4AT-L} and then with 4G8 (**Supplemental Fig. 2.4 M-O**). Regardless of the order of antibody addition between 4G8 and pAb_{4AT-L}, the cores of cored plaques were consistently recognized by pAb_{4AT-L} while 4G8 consistently recognized the halo of Aβ around the cores of cored plaques. These observations indicate that pAb_{4AT-L} is recognizing features of plaques that are distinct from the sequence recognition provided by 4G8.

We also compared pAb_{4AT-L} to the 11A50-B10 and 12F4 antibodies, which recognize the respective *C*-termini of $A\beta_{40}$ and of $A\beta_{42}$ [26,27]. The 11A50-B10 and 12F4 antibodies recognize different regions of the plaques. 11A50-B10 stains the periphery of the cores of cored plaques (**Figure 2.5 G**), while 12F4 recognizes distinct halos and standard dense plaques (**Figure 2.5 J**). These differences in staining of 11A50-B10 and 12F4 reflect differences in how $A\beta_{40}$ and $A\beta_{42}$

deposit in forming the plaques, with $A\beta_{40}$ depositing later than the more aggregation-prone $A\beta_{42}$. $A\beta_{42}$ is the dominant isoform in plaques and serves as a foundation for plaque formation, because the additional two hydrophobic *C*-terminal amino acids increase peptide self-assembly.[23,28,29] Thus, 12F4 strongly stains more regions of the plaques reflecting their predominant $A\beta_{42}$ composition (**Figure 2.5 J**). In contrast, the less pronounced and more diffuse staining by 11A50-B10 reflects the later $A\beta_{40}$ deposition.[28,29]

$pAb_{4AT\text{-}L}$ is more similar to 12F4 than 11A50-B10. Thus, 11A50-B10 recognizes the periphery of the cores of cored plaques recognized by $pAb_{4AT\text{-}L}$ (**Figure 2.5 H-I**). In contrast, 12F4 staining slightly overlaps with $pAb_{4AT\text{-}L}$, especially in the transition areas between the halo and cores of cored plaques (**Figure 2.5 K-L**). These observations demonstrate that $pAb_{4AT\text{-}L}$ strongly recognizes plaques composed of $A\beta_{42}$ than plaques composed of $A\beta_{40}$.

We performed additional immunofluorescent staining swapping the order of antibody addition to ensure that steric hindrance was not interfering with antibody staining (and therefore epitope recognition) of 6E10, 11A50-B10, and 12F4 in the presence of $pAb_{4AT\text{-}L}$. We thus swapped the order of staining, first staining LOAD brain slices with these commercially available antibodies and a fluorescent goat-anti mouse secondary antibody, then staining with $pAb_{4AT\text{-}L}$ and as fluorescent goat anti-rabbit secondary antibody. Swapping the order of addition between commercially available anti-Aβ antibodies and $pAb_{4AT\text{-}L}$ does not change the staining we observe from micrographs and therefore epitope recognition (**Figure 2.5** and **Supplemental Figure 2.4 A-C** and **2.4 G-L**).

Collectively, these experiments indicate that $pAb_{4AT\text{-}L}$ consistently recognizes the cores of cored plaques more strongly than 6E10, 4G8, 11A50-B10, and 12F4. $pAb_{4AT\text{-}L}$ has little to no

recognition of the halos around plaques. pAb_{4AT-L} recognition of plaques is more similar to 12F4 than 11A50-B10 and therefore recognizes plaques comprised of $A\beta_{42}$.

pAb_{4AT-L} recognizes plaques associated with glial response and neuropil threads.

We performed plaque phenotyping studies to better understand the types of plaques recognized by pAb_{4AT-L}. We thus co-stained brain slices with pAb_{4AT-L} and with IBA-1, GFAP, or AT8 to identify microglia (**Figure 2.6 A-C**), astrocytes (**Figure 2.6 D-F**), or tau (**Figure 2.6 G-I**).

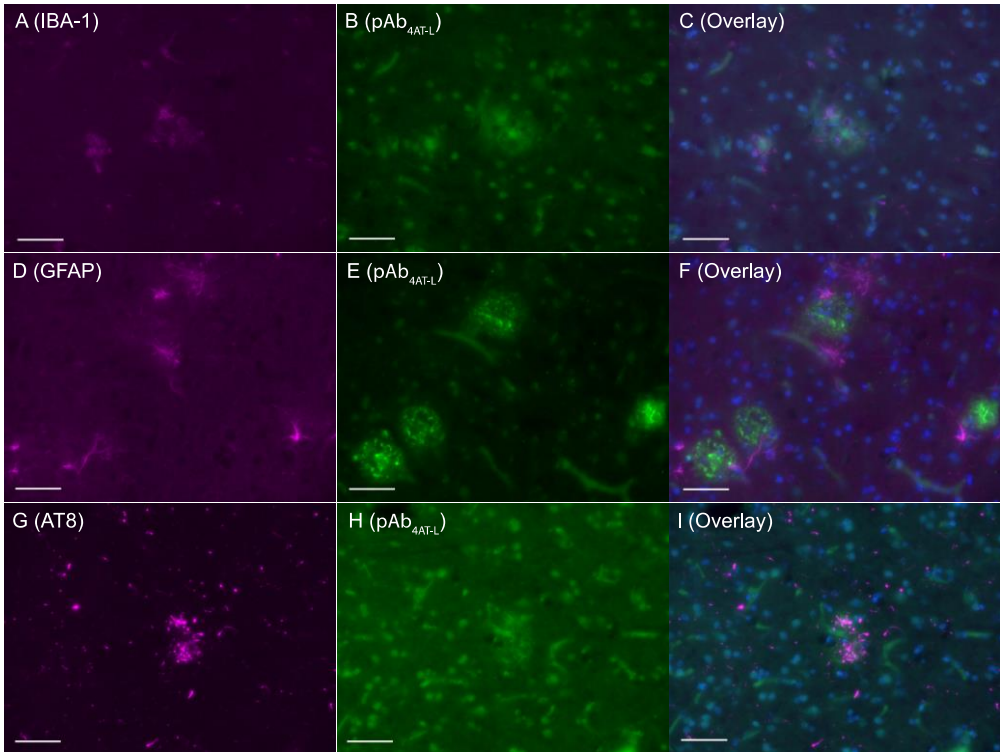

Figure 2.6 Characterization of plaque phenotypes identified by pAb_{4AT-L} in a person who lived with LOAD: Immunofluorescence micrographs illustrating staining with pAb_{4AT-L}, IBA-1 (microglia), GFAP (astrocytes), and AT8 (tau). The left column contains images of antibodies staining for associated AD pathology (magenta); the middle column contains images of pAb_{4AT-L} (green); the right column shows the corresponding overlay, as well as the staining of cell nuclei by DAPI (blue). **A-C** are images from coincubation with IBA-1 and pAb_{4AT-L}; **D-F** are images from coincubation with GFAP and pAb_{4AT-L}; **G-I** are images from coincubation with AT8 and pAb_{4AT-L}. Images were acquired at 40X; the scale bar is 50 μm.

Microglia and astrocytes are glial cells in the brain involved with neuroinflammation and Aβ clearance.[30] Dense core plaques are also defined by the presence of activated microglia and astrocytes surrounding the core of the plaque.[31–33] The activation of glial cells occurs in response to inflammatory cytokines, or neuritic damage caused by Aβ, indicating Aβ clearance.[31–33] In a micrograph of plaques stained with $pAb_{4AT\text{-}L}$, microglia stained with IBA-1 (Ionized calcium-Binding Adapter molecule 1), are embedded in the halo of Aβ and appear to engage with the core of the cored plaques (**Figure 2.6 A-C**). In another micrograph of dense core plaques stained with $pAb_{4AT\text{-}L}$, astrocytes stained with GFAP (Glial Fibrillary Acidic Protein) surround the halo of dense core plaques (**Figure 2.6 D-F**).

Neuropil threads are phosphorylated tau that forms paired helical filaments which accumulate in the dendrites and soma of neurons; this species of tau pathology is one of the earliest forms of tau accumulation and is evidence that supports the synergistic relationship between Aβ and tau where the accumulation of Aβ precedes tau in the pathogenesis of AD.[4,20,21,27,34] Neuritic plaques contain tau-positive dystrophic neurites and may or may not contain dense cores.[35] The AT8 antibody recognizes phosphorylated tau-associated AD pathology.[21,23] In a micrograph of a plaque stained with $pAb_{4AT\text{-}L}$, the AT8 recognizes neuropil threads that appear to be intertwined and matted on the plaque (**Figure 2.6 G-I**).

$pAb_{4AT\text{-}L}$ recognizes Cerebral Amyloid Angiopathy (CAA) in people with LOAD.

In staining brain slices from an individual LOAD, we observed that $pAb_{4AT\text{-}L}$ also recognizes Cerebral Amyloid Angiopathy (CAA) (**Figure 2.7**). CAA results from the accumulation of $A\beta_{40}$ in blood vessels of the brain.[23,36,37] Brain slices co-stained with $pAb_{4AT\text{-}L}$ and 6E10, 4G8, or 11A50-B10 reveal co-localization of $pAb_{4AT\text{-}L}$ and the corresponding anti-Aβ antibodies in CAA pathology (**Figure 2.7 A-I**). In contrast, 12F4 shows little staining of CAA

pathology demonstrating that the CAA deposits are composed primarily of $A\beta_{40}$, instead of $A\beta_{42}$ (**Figure 2.7 J-L**). Because of the propensity for CAA autofluorescence in the green channel, and to confirm that $pAb_{4AT\text{-}L}$ is recognizing CAA, we swapped Alexa Fluor dyes between 4G8 and 4AT-L. In both staining experiments with $pAb_{4AT\text{-}L}$ and 4G8, we observe that $pAb_{4AT\text{-}L}$ distinctly stains CAA (**Supplemental Figure 2.5 D-F**). These experiments demonstrate that $pAb_{4AT\text{-}L}$ recognizes CAA, as well as Aβ plaques and present regions of $A\beta_{17\text{-}36}$ in an arrangement or conformation that resembles the 4AT-L trimer.

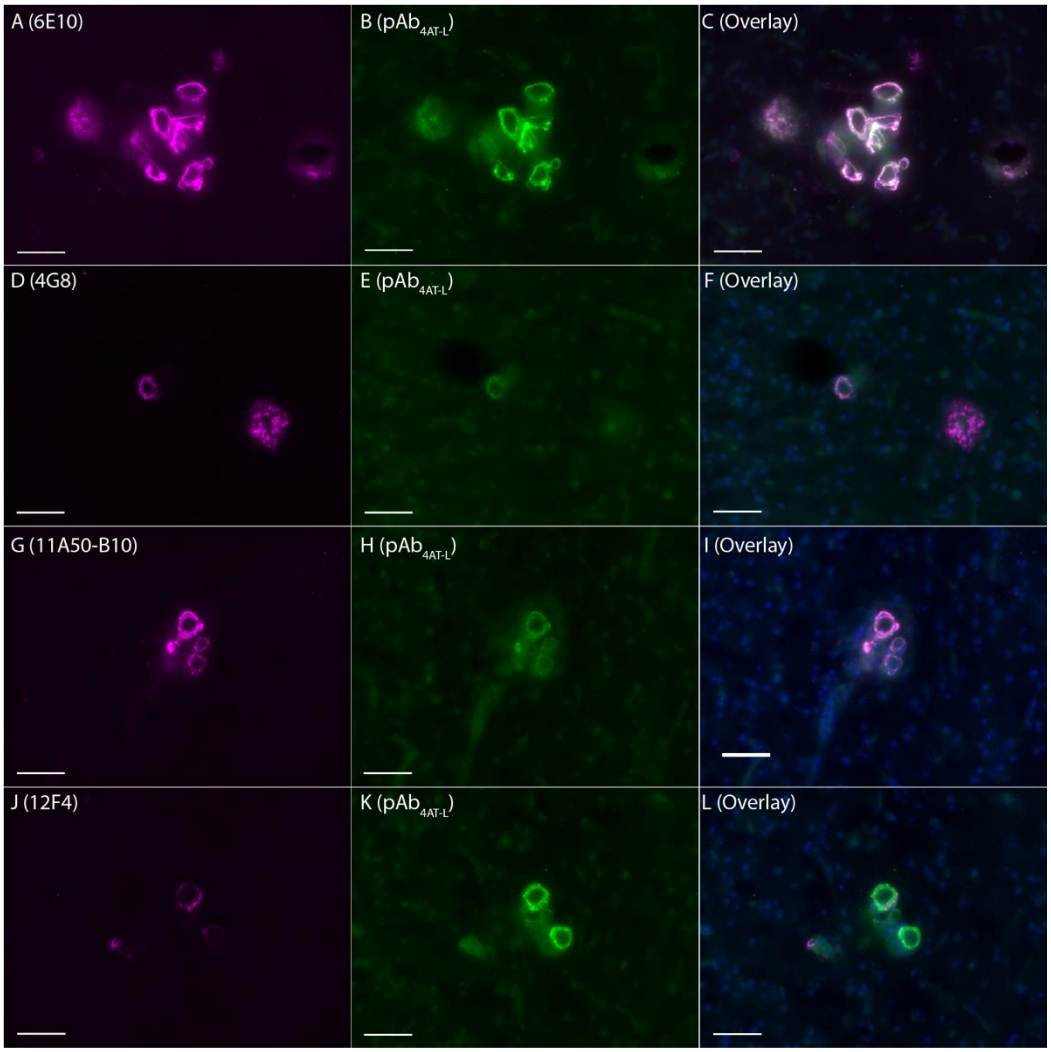

Figure 2.7 Immunofluorescence micrographs comparing the staining of cerebral amyloid angiopathy (CAA) by $pAb_{4AT\text{-}L}$ to four commercially available anti-Aβ antibodies in brain slices from a person who lived with LOAD. The left column shows the staining of each commercially

available antibody (magenta); the middle column shows the staining of $pAb_{4AT\text{-}L}$ (green); the right column shows the corresponding overlay, as well as the staining of cell nuclei by DAPI (blue). **A-C** are images from coincubation with 6E10 and $pAb_{4AT\text{-}L}$; **D-F** are images from coincubation with 4G8 and $pAb_{4AT\text{-}L}$; **G-I** are images from coincubation with 11A50-B10 and $pAb_{4AT\text{-}L}$; **J-L** are images from coincubation with 12F4 and $pAb_{4AT\text{-}L}$. Images were acquired at 40X; the scale bar is 50 μm.

Discussion

Antibodies against Aβ are critical tools in identifying amyloid-related pathological features in brain tissue. A unique feature of $pAb_{4AT\text{-}L}$ is that it was generated against a conformationally well-defined oligomer derived from Aβ, with a trimeric structure that is characterized at atomic resolution (PDB 7JXO). In contrast, other antibodies used to characterize Aβ (e.g., 6E10, 4G8, 11A50-B10, and 12F4) are generated against Aβ, fragments of Aβ, or in some cases, preparations of Aβ oligomers or fibrils for which the three-dimensional structures are not known. Some of the features recognized by $pAb_{4AT\text{-}L}$ may thus reflect structural and conformational similarities with the 4AT-L trimer used to generate $pAb_{4AT\text{-}L}$.

Although monoclonal antibodies, such as 6E10, 4G8, 11A50-B10, and 12F4, have the advantages of being homogenous and recognizing a single epitope, polyclonal antibodies have the potential to recognize multiple epitopes with similar features, such as conformation. The A11 polyclonal antibody has been used widely to recognize Aβ oligomers, but the Aβ antigen used to generate A11 is heterogenous and structurally less well-defined, and different commercial sources of A11 have provided variable results.[12,38] In contrast, the 4AT-L antigen used to generate $pAb_{4AT\text{-}L}$ is homogenous and structurally well-defined.

The recognition of the cores of cored plaques by $pAb_{4AT\text{-}L}$ may reflect that the cores present regions of $A\beta_{17\text{-}36}$ in an arrangement or conformation that resembles the 4AT-L trimer. Studies on the Aβ composition of plaques have sought to connect the relationship between Aβ oligomers and

plaques. Aβ antibodies that target a specific species of Aβ (Aβ conformation-specific antibodies) are used to elucidate different conformations of Aβ among plaque phenotypes and provide functional insight into the plaque morphology.[38–42] The A11 and OC polyclonal antibodies and the OC monoclonal antibodies are conformation-specific antibodies that recognize cored plaques.[38,39,41] Immunohistochemical studies in brain slices from a transgenic mouse model using the Aβ oligomer-specific antibody NAB61 demonstrate that Aβ oligomers in cored plaques results in synaptic loss and ultimately contribute to cognitive decline.[40] Immunofluorescent staining of AD mouse and human brain tissue with the OC pAb displayed Aβ oligomers in cored plaques associated with synaptic loss. Results from these studies support a model in which the cores of cored plaques are surrounded by Aβ oligomers which then spread to elicit their neurotoxic properties.

The cores of cored plaques may serve as a site on the plaque to collect Aβ oligomers. The cores and halos of plaques recognized by $pAb_{4AT\text{-}L}$ might thus be composed of oligomeric Aβ which may then recruit additional Aβ oligomers to elicit their neurotoxic effects leading to the progression of AD. The cores, for example, may be composed of Aβ oligomers similar in structure to 4AT-L, that then serve as sites for Aβ oligomers to induce dystrophic neurons and ultimately contribute to AD pathogenesis.

Although CAA is primarily composed of $Aβ_{40}$ and plaques primarily composed of Aβ42, previous studies report conformation-specific antibodies recognizing CAA. The OC polyclonal antibody and the OC monoclonal antibody mOC31, recognize vascular amyloid, suggesting that vascular amyloid is composed of distinct conformations.[11,12,39] The strong staining CAA suggests that the $pAb_{4AT\text{-}L}$ antibody may also recognize distinct conformations of Aβ, in a similar arrangement to the 4AT-L trimer.

Conclusion

The 4AT-L trimer is a conformationally defined Aβ-derived peptide consisting of three β-hairpins in a triangular arrangement that can be synthesized in milligram quantities. It can be used to generate the polyclonal antibody $pAb_{4AT\text{-}L}$, which can also be generated in milligram quantities. $pAb_{4AT\text{-}L}$ recognizes cored plaques in brain slices from 5xFAD mice in immunofluorescent staining experiments. Unlike the anti-Aβ monoclonal antibodies (6E10, 4G8, 11A50-B10, and 12F4), $pAb_{4AT\text{-}L}$ strongly recognizes the cores of cored plaques in LOAD. $pAb_{4AT\text{-}L}$ also recognizes neuritic plaques and CAA. The pathological features recognized by $pAb_{4AT\text{-}L}$ and unique conformationally defined antigen 4AT-L make $pAb_{4AT\text{-}L}$ a valuable tool for identifying Aβ plaque composition and providing functional insights into Aβ plaque morphology.

Materials and Methods

Synthesis of peptide monomer 4AT-L_{cc} and cross linked trimer 4AT-L

The chemicals and instruments required for peptide synthesis are similar to those used in our laboratory's previous publications.[15,17] Complete procedures are provided in the supplemental information.

Curation of 5xFAD mice and wild type littermates

All animal experiments were approved by the UC Irvine Institutional Animal Care and Use Committee (UCI IACUC). All animals were bred by the Transgenic Mouse Facility at UC Irvine. The process of breeding, genotyping, raising, and aging of 5xFAD hemizygous mice (B6.Cg Tg(APPSwFlLon,PSEN1*M146L*L286V)6799Vas/Mmjax, Stock number 34848-JAX, MMRRC) and wild type littermates for the purposes of tissue harvesting were followed as

described in Forner et al. 2021.[19] For more information about the curation and preparation of mouse brain tissue, refer to the supplemental information.

Tissue curation from ADRC

Human brain tissue samples were provided by the UC Irvine Alzheimer's Disease Research Center (UCI ADRC). The ADRC obtains, fixes, processes, and curates human brain tissue samples, and provides them in a de-identified format, thus rendering their application exempt from human subjects protocols. After the fixation process for at least two weeks in 4% paraformaldehyde, brains are submerged in 1 X phosphate-buffered saline (PBS) + 0.02% sodium azide, coronally sectioned, and sampled for diagnostic Formalin-Fixed Paraffin-Embedded (FFPE) tissue blocks. The coronal sections were then placed in individual heat-sealed bags filled with 1 X PBS + 0.02% sodium azide and stored at 4ºC for long-term storage for ongoing dissemination to investigators for their research studies.

Mouse and human tissue sectioning

Mouse brain tissue was sectioned using an HM 430 Sliding Microtome (Cat No. 22-050-855) with a sharp MX35 ultra microtome blade (REF 3053835). The stage was chilled with powdered dry ice. The brain tissue was submerged in powdered dried ice for 5 minutes and then mounted coronally with Tissue-Tek O.C.T. Compound (Sakura Finetek). After the mouse brain tissue was sectioned at 40 microns, and each slice was transferred with a paintbrush to a 48-well plate containing 1 X PBS + 0.02% sodium azide, the plate was then stored at 4 ºC for long-term storage (ThermoFisher, Cat. No. 3548).

Human occipital cortex was sectioned using a vibratome (Leica VT1000S) at 30 µm. Sequential tissue sections were then transferred to a 24-well plate containing 1 X PBS + 0.02% sodium azide and were stored at 4 ºC for long-term storage (ThermoFisher, Cat. No. 142485).

Generation of rabbit polyclonal antibodies

The conjugation chemistry and immunizations to generate $pAb_{4AT\text{-}L}$ were performed under contract with Pacific Immunology (Ramona, CA). The 4AT-L trimer was conjugated to the carrier protein keyhole limpet hemocyanin (KLH) using standard 1-ethyl-3-(3 dimethylaminopropyl) carbodiimide (EDC) coupling chemistry following vendor protocols (Thermo Scientific, MAN0017125 Rev. A.0 Pub. Part No. 2160475.7). Two New Zealand white rabbits, 9-10 weeks of age, were used to generate rabbit polyclonal antibodies. Rabbits were primed with 200 µg of the 4AT-L trimer in AdjuLite Complete Freund's Adjuvant (CFA) (Cat. #A5001), by subcutaneous injection using a 19-gauge needle in the neck/shoulder region. Pacific Immunology uses a highly purified mineral oil base Freund's Adjuvant that allows antigen presentation and elimination of injection site abscesses and granulomas. On days 21, 42, and 70 the rabbits received booster injections of 100 µg of the 4AT-L timer in AdjuLite Incomplete Freund's Adjuvant (IFA) (Cat. #A5002). Blood samples for testing were drawn from the central ear artery using a 19-gauge needle on Days 0 (10 mL), 49 (45-50 mL), 63, (45-50 mL) 77 (45-50 mL), and Day 91 (45-50 mL).

As whole blood was collected, it was diluted in Anticoagulant Citrate Dextrose Solution USP (ACD) Solution A (0.80 g citric acid monohydrate, 2.45 g dextrose monohydrate, and 2.20 g of sodium citrate dihydrate in 100 mL) in a 1:10 ratio. The blood and ACD solution was diluted 1:1 with sterile 1 X PBS containing 2.5 mM EDTA and 0.5% BSA. 20 mL of StemCell Lymphoprep was added to a 50-mL StemCell SepMate-50 separation tube, then 30 mL of the

blood and ACD solution was added over the Lymphoprep, then centrifuged for 30 minutes at 3,000 RPM. The supernatant (plasma) was retrieved and decanted once the PBMCs have been spun down to form a pellet. Plasma was then shipped for affinity purification and ELISA followed by experiments and antibody characterization. PBMCs were also isolated for the future generation of monoclonal antibodies. For information about affinity purification and ELISA, refer to the supplemental information.

Immunofluorescent staining on 5xFAD mice brain slices

All steps were performed on a plate shaker at 90 rpm and ambient temperature (ca. 25 ºC) unless otherwise noted. Free-floating tissue was transferred to a 24-well plate (Cell Treat Scientific Products Polystyrene 24-well Non-treated Plate, Sterile, Part Number: 229524) with 10 X Tris Buffered Saline (500 mM Tris, 1 M NaCl) that was diluted to 1 X TBS with Milli-Q® water. The tissue was washed with 1 X TBS for 5 minutes and pretreated with 88% formic acid (Certified ACS, Fisher Chemical, Cat. No. A118P-100) for 5 minutes in the fume hood to enhance detection. After incubation, the antigen retrieval solution was aspirated by a pipette, and then the tissue was washed with 1 X TBS three times for 5 minutes each. Tissues were then treated with 3% H_2O_2 (Hydrogen Peroxide, 30% (Stabilized with Sodium Stannate/Certified), Fisher Chemical, Cat. No. H323-500) with 10% methanol (Methanol (Certified ACS), Fisher Chemical, Cat. No. A412-4) for 30 minutes in the fume hood. The tissue was then washed with 1 X TBS for 5 minutes, permeabilized with 500 µL 1 X TBS-A (0.1% Triton-X) for 15 minutes, and incubated in blocking solution (1 X TBS-B, 0.1% Triton, and 3% BSA (Bovine Serum Albumin, Fraction V, Heat Shock Treated, Fisher BioReagents, Cat. No. BP1600-100) for 30 minutes. After the previous blocking reagent was aspirated from the well, the tissue was incubated in supplemented blocking solution (which includes 5% normal horse serum (Vector Laboratories, REF S-2000)) for 30 minutes. After

aspirating the supplemented blocking solution from the wells, primary antibody (1:5000 diluted $pAb_{4AT\text{-}L}$ in blocking buffer) was added to the wells of a new 24-well plate. The tissue was then transferred to the 24-well plate, sealed with Parafilm, and placed on an orbit shaker at room temperature overnight (16 hours).

The next day, tissues were washed twice with 1 X TBS-A for 5 minutes. After the last wash was aspirated, the tissue was incubated in blocking solution for 15 minutes. After aspirating the blocking solution from the wells, 500 µL of diluted horse anti-rabbit biotinylated secondary antibody (1:1000) (Vector Laboratories, BA-1100-1.5) in blocking solution was added to the wells and the tissue incubated for 1 hour at room temperature. After a 1-hour incubation, the tissues were washed in 1 X TBS-A twice for 5 minutes each then placed in ABC solution (Vectastain Elite ABC-HRP Kit, Peroxidase, Cat. No. PK-6100) for 1 hour. The tissue was washed with 1 X TBS three times, for 5 minutes each. During the last of the three washes in 1 X TBS, the DAB (3, 3 - diaminobenzidine) reagent was prepared in the fume hood and according to manufacturer's instructions (DAB Substrate Kit, Peroxidase (HRP), with Nickel, Cat. No. SK-4100). Tissue was incubated in DAB for 5 minutes. The tissue was washed with 1 X TBS three times, 5 minutes each. Tissues were mounted on slides (Fisherbrand Superfrost Plus Microscope Slides, 25mm x 75mm x 1.0mm, Glass, Regular Corner, 3/4" SuperFrost Tab, Part Num. 22-037-246) until dry in the fume hood.

DAB staining

All steps were performed on a plate shaker at 90 rpm and ambient temperature (ca. 25 ºC) unless otherwise noted. Free-floating tissue was transferred to a 24-well plate (Cell Treat Scientific Products Polystyrene 24-well Non-treated Plate, Sterile, Part Number: 229524) with 10 X Tris Buffered Saline (500 mM Tris, 1 M NaCl) that was diluted to 1 X TBS with Milli-Q® water. The

tissue was washed with 500 µL of 1 X TBS for 5 minutes. After removing the wash, the tissue was subjected to 300 µL 88% formic acid (Certified ACS, Fisher Chemical, Cat. No. A118P-100) antigen retrieval for 5 minutes in the fume hood. After incubation, the antigen retrieval solution was aspirated by a pipette, and then the tissue was washed with 500 µL of 1 X TBS three times for 5 minutes each. Tissues were then treated with 3% H_2O_2 (Hydrogen Peroxide, 30% (Stabilized with Sodium Stannate/Certified), Fisher Chemical, Cat. No. H323-500) with 10% methanol (Methanol (Certified ACS), Fisher Chemical, Cat. No. A412-4) for 30 minutes in the fume hood. After transferring the tissue with a paintbrush to a new 24-well plate, the tissue was then washed with 500 µL of 1 X TBS for 5 minutes. After the last wash was aspirated, the tissue membrane was then permeabilized in 500 µL 1 X TBS-A (0.1% Triton-X) for 15 minutes. After the last wash was aspirated, 475 µL of blocking solution, (1 X TBS-B, 0.1% Triton, and 3% BSA (Bovine Serum Albumin, Fraction V, Heat Shock Treated, Fisher BioReagents, Cat. No. BP1600-100) were added to each tissue and incubated for 30 minutes. After the previous blocking reagent was aspirated from the well, the tissue was incubated in 475 µL of supplemented blocking solution (which includes 5% normal horse serum (Vector Laboratories, REF S-2000)) for 30 minutes. After aspirating the supplemented blocking solution from the wells, 500 µL of primary antibody (1:5000 diluted $pAb_{4AT\text{-}L}$ in blocking buffer) was added to the wells of a new 24-well plate. The tissue was then transferred to the 24-well plate, sealed with Parafilm, and placed on an orbit shaker at room temperature overnight (16 hours).

The next day, tissues were washed twice with 500 µL of 1 X TBS-A for 5 minutes. After the last wash was aspirated, the tissue was incubated in 500 µL of blocking solution for 15 minutes. After aspirating the blocking solution from the wells, 500 µL of diluted horse anti-rabbit biotinylated secondary antibody (1:1000) (Vector Laboratories, BA-1100-1.5) in blocking solution

was added to the wells and the tissue incubated on tissue for 1 hour at room temperature. After a 1-hour incubation, the tissues were washed in 500 µL of 1 X TBS-A twice for 5 minutes each then placed in ABC solution (Vectastain Elite ABC-HRP Kit, Peroxidase, Cat. No. PK-6100) for 1 hour. The tissue was washed with 500 µL of 1 X TBS three times, for 5 minutes each. During the last of the three washes in 1 X TBS, the DAB (3, 3 -diaminobenzidine) reagent was prepared in the fume hood and according to manufacturer's instructions (DAB Substrate Kit, Peroxidase (HRP), with Nickel, Cat. No. SK-4100). The tissue was incubated in DAB for 5 minutes. The tissue was washed with 500 µL of 1 X TBS three times, 5 minutes each. Tissues were mounted on slides (Fisherbrand Superfrost Plus Microscope Slides, 25mm x 75mm x 1.0mm, Glass, Regular Corner, 3/4" SuperFrost Tab, Part Num. 22-037-246) until dry in the fume hood.

The slides were counterstained in 0.1% Cresyl Violet (ab246817, abcam) in Milli-Q® water for 3 minutes followed by Milli-Q® water for 1 minute. Slides were dehydrated through progressively increasing ethanol solutions and then transferred to xylene and were cover slipped (Globe Scientific 1419-10 Cover Glass, 24 x 60mm, No. 1 Thickness) with DPX mounting media (Sigma-Aldrich, SKU 06522). Slides were left to harden for 3 days before undergoing imaging analysis.

Preabsorption of 4AT-L trimer with $pAb_{4AT\text{-}L}$. To confirm antibody specificity, tissue was incubated in a solution of $pAb_{4AT\text{-}L}$ (1:1000) in blocking buffer with 1:100 of 4AT-L trimer for 30 minutes before being added to the tissue during the primary antibody step. The rest of the experiment was performed as previously described

Immunofluorescent staining on brain slices from LOAD

Double-label immunofluorescence with amyloid antibodies. All steps were performed on a plate shaker at 90 rpm and ambient temperature (ca. 25 ºC) unless otherwise noted. All wells were filled with 500 µL of buffer unless otherwise noted. Free-floating tissue was transferred to a well of a 24-well plate (Cell Treat Scientific Products Polystyrene 24 Well Non-treated Plate, Sterile, Part Number: 229524) filled with 10 X Tris Buffered Saline (500 mM Tris, 1 M NaCl) that was diluted to 1 X TBS with Milli-Q® water. This tissue was washed in 1 X TBS for 5 minutes. After removing the wash, the tissue was subjected to 300 µL 88% formic acid (Certified ACS, Fisher Chemical, Cat. No. A118P-100) antigen retrieval for 5 minutes in the fume hood. After incubation, the antigen retrieval solution was aspirated by a pipette, and then the tissue was washed with 1 X TBS twice for 5 minutes each and then 1 X TBS -A (1 X TBS, 0.1% Triton-X) for 15 minutes. After the last wash, 475 µL of blocking solution, (1 X TBS-B, 0.1% Triton and 3% BSA (Bovine Serum Albumin, Fraction V, Heat Shock Treated, Fisher BioReagents, Cat. No. BP1600-100) was added for 30 minutes. The primary antibodies, a monoclonal anti-amyloid beta antibody (Anti-β-Amyloid, 1-16 [6E10], BioLegend, Cat. No. 803015; Anti-β-Amyloid, 17-24 [4G8, BioLegend, Cat. No. 800708; β-Amyloid 1-40 [11A50-B10], BioLegend, Cat. No. 805404; Purified anti-β-Amyloid, 1-42 Antibody [12F4], BioLegend, Cat. No. 805509) was diluted blocking buffer and added to the wells (1:1000). The plate was then placed on an orbit shaker at 4° C for overnight incubation (16 hours).

The next day, the primary antibody solution was aspirated from the well and the tissue was washed in 1 X TBS-A twice for 5 minutes and then in blocking buffer for 15 minutes. Next, tissue was incubated in blocking buffer supplemented with 5% normal goat serum (Vector laboratories, REF S-1000) and diluted secondary antibody (1:1000) for 1 hour (Goat anti-Mouse IgG (H+L)

Cross-Adsorbed Secondary Antibody Alexa Fluor 647, Invitrogen, Cat. No. A-21235). Subsequently the tissue was washed in 1 X TBS-A twice for 5 minutes and then blocking buffer for 15 minutes. At this time, the second primary antibody ($pAb_{4AT\text{-}L}$),diluted in blocking buffer (1:1000) was added and tissue incubated on an orbit shaker 4°C overnight (16 hours).

The tissue was washed in 1 X TBS-A twice for 5 minutes each and then in blocking buffer for 15 minutes. Next, tissue was placed in blocking buffer supplemented with 5% normal goat serum and diluted secondary antibody for 1 hour (1:1000, Goat anti-Rabbit IgG (H+L) Cross-Adsorbed Secondary Antibody, Alexa Fluor 488, Invitrogen, Cat. No. A-11008). The tissue was washed in 1 X TBS-A twice for 5 minutes each and then in 1 X TBS for an additional three times for 5 minutes each. To quench lipofuscin the tissue was then incubated in True black (Gold Biotechnology) in 70% EtOH (as prepared by manufacturer's instructions) with for 5 mins. The tissue was washed in 1 X TBS six times for 5 minutes each and mounted on slides (Fisherbrand Superfrost Plus Microscope Slides, 25mm x 75mm x 1.0mm, Glass, Regular Corner, 3/4" SuperFrost Tab, Part Num. 22-037-246), coated in mounting media (VECTASHIELD Vibrance® Antifade Mounting Medium with DAPI, H-1800), then coverslipped (Globe Scientific 1419-10 Cover Glass, 24 x 60mm, No. 1 Thickness). The slides were then placed in a dark location until dry. For more information about staining with IBA-1, GFAP, and AT8 refer to the supplemental information.

Bright-field and fluorescence image acquisition

All images were acquired on the Keyence BZ-X800 fluorescent microscope. Objective lenses plan apochromat 40 X (Model BZ-PA40, NA 0.95, WD 0.17 to 0.25 mm, slide thickness 0.11 to 0.23, depth of field approx.0.6 µm, field of view, 362×273 µm) and plan apochromat 20 X (Model BZ-PA20, NA 0.75, WD 0.6 mm, slide thickness 0.17, depth of field approx.1.0 µm, field

of view 725×546 µm) were used for image acquisition. For immunofluorescent staining experiments, Keyence filter cubes were used to excite fluorophores while brightfield was used to image immunohistochemistry staining. The filter cubes are notated as set name model, excitation wavelength, emission wavelength, dichroic mirror wavelength. The following filter cubes were used in this manuscript: BZ-X filter DAPI OP-87762 360/40 460/50 400, BZ-X filter GFP OP-87763 470/40 525/50 495, BZ-X filter TRITC OP-87764 545/25 605/70 56, and BZ-X filter Cy5 OP-87766 620/60 700/75 660. For specific acquisition parameters used for every microscopy image, see Supplemental Tables 3-4 and 6-7. All images of plaques were obtained with a z-stack taking 25 images with a pitch of 0.3 microns unless otherwise noted. All images of cerebral amyloid angiopathy were obtained with a z-stack taking 12-25 images depending on the size of the blood vessel with a pitch of 0.6 microns.

The Keyence analyzing software (BZ-X800E Analyzer, Osaka, Japan) was used to process images. Acquired z-stack images were loaded in the analyzing software and complied by full focus to sectioned images. Original full-focus sectioned images were saved. All images were additionally processed by adjusting the shadow on the look-up table without removing signal. Supplemental Table 5 and 8 lists the processing parameters of each image.

Quantitative digital neuropathology and statistics

The Aperio Versa 200 slide scanner (Leica) was used to obtain whole slide images (WSI) of human tissue stained with $pAb_{4AT\text{-}L}$ using 20X brightfield imaging. Images of these slides were then uploaded to Aperio eSlideManager (eSM) (Leica) and were annotated using Aperio ImageScope (v12.4.6.5003). In ImageScope, both white matter and grey matter were analyzed by placing 5 boxes (600 *h* x 600 *w* x 600 *l*) in a systematic manner on the tissue. The first box was placed in an area of white matter with the least amount of pathology that contained enough space

to ultimately align all 5 boxes. The next box was placed one box length over to the left of the first box, then up. The following box was placed in a similar manner until all 5 boxes are placed. Boxes that contained areas with uneven sectioning, holes, tissue tears, foreign particles, and tissue overlap, were moved one box length to the right. The same process was repeated with gray matter. After the tissue was annotated, the "Positive Pixel Count V9" algorithm was used to quantify plaques with the only setting in the input setting of Intensity Threshold (Lower Limit) of WEAK positive pixels (Iwp (Low) = Ip (High)) changed to 175. The algorithm was then processed on the Aperio eSM. After the data was exported, the percent load for each annotation was calculated with *Np* (Number Positive), *Nsp* (Number Strong Positive), *Nwp* (Number Weak Positive) using the following equation:

$$\frac{Nwp+Np+Nsp}{Total\ Area}$$

Statistical analysis was performed on Microsoft Excel (version 16.70) and GraphPad Prism (version 9.0).

Acknowledgments

We thank the National Institutes of Health (NIH) National Institute on Aging (NIA) for funding (AG062296) for funding support. We acknowledge the support of the Chao Family Comprehensive Cancer Center Transgenic Mouse Facility Shared Resource, supported by the National Cancer Institute of the National Institutes of Health under award number P30CA062203. Tissue from cases with LOAD and nondemented controls were from the UCI Alzheimer disease research center (NIH/NIA P30AG066519). The content is solely the responsibility of the authors and does not necessarily represent the official views of the National Institutes of Health. Thank you to Ryan Sargent and the team at Pacific Immunology for

immunizing rabbits for the generation of $pAb_{4AT\text{-}L}$. Thank you to Dr. Shimako Kawauchi and UCI Transgenic Mouse Facility for providing mice for these studies. Thank you Sierra Wright and Briana Gawronski at the UCI ADRC for providing human tissue samples and relevant information essential for these experiments. Figures were created with Biorender.com.

References

(1) Yakupova, E. I.; Bobyleva, L. G.; Vikhlyantsev, I. M.; Bobylev, A. G. Congo Red and Amyloids: History and Relationship. *Biosci Rep* **2019**, *39* (1), BSR20181415. https://doi.org/10.1042/BSR20181415.

(2) Masters, C. L.; Bateman, R.; Blennow, K.; Rowe, C. C.; Sperling, R. A.; Cummings, J. L. Alzheimer's Disease. *Nat Rev Dis Primers* **2015**, *1* (1), 1–18. https://doi.org/10.1038/nrdp.2015.56.

(3) Goldman, R. D. Antibodies: Indispensable Tools for Biomedical Research. *Trends in Biochemical Sciences* **2000**, *25* (12), 593–595. https://doi.org/10.1016/S0968-0004(00)01725-4.

(4) Salloway, S.; Chalkias, S.; Barkhof, F.; Burkett, P.; Barakos, J.; Purcell, D.; Suhy, J.; Forrestal, F.; Tian, Y.; Umans, K.; Wang, G.; Singhal, P.; Budd Haeberlein, S.; Smirnakis, K. Amyloid-Related Imaging Abnormalities in 2 Phase 3 Studies Evaluating Aducanumab in Patients With Early Alzheimer Disease. *JAMA Neurol* **2022**, *79* (1), 13–21. https://doi.org/10.1001/jamaneurol.2021.4161.

(5) Yang, T.; O'Malley, T. T.; Kanmert, D.; Jerecic, J.; Zieske, L. R.; Zetterberg, H.; Hyman, B. T.; Walsh, D. M.; Selkoe, D. J. A Highly Sensitive Novel Immunoassay Specifically Detects Low Levels of Soluble Aβ Oligomers in Human Cerebrospinal Fluid. *Alzheimer's Research & Therapy* **2015**, *7* (1), 14. https://doi.org/10.1186/s13195-015-0100-y.

(6) Aprile, F. A.; Sormanni, P.; Perni, M.; Arosio, P.; Linse, S.; Knowles, T. P. J.; Dobson, C. M.; Vendruscolo, M. Selective Targeting of Primary and Secondary Nucleation Pathways in Aβ42 Aggregation Using a Rational Antibody Scanning Method. *Science Advances* **2017**, *3* (6), e1700488. https://doi.org/10.1126/sciadv.1700488.

(7) Aprile, F. A.; Sormanni, P.; Podpolny, M.; Chhangur, S.; Needham, L.-M.; Ruggeri, F. S.; Perni, M.; Limbocker, R.; Heller, G. T.; Sneideris, T.; Scheidt, T.; Mannini, B.; Habchi, J.; Lee, S. F.; Salinas, P. C.; Knowles, T. P. J.; Dobson, C. M.; Vendruscolo, M. Rational Design of a Conformation-Specific Antibody for the Quantification of Aβ Oligomers. *Proceedings of the National Academy of Sciences* **2020**, *117* (24), 13509–13518. https://doi.org/10.1073/pnas.1919464117.

(8) Broersen, K.; Jonckheere, W.; Rozenski, J.; Vandersteen, A.; Pauwels, K.; Pastore, A.; Rousseau, F.; Schymkowitz, J. A Standardized and Biocompatible Preparation of Aggregate-Free Amyloid Beta Peptide for Biophysical and Biological Studies of Alzheimer's Disease. *Protein Engineering, Design and Selection* **2011**, *24* (9), 743–750. https://doi.org/10.1093/protein/gzr020.

(9) Baghallab, I.; Reyes-Ruiz, J. M.; Abulnaja, K.; Huwait, E.; Glabe, C. Epitomic Characterization of the Specificity of the Anti-Amyloid Aβ Monoclonal Antibodies 6E10 and 4G8. *J Alzheimers Dis 66* (3), 1235–1244. https://doi.org/10.3233/JAD-180582.

(10) Glabe, C. G. Structural Classification of Toxic Amyloid Oligomers *. *Journal of Biological Chemistry* **2008**, *283* (44), 29639–29643. https://doi.org/10.1074/jbc.R800016200.

(11) Hatami, A.; Albay, R.; Monjazeb, S.; Milton, S.; Glabe, C. Monoclonal Antibodies against Aβ42 Fibrils Distinguish Multiple Aggregation State Polymorphisms in Vitro and in Alzheimer Disease Brain *. *Journal of Biological Chemistry* **2014**, *289* (46), 32131–32143. https://doi.org/10.1074/jbc.M114.594846.

(12) Kayed, R.; Canto, I.; Breydo, L.; Rasool, S.; Lukacsovich, T.; Wu, J.; Albay, R.; Pensalfini, A.; Yeung, S.; Head, E.; Marsh, J. L.; Glabe, C. Conformation Dependent Monoclonal

Antibodies Distinguish Different Replicating Strains or Conformers of Prefibrillar Aβ Oligomers. *Mol Neurodegener* **2010**, *5*, 57. https://doi.org/10.1186/1750-1326-5-57.

(13) Stine, W. B.; Jungbauer, L.; Yu, C.; LaDu, M. J. Preparing Synthetic Aβ in Different Aggregation States. *Methods Mol Biol* **2011**, *670*, 13–32. https://doi.org/10.1007/978-1-60761-744-0_2.

(14) Kreutzer, A. G.; Parrocha, C. M. T.; Haerianardakani, S.; Guaglianone, G.; Nguyen, J. T.; Diab, M. N.; Yong, W.; Perez-Rosendahl, M.; Head, E.; Nowick, J. S. Antibodies Raised Against an Aβ Oligomer Mimic Recognize Pathological Features in Alzheimer's Disease and Associated Amyloid-Disease Brain Tissue. bioRxiv May 12, 2023, p 2023.05.11.540404. https://doi.org/10.1101/2023.05.11.540404.

(15) Haerianardakani, S.; Kreutzer, A. G.; Salveson, P. J.; Samdin, T. D.; Guaglianone, G. E.; Nowick, J. S. Phenylalanine Mutation to Cyclohexylalanine Facilitates Triangular Trimer Formation by β-Hairpins Derived from Aβ. *J. Am. Chem. Soc.* **2020**, *142* (49), 20708–20716. https://doi.org/10.1021/jacs.0c09281.

(16) Samdin, T. D.; Kreutzer, A. G.; Nowick, J. S. Exploring Amyloid Oligomers with Peptide Model Systems. *Current Opinion in Chemical Biology* **2021**, *64*, 106–115. https://doi.org/10.1016/j.cbpa.2021.05.004.

(17) Kreutzer, A. G.; Yoo, S.; Spencer, R. K.; Nowick, J. S. Stabilization, Assembly, and Toxicity of Trimers Derived from Aβ. *J. Am. Chem. Soc.* **2017**, *139* (2), 966–975. https://doi.org/10.1021/jacs.6b11748.

(18) Oakley, H.; Cole, S. L.; Logan, S.; Maus, E.; Shao, P.; Craft, J.; Guillozet-Bongaarts, A.; Ohno, M.; Disterhoft, J.; Eldik, L. V.; Berry, R.; Vassar, R. Intraneuronal β-Amyloid Aggregates, Neurodegeneration, and Neuron Loss in Transgenic Mice with Five Familial

Alzheimer's Disease Mutations: Potential Factors in Amyloid Plaque Formation. *J. Neurosci.* **2006**, *26* (40), 10129–10140. https://doi.org/10.1523/JNEUROSCI.1202-06.2006.

(19) Forner, S.; Kawauchi, S.; Balderrama-Gutierrez, G.; Kramár, E. A.; Matheos, D. P.; Phan, J.; Javonillo, D. I.; Tran, K. M.; Hingco, E.; da Cunha, C.; Rezaie, N.; Alcantara, J. A.; Baglietto-Vargas, D.; Jansen, C.; Neumann, J.; Wood, M. A.; MacGregor, G. R.; Mortazavi, A.; Tenner, A. J.; LaFerla, F. M.; Green, K. N. Systematic Phenotyping and Characterization of the 5xFAD Mouse Model of Alzheimer's Disease. *Sci Data* **2021**, *8* (1), 270. https://doi.org/10.1038/s41597-021-01054-y.

(20) Boon, B. D. C.; Bulk, M.; Jonker, A. J.; Morrema, T. H. J.; van den Berg, E.; Popovic, M.; Walter, J.; Kumar, S.; van der Lee, S. J.; Holstege, H.; Zhu, X.; Van Nostrand, W. E.; Natté, R.; van der Weerd, L.; Bouwman, F. H.; van de Berg, W. D. J.; Rozemuller, A. J. M.; Hoozemans, J. J. M. The Coarse-Grained Plaque: A Divergent Aβ Plaque-Type in Early-Onset Alzheimer's Disease. *Acta Neuropathol* **2020**, *140* (6), 811–830. https://doi.org/10.1007/s00401-020-02198-8.

(21) Duyckaerts, C.; Delatour, B.; Potier, M.-C. Classification and Basic Pathology of Alzheimer Disease. *Acta Neuropathol* **2009**, *118* (1), 5–36. https://doi.org/10.1007/s00401-009-0532-1.

(22) Sanchez-Varo, R.; Mejias-Ortega, M.; Fernandez-Valenzuela, J. J.; Nuñez-Diaz, C.; Caceres-Palomo, L.; Vegas-Gomez, L.; Sanchez-Mejias, E.; Trujillo-Estrada, L.; Garcia-Leon, J. A.; Moreno-Gonzalez, I.; Vizuete, M.; Vitorica, J.; Baglietto-Vargas, D.; Gutierrez, A. Transgenic Mouse Models of Alzheimer's Disease: An Integrative Analysis.

International Journal of Molecular Sciences **2022**, *23* (10), 5404. https://doi.org/10.3390/ijms23105404.

(23) Serrano-Pozo, A.; Frosch, M. P.; Masliah, E.; Hyman, B. T. Neuropathological Alterations in Alzheimer Disease. *Cold Spring Harb Perspect Med* **2011**, *1* (1), a006189. https://doi.org/10.1101/cshperspect.a006189.

(24) Rahman, M. M.; Lendel, C. Extracellular Protein Components of Amyloid Plaques and Their Roles in Alzheimer's Disease Pathology. *Molecular Neurodegeneration* **2021**, *16* (1), 59. https://doi.org/10.1186/s13024-021-00465-0.

(25) Hampel, H.; Hardy, J.; Blennow, K.; Chen, C.; Perry, G.; Kim, S. H.; Villemagne, V. L.; Aisen, P.; Vendruscolo, M.; Iwatsubo, T.; Masters, C. L.; Cho, M.; Lannfelt, L.; Cummings, J. L.; Vergallo, A. The Amyloid-β Pathway in Alzheimer's Disease. *Mol Psychiatry* **2021**, *26* (10), 5481–5503. https://doi.org/10.1038/s41380-021-01249-0.

(26) Lloyd, G. M.; Trejo-Lopez, J. A.; Xia, Y.; McFarland, K. N.; Lincoln, S. J.; Ertekin-Taner, N.; Giasson, B. I.; Yachnis, A. T.; Prokop, S. Prominent Amyloid Plaque Pathology and Cerebral Amyloid Angiopathy in APP V717I (London) Carrier – Phenotypic Variability in Autosomal Dominant Alzheimer's Disease. *Acta Neuropathologica Communications* **2020**, *8* (1), 31. https://doi.org/10.1186/s40478-020-0891-3.

(27) Ramakrishnan, M.; Kandimalla, K. K.; Wengenack, T. M.; Howell, K. G.; Poduslo, J. F. Surface Plasmon Resonance Binding Kinetics of Alzheimer's Disease Amyloid β Peptide Capturing- and Plaque Binding- Monoclonal Antibodies. *Biochemistry* **2009**, *48* (43), 10405–10415. https://doi.org/10.1021/bi900523q.

(28) Findeis, M. A. The Role of Amyloid β Peptide 42 in Alzheimer's Disease. *Pharmacology & Therapeutics* **2007**, *116* (2), 266–286. https://doi.org/10.1016/j.pharmthera.2007.06.006.

(29) Haass, C. Initiation and Propagation of Neurodegeneration. *Nat Med* **2010**, *16* (11), 1201–1204. https://doi.org/10.1038/nm.2223.

(30) González-Reyes, R. E.; Nava-Mesa, M. O.; Vargas-Sánchez, K.; Ariza-Salamanca, D.; Mora-Muñoz, L. Involvement of Astrocytes in Alzheimer's Disease from a Neuroinflammatory and Oxidative Stress Perspective. *Frontiers in Molecular Neuroscience* **2017**, *10*.

(31) Pan, X.; Zhu, Y.; Lin, N.; Zhang, J.; Ye, Q.; Huang, H.; Chen, X. Microglial Phagocytosis Induced by Fibrillar β-Amyloid Is Attenuated by Oligomeric β-Amyloid: Implications for Alzheimer's Disease. *Molecular Neurodegeneration* **2011**, *6* (1), 45. https://doi.org/10.1186/1750-1326-6-45.

(32) Bouvier, D. S.; Jones, E. V.; Quesseveur, G.; Davoli, M. A.; A. Ferreira, T.; Quirion, R.; Mechawar, N.; Murai, K. K. High Resolution Dissection of Reactive Glial Nets in Alzheimer's Disease. *Sci Rep* **2016**, *6*, 24544. https://doi.org/10.1038/srep24544.

(33) Serrano-Pozo, A.; Muzikansky, A.; Gómez-Isla, T.; Growdon, J. H.; Betensky, R. A.; Frosch, M. P.; Hyman, B. T. Differential Relationships of Reactive Astrocytes and Microglia to Fibrillar Amyloid Deposits in Alzheimer Disease. *J Neuropathol Exp Neurol* **2013**, *72* (6), 462–471. https://doi.org/10.1097/NEN.0b013e3182933788.

(34) Sudol, K. L.; Mastrangelo, M. A.; Narrow, W. C.; Frazer, M. E.; Levites, Y. R.; Golde, T. E.; Federoff, H. J.; Bowers, W. J. Generating Differentially Targeted Amyloid-β Specific Intrabodies as a Passive Vaccination Strategy for Alzheimer's Disease. *Mol Ther* **2009**, *17* (12), 2031–2040. https://doi.org/10.1038/mt.2009.174.

(35) Jellinger, K. A. Understanding Conflicting Neuropathological Findings. *JAMA Neurology* **2016**, *73* (4), 479–480. https://doi.org/10.1001/jamaneurol.2015.4879.

(36) Walker, L. C. Aβ Plaques. *Free Neuropathol* **2020**, *1*, 31. https://doi.org/10.17879/freeneuropathology-2020-3025.

(37) Greenberg, S. M.; Bacskai, B. J.; Hernandez-Guillamon, M.; Pruzin, J.; Sperling, R.; van Veluw, S. J. Cerebral Amyloid Angiopathy and Alzheimer Disease — One Peptide, Two Pathways. *Nat Rev Neurol* **2020**, *16* (1), 30–42. https://doi.org/10.1038/s41582-019-0281-2.

(38) Kayed, R.; Head, E.; Thompson, J. L.; McIntire, T. M.; Milton, S. C.; Cotman, C. W.; Glabe, C. G. Common Structure of Soluble Amyloid Oligomers Implies Common Mechanism of Pathogenesis. *Science* **2003**, *300* (5618), 486–489. https://doi.org/10.1126/science.1079469.

(39) Kayed, R.; Head, E.; Sarsoza, F.; Saing, T.; Cotman, C. W.; Necula, M.; Margol, L.; Wu, J.; Breydo, L.; Thompson, J. L.; Rasool, S.; Gurlo, T.; Butler, P.; Glabe, C. G. Fibril Specific, Conformation Dependent Antibodies Recognize a Generic Epitope Common to Amyloid Fibrils and Fibrillar Oligomers That Is Absent in Prefibrillar Oligomers. *Mol Neurodegener* **2007**, *2*, 18. https://doi.org/10.1186/1750-1326-2-18.

(40) Koffie, R. M.; Meyer-Luehmann, M.; Hashimoto, T.; Adams, K. W.; Mielke, M. L.; Garcia-Alloza, M.; Micheva, K. D.; Smith, S. J.; Kim, M. L.; Lee, V. M.; Hyman, B. T.; Spires-Jones, T. L. Oligomeric Amyloid β Associates with Postsynaptic Densities and Correlates with Excitatory Synapse Loss near Senile Plaques. *Proceedings of the National Academy of Sciences* **2009**, *106* (10), 4012–4017. https://doi.org/10.1073/pnas.0811698106.

(41) Reyes-Ruiz, J. M.; Nakajima, R.; Baghallab, I.; Goldschmidt, L.; Sosna, J.; Mai Ho, P. N.; Kumosani, T.; Felgner, P. L.; Glabe, C. An "Epitomic" Analysis of the Specificity of Conformation-Dependent, Anti-Aß Amyloid Monoclonal Antibodies. *Journal of Biological Chemistry* **2021**, *296*, 100168. https://doi.org/10.1074/jbc.RA120.015501.

(42) Sanchez-Varo, R.; Sanchez-Mejias, E.; Fernandez-Valenzuela, J. J.; De Castro, V.; Mejias-Ortega, M.; Gomez-Arboledas, A.; Jimenez, S.; Sanchez-Mico, M. V.; Trujillo-Estrada, L.; Moreno-Gonzalez, I.; Baglietto-Vargas, D.; Vizuete, M.; Davila, J. C.; Vitorica, J.; Gutierrez, A. Plaque-Associated Oligomeric Amyloid-Beta Drives Early Synaptotoxicity in APP/PS1 Mice Hippocampus: Ultrastructural Pathology Analysis. *Front Neurosci* **2021**, *15*, 752594. https://doi.org/10.3389/fnins.2021.752594.

Supporting Information for

Antibodies generated from a triangular trimer from Aβ recognize cored and neuritic plaques in brain sections of people who lived with late-onset Alzheimer's disease

Synthesis of peptide monomer 4AT-L_{cc} and cross-linked trimer 4AT-L

The chemicals and instruments required for peptide synthesis are similar to those used in our laboratory's previous publications,[15, 17]. Information for the synthesis of peptide monomer 4AT-L_{cc} and cross-linked trimer 4AT-L was adapted or taken verbatim from Haerianardakani et al. 2020,[15] and Kreutzer et al. 2017.[17]

All chemicals were used as received except where noted otherwise. Prior to use, methylene chloride (CH_2Cl_2) and anhydrous, amine-free dimethylformamide (DMF) purchased from Alfa Aesar was passed through alumina under argon in a solvent purification system. DMF purchased from Alfa Aesar and DMF purchased from Thermofisher were used in the synthesis. 24 hours before use, an amine scavenger was added to a bottle of DMF purchased from ThermoFisher. Amino acids, coupling agents, and resins were purchased from Chem-Impex. All reactions were performed at ambient temperature (ca. 25 °C), unless otherwise noted. HPLC grade acetonitrile (ACN) and 18 MΩ deionized water, each containing 0.1% trifluoracetic acid (TFA), were used for analytical and preparative reverse-phase HPLC. A Biotage Isolera Liquid Chromatography System using a Reverse Phase Biotage Sfär Bio C18 D – Duo 300 Å 20 µm, 25g column was used for initial purification of the cyclized peptide and oxidized trimer. Analytical reverse-phase HPLC

was performed on an Agilent 1260 system equipped with an Aeris PEPTIDE 2.6 μm XB-C18 column (Phenomonex). The peptide was then purified using preparative reverse-phase HPLC on a Rainin Dynamax system equipped with a ZORBAX 300SB-C18 7 μm, 21.2 x 250 mm, PrepHT column (Agilent). Mass spectrometry was performed either on an AB SCIEX TOF/TOF 5800 system (MALDI-TOF) or a Waters Xevo G2-XS QTof mass spectrometer (LC/MS with ESI).

After HPLC purification and lyophilization, all peptides were prepared and used as the trifluoroacetate (TFA) salt and were assumed to have one TFA ion per ammonium group present in each peptide. In previously reported procedures, a typical oxidation of 32 mg of peptide 4AT-L_{cc} afforded ca. 7 mg (22%) of trimer 4AT-L [15]. The following procedure is an improved synthesis of 4AT-L_{cc} and 4AT-L which includes oxidation of 50 mg of peptide 4AT-L_{cc} to afford ca. 12 mg (24%) of trimer 4AT-L.

Synthesis of monomer 4AT-L_{cc}

Loading the resin. To synthesize 4AT-L_{cc}, 2-chlorotrityl chloride resin (600 mg, 1.6 mmol/g) was transferred to a Bio-Rad Poly-Pep chromatography column (20 mL). A solution of Fmoc-Gly-OH (94 mg, 0.15 mmol) in 3.75% (v/v) 2,4,6-collidine in dry CH_2Cl_2 (16 mL) was added to the resin and the suspension was gently agitated for 12 hours. The solution was then drained and a solution of CH_2Cl_2/MeOH/*N*,*N*-diisopropylethylamine (DIPEA) (17:2:1, 8 mL) was added to the resin and agitated for 1 hour to cap the unreacted 2-chlorotrityl chloride sites of the resin. After an hour, the capping solution was drained, and the resin was washed with DMF (5 X, total column volume).

Peptide coupling. The Fmoc-Gly-2-chlorotrityl resin was then transferred to a 250-mL ChemGlass peptide synthesis vessel connected to a nitrogen/vacuum Schlenk line. The linear

peptide was then synthesized from the *C*-terminus to the *N*-terminus in consecutive cycles of amino acid coupling. Each cycle of amino acid coupling consists of i. Fmoc-deprotection with a solution of 20% (v/v) piperidine in DMF (8 mL) for 5 minutes, ii. washing with DMF (8 mL, 7 X), iii. coupling of amino acid (0.75 mmol, 5 equiv) in the presence of HCTU (0.75 mmol, 5 equiv) dissolved in 20 % (v/v) 2,4,6-collidine in DMF (8 mL) for 20 minutes, iv. washing with DMF (8 mL, 7 X). We used a special coupling procedure for the phenylalanine residue that follows the *N*-methylphenylalanine: the phenylalanine was coupled twice (0.75 mmol, 5 equiv, each time) and allowed to react for 1 hour the first time, and 20 minutes the second time each in the presence of HATU (5 equiv) and HOAt (5 equiv) dissolved in 20 % (v/v) 2,4,6-collidine in DMF (8 mL). After the last amino acid was coupled, the terminal Fmoc protecting group was cleaved using a solution of 20% (v/v) piperidine in DMF (8 mL for 5 minutes). Once the linear peptide was prepared on resin, the resin was divided evenly between two 10-mL Bio-Rad Poly-Prep chromatography columns and the following procedures were performed separately on each portion.

Cleavage of the peptide from the resin. After the resin was transferred to the Bio-Rad Poly-Prep chromatography column, the resin was washed with CH_2Cl_2 (10 X total column volume). To cleave the linear-protected peptide from the resin, a solution of 20% (v/v) 1,1,1,3,3,3-hexafluoroisopropanol (HFIP) in CH_2Cl_2 (7 mL) was added to the resin and the suspension was agitated for 1 hour. After an hour, the HFIP solution was filtered through the Bio-Rad column and the filtrate was collected in a 250-mL round-bottom flask. The resin was treated with a fresh solution of 20% (v/v) HFIP in CH_2Cl_2 (7 mL) and the suspension was agitated for an additional 30 minutes. After 30 minutes, the solution was filtered. The combined filtrates were concentrated to dryness by rotary evaporation to yield the linear protected peptide.

Cyclization of the linear peptide. The linear protected peptide was dissolved in dry DMF from Alfa Aesar (125 mL). HOAt (150 mg, 1.0 mmol, 13 equiv) and HATU (375 mg, 1.0 mmol, 13 equiv) were added to the solution. 4-Methylmorpholine (0.33 mL, 3.0 mmol, 40 equiv) was added and the solution was stirred under nitrogen for 48 hours. The solution was then concentrated to dryness by rotary evaporation with the water bath at 60 ºC to afford the cyclic protected peptide.

Global deprotection of the cyclic protected peptide. A solution of TFA/triisopropylsilane (TIPS)/water (18:1:1, 20 mL) was added to the dry cyclic protected peptide. The solution was stirred under nitrogen for 1.5 hours to remove acid-labile side chain protecting groups and yield the crude cyclic deprotected peptide.

Diethyl ether precipitation of the cyclic deprotected peptide. As the crude peptide was undergoing global deprotection two 50-mL conical vials of diethyl ether were placed on ice and chilled for at least an hour. Diethyl ether precipitation was performed to isolate the crude cyclic deprotected peptide and to remove deprotection reagents and byproducts. The global deprotection mixture was divided between an additional two 50-mL conical tubes (ca. 10 mL each) and mixed with cold diethyl ether (ca. 10 mL each). The mixtures of global deprotection solution and diethyl ether were incubated on ice for 5 minutes and then centrifuged at 700 rpm (107 x *G*) for 10 minutes. The crude cyclic deprotected peptide forms a pellet upon centrifugation. The supernatant in each conical tube was discarded and the pellet was gently resuspended in cold diethyl ether (ca. 10 mL each) and incubated on ice for an additional 5 minutes before being centrifuged again at 700 rpm (107 x *G*) for 10 minutes. This process of resuspending, decanting, incubating, and centrifuging was repeated one additional time. The pellet was suspended in ca. 4 mL of diethyl ether and the suspension was transferred into a clean 250-mL round-bottom flask. The mixture was concentrated to dryness by rotary evaporation. The crude cyclic deprotected peptide was immediately subjected

to reverse-phase HPLC purification. The crude cyclic deprotected peptide was immediately subjected to reverse-phase chromatographic purification.

Reverse-phase HPLC purification. The crude cyclic deprotected peptide was purified by reverse-phase liquid chromatography using either a Biotage Isolera Liquid Chromatography System (Method A) or a preparative HPLC instrument (Method B). Method A: The crude cyclic deprotected peptide was dissolved in 10% (v/v) diluted ACN (10 mL) and purified in 10% ACN and injected into a Biotage Isolera Liquid Chromatography System System using a Reverse Phase Biotage Sfär Bio C18 D – Duo 300 Å 20 µm, 25g column (10–50% ACN gradient). Method B: The crude cyclic deprotected peptide was dissolved in 20% (v/v) ACN in water (4 mL) and filtered through a 0.2 µm PVDF syringe filter. RP-HPLC was performed on the solution using a Rainin Dynamax system equipped with a ZORBAX 300SB-C18 7 µm, 21.2 x 250 mm, PrepHT column (20–45% ACN over 70 minutes).

Pure fractions, as determined by MALDI-TOF and analytical HPLC, were combined, concentrated to dryness by rotary evaporation, and lyophilized in two 50-mL conical vials. [The monoisotopic mass of 4AT-L_{cc} is 2200.0594 in the uncharged state. 4AT-L_{cc} thus gives a characteristic peak at m/z 2201 in the MALDI mass spectrum.] After two days of lyophilization, this 600 mg synthesis typically yields ca. 75-90 mg of 4AT-L_{cc}.

Oxidation of 4AT-L_{cc} to form cross-linked trimer 4AT-L. 30-50 mg of the 4AT-L_{cc} was subjected to oxidation as follows. [We have found that oxidizing more than 50 mg of material results in a decreased yield of the trimer.] 4AT-L was prepared by oxidizing peptide 4AT-L_{cc} (6 mM) in 20% aqueous dimethyl sulfoxide (DMSO) in the presence of triethylamine (TEA) (60 mM) as follows: The dry lyophilized peptide 4AT-L_{cc} was weighed and then transferred to a 20-mL scintillation vial and dissolved in an appropriate volume of 20% (v/v) aqueous DMSO to make

a 6 mM (13.2 mg/mL) solution of the peptide. An appropriate volume of TEA was added to the solution to make a 60 mM solution of TEA. The reaction mixture was incubated on a plate shaker at ambient temperature (ca. 25 ºC) for 48 hours. After incubation, the peptide solution was diluted with a total of ca. 10 mL of 10% ACN and injected into a Biotage Isolera Liquid Chromatography System using a Reverse Phase Biotage Sfär Bio C18 D – Duo 300 Å 20 µm, 25 g column (10–50% ACN). Fractions that contained the targeted mass by LC/MS with ESI were collected and lyophilized for three days. [The monoisotopic mass of 4AT-L is 6594.1362 in the uncharged state. The 4AT-L trimer gives a characteristic $[M+7H]^{7+}$ peak at m/z 943 in the ESI mass spectrum.]

The peptide was further purified using preparative reverse-phase HPLC on a Rainin Dynamax system equipped with a ZORBAX 300SB-C18 7 µm, 21.2 x 250 mm, PrepHT column (20–45% ACN over 70 mins) with the HPLC column heated to 60 ºC in a water bath. Pure fractions were determined by analytical HPLC with the column heated to 60 ºC and LC/MS with ESI. Pure fractions that contained the targeted mass were collected and lyophilized resulting in 4AT-L trimer as a TFA salt.

Mouse and human tissue sectioning

Mouse brain tissue was sectioned using an HM 430 Sliding Microtome (Cat No. 22-050-855) with a sharp MX35 ultra microtome blade (REF 3053835). The stage was chilled with powdered dry ice. The brain tissue was submerged in powdered dried ice for 5 minutes and then mounted coronally with Tissue-Tek O.C.T. Compound (Sakura Finetek). After the mouse brain tissue was sectioned at 40 microns, and each slice was transferred with a paintbrush to a 48-well plate containing 1 X PBS + 0.02% sodium azide, the plate was then stored at 4 ºC for long-term storage (ThermoFisher, Cat. No. 3548).

Human occipital cortex was sectioned using a vibratome (Leica VT1000S) at 30 µm. Sequential tissue sections were then transferred to a 24-well plate containing 1 X PBS + 0.02% sodium azide and were stored at 4 ºC for long-term storage (ThermoFisher, Cat. No. 142485).

Affinity purification of $pAb_{4AT\text{-}L}$

Preparation of the Affinity Column. To create the affinity purification column, 300 mg of dry NHS-activated agarose (Pierce™ NHS-Activated Agarose, Dry Cat. No. 26197) was added to a Bio-Rad Poly-Prep chromatography column (10 mL). The column was then loaded with 2.0 mg of 4AT-L trimer dissolved in 4 mL of 20% DMSO in 1 X PBS (pH = 7.4) and was added to the 10-mL Bio-Rad Poly-Prep chromatography column. The column was placed on a rocker at ambient temperature (25 ºC) for 2 ½ hours. The peptide resin conjugate was transferred to a 50-mL glass Kontes Flex-Column chromatography column (Kimble Chase). The resin was then washed 5 X (total column volume) with 1 X PBS followed by 18 MΩ deionized water and 2 X (total column volume) with 1 M Tris Buffer (pH = 8.5). An additional column volume of 1 M Tris buffer (pH = 8.5) was added, and the column was rocked overnight (ca. 12 hr) at 4°C to quench unreacted NHS esters.

Affinity Purification. For the following steps, all washes were chilled on ice before being added to the column. The column was washed 5 X (total column volume) with 1 X PBS (pH = 7.4). After aspirating the column, the plasma of two rabbits from Pacific Immunology was pooled (ca. 50 mL total), syringe filtered through a 0.45 micron hydrophilic PVDF syringe filter (25 mm, Millex – HV, REF SLHV033RB), before being added to the column. The column was then placed on a rocker overnight (ca. 12 hr) at 4°C. After the overnight incubation, the column was washed with 750 mL of 1 X PBS. The elution buffer, 0.2 M glycine buffer (pH = 1.85), was added to the column and 1 mL, ca. 20-30 fractions were collected with Eppendorf tubes chilled on ice and filled

with 500 µL of 1 M Tris Buffer (pH = 8.5). Fractions were checked for the presence of eluted antibodies at 280 nm using the Thermo Scientific NanoDrop One microvolume UV-Vis spectrophotometer (Cat. No. 13-400-519). Fractions containing antibodies were pooled, then concentrated with a 30 kDA buffer exchange column (Thermo Scientific Pierce™ Protein Concentrator PES, 30K MWCO, 5-20 mL, Cat. No. 88529) for a minimum of 6 buffer exchanges with 1 X PBS. Success of affinity purifications was measured by ELISA. Affinity purifications were performed three times to deplete as much antibody as possible from the plasma. The concentrated antibody was then quantified by BCA assay (Thermo Scientific Pierce BCA Protein Assay Kit, Cat. No. 23227) per the manufacturer's instructions. The concentrated antibody was then diluted with 1 X PBS + 0.02% sodium azide to a workable concentration and was stored at 4 ºC for long-term storage.

Enzyme-linked immunosorbent assays (ELISAs)

All procedures for this assay were performed in ambient temperature (25 ºC). 96-well flat bottom MaxiSorp immunoplates (Thermo Scientific Clear Flat-Bottom Immuno Nonsterile 96-Well Plates, Cat. No.442404) were coated in triplicate with 50 µL of 2 ng/µL of 4AT-L trimer in 1 X carbonate buffer (pH = 9.0). The plates were sealed with Axygen AxySeal Sealing Film (REF PCR-SP), and placed on a plate shaker overnight. The next day, plates were aspirated, washed with 100 µL of 1 X PBS + 0.05% Tween 20, rinsed with 18 MΩ deionized water, and aspirated using the Fisherbrand accuWash and accuWash Versa plate washer (Cat. No.14-377-577). One complete wash cycle consists of aspirating, washing, rinsing, and aspirating the plate. Plates were coated with 75 µL of blocking solution, 1% BSA (Bovine Serum Albumin, Fraction V, Heat Shock Treated, Fisher BioReagents, Cat. No. BP1600-100) in 1 X PBS, sealed, and then placed on the plate shaker for at least 1 hour. Primary antibodies were diluted to 1 µg/mL in 250 µL of blocking

solution. Plates were aspirated, washed, rinsed, and aspirated once, then primary antibodies were plated in triplicates in the top row of the 96-well plate, followed by a 1:3 dilution down the plate in blocking solution. Plates were sealed and incubated on the plate shaker for 2 hours. After incubation plates were aspirated, washed, rinsed, and aspirated three times. Plates were coated with 50 µL goat-anti-rabbit HRP (1:10,000) (Jackson ImmunoResearch Cat No. 111-035-144) in blocking solution, sealed, and incubated on the plate shaker for 1 hour. After incubation, plates were aspirated, washed, rinsed, and aspirated three times and developed with 50 µL of TMB/E substrate (Millipore, ES001-500ML) followed by 50 µL of 1 M HCl and scanned at 450 nm using the Skant It 5.0 Software and Thermofisher Multiskan Go plate reader (Cat. No. N10588).

Double-label immunofluorescence for plaque phenotyping

Staining for IBA-1 with $pAb_{4AT\text{-}L}$. Because both IBA-1 and $pAb_{4AT\text{-}L}$ were generated in rabbits, we performed a three-day staining procedure to prevent antibody cross-reactivity. The first day of experiments was performed as previously described with IBA-1 as the diluted primary antibody diluted in blocking buffer (1:1000), and incubated at 4 °C on a plate shaker overnight (16 hours).

The next day, after the primary antibody was aspirated, the tissue was washed twice in 1X TBS-A for 5 minutes each. After aspirating the last wash, the tissue was then incubated in blocking buffer for 15 minutes. After aspirating the blocking buffer, the tissue was incubated in blocking buffer supplemented with 5% normal goat serum and diluted secondary antibody for 1 hour (1:1000, Goat anti-Rabbit IgG (H+L) Cross-Adsorbed Secondary Antibody, Alexa Fluor 647, Invitrogen, Cat. No. A-21244). For the duration of the experiment, the plate was wrapped in aluminum foil to avoid fluorescent quenching. After aspirating the secondary antibody solution, the tissue was washed in 1 X TBS-A twice for 5 minutes each. After the last wash was aspirated,

the tissue was incubated in blocking buffer for 15 minutes. After the last wash was removed, the tissue was washed in 1 X TBS for an additional three times for 5 minutes each. The tissues were then transferred with a paintbrush to 20-mL scintillation vials filled with 37% formaldehyde (Fisher Chemical, Cat. No. F79-4), then incubated in a water bath at 37 °C for 2 hours. After incubating, the tissue was then transferred with a paintbrush back to the 24-well plate with each well filled with fresh 1 X TBS. The tissue was then washed three times for 5 minutes each. After the last wash, the tissue was then washed 1 X TBS-A for 15 minutes. Once the last wash was aspirated, the tissue was incubated in blocking buffer for 30 minutes. A second primary antibody solution was prepared in blocking buffer with diluted $pAb_{4AT\text{-}L}$ (1:1000). The tissue was then incubated in the second primary antibody solution on a plate shaker at 4° C overnight (16 hours).

The next day, the second primary antibody solution was aspirated and washed twice in 1 X TBS-A for 5 minutes each. After the last wash was aspirated, the tissue was then incubated in blocking buffer for 15 minutes. Once the blocking buffer was aspirated, the tissue was incubated in blocking buffer supplemented with 5% normal goat serum and diluted secondary antibody (1:1000) for 1 hour (Goat anti-Rabbit IgG (H+L) Cross-Adsorbed Secondary Antibody, Alexa Fluor 488, Invitrogen, Cat. No. A-11008). After aspirating the secondary antibody solution, the tissue was washed in 1 X TBS-A twice for 5 minutes each. After the last wash was removed, the tissue was washed in 1 X TBS for an additional three times for 5 minutes each. Following the aspiration of the last wash, to quench lipofuscin the tissue was then incubated in True black in 70% EtOH (as prepared by manufactures instructions) with for 5 mins. Once True black (Gold Biotechnology) was aspirated, the tissue was washed in 1 X TBS six times for 5 minutes each. With a paintbrush, the tissues were mounted on slides (Fisherbrand Superfrost Plus Microscope Slides, 25mm x 75mm x 1.0mm, Glass, Regular Corner, 3/4" SuperFrost Tab, Part Num. 22-037-

246), coated in mounting media (Vectashield Vibrance® Antifade Mounting Medium with DAPI, H-1800), then coverslipped (Globe Scientific 1419-10 Cover Glass, 24 x 60mm, No. 1 Thickness). The slides were then placed in a dark location until the slides were dry.

Staining for GFAP or AT8 with pAb_{4AT-L}. All procedures for preparing the tissue for primary antibody incubation were also performed when co-staining with GFAP and pAb_{4AT-L}, and AT8 with pAb_{4AT-L}. To prepare the primary antibody solution, diluted GFAP or AT8 (1:1000) with diluted pAb_{4AT-L} (1:1000) in blocking buffer. This primary antibody solution was added after the tissue was incubated in blocking buffer. The plate containing the tissue was then incubated on a plate shaker at 4° C overnight (16 hours).

The next day, the tissue was then subjected to procedures similar to the third day of experiments listed previously. The primary antibody was aspirated and the tissue was washed in 1 X TBS-A twice for 5 minutes each. After the last wash was aspirated, the tissue was incubated in blocking buffer for 15 minutes. Once the blocking buffer was aspirated, the tissue was incubated in blocking buffer supplemented with 5% normal goat serum and diluted in two secondary antibodies for 1 hour (1:1000, Goat anti-Rabbit IgG (H+L) Cross-Adsorbed Secondary Antibody, Alexa Fluor 488, Invitrogen, Cat. No. A-11008; Goat anti-Mouse IgG (H+L) Cross-Adsorbed Secondary Antibody, Alexa Fluor 647, Invitrogen, Cat. No. A-21235). The rest of the procedure was performed as previously described after the secondary antibody solution was aspirated.

Supplemental Figure S2.1

Characterization data of peptide monomer 4AT-Lcc and cross-linked trimer 4AT-L

Characterization of 4AT-L_{cc}

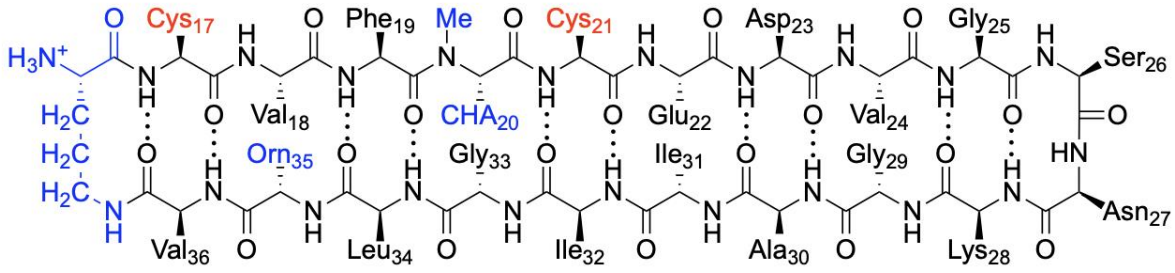

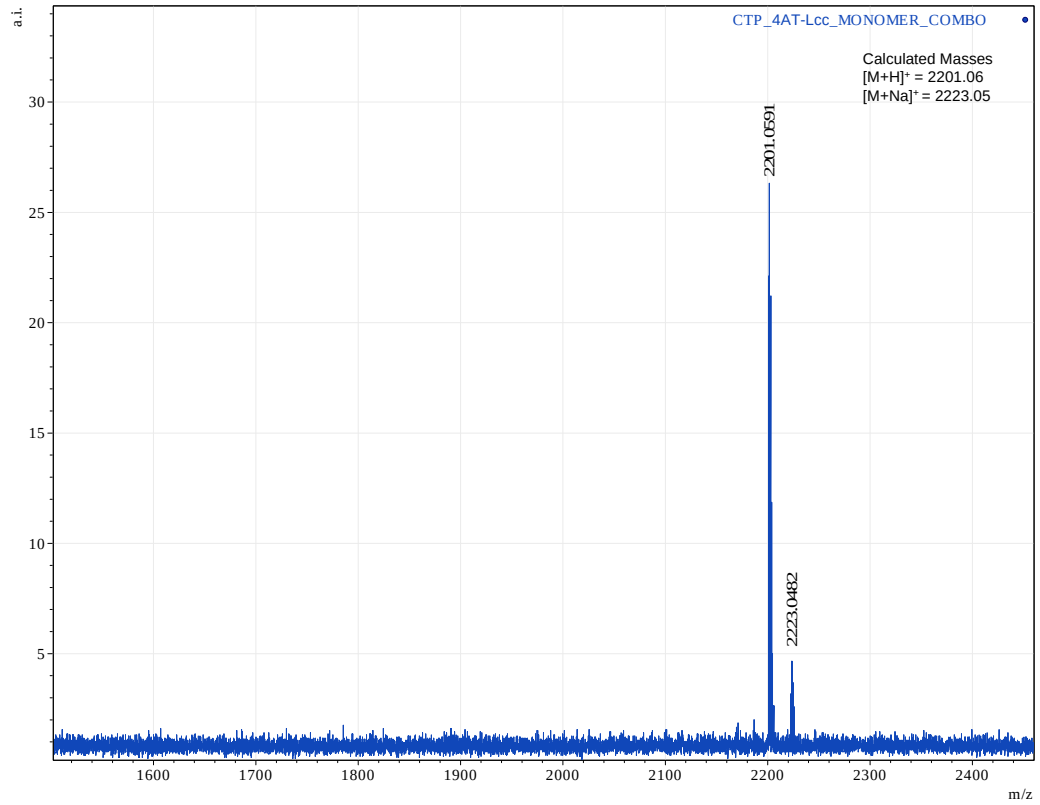
CTP_4AT-Lcc_MONOMER_COMBO
Calculated Masses
[M+H]+ = 2201.06
[M+Na]+ = 2223.05
2201.0591
2223.0482
a.i.
m/z

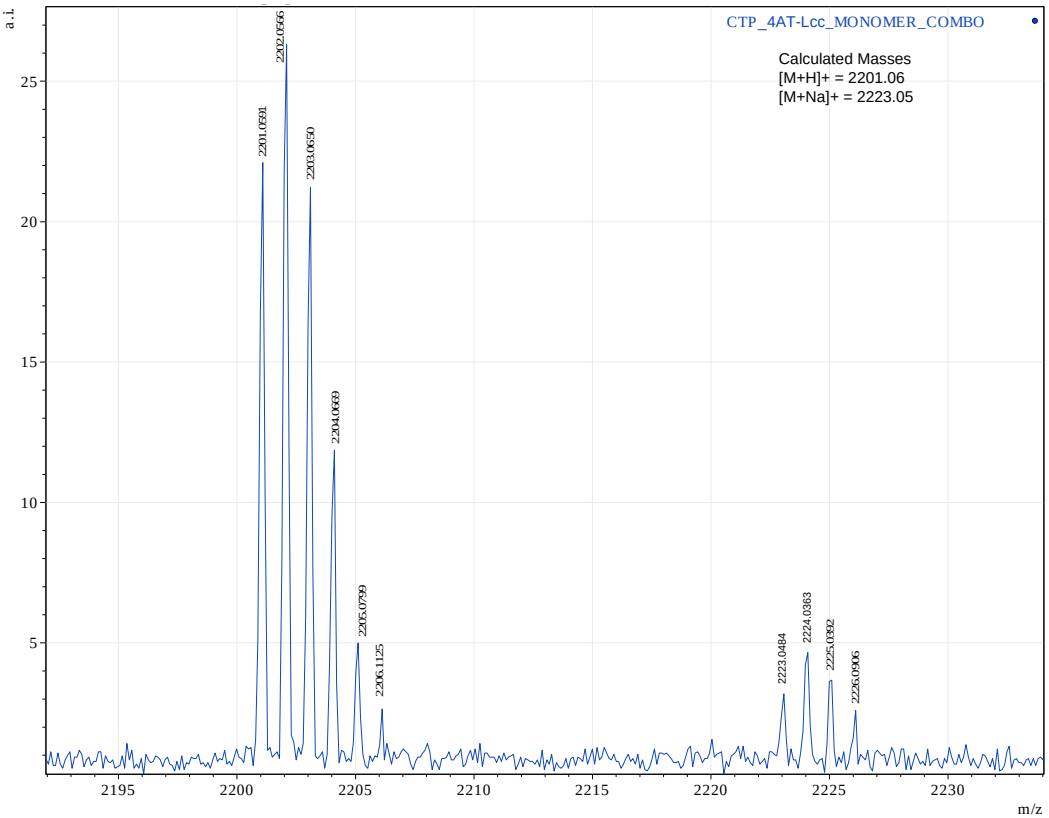
CTP_4AT-Lcc_MONOMER_COMBO
Calculated Masses
[M+H]+ = 2201.06
[M+Na]+ = 2223.05
2201.0591
2202.0666
2203.0650
2204.0669
2205.0799
2206.1125
2223.0484
2224.0363
2225.0392
2226.0906
a.i.
m/z

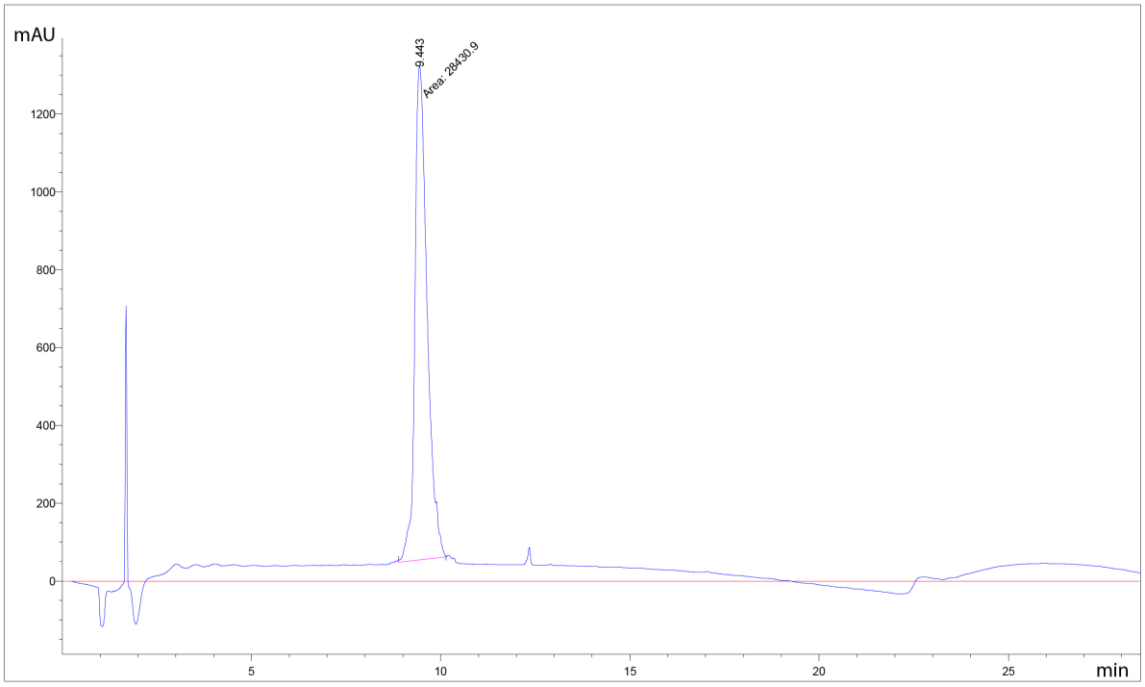

Signal 1: MWD1 A, Sig=214,4 Ref=off

Peak #	RetTime [min]	Type	Width [min]	Area [mAU*s]	Height [mAU]	Area %
1	9.443	MM	0.3736	2.84309e4	1268.33105	100.0000

Characterization of 4AT-L

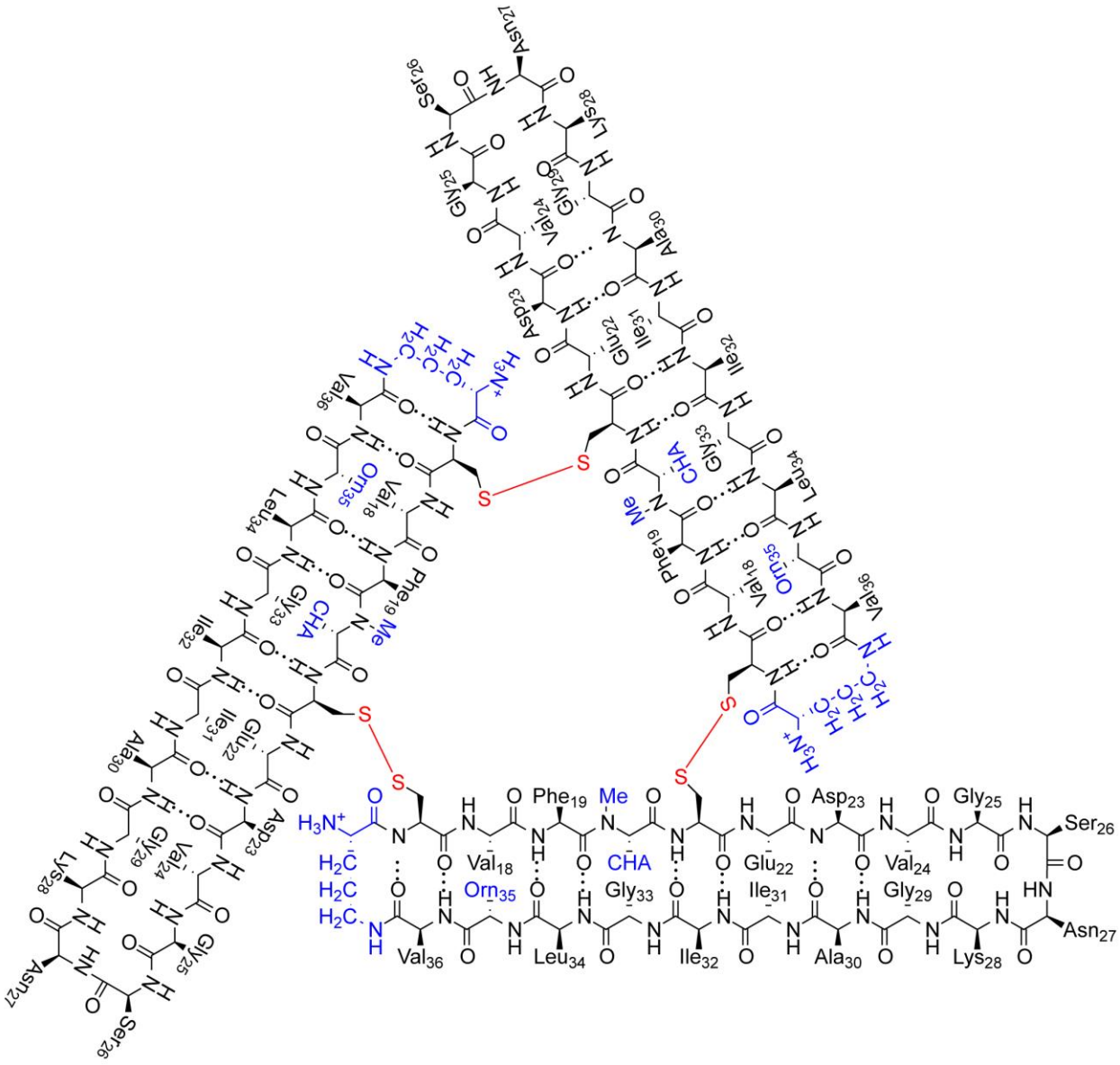

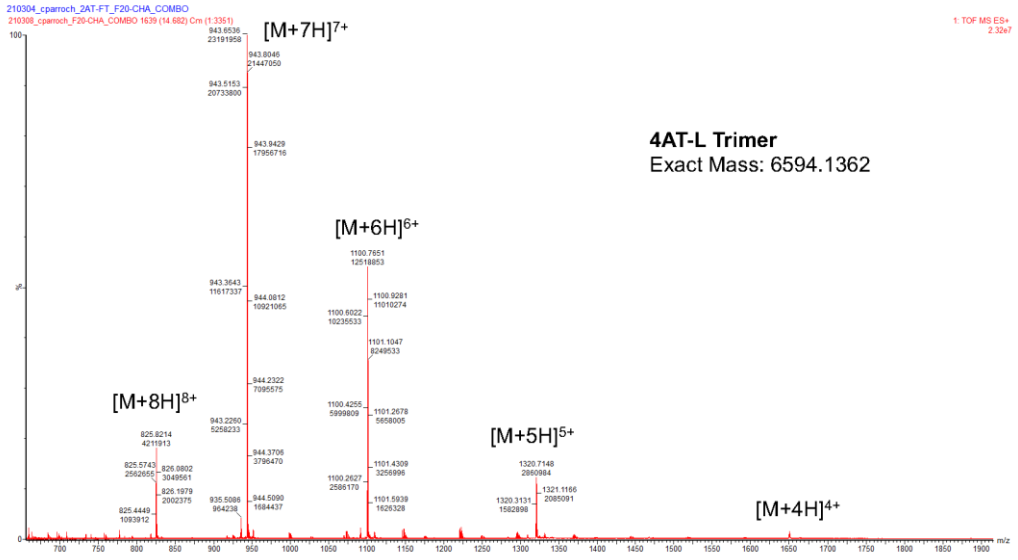
210304_cparroch_2AT-FT_F20-CHA_COMBO
210308_cparroch_F20-CHA_COMBO 1639 (14.682) Cm (1:3351)
1: TOF MS ES+
2.32e7
[M+7H]7+
[M+6H]6+
[M+8H]8+
[M+5H]5+
[M+4H]4+
4AT-L Trimer
Exact Mass: 6594.1362
m/z

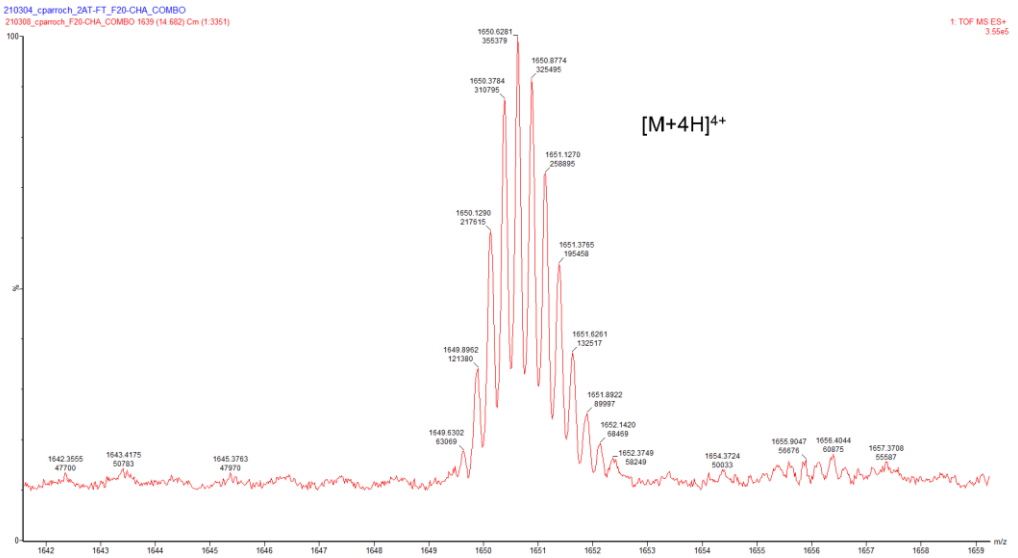
210304_cparroch_2AT-FT_F20-CHA_COMBO
210308_cparroch_F20-CHA_COMBO 1639 (14.682) Cm (1:3351)
1: TOF MS ES+
3.55e5
[M+4H]4+
m/z

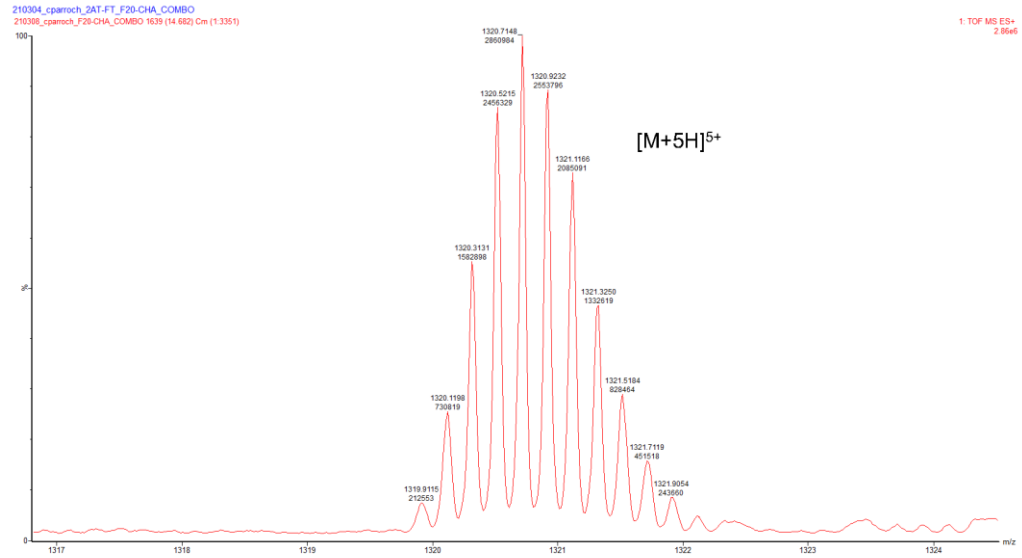
210304_cparroch_2AT-FT_F20-CHA_COMBO
210308_cparroch_F20-CHA_COMBO 1639 (14.682) Cm (1:3351)
1: TOF MS ES+
2.86e6
[M+5H]5+
1320.7148
2860984
1320.9232
2553796
1320.5215
2456329
1321.1166
2085091
1320.3131
1582898
1321.3250
1332619
1321.5184
828464
1320.1198
730819
1321.7119
451518
1319.9115
212553
1321.9054
243660
%
m/z
1317
1318
1319
1320
1321
1322
1323
1324

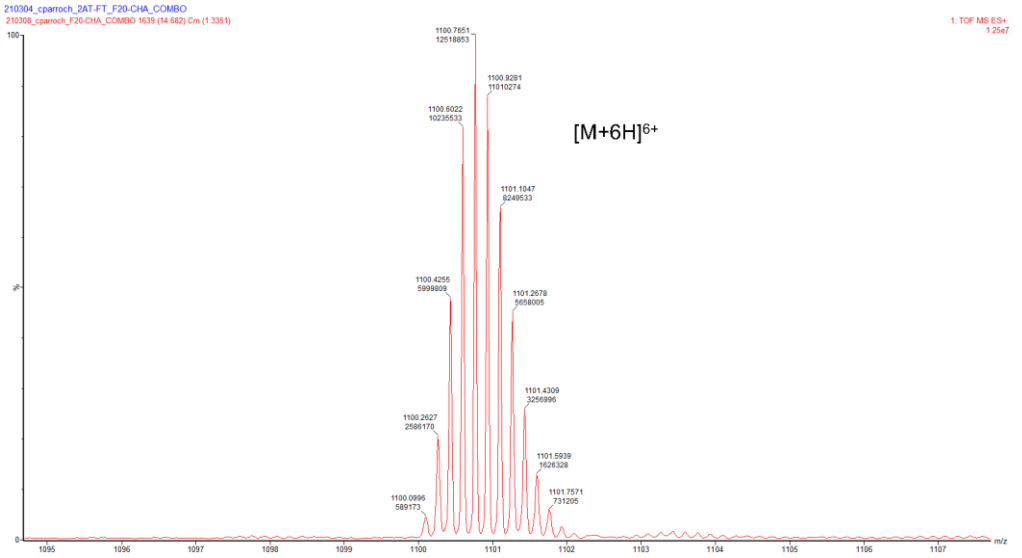
210304_cparroch_2AT-FT_F20-CHA_COMBO
210308_cparroch_F20-CHA_COMBO 1639 (14.682) Cm (1:3351)
1: TOF MS ES+
1.25e7
[M+6H]6+
1100.7651
12518853
1100.9281
11010274
1100.6022
10235533
1101.1047
9249533
1100.4255
5999809
1101.2678
5658005
1101.4309
3256996
1100.2627
2586170
1101.5939
1626328
1100.0996
589173
1101.7571
731205
%
m/z
1095
1096
1097
1098
1099
1100
1101
1102
1103
1104
1105
1106
1107

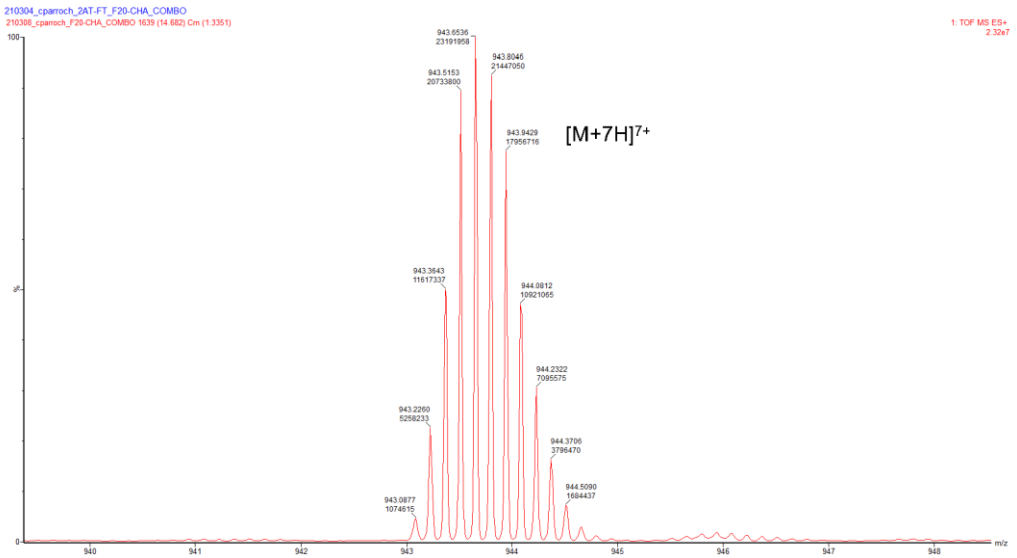
210304_cparroch_2AT-FT_F20-CHA_COMBO
210308_cparroch_F20-CHA_COMBO 1639 (14.682) Cm (1:3351)
1: TOF MS ES+
2.32e7
943.6536
23191958
943.8046
21447050
943.5153
20733800
943.9429
17956716
[M+7H]7+
943.3643
11617337
944.0812
10921065
944.2322
7095575
943.2260
5258233
944.3706
3796470
944.5090
1684437
943.0877
1074615
%
0
940
941
942
943
944
945
946
947
948
m/z

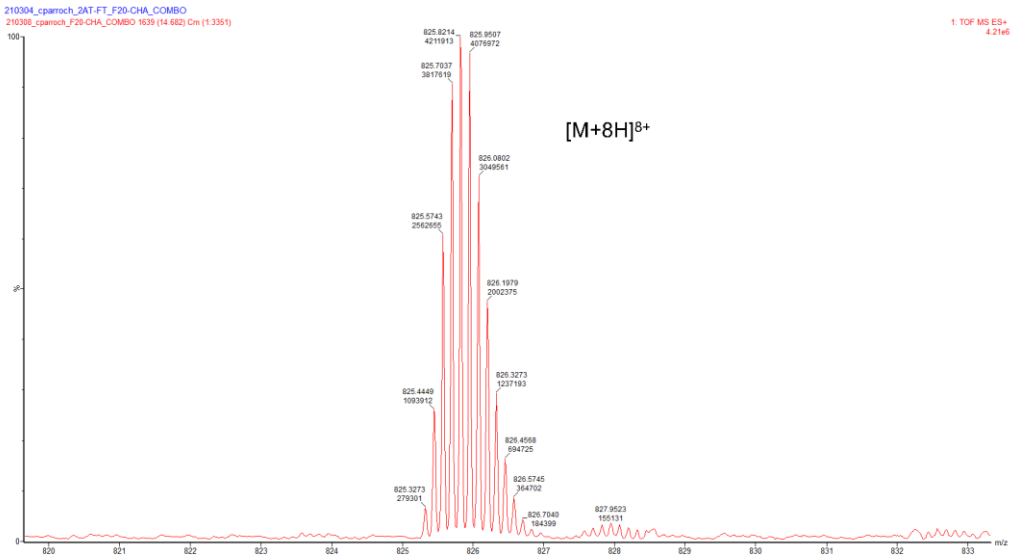
210304_cparroch_2AT-FT_F20-CHA_COMBO
210308_cparroch_F20-CHA_COMBO 1639 (14.682) Cm (1:3351)
1: TOF MS ES+
4.21e6
825.8214
4211913
825.9507
4076972
825.7037
3817619
[M+8H]8+
826.0802
3049561
825.5743
2562655
826.1979
2002375
826.3273
1237193
825.4449
1093912
826.4568
594725
826.5745
364702
825.3273
279301
826.7040
184399
827.9523
155131
%
0
820
821
822
823
824
825
826
827
828
829
830
831
832
833
m/z

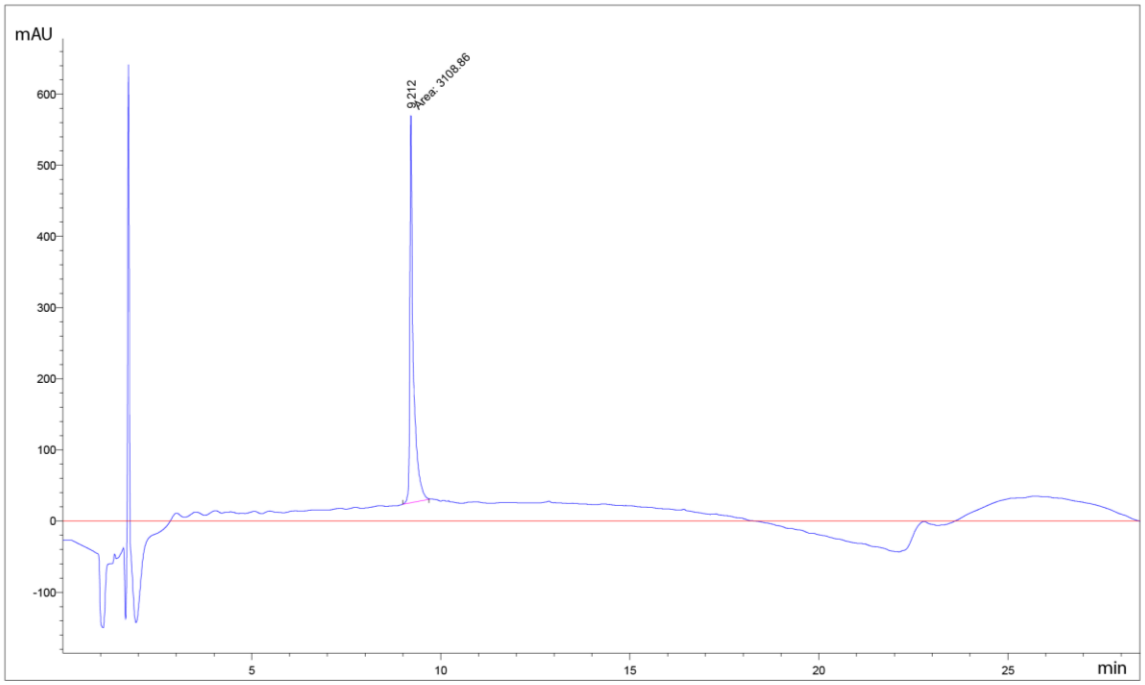

Signal 1: MWD1 A, Sig=214, 4 Ref =off

Peak #	RetTime [min]	Type	Width [min]	Area [mAU*s]	Height [mAU]	Area %
1	9.213	MM	0.1046	3108.86206	495.36078	100.0000

Succession of isolating 4AT-L specific antibodies through affinity purification by ELISA.

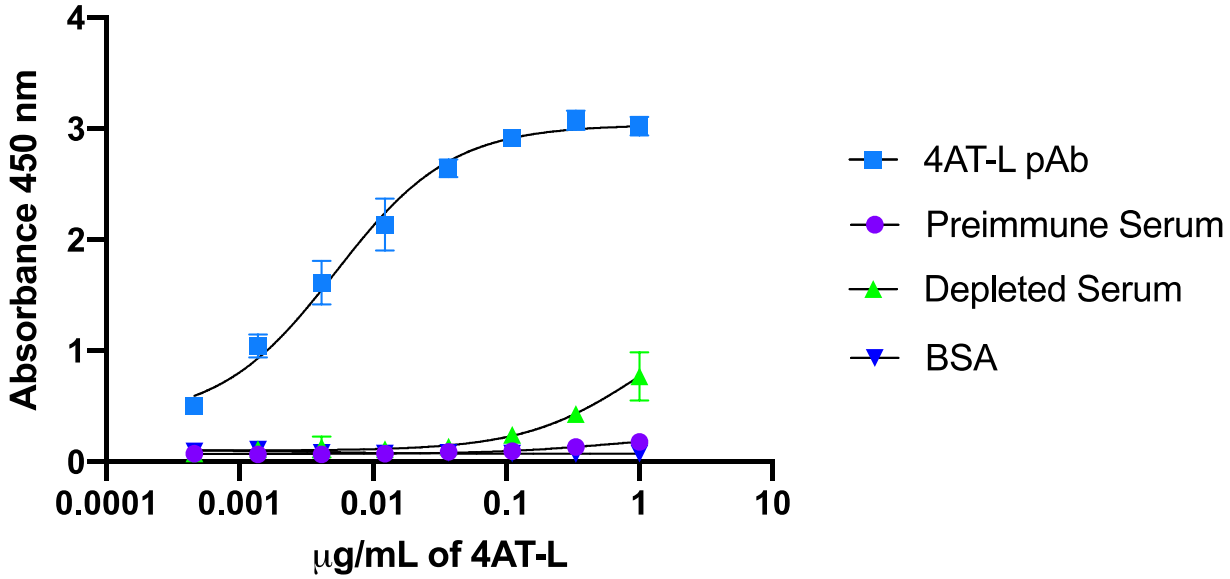

Supplemental Figure S2.2 ELISA graph demonstrating the recognition of affinity purified 4AT-L with 4AT-L peptide and serum depleted of antibodies recognizing the 4AT-L trimer.

4AT-L pAb recognition of Aβ plaques on human brain tissue is blocked with the addition of the 4AT-L trimer.

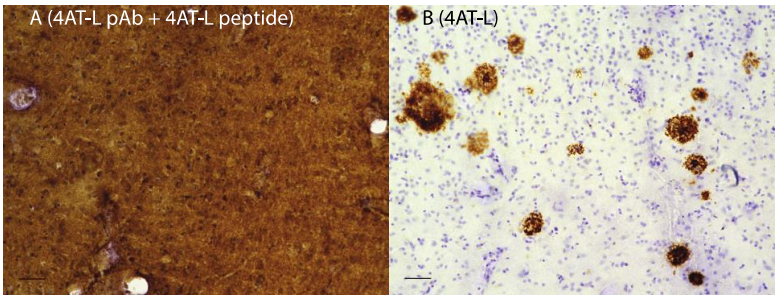

Supplemental Figure S2.3 Immunohistochemistry micrographs of brain sections from a person who lived with LOAD that was either stained with (**A**) $pAb_{4AT\text{-}L}$ with the 4AT-L trimer (preabsorbed) or (**B**) $pAb_{4AT\text{-}L}$. All images were acquired at 40X; the scale bar is 50 µm.

4AT-L pAb recognition is not affected by antibody order.

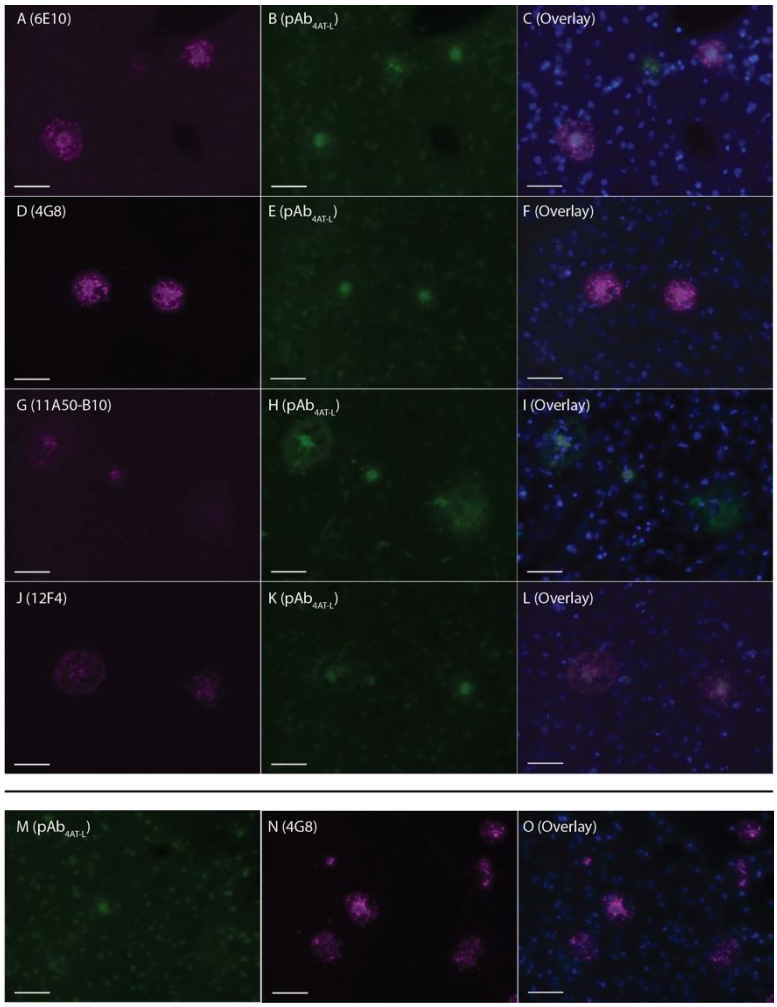

Supplemental Figure S2.4. Immunofluorescence micrographs comparing the staining quality of Aβ plaques by swapping antibody order of addition between four commercially available anti-Aβ antibodies and $pAb_{4AT\text{-}L}$ to brain slices from a person who lived with LOAD. The left column shows the staining of the primary antibody (and respective secondary antibody) that was added to the brain slice; the middle column shows the staining of the second primary antibody (and a respective secondary antibody) that was added to the brain slice; the right column shows the corresponding overlay, as well as the staining of cell nuclei by DAPI (blue). **(A-C)** shows the staining of Aβ plaques when 6E10 (magenta) was added to the brain section first before the addition of $pAb_{4AT\text{-}L}$ (green); **(D-F)** shows the staining of Aβ plaques when 4G8 (magenta) was added to the brain section first before the addition of $pAb_{4AT\text{-}L}$ (green); **(G-I)** shows the staining of Aβ plaques when 11A10-B50 (magenta) was added to the brain section first before the addition of $pAb_{4AT\text{-}L}$ (green); **(J-L)** shows the staining of Aβ plaques when 12F4 (magenta) was added to the brain section first before the addition of $pAb_{4AT\text{-}L}$ (green); **(M-O)** shows the staining of Aβ plaques when $pAb_{4AT\text{-}L}$ (green) was added to the brain section first before the addition of 4G8 (magenta). All images were acquired at 40X; the scale bar is 50 μm.

4AT-L pAb recognition is consistent despite the exchange of fluorophores.

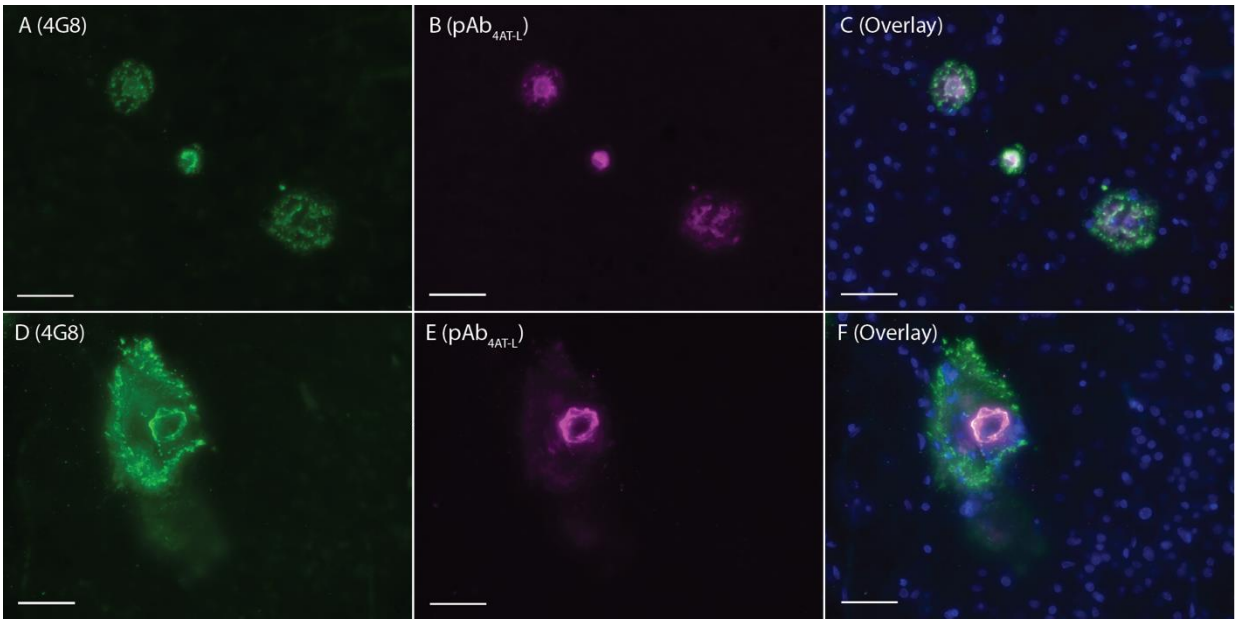

Supplemental Figure S2.5. Immunofluorescence micrographs comparing the staining of Aβ plaques and cerebral amyloid angiopathy (CAA) by $pAb_{4AT\text{-}L}$ to 4G8 with swapped fluorophores in brain slices from a person who lived with LOAD. The left column shows the staining of 4G8 (green); the middle column shows the staining of $pAb_{4AT\text{-}L}$ (magenta); the right column shows the corresponding overlay, as well as the staining of cell nuclei by DAPI (blue). **(A-C)** are images of Aβ plaques stained by the coincubation with 4G8 and $pAb_{4AT\text{-}L}$; (**D-F)** are images of CAA stained by the coincubation with 4G8 and $pAb_{4AT\text{-}L}$. All images were acquired at 40 X; the scale bar is 50 μm.

Supplemental Table S2.1.

Table of Antibodies and Reagents

Item	Supplier	Cat No	Storage	Concentration for IF and IHC	Application
Peroxidase AffiniPure Goat Anti-Rabbit IgG (H+L)	Jackson ImmunoResearch	111-035-144	-80 ℃	1: 5000	ELISA
500 ml TMB/E Single Reagent, Blue color, Horseradish Peroxidase *Substrate*	Millipore	ES001-500ML	4 ℃	50 uL per well	ELISA
Thioflavine S (Practical Grade)	Sigma-Aldrich	T1892-25G	RT	0.5% in 50% EtOH	IF
TrueBlack™ Lipofuscin Autofluorescence Quencher	GoldBiotechnology	TB-250-1	RT	50 uL per 1 mL of 70% EtOH	IF
88% formic acid (Certified ACS)	Fisher Chemical,	A118P-100	RT	88%	IHC and IF
Normal goat serum	Vector laboratories	REF S-1000	4 ℃	5% (v/v)	IHC and IF
Goat anti-Rabbit IgG (H+L) Cross-Adsorbed Secondary Antibody, Alexa Fluor™ 488	Invitrogen	A-11008	4 ℃	1:1000	IF
Goat anti-Rabbit IgG (H+L) Cross-Adsorbed Secondary Antibody, Alexa Fluor™ 647	Invitrogen	A-21244	4 ℃	1:1000	IF
Goat anti-Mouse IgG (H+L) Cross-Adsorbed Secondary Antibody, Alexa Fluor™ 647	Invitrogen	A-21235	4 ℃	1:1000	IF
Goat anti-Mouse IgG (H+L) Cross-Adsorbed Secondary Antibody, Alexa Fluor™ 488	Invitrogen	A-11001	4 ℃	1:1000	IF
Anti-β-Amyloid, 1-16 [6E10]	BioLegend	803015	-20 ℃	1:1000	IF

Anti-β-Amyloid, 17-24 [4G8]	BioLegend	800708	4 ℃	1:1000	IF
β-Amyloid 1-40, [11A50-B10]	BioLegend	805404	4 ℃	1:1000	IF
Purified anti-β-Amyloid,1-42 Antibody [12F4]	BioLegend	805509	4 ℃	1:1000	IF
Phospho-Tau (Ser202, Thr205) Monoclonal Antibody (AT8)	Invitrogen	MN1020	-20 ℃	1:1000	IF
GFAP Antibody	Abcam	ab4648	-20 ℃	1:1000	IF
Anti-IBA-1 (for ICC)	Wako	019-19741	-20 ℃	1:1500	IF
37% Formaldehyde	Fisher Chemical	F79-4	RT	N/A	IF
DAPI Fluoromount-G Mounting Medium	Southern Biotech	0100-20	4 ℃	N/A	IF
VECTASHIELD Vibrance® Antifade Mounting Medium with DAPI	Vector laboratories	H-1800	N/A	N/A	IF
DPX Mounting Media	Sigma-Aldrich	SKU 06522x	RT	N/A	IHC
Vectastain Elite ABC-HRP Kit Peroxidase	Vector Laboratories	PK-6100	4 ℃	Manufacturer's instructions	IHC
DAB Substrate Kit, Peroxidase (HRP), with Nickel	Vector Laboratories	SK-4100	4 ℃	Manufacturer's instructions	IHC
Normal Horse Serum	Vector Laboratories	REF S-2000	4 ℃	5% (v/v)	IHC
Horse Anti-Rabbit IgG Antibody (H+L), Biotinylated	Vector Laboratories	BA-1100-1.5	4 ℃	1:1000	IHC
1% Cresyl Violet	Abcam	ab246817	4 ℃	0.1%	IHC

Supplemental Table S2.2

Magnification and channel settings for images in the main body of the manuscript

Figure	Magnification	DAPI Channel	GFAP Channel	Cy5 Channel
2A	4X stitch	–	1/50s	–
2B-D	20 X	–	1/50s	–
3A-C	20 X	1/500s	1/200s	1/150s
5A-B	40 X	–	1/50s	1/15s
5C	40 X	1/120s	1/50s	1/15s
5D-E	40 X	–	1/50s	1/80s
5F	40 X	1/120s	1/50s	1/80s
5G-H	40 X	–	1/50s	1/15s
5I	40 X	1/120s	1/50s	1/15s
5J-K	40 X	–	1/50s	1/12s
5L	40 X	1/120s	1/50s	1/12s
6A-B	40 X	–	1/50s	1/1.7s
6C	40 X	1/120s	1/50s	1/1.7s
6D-E	40 X	–	1/50s	1/6s
6F	40 X	1/120s	1/50s	1/6s
6G-H	40 X	–	1/30s	1/15s
6I	40 X	1/120s	1/30s	1/15s
7A-B	40 X	–	1/50s	1/12s
7C	40 X	1/120s	1/50s	1/12s
7D-E	40 X	–	1/50s	1/50s
7F	40 X	1/120s	1/50s	1/50s
7G-H	40 X	–	1/30s	1/20s
7I	40 X	–	1/30s	1/20s
7J-K	40 X	–	1/30s	1/20s
7L	40 X	1/120s	1/30s	1/20s

Supplemental Table S2.3

Z-stack settings for images in the main body of the manuscript

Figure	Current Setting	Upper Limit	Lower Limit	Pitch	Images
2B-D, 3A-C	2741.9	2745.7	2725.1	0.6 um	35
5A-C	2936.0 um	2939.6um	2932.4 um	0.3 um	25
5D-F	2760.4 um	2764 um	2756.8 um	0.3 um	25
5G-I	2703.1 um	2706.7	2699.5	0.3 um	25
5J-L	2792.4 um	2796.0	2788.8	0.3 um	25
6A-C	2708.7 um	2710.6	2706.8	0.3 um	25
6D-F	2755.0	2758.6um	2751.4 um	0.3 um	25
6G-I	2785.7	2789.3um	2782.1 um	0.3 um	25
7A-C	2691.7 um	2702.5 um	2689.0 um	0.6 um	24
7 D-F	2792.7	2799.0 um	2788.2 um	0.6 um	18
7G-I	2687.0	2690.0 um	2683.4 um	0.6 um	19
7J-L	2755.2 um	2758.7um	2751.6 um	0.6 um	15

Supplemental Table S2.4

Shadow and brightness adjustments for images in the main body of the manuscript

Figure	**Shadow** (Green)	**Shadow** (Magenta)	**Shadow** (Blue)	**Shadow** (Combo)	**Brightness**
2A	–	–	–	–	–
2B-D	9	–	–	–	190
3A-C	9	2	1	–	190
5A-B	8	7	–	–	160
5C	–	–	–	9	160
5D-E	–	–	–	9	160
5F	–	–	–	9	160
5G-H	8	7	–	–	160
5I	–	–	–	9	160
5J-K	–	–	–	9	160
5L	–	–	–	9	160
6A-B	5	12	1	–	145, 160,110
6C	–	–	–	19	160
6D-E	5	12	20	–	80, 160, 160
6F	–	–	–	20	160
6G-H	7	6	1	–	160
6I	–	–	–	14	160
7A-B	8	9	–	–	–
7C	–	–	–	19	–
7D-E	2	–	–	–	–
7F	–	–	–	5	–
7G-H	10	5	–	–	–
7I	–	–	–	19	–
7J-K	10	5	–	–	–
7L	–	–	–	18	–

Supplemental Table S2.5

Magnification and channel settings for images in the supplemental information

Supplemental Figure	Magnification	DAPI Channel Exposure	GFAP Channel Exposure	Cy5 Channel Exposure
S3, A	–	–	–	–
S3, B	–	–	–	–
S3, C	20x	–	–	–
S4, A and B	40x	1/120s	1/50s	1/15s
S4, C	40x	1/120s	1/50s	1/15s
S4, D and E	40x	–	1/50s	1/50s
S4, F	40x	1/120s	1/50s	1/50s
S4, G and H	40x	–	1/50s	1/15s
S4, I	40x	1/120s	1/50s	1/15s
S4, J and K	40x	–	1/80s	1/25s
S4, L	40x	1/120s	1/80s	1/25s
S4, M and N	40x	–	1/50s	1/50s
S4, O	40x	1/120s	1/50s	1/50s
S5, A and B	40x	–	1/120s	1/25s
S5, C	40x	1/120s	1/120s	1/25s
S5, D and E	40x	–	1/120s	1/30s
S5, F	40x	1/120s	1/120s	1/30s

Supplemental Table S2.6

Z-stack settings for images in the main body of the supplemental information

Figure	Current Setting	Upper Limit	Lower Limit	Pitch	Images
S3, A	–	–	–	–	–
S3, B	2781.2	2784.8	2777.6	0.3	25
S3, C	2760.5	2764.4	2756.9	0.3	25
S4, A-C	2704.1 um	2707.7um	2700.5um	0.3 um	25
S4, D-F	2747.6um	2751.2um	2744 um	0.3 um	25
S4, G-I	2880.8	2884.4	2877.2	0.3	25
S4, J-L	2835 um	2838.6um	2831.4um	0.3 um	25
S4, M-O	2703.8	2706.6	2699.4	0.3 um	22
S5, A-C	2748.2 um	2757.8um	2744.6 um	0.3	25
S4, D-F	2737.1	2741.6	2731.7	0.6	18

Supplementary Table S2.7

Shadow and brightness adjustments for images in the supplemental information

Supplemental Figure	**Shadow** (Green)	**Shadow** (Magenta)	**Shadow** (Blue)	**Shadow** (Combo)	**Brightness**
S3, A	–	–	–	–	–
S3, B	–	–	–	–	–
S3, C	–	–	–	23	156
S4, A and B	0	4	–		160, 160
S4, C	–	–	–	6	160
S4, D and E	7	–	–	–	160
S4, F	–	–	–	–	–
S4, G and H	5	–	4	–	160,160
S4, I	–	–	–	11	160
S4, J and K	5	4	–	–	160, 160
S4, L	–	–	–	13	–
S4, M and N	2	–	–	–	160
S4, O	–	–	–	5	–
S5, A and B	–	3	–		160
S5, C	–	3	–	9	160, 160
S5, D and E	5	–	–	–	160
S5, F	–	–	–	9	177

Chapter 3[b]

Current Peptide Vaccine and Immunotherapy Approaches Against Alzheimer's Disease

Introduction

Alzheimer's disease (AD) is the most common form of dementia, affecting ca. 6.2 million Americans.[1] It is expected to increase to 13.8 million by 2060. Four cognition-enhancing drugs have been used to treat the symptoms of AD, by inhibiting cholinesterase (rivastigmine, galantamine, and donepezil) or targeting the NMDA receptor (memantine).[2] Psychotropic agents have also been used to treat behavioral disturbances. These small-molecule drugs do not prevent the inevitable decline associated with AD but only mitigate the symptoms.[2] There are currently no therapeutic agents that substantially alter the progression of the disease in the growing number of patients diagnosed with AD. Peptide vaccines and immunotherapies with monoclonal antibodies have thus far demonstrated promise in slowing the cognitive decline associated with AD. Vaccines involve administration of an antigen associated with the disease. The annual flu shot or the Johnson & Johnson vaccine against COVID-19 are typical examples. In vaccination, a patient's immune system is trained to produce antibodies against a pathogen or molecule associated with the disease.

Immunotherapies involve administration of exogenously produced antibodies that recognize molecules or pathogens associated with the disease. HUMIRA is a monoclonal antibody that neutralizes tumor necrosis factor α (TNFα) to reduce inflammation associated with rheumatoid

[b] [a]This chapter is adapted from Parrocha, C. M. T.; Nowick, J. S. Pept. Sci. 2022, e24289

arthritis and other inflammatory disease. Immunotherapy does not involve training the immune system, but instead just provides the antibodies needed to treat the disease.

The vaccines and immunotherapies that have been pursued thus far for AD have focused on sequestering and clearing the aggregating peptides and proteins involved in the pathogenesis and progression of the disease, the β-amyloid peptide (Aβ) and tau. In AD, Aβ aggregates to form fibrils and plaques in the brain[3], and hyperphosphorylated tau aggregates to form neurofibrillary tangles.[4] Aβ, tau, and peptide fragments thereof have been used in peptide vaccine and immunotherapy development against AD. This review will cover the design and development of peptide vaccines and immunotherapies with a peptide or protein that contributes to the progression and pathogenesis of AD.

β-Amyloid Peptide Vaccines

The earliest Aβ peptide vaccine, AN-1792, consisted of the $A\beta_{1-42}$ peptide formulated with the QS21 adjuvant.[5] The AN-1792 vaccine was designed to train the immune system to generate antibodies that target and sequester endogenous Aβ and thus prevent the formation of Aβ plaques in the brain and the associated cognitive decline.

Even though the AN-1792 vaccine showed promising safety and tolerability in a phase I clinical trial which began in 2001, the vaccine failed two years later in a phase II clinical trial because it induced meningoencephalitis, a form of brain inflammation.[6] Subsequent studies have suggested that the QS21 adjuvant may have exacerbated the inflammatory T-cell response — a Th-1 response — that produced the meningoencephalitis.[3] Epitope mapping and additional studies of $A\beta_{1-42}$ further established that the central region, between residues 14 and 34, induces a Th-1 response.[6,7] In contrast, the *N*-terminal region of Aβ, between residues 1 and 15, induces the

production of antibodies against Aβ through a B-cell response — a Th-2 response.[6,7] A follow-up study, performed 14 years after the phase I clinical trial, showed plaque removal associated with the antibodies that AN-1792 induced.[7,8] Although the AN-1792 peptide vaccine failed in clinical trials, it inspired the second generation of Aβ peptide vaccines.

Nine Aβ peptide vaccines have subsequently entered clinical trials (**Supplemental Table S3.1**). **Figure 3.1** summarizes the four most promising peptide vaccine candidates tested in at least phase II clinical trials (CAD-106, ACI-24, ABvac40, and UB-311) and illustrates the region of Aβ that was used as an antigen and the means of antigen presentation. Most of the second-generation peptide vaccines were designed with the *N*-terminus of Aβ to direct a Th-2 response while not inducing a Th-1 response, thus building on the lessons learned from the failure of the AN-1792 peptide vaccine.

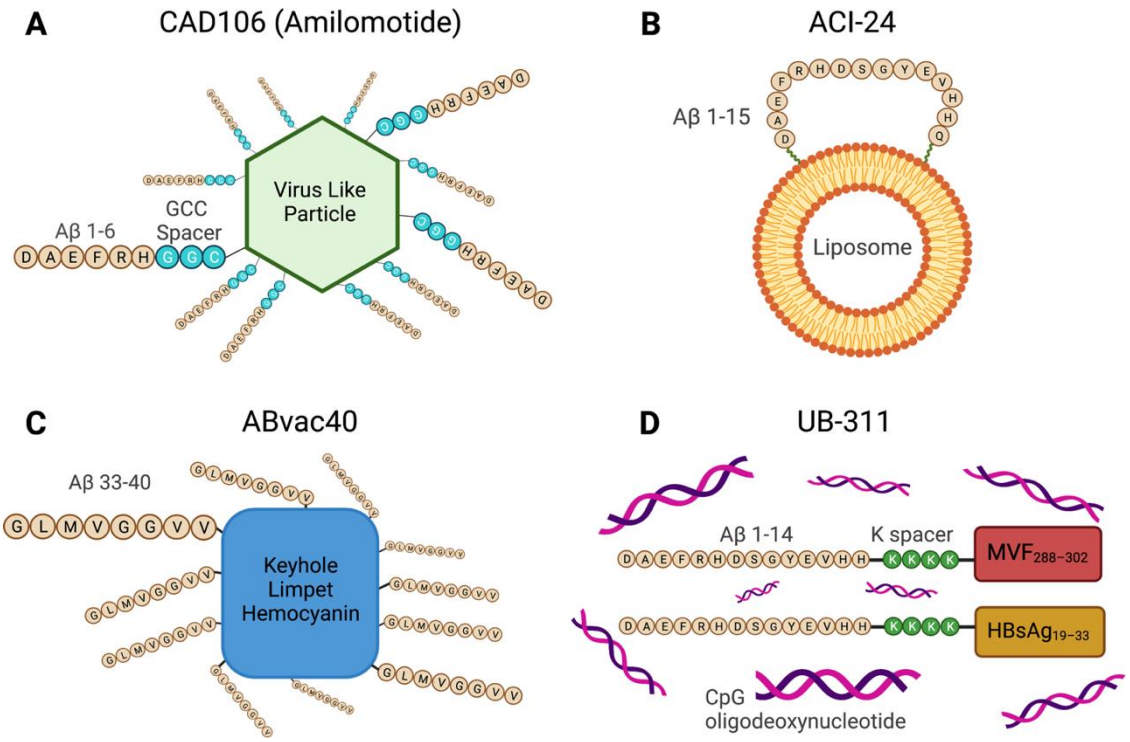

Figure 3.1. Four Aβ peptide vaccines that have advanced to phase II clinical trials. (**A**) CAD106, (**B**) ACI-24, (**C**) ABvac40, and (**D**) UB-311. The figure was designed by Chelsea Marie T. Parrocha and created with BioRender.com.

CAD-106 (Amilomotide: Novartis Pharmaceuticals) is the only AD peptide vaccine to enter phase II/III clinical trials. CAD-106 contains $A\beta_{1-6}$ followed by a three amino acid spacer (GGC) conjugated to an *E. coli* RNA phage Qβ virus-like particle (VLP) delivery system.[9] The VLP promotes multivalent antigen presentation of Aβ peptide fragments (**Figure 3.1 A**). The peptide vaccine was well tolerated and generated an immune response. In a phase IIB clinical trial, PET imaging studies showed a decrease of plaques in patients treated with CAD-106 for 78 weeks.[10] In a separate phase II/III clinical trial, the efficacy of CAD-106 was compared to a small-molecule inhibitor of beta-secretase-1 (BACE-1). Although no cases of meningoencephalitis with CAD-106 occurred,[7] the trial was ended prematurely because of adverse effects in the control (BACE-1) group and further development of CAD-106 was discontinued.[11,12]

ACI-24 (AC Immune) is designed to avoid eliciting a Th-1 response to Aβ. ACI-24 is made from $A\beta_{1-15}$ anchored to a liposome by tetra-palmitoylated lysine followed by a polyethylene glycol spacer on each end which allows anchoring to liposomes (**Figure 3.1 B**).[13] This liposome peptide delivery system, termed a SupraAntigen platform, was developed by AC Immune.[14] CD spectroscopy established that the anchored peptide adopts an ordered β-sheet conformation and thus indicates that the antigen is conformationally defined.[13] In 2016, ACI-24 was the first Aβ peptide vaccine used against AD in Down syndrome.[15] Although a phase II clinical trial was scheduled to be completed in 2024, the trial was withdrawn in 2021 to continue optimizing vaccine formulation and improve study design.[15,16]

ABvac40 (Axon Neuroscience SE) is designed to target the *C*-terminus of $A\beta_{1-40}$. $A\beta_{1-40}$ is the predominant alloform of Aβ, and elevated levels of $A\beta_{40}$ are correlated with AD severity.[17] This peptide vaccine contains $A\beta_{33-40}$ conjugated with the carrier protein keyhole limpet

hemocyanin (KLH) (**Figure 3.1 C**) . In a phase I clinical trial, 11 out of 12 immunized patients produced antibodies against $A\beta_{1-40}$. None of the patients developed amyloid-related imaging abnormalities (ARIA), involving edema (ARIA-E), microhemorrhage (ARIA-H), or other signs of brain pathology.[17] A phase II clinical trial is currently ongoing and is expected to be completed by the end of 2022.[18]

UB-311 (Vaxxinity) targets the *N*-terminus of Aβ and is made with the UBITh platform technology developed by United Biomedical.[19,20] UB-311 contains a mixture of two different $A\beta_{1-14}$ peptide antigens, both designed to induce a helper T-cell response (**Figure 3.1 D**).[21] In one, $A\beta_{1-14}$ is linked to measles virus fusion protein ($MVF_{288-302}$); in the other, $A\beta_{1-14}$ is linked to the surface antigen from a hepatitis B virus ($HBsAg_{19-33}$). These peptide conjugates are mixed with polyanionic CpG oligodeoxynucleotide to form micron-sized immunostimulatory complexes and then with the Adju-Phos adjuvant to create a Th-2 biased peptide vaccine.[21] In phase I, IIA, and IIB clinical trials, patients treated with UB-311 tolerated the peptide vaccine and did not show any signs of ARIA-E.[22] Although phase II clinical trials were terminated in 2019 due to a treatment design error, there are plans for an additional phase IIB clinical trial.[23,24]

Tau Peptide Vaccines

Tau peptide vaccines were developed in response to the discouraging outcomes of earlier Aβ peptide vaccines and immunotherapies. The AN-1792 peptide vaccine showed modest clearance of tau and immunotherapies that target Aβ failed to significantly alter cerebrospinal fluid (CSF) levels of tau.[4] Preclinical studies have focused on developing tau peptide vaccines against pathological forms of tau. However, identifying epitopes that produce therapeutic antibodies specific to pathological forms of tau remains challenging. **Figure 3.2** summarizes the two tau

peptide vaccine candidates tested in clinical trials (ACI-35 and AADvac1) and illustrates the regions of tau used as antigens and the means of antigen presentation.

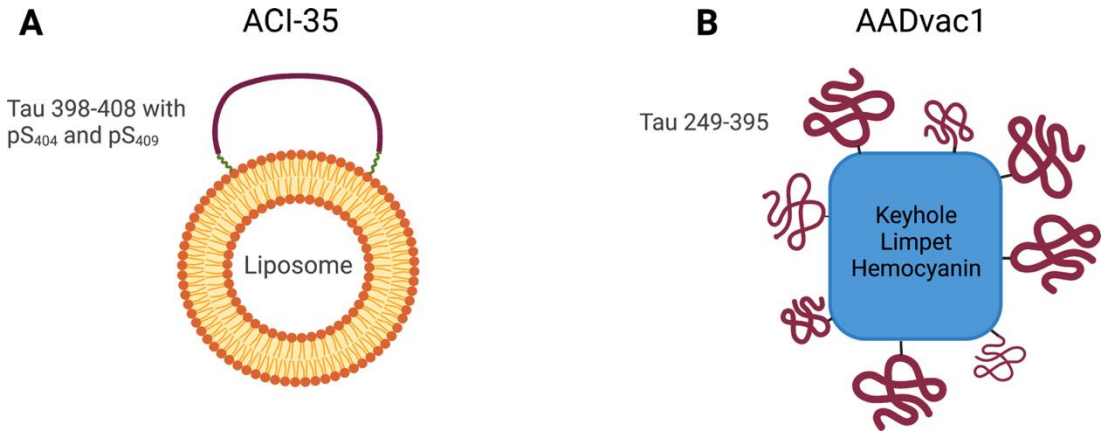

Figure 3.2. Two tau peptide vaccines that have advanced to phase II clinical trials. (**A**) ACI-35, (**B**) AADvac1. The figure was designed by Chelsea Marie T. Parrocha and created with BioRender.com.

One of the first tau peptide vaccines was created by Asuni and co-workers in 2007 and was tested in an AD tau mouse model.[25] The vaccine consists of $tau_{393–408}$ with phosphorylated serine at positions 396 and 404 in Adju-Phos adjuvant. P301 transgenic AD mice immunized with the vaccine showed decreased aggregated tau in the brain, increased anti-tau antibody titers, and slowed cognitive decline. The same peptide epitope was then used to create the ACI-35 vaccine, which is one of only two tau peptide vaccines to enter clinical trials.[25] This tau peptide vaccine was created with the same liposome-based vaccine technology used to make ACI-24.[26]

In ACI-35 (AC Immune and Janssen), AC Immune's SupraAntigen platform takes the phosphorylated $tau_{398–408}$ peptide and flanks the peptide by pairs of lipid-bearing lysine residues thus anchoring the peptide to the liposome (**Figure 3.2 A**). CD spectroscopy established that the anchored peptide adopts an ordered β-sheet conformation and thus indicates that the antigen is conformationally defined.[27] Phase IB clinical trials in 2013 tested AC1-35 for safety, tolerability, and therapeutic efficacy. The vaccine formulation elicited only a weak immune response, even

with the administration of booster shots.[27,28] An improved formulation of the vaccine was subsequently designed, ACI-35.030, with a second adjuvant and helper T-cell epitopes. The ACI-35.030 vaccine provided increased immune response in rhesus monkeys. Phase IB/IIA clinical trials began in August 2019, and results thus show high titers and antibodies specific for phosphorylated tau and aggregated tau.[29,30]

AADvac1 (Axon Neuroscience) was inspired by epitopes recognized by the tau antibody, DC8E8.[31,32,33] Epitope mapping studies, competition assays, and X-ray crystallography revealed that DC8E8 binds to the amino acid sequence HXPGGG, which is found in the microtubule binding region of the 3R and 4R tau isoforms.[4] In AADvac1, $tau_{294–395}$ of the microtubule binding region is conjugated to KLH and formulated with Adju-Phos adjuvant (**Figure 3.2 B**).[34] Tau transgenic rats that were immunized with AADvac1 exhibited a Th-2 immune response and high levels of anti-tau antibodies. In 2013 phase I clinical trial, patients developed titers against AADvac1 and had no signs of brain inflammation.[35,36] Phase II clinical trials ended in 2019 and assessed for long-term safety, tolerability, and efficacy in patients.[37,38] AADvac1 was safe and well-tolerated but did not demonstrate improvement in cognitive impairment.[39]

β-Amyloid Immunotherapies

Two decades of effort have led to the controversial FDA approval of the Aβ monoclonal antibody Aducanumab (Aduhelm), which has subsequentially sparked the revival of three additional monoclonal antibodies against Aβ (Gantenerumab, Solanezumab, and Crenezumab) that were previously terminated in the drug pipeline. Two additional anti-Aβ monoclonal antibodies, Donanemab and Lecanemab, are now in phase III clinical trials. **Figure 3.3** illustrates the antigen that was used to generate each of these monoclonal antibodies. Additional details are summarized in **Table S3.2**.

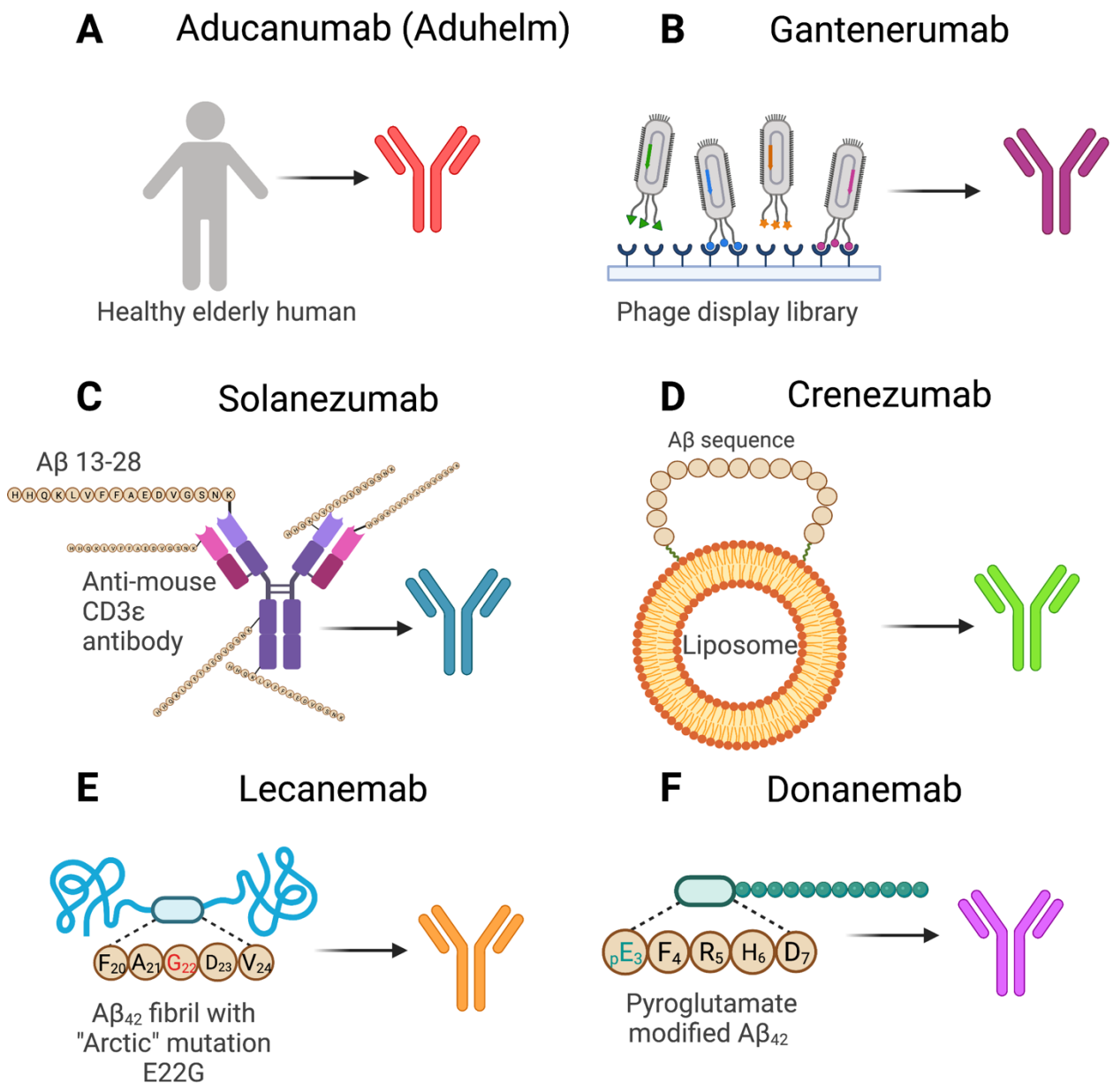

Figure 3.3. Derivation of six Aβ immunotherapies. (**A**) Aducanumab, (**B**) Gantenerumab, (**C**) Solanezumab, (**D**) Crenezumab, (**E**) Lecanemab, and (**F**) Donanemab. The figure was designed by Chelsea Marie T. Parrocha and created with BioRender.com.

Aducanumab (Aduhelm: Biogen, Eisai, Neurimmune) was derived from B-cells of healthy elderly donors that display antibodies that recognize aggregated Aβ (**Figure 3.3 A**), and its discovery was driven by the rationale that the cognitively normal patients had antibodies that could benefit AD patients.[40] The FDA approved Aducanumab in June 2021 as the first drug in its class

to treat AD.[41] The approval was controversial, because Aducanumab had only marginal effects on cognitive impairment despite clearing plaques, and because it displayed side effects in a large percentage of patients (ARIA, confusion, dizziness, nausea, and headache).[42,43,44,45,46] For these reasons, Aducanumab has not been widely adopted as a treatment for AD and has been rejected by many medical providers,[47] insurance companies,[48,49] and international drug and regulatory agencies.[50] Biogen plans to submit a final protocol to perform phase IV clinical trials for FDA review. The approval of Aducanumab has revived previously terminated monoclonal antibodies and reinvigorated efforts to develop immunotherapies against AD.[51]

Gantenerumab (Roche and Chugai Pharmaceutical) was generated to target and sequester Aβ plaques by stimulating microglia to clear Aβ through phagocytosis. Gantenerumab was created from a synthetic human antibody phage display library and *in vitro* maturation on Aβ fibrils (**Figure 3.3 B**).[52] In October 2021, the FDA granted accelerated development and review in a fashion similar to Aducanumab.[53] Two active phase III clinical trials[54,55] and one phase II[56] clinical trial are currently underway to assess the efficacy of Gantenerumab, with the phase II clinical trial and one of the phase III clinical trials[55] assessing in prodromal or mild AD patients. Two open-label phase III clinical trials are actively recruiting patients and are expected to end in 2024[57] and 2026.[58] Washington University in St. Louis has initiated a collaboration with Roche to test Gantenerumab on patients with mutations that cause AD at as young as 30 years old, making it the first monoclonal antibody to be tested in such a young demographic of patients.[59]

Solanezumab (Eli Lilly) is a humanized IgG1 monoclonal antibody against Aβ that was derived from a murine precursor raised against the central region of Aβ. The murine antibody was generated by immunizing mice with $A\beta_{13\text{-}28}$ conjugated to an anti-mouse CD3ε antibody using the heterobifunctional crosslinker MBS and formulated in Freund's complete adjuvant (**Figure 3.3**

C).[60] Although four phase III clinical trials were completed in 2012[61,62] and terminated in 2017,[63,64] one phase III clinical trial assessing the efficacy in slowing plaque production and cognitive impairment will be completed in 2023.[68] Phase II/III clinical studies comparing the efficacy of Gantenerumab and Solanezumab showed that these monoclonal antibodies failed to reverse cognitive impairment.[69] Despite these previous results, another trial is recruiting patients and is expected to be completed in 2022.[70]

Crenezumab (Genentech and Roche) is a humanized IgG4 antibody selected to target Aβ while preventing over-activation of microglia-mediated brain inflammation.[65] Crenezumab was generated by immunizing AD transgenic mice with an Aβ peptide displayed on AC Immune's SupraAntigen platform (**Figure 3.3 D**).[65,13,27] Three phase III clinical trials were terminated in 2019 because interim analysis suggested that the treatment was unlikely to meet clinical endpoints.[66,67,68,69] Current efforts in accessing the therapeutic potential of Crenezumab have shifted to patients with familial AD. A phase II clinical trial evaluating the safety and efficacy of Crenezumab in familial AD patients began in 2013 and is expected to be completed in 2022.[70] A subsequent phase II clinical trial using PET imaging to access for tau burden in treated patients was initiated in 2019. This study is continuing to recruit patients and is planned to be completed by March 2022.[71]

Lecanemab (Biogen, Eisai, and BioArctic) is an IgG1 monoclonal antibody against Aβ that was derived from a murine antibody generated against the "Arctic" mutation E22G of Aβ, which leads to high levels of fibrils without plaque deposition.[72,73,74,75] The murine antibody was created by immunizing mice with E22G Aβ fibrils in Freund's complete adjuvant (**Figure 3.3 E**).[75] In a phase IIB clinical trial, which is expected to be completed by 2025[76], treatment reduced 93% of plaques and slowed cognitive decline by 27–56%, as assessed by multiple statistical models.[77] A

phase III clinical trial is ongoing accessing safety and efficacy in patients with early AD and is expected to end in 2024.[78] Two weeks after the FDA approval of Aducanumab, the FDA granted accelerated approval of Lecanemab in early AD.[79] The FDA subsequently granted "Fast Track Designation" to further expedite development.[80] Phase II/III clinical trials are currently assessing patients with familial AD receiving either the Aβ antibody Lecanemab or the tau antibody E2814 and are expected to end October 2027.[81,82]

Donanemab (Eli Lilly) is the humanized IgG1 monoclonal antibody of a murine antibody that was developed to specifically target existing Aβ plaques, rather than prevent plaque development. In contrast to previous Aβ monoclonal antibodies, the mice were immunized with a pyroglutamate form of Aβ found in aggregated Aβ ($Aβ_{p3-42}$ peptide, **Figure 3.3 F**).[83] Donanemab is currently in a phase III clinical trial assessing AD patients with prodromal to mild AD[84] and has been granted accelerated approval, in a fashion similar to Aducanumab and Lecanemab.[85] Two additional phase III clinical trials are recruiting patients, with one trial treating patients at risk of cognitive decline with AD[86] and the other comparing plaque clearance in patients treated either with Donanemab or Aducanumab.[87]

Tau Immunotherapies

Monoclonal antibody immunotherapies against tau are starting to show promise in treating AD, with four notable examples in or about to be in phase II clinical trials (Semorinemab, JNJ-63733657, E2814, and Bepranemab). **Figure 3.4** illustrates the antigen that was used to generate each of these monoclonal antibodies. Additional details are summarized in **Supplemental Table S3.3**

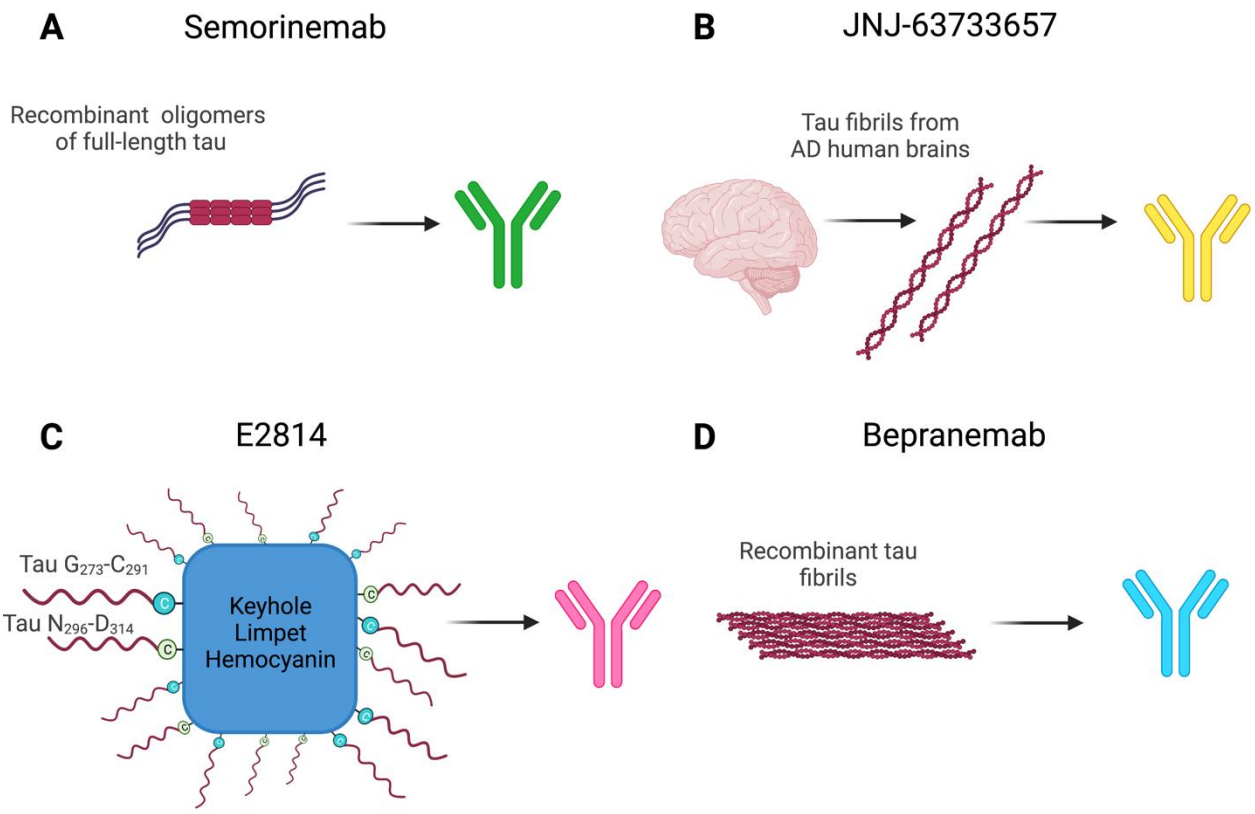

Figure 3.4. Derivation of four tau immunotherapies. (**A**) Semorinemab, (**B**) JNJ-63733657, (**C**) E2814, and (**D**) Bepranemab. The figure was designed by Chelsea Marie T. Parrocha and created with BioRender.com.

Semorinemab (AC Immune SA, Genentech, and Roche) is a humanized IgG4 antibody against tau that was designed to reduce microglia-mediated brain inflammation though mutation of the Fc region. Its murine precursor was derived from oligomers generated from recombinant full-length human tau isoform 2N4R (**Figure 3.4 A**).[88,89] In a 2017 phase II clinical trial, 0.3% of Semorinemab was found to enter the CSF, and the concentration of *N*-terminal tau in the CSF increased, suggesting that the antibody was targeting tau.[90,91] Nevertheless, Semorinemab did not decrease markers of neurodegeneration and inflammation.[95] The launch of a phase III clinical trial is pending on results from a separate 2019 phase II clinical study that will be completed in 2023.[92]

JNJ-63733657 (Janssen) is a humanized IgG1 monoclonal antibody that was selected for targeting the microtubule-binding region of tau and disrupting cell-to-cell propagation of aggregated tau.[93,73] Its murine precursor was derived by immunizing mice with tau paired-helical filaments isolated from AD human brain (**Figure 3.4 B**).[81,98] JNJ-63733657 was tested in two phase I clinical trials. The 2017 phase I clinical trial reported the monoclonal antibody to be safe and well tolerated. The 2019 phase I clinical trial reported ~0.2% of JNJ-63733657 entering into the CSF and a dose-dependent reduction of pS_{217} tau.[94] A phase II clinical trial began in January 2021 and is expected to run until 2025.[95]

E2814 (Eisai) is a humanized IgG1 monoclonal antibody that was selected for its affinity to the microtubule binding region of tau.[96] Its murine precursor was generated by immunizing transgenic mice with two 19-mer peptide fragments from the 4R tau isoform that is essential for tau seeding and aggregation. The fragments (G_{273}–C_{291} and N_{296}–D_{314} with an *N*-terminal cysteine) contain the R2 and R3 repeats and are designed to present key epitopes and to co-assemble and thus minimize further aggregation. The fragments were conjugated to KLH and administered with Freund's complete adjuvant (**Figure 3.4 C**).[96] A phase I clinical trial began in December 2019 and is expected to be completed in November 2022.[97] A phase I/II clinical trial began in June 2021 and is currently recruiting patients.[98]

Bepranemab (UCB Biopharma SRL) is a humanized IgG4 monoclonal antibody selected for its efficacy in blocking human tau seeds *in vitro* and was generated by immunizing Sprague–Dawley rats with fibrils of recombinant tau (**Figure 3.4 D**).[25,99] Bepranemab was originally tested in phase I clinical trials for safety, tolerability, and efficacy against progressive supranuclear palsy.[100,101] It is now being tested in a phase II clinical trial for AD, which is expected to be completed in 2025.[102]

Conclusion and Perspective

More than two decades of effort to develop peptide vaccines and monoclonal antibody immunotherapies that target Aβ and tau have revealed that there is much left to be explored to create safe and effective peptide vaccines and immunotherapies against AD. Although peptide vaccines may hold the ultimate promise of being widely administered to prevent AD, their development has proven challenging because of adverse reactions such as ARIA. Immunotherapies are currently showing the most immediate promise in spite of being costly and requiring repeated intravenous administration. Aducanumab currently costs $56,000 per year,[48,49] requires high dosing (10 mg/kg) every 4 weeks,[103] has marginal efficacy, and risks inducing ARIA. It is now thought that beginning treatment early is important for slowing or preventing the decline associated with AD.[104] For this reason, some of the current clinical trials are focusing on patients with mild or prodromal AD. Other clinical trials have focused on younger patients who are at risk of familial AD[59] or who have Down syndrome.[15]

A major limitation of the immunotherapies that have been developed thus far is that antibodies do not easily cross the blood-brain barrier and only small amounts (<1%) of the antibodies administered enter the brain. New technology for antibody delivery to the brain may allow the development of more efficacious immunotherapies. Antibodies that bind to the transferrin receptor can cross the blood-brain barrier by transcytosis, binding to the transferrin receptor and then being transported across the epithelial cells lining blood vessels in the brain.[105] Roche has thus created a derivative of Gantenerumab (RO7126209) that enters the CSF with eightfold greater efficacy by conjugating Gantenerumab to a Fab fragment that binds to the transferrin receptor. In phase I clinical trials, this bioconjugate showed no signs of inducing ARIA.[106] Phase IB/IIA clinical trials are ongoing and are expected to be completed by 2024.[107]

Other approaches to targeting the transferrin receptor for improved transport of antibodies have also been developed.[128]

Additional improvements in immunotherapies may emerge. Apolipoprotein E (APOE) is another promising target for monoclonal antibody immunotherapies in AD that has begun to be explored in preclinical trials.[108,109,110] Combination therapies involving multiple immunotherapies or immunotherapies in combination with other drugs are also being explored.[111,81]

Even if monoclonal antibody immunotherapies become safer and more efficacious, it is unlikely that they will be widely administered at an early enough age to prevent AD, because they will likely require repeated intravenous administration starting in middle age. In this sense, immunotherapies are unlikely to ever be used widely, like drugs for high blood pressure or high cholesterol. Nevertheless, monoclonal antibody immunotherapies are likely to continue to be developed, we hope with increased efficacy. In the long run, we hope that safe and efficacious peptide vaccines can be created for prophylaxis in the broad population of middle-aged adults.

Patients receiving Aβ peptide vaccines are typically immunized with the *N*-terminus of Aβ because it is a B-cell epitope. Although the middle region of Aβ, between residues 16 and 32, has been avoided out of concerns that it can induce a Th-1 response, it deserves further study, particularly as the development of Th-2 biased vaccine formulations continues to advance.[3] This region of Aβ can present unique peptide epitopes in loop-like conformations when folded into β-hairpins, which are thought to make up the toxic amyloid oligomers associated with neurodegeneration.[112–114] Peptide vaccines containing the middle region of Aβ in β-hairpin conformations may thus lead to conformation-specific antibodies with potential to bind and detoxify these amyloid oligomers. The epitopes presented by this region of Aβ should be distinct

from those presented by the *N*-terminal region of Aβ, which can also fold into a β-hairpin-like structure. [115-119]

Much work also remains to be done in the development of tau vaccines, because there are a multitude of different hyperphosphorylated tau epitopes that need to be explored.[120] Tau contains more than 80 potential sites of phosphorylation on serine, threonine, and tyrosine residues,[121] which create a daunting challenge in selecting and exploring biologically relevant antigens.[122–124] Exploration of these antigens may ultimately provide a better molecular understanding of AD, which can further guide peptide vaccine and monoclonal antibody immunotherapy development.

ACKNOWLEDGMENTS

We thank the National Institutes of Health (NIH) and National Institute on Aging (NIA) for funding (AG062296) for funding support. Figures were created with BioRender.com.

CONFLICTS OF INTEREST

James S. Nowick serves as an Advisory Board member of Peptide Science, and was excluded from both the peer-review process and all editorial decisions related to the publication of this article. We have no additional conflicts of interest.

References

(1) 2021 Alzheimer's Disease Facts and Figures. *Alzheimer's & dementia : the journal of the Alzheimer's Association* **2021**, *17* (3), 327–406. https://doi.org/10.1002/ALZ.12328.

(2) Masters, C. L.; Bateman, R.; Blennow, K.; Rowe, C. C.; Sperling, R. A.; Cummings, J. L. Alzheimer's Disease. *Nat Rev Dis Primers* **2015**, *1* (1), 1–18. https://doi.org/10.1038/nrdp.2015.56.

(3) Marciani, D. J. A Retrospective Analysis of the Alzheimer's Disease Vaccine Progress – The Critical Need for New Development Strategies. *Journal of Neurochemistry* **2016**, *137* (5), 687–700. https://doi.org/10.1111/jnc.13608.

(4) Congdon, E. E.; Sigurdsson, E. M. Tau-Targeting Therapies for Alzheimer Disease. *Nat Rev Neurol* **2018**, *14* (7), 399–415. https://doi.org/10.1038/s41582-018-0013-z.

(5) Schenk, D.; Barbour, R.; Dunn, W.; Gordon, G.; Grajeda, H.; Guido, T.; Hu, K.; Huang, J.; Johnson-Wood, K.; Khan, K.; Kholodenko, D.; Lee, M.; Liao, Z.; Lieberburg, I.; Motter, R.; Mutter, L.; Soriano, F.; Shopp, G.; Vasquez, N.; Vandevert, C.; Walker, S.; Wogulis, M.; Yednock, T.; Games, D.; Seubert, P. Immunization with Amyloid-β Attenuates Alzheimer-Disease-like Pathology in the PDAPP Mouse. *Nature* **1999**, *400* (6740), 173–177. https://doi.org/10.1038/22124.

(6) Gallardo, G.; Holtzman, D. M. Antibody Therapeutics Targeting Aβ and Tau. *Cold Spring Harb Perspect Med* **2017**, *7* (10), a024331. https://doi.org/10.1101/cshperspect.a024331.

(7) Mantile, F.; Prisco, A. Vaccination against β-Amyloid as a Strategy for the Prevention of Alzheimer's Disease. *Biology* **2020**, *9* (12), 425. https://doi.org/10.3390/biology9120425.

(8) Nicoll, J. A. R.; Buckland, G. R.; Harrison, C. H.; Page, A.; Harris, S.; Love, S.; Neal, J. W.; Holmes, C.; Boche, D. Persistent Neuropathological Effects 14 Years Following Amyloid-β

Immunization in Alzheimer's Disease. *Brain* **2019**, *142* (7), 2113–2126. https://doi.org/10.1093/brain/awz142.

(9) Wiessner, C.; Wiederhold, K.-H.; Tissot, A. C.; Frey, P.; Danner, S.; Jacobson, L. H.; Jennings, G. T.; Lüönd, R.; Ortmann, R.; Reichwald, J.; Zurini, M.; Mir, A.; Bachmann, M. F.; Staufenbiel, M. The Second-Generation Active Aβ Immunotherapy CAD106 Reduces Amyloid Accumulation in APP Transgenic Mice While Minimizing Potential Side Effects. *J Neurosci* **2011**, *31* (25), 9323–9331. https://doi.org/10.1523/JNEUROSCI.0293-11.2011.

(10) Vandenberghe, R.; Riviere, M.-E.; Caputo, A.; Sovago, J.; Maguire, R. P.; Farlow, M.; Marotta, G.; Sanchez-Valle, R.; Scheltens, P.; Ryan, J. M.; Graf, A. Active Aβ Immunotherapy CAD106 in Alzheimer's Disease: A Phase 2b Study. *Alzheimers Dement (N Y)* **2016**, *3* (1), 10–22. https://doi.org/10.1016/j.trci.2016.12.003.

(11) Huang, L.-K.; Chao, S.-P.; Hu, C.-J. Clinical Trials of New Drugs for Alzheimer Disease. *Journal of Biomedical Science* **2020**, *27* (1), 18. https://doi.org/10.1186/s12929-019-0609-7.

(12) Novartis Pharmaceuticals. *A Randomized, Double-Blind, Placebo-Controlled, Two-Cohort, Parallel Group Study to Evaluate the Efficacy of CAD106 and CNP520 in Participants at Risk for the Onset of Clinical Symptoms of Alzheimer's Disease.*; Clinical trial registration results/NCT02565511; clinicaltrials.gov, 2021. https://clinicaltrials.gov/ct2/show/results/NCT02565511 (accessed 2022-02-22).

(13) Muhs, A.; Hickman, D. T.; Pihlgren, M.; Chuard, N.; Giriens, V.; Meerschman, C.; van der Auwera, I.; van Leuven, F.; Sugawara, M.; Weingertner, M.-C.; Bechinger, B.; Greferath, R.; Kolonko, N.; Nagel-Steger, L.; Riesner, D.; Brady, R. O.; Pfeifer, A.; Nicolau, C. Liposomal Vaccines with Conformation-Specific Amyloid Peptide Antigens Define

Immune Response and Efficacy in APP Transgenic Mice. *Proceedings of the National Academy of Sciences* **2007**, *104* (23), 9810–9815. https://doi.org/10.1073/pnas.0703137104.

(14) *AC Immune | Technology platforms*. https://www.acimmune.com/en/technology-platforms/ (accessed 2022-02-24).

(15) AC Immune SA. *A Phase 2 Double-Blind, Randomized, Placebo-Controlled Study to Assess the Safety, Tolerability and Target Engagement of ACI-24 in Adults With Down Syndrome*; Clinical trial registration study/NCT04373616; clinicaltrials.gov, 2021. https://clinicaltrials.gov/ct2/show/study/NCT04373616 (accessed 2022-02-22).

(16) Department of Psychiatry and Psychotherapy, University Medical Center (UMG), Georg-August-University, Goettingen, Germany; Zampar, S.; Wirths, O.; Department of Psychiatry and Psychotherapy, University Medical Center (UMG), Georg-August-University, Goettingen, Germany. Immunotherapy Targeting Amyloid-β Peptides in Alzheimer's Disease. In *Alzheimer's Disease: Drug Discovery*; Neurochemistry Laboratory, Department of Psychiatry, Massachusetts General Hospital and Harvard Medical School, Charlestown, MA, USA, Huang, X., Eds.; Exon Publications, 2020; pp 23–49. https://doi.org/10.36255/exonpublications.alzheimersdisease.2020.ch2.

(17) Lacosta, A.-M.; Pascual-Lucas, M.; Pesini, P.; Casabona, D.; Pérez-Grijalba, V.; Marcos-Campos, I.; Sarasa, L.; Canudas, J.; Badi, H.; Monleón, I.; San-José, I.; Munuera, J.; Rodríguez-Gómez, O.; Abdelnour, C.; Lafuente, A.; Buendía, M.; Boada, M.; Tárraga, L.; Ruiz, A.; Sarasa, M. Safety, Tolerability and Immunogenicity of an Active Anti-Aβ40 Vaccine (ABvac40) in Patients with Alzheimer's Disease: A Randomised, Double-Blind, Placebo-Controlled, Phase I Trial. *Alzheimers Res Ther* **2018**, *10*, 12. https://doi.org/10.1186/s13195-018-0340-8.

(18) Araclon Biotech S.L. *A Multi-Center, Randomized, Double-Blind, Placebo-Controlled, 24 Months Study in Patients With Amnestic Mild Cognitive Impairment or Very Mild Alzheimer's Disease to Investigate the Safety, Tolerability and Immune Response of Repeated Subcutaneous Injections of ABvac40*; Clinical trial registration NCT03461276; clinicaltrials.gov, 2021. https://clinicaltrials.gov/ct2/show/NCT03461276 (accessed 2022-02-22).

(19) Sokoll, K. K. Stabilized Synthetic Immunogen Delivery System. US8088388B2, January 3, 2012. https://patents.google.com/patent/US8088388B2/en (accessed 2022-02-23).

(20) Wang, C. Y.; Walfield, A. M. Site-Specific Peptide Vaccines for Immunotherapy and Immunization against Chronic Diseases, Cancer, Infectious Diseases, and for Veterinary Applications. *Vaccine* **2005**, *23* (17), 2049–2056. https://doi.org/10.1016/j.vaccine.2005.01.007.

(21) Wang, C. Y.; Wang, P.-N.; Chiu, M.-J.; Finstad, C. L.; Lin, F.; Lynn, S.; Tai, Y.-H.; De Fang, X.; Zhao, K.; Hung, C.-H.; Tseng, Y.; Peng, W.-J.; Wang, J.; Yu, C.-C.; Kuo, B.-S.; Frohna, P. A. UB-311, a Novel UBITh® Amyloid β Peptide Vaccine for Mild Alzheimer's Disease. *Alzheimers Dement (N Y)* **2017**, *3* (2), 262–272. https://doi.org/10.1016/j.trci.2017.03.005.

(22) *Our Pipeline*. Vaxxinity. https://vaxxinity.com/our-pipeline/ (accessed 2022-02-23).

(23) United Neuroscience Ltd. *An Extension Study of a Phase IIa Study in Patients With Mild Alzheimer's Disease to Evaluate the Safety, Tolerability, Immunogenicity, and Efficacy of UBITh® AD Immunotherapeutic Vaccine (UB-311)*; Clinical trial registration NCT03531710; clinicaltrials.gov, 2021. https://clinicaltrials.gov/ct2/show/NCT03531710 (accessed 2022-02-22).

(24) Cowdell, P. Hi James - There Have Been 4 Clinical Trials, Conducted in Taiwan. For Details of the Completed Ph2 Study It Is Listed on Clinicaltrials.Gov (Https://Clinicaltrials.Gov/Ct2/Results?Term=Ub-311) and It Is Stated in Our S1 Filing That We Are Planning a Ph2b Study. Hope This Helps. Good Luck. Phil, 2022.

(25) Ji, C.; Sigurdsson, E. M. Current Status of Clinical Trials on Tau Immunotherapies. *Drugs* **2021**, *81* (10), 1135–1152. https://doi.org/10.1007/s40265-021-01546-6.

(26) Theunis, C.; Crespo-Biel, N.; Gafner, V.; Pihlgren, M.; López-Deber, M. P.; Reis, P.; Hickman, D. T.; Adolfsson, O.; Chuard, N.; Ndao, D. M.; Borghgraef, P.; Devijver, H.; Leuven, F. V.; Pfeifer, A.; Muhs, A. Efficacy and Safety of A Liposome-Based Vaccine against Protein Tau, Assessed in Tau.P301L Mice That Model Tauopathy. *PLOS ONE* **2013**, *8* (8), e72301. https://doi.org/10.1371/journal.pone.0072301.

(27) Hickman, D. T.; López-Deber, M. P.; Ndao, D. M.; Silva, A. B.; Nand, D.; Pihlgren, M.; Giriens, V.; Madani, R.; St-Pierre, A.; Karastaneva, H.; Nagel-Steger, L.; Willbold, D.; Riesner, D.; Nicolau, C.; Baldus, M.; Pfeifer, A.; Muhs, A. Sequence-Independent Control of Peptide Conformation in Liposomal Vaccines for Targeting Protein Misfolding Diseases*. *Journal of Biological Chemistry* **2011**, *286* (16), 13966–13976. https://doi.org/10.1074/jbc.M110.186338.

(28) *Active Tau Vaccine: Hints of Slowing Neurodegeneration | ALZFORUM*. https://www.alzforum.org/news/conference-coverage/active-tau-vaccine-hints-slowing-neurodegeneration (accessed 2022-02-23).

(29) *AC Immune Announces Interim Phase 1b/2a Data Showing that its ACI-35.030 Anti-pTau Alzheimer's Vaccine Generates a Potent Immune Response | AC Immune SA*.

https://ir.acimmune.com/news-releases/news-release-details/ac-immune-announces-interim-phase-1b2a-data-showing-its-aci (accessed 2022-02-23).

(30) AC Immune SA. *A Phase Ib/IIa Multicenter, Double-Blind, Randomized, Placebo-Controlled Study to Evaluate the Safety, Tolerability and Immunogenicity of Different Doses, Regimens and Combinations of Tau Targeted Vaccines in Subjects With Early Alzheimer's Disease*; Clinical trial registration NCT04445831; clinicaltrials.gov, 2021. https://clinicaltrials.gov/ct2/show/NCT04445831 (accessed 2022-02-22).

(31) Kontsekova, E.; Zilka, N.; Kovacech, B.; Skrabana, R.; Novak, M. Identification of Structural Determinants on Tau Protein Essential for Its Pathological Function: Novel Therapeutic Target for Tau Immunotherapy in Alzheimer's Disease. *Alzheimer's Research & Therapy* **2014**, *6* (4), 45. https://doi.org/10.1186/alzrt277.

(32) Ng, P. Y.; Chang, I. S.; Koh, R. Y.; Chye, S. M. Recent Advances in Tau-Directed Immunotherapy against Alzheimer's Disease: An Overview of Pre-Clinical and Clinical Development. *Metab Brain Dis* **2020**, *35* (7), 1049–1066. https://doi.org/10.1007/s11011-020-00591-6.

(33) Novak, P.; Zilka, N.; Zilkova, M.; Kovacech, B.; Skrabana, R.; Ondrus, M.; Fialova, L.; Kontsekova, E.; Otto, M.; Novak, M. AADvac1, an Active Immunotherapy for Alzheimer's Disease and Non Alzheimer Tauopathies: An Overview of Preclinical and Clinical Development. *J Prev Alzheimers Dis* **2019**, *6* (1), 63–69. https://doi.org/10.14283/jpad.2018.45.

(34) Kontsekova, E.; Zilka, N.; Kovacech, B.; Novak, P.; Novak, M. First-in-Man Tau Vaccine Targeting Structural Determinants Essential for Pathological Tau–Tau Interaction Reduces

Tau Oligomerisation and Neurofibrillary Degeneration in an Alzheimer's Disease Model. *Alzheimer's Research & Therapy* **2014**, *6* (4), 44. https://doi.org/10.1186/alzrt278.

(35) Axon Neuroscience SE. *A 3-Months Randomized, Placebo-Controlled, Parallel Group, Double-Blinded, Multi-Centre, Phase I Study to Assess Tolerability & Safety of AADvac1 Applied to Patients With Mild-Moderate Alzheimer's Disease With 3-Months Open Label Extension*; Clinical trial registration NCT01850238; clinicaltrials.gov, 2015. https://clinicaltrials.gov/ct2/show/NCT01850238 (accessed 2022-02-22).

(36) Novak, P.; Schmidt, R.; Kontsekova, E.; Zilka, N.; Kovacech, B.; Skrabana, R.; Vince-Kazmerova, Z.; Katina, S.; Fialova, L.; Prcina, M.; Parrak, V.; Dal-Bianco, P.; Brunner, M.; Staffen, W.; Rainer, M.; Ondrus, M.; Ropele, S.; Smisek, M.; Sivak, R.; Winblad, B.; Novak, M. Safety and Immunogenicity of the Tau Vaccine AADvac1 in Patients with Alzheimer's Disease: A Randomised, Double-Blind, Placebo-Controlled, Phase 1 Trial. *The Lancet Neurology* **2017**, *16* (2), 123–134. https://doi.org/10.1016/S1474-4422(16)30331-3.

(37) Axon Neuroscience SE. *A 24 Months Randomised, Placebo-Controlled, Parallel Group, Double Blinded, Multi Centre, Phase 2 Study to Assess Safety and Efficacy of AADvac1 Applied to Patients With Mild Alzheimer's Disease*; Clinical trial registration NCT02579252; clinicaltrials.gov, 2019. https://clinicaltrials.gov/ct2/show/NCT02579252 (accessed 2022-02-22).

(38) Ondrus, M.; Novak, P. Design of the Phase II Clinical Study of the Tau Vaccine AADvac1 in Patients with Mild Alzheimer's Disease. *Neurobiology of Aging* **2016**, *39*, S26. https://doi.org/10.1016/j.neurobiolaging.2016.01.115.

(39) Novak, P.; Kovacech, B.; Katina, S.; Schmidt, R.; Scheltens, P.; Kontsekova, E.; Ropele, S.; Fialova, L.; Kramberger, M.; Paulenka-Ivanovova, N.; Smisek, M.; Hanes, J.; Stevens,

E.; Kovac, A.; Sutovsky, S.; Parrak, V.; Koson, P.; Prcina, M.; Galba, J.; Cente, M.; Hromadka, T.; Filipcik, P.; Piestansky, J.; Samcova, M.; Prenn-Gologranc, C.; Sivak, R.; Froelich, L.; Fresser, M.; Rakusa, M.; Harrison, J.; Hort, J.; Otto, M.; Tosun, D.; Ondrus, M.; Winblad, B.; Novak, M.; Zilka, N. ADAMANT: A Placebo-Controlled Randomized Phase 2 Study of AADvac1, an Active Immunotherapy against Pathological Tau in Alzheimer's Disease. *Nat Aging* **2021**, *1* (6), 521–534. https://doi.org/10.1038/s43587-021-00070-2.

(40) Sevigny, J.; Chiao, P.; Bussière, T.; Weinreb, P. H.; Williams, L.; Maier, M.; Dunstan, R.; Salloway, S.; Chen, T.; Ling, Y.; O'Gorman, J.; Qian, F.; Arastu, M.; Li, M.; Chollate, S.; Brennan, M. S.; Quintero-Monzon, O.; Scannevin, R. H.; Arnold, H. M.; Engber, T.; Rhodes, K.; Ferrero, J.; Hang, Y.; Mikulskis, A.; Grimm, J.; Hock, C.; Nitsch, R. M.; Sandrock, A. The Antibody Aducanumab Reduces Aβ Plaques in Alzheimer's Disease. *Nature* **2016**, *537* (7618), 50–56. https://doi.org/10.1038/nature19323.

(41) Research, C. for D. E. and. FDA's Decision to Approve New Treatment for Alzheimer's Disease. *FDA* **2021**.

(42) Salloway, S.; Chalkias, S.; Barkhof, F.; Burkett, P.; Barakos, J.; Purcell, D.; Suhy, J.; Forrestal, F.; Tian, Y.; Umans, K.; Wang, G.; Singhal, P.; Budd Haeberlein, S.; Smirnakis, K. Amyloid-Related Imaging Abnormalities in 2 Phase 3 Studies Evaluating Aducanumab in Patients With Early Alzheimer Disease. *JAMA Neurol* **2022**, *79* (1), 13–21. https://doi.org/10.1001/jamaneurol.2021.4161.

(43) Knopman, D. S.; Jones, D. T.; Greicius, M. D. Failure to Demonstrate Efficacy of Aducanumab: An Analysis of the EMERGE and ENGAGE Trials as Reported by Biogen,

December 2019. *Alzheimer's & Dementia* **2021**, *17* (4), 696–701. https://doi.org/10.1002/alz.12213.

(44) Alexander, G. C.; Karlawish, J. The Problem of Aducanumab for the Treatment of Alzheimer Disease. *Ann Intern Med* **2021**, *174* (9), 1303–1304. https://doi.org/10.7326/M21-2603.

(45) Fleck, L. M. Alzheimer's and Aducanumab: Unjust Profits and False Hopes. *Hastings Center Report* **2021**, *51* (4), 9–11. https://doi.org/10.1002/hast.1264.

(46) Perlmutter, J. S. FDA's Green Light, Science's Red Light. *Science* **2021**, *372* (6549), 1371–1371. https://doi.org/10.1126/science.abk0575.

(47) *Doctors refuse to prescribe Biogen's Alzheimer's drug*. Fortune. https://fortune.com/2021/07/08/biogen-aduhelm-aducanumab-alzheimers-doctors-disapprove/ (accessed 2022-02-23).

(48) *Some Blues Plans Won't Cover New Alzheimer's Therapy Aduhelm*. Formulary Watch. https://www.formularywatch.com/view/some-blues-plans-won-t-cover-new-alzheimer-s-therapy-aduhelm (accessed 2022-02-23).

(49) *Doctors Remain Divided Over First Drug to Treat Alzheimer's, But Patients Are Eager to Try It*. Time. https://time.com/6081333/biogen-alzheimers-drug-aduhelm-fda-controversy/ (accessed 2022-02-23).

(50) Alzheimer's Drug Aducanumab Not Approved for Use in EU. *BBC News*. December 17, 2021. https://www.bbc.com/news/health-59699907 (accessed 2022-02-23).

(51) *Update on the Phase 4 Confirmatory Study of ADUHELM® | Biogen*. https://investors.biogen.com/news-releases/news-release-details/update-phase-4-confirmatory-study-aduhelmr (accessed 2022-02-23).

(52) Bohrmann, B.; Baumann, K.; Benz, J.; Gerber, F.; Huber, W.; Knoflach, F.; Messer, J.; Oroszlan, K.; Rauchenberger, R.; Richter, W. F.; Rothe, C.; Urban, M.; Bardroff, M.; Winter, M.; Nordstedt, C.; Loetscher, H. Gantenerumab: A Novel Human Anti-Aβ Antibody Demonstrates Sustained Cerebral Amyloid-β Binding and Elicits Cell-Mediated Removal of Human Amyloid-β. *Journal of Alzheimer's Disease* **2012**, *28* (1), 49–69. https://doi.org/10.3233/JAD-2011-110977.

(53) *Roche - Doing now what patients need next*. https://www.roche.com/investors/updates/inv-update-2021-10-08 (accessed 2022-02-23).

(54) Hoffmann-La Roche. *An Open-Label, Multicenter, Rollover Study to Evaluate the Safety and Tolerability of Long-Term Administration of Gantenerumab in Participants With Alzheimer's Disease*; Clinical trial registration NCT04339413; clinicaltrials.gov, 2022. https://clinicaltrials.gov/ct2/show/NCT04339413 (accessed 2022-02-22).

(55) Hoffmann-La Roche. *A Phase III, Multicenter, Randomized, Double-Blind, Placebo-Controlled, Parallel-Group, Efficacy, and Safety Study of Gantenerumab in Patients With Early (Prodromal to Mild) Alzheimer's Disease*; Clinical trial registration NCT03443973; clinicaltrials.gov, 2022. https://clinicaltrials.gov/ct2/show/NCT03443973 (accessed 2022-02-22).

(56) Hoffmann-La Roche. *A Phase II, Multicenter, Open-Label, Single Arm Study to Evaluate the Pharmacodynamic Effects of Once Weekly Administration of Gantenerumab in Participants With Early (Prodromal to Mild) Alzheimer's Disease*; Clinical trial registration NCT04592341; clinicaltrials.gov, 2022. https://clinicaltrials.gov/ct2/show/NCT04592341 (accessed 2022-02-22).

(57) Hoffmann-La Roche. *An Open-Label, Multicenter, Rollover Study to Evaluate the Safety, Tolerability, and Efficacy of Long-Term Gantenerumab Administration in Participants With Alzheimer's Disease*; Clinical trial registration NCT04374253; clinicaltrials.gov, 2022. https://clinicaltrials.gov/ct2/show/NCT04374253 (accessed 2022-02-22).

(58) Hoffmann-La Roche. *A Phase III, Multicenter, Randomized, Double-Blind, Placebo-Controlled, Parallel-Group, Efficacy, and Safety Study of Gantenerumab in Patients With Early (Prodromal to Mild) Alzheimer's Disease*; Clinical trial registration NCT03444870; clinicaltrials.gov, 2022. https://clinicaltrials.gov/ct2/show/NCT03444870 (accessed 2022-02-22).

(59) *New Alzheimer's prevention trial in young people*. Washington University School of Medicine in St. Louis. https://medicine.wustl.edu/news/new-alzheimers-prevention-trial-in-young-people/ (accessed 2022-02-23).

(60) Schlossmacher, M. G.; Selkoe, D. J. Methods of Screening for Compounds Which Inhibit Soluble β-Amyloid Peptide Production. US5766846A, June 16, 1998. https://patents.google.com/patent/US5766846A/en (accessed 2022-02-23).

(61) Eli Lilly and Company. *Effect of Passive Immunization on the Progression of Alzheimer's Disease: LY2062430 Versus Placebo*; Clinical trial registration NCT00904683; clinicaltrials.gov, 2012. https://clinicaltrials.gov/ct2/show/NCT00904683 (accessed 2022-02-22).

(62) Eli Lilly and Company. *Effect of LY2062430, an Anti-Amyloid Beta Monoclonal Antibody, on the Progression of Alzheimer's Disease as Compared With Placebo*; Clinical trial registration NCT00905372; clinicaltrials.gov, 2012. https://clinicaltrials.gov/ct2/show/NCT00905372 (accessed 2022-02-22).

(63) Eli Lilly and Company. *Continued Efficacy and Safety Monitoring of Solanezumab, an Anti-Amyloid β Antibody in Patients With Alzheimer's Disease*; Clinical trial registration NCT01127633; clinicaltrials.gov, 2019. https://clinicaltrials.gov/ct2/show/NCT01127633 (accessed 2022-02-22).

(64) Eli Lilly and Company. *Effect of Passive Immunization on the Progression of Mild Alzheimer's Disease: Solanezumab (LY2062430) Versus Placebo*; Clinical trial registration NCT01900665; clinicaltrials.gov, 2019. https://clinicaltrials.gov/ct2/show/NCT01900665 (accessed 2022-02-22).

(65) Adolfsson, O.; Pihlgren, M.; Toni, N.; Varisco, Y.; Buccarello, A. L.; Antoniello, K.; Lohmann, S.; Piorkowska, K.; Gafner, V.; Atwal, J. K.; Maloney, J.; Chen, M.; Gogineni, A.; Weimer, R. M.; Mortensen, D. L.; Friesenhahn, M.; Ho, C.; Paul, R.; Pfeifer, A.; Muhs, A.; Watts, R. J. An Effector-Reduced Anti-β-Amyloid (Aβ) Antibody with Unique Aβ Binding Properties Promotes Neuroprotection and Glial Engulfment of Aβ. *J. Neurosci.* **2012**, *32* (28), 9677–9689. https://doi.org/10.1523/JNEUROSCI.4742-11.2012.

(66) Hoffmann-La Roche. *A Phase III, Multicenter, Randomized, Double-Blind, Placebo-Controlled, Parallel-Group, Efficacy And Safety Study of Crenezumab in Patients With Prodromal to Mild Alzheimer's Disease.*; Clinical trial registration NCT02670083; clinicaltrials.gov, 2020. https://clinicaltrials.gov/ct2/show/NCT02670083 (accessed 2022-02-22).

(67) Hoffmann-La Roche. *A Phase III, Multicenter, Randomized, Double-Blind, Placebo-Controlled, Parallel-Group, Efficacy and Safety Study of Crenezumab in Patients With Prodromal to Mild Alzheimer's Disease*; Clinical trial registration NCT03114657;

clinicaltrials.gov, 2020. https://clinicaltrials.gov/ct2/show/NCT03114657 (accessed 2022-02-22).

(68) Hoffmann-La Roche. *A Multicenter, Open-Label, Long-Term Extension Of Phase III Studies (BN29552/BN29553) Of Crenezumab In Patients With Alzheimer's Disease*; Clinical trial registration NCT03491150; clinicaltrials.gov, 2020. https://clinicaltrials.gov/ct2/show/NCT03491150 (accessed 2022-02-22).

(69) *Roche - Doing now what patients need next.* https://www.roche.com/media/releases/med-cor-2019-01-30 (accessed 2022-02-23).

(70) Genentech, Inc. *A Double-Blind, Placebo-Controlled Parallel-Group Study in Preclinical PSEN1 E280A Mutation Carriers Randomized to Crenezumab or Placebo, and in Non-Randomized, Placebo-Treated Non-Carriers From the Same Kindred, to Evaluate the Efficacy and Safety of Crenezumab in the Treatment of Autosomal-Dominant Alzheimer's Disease*; Clinical trial registration NCT01998841; clinicaltrials.gov, 2021. https://clinicaltrials.gov/ct2/show/NCT01998841 (accessed 2022-02-22).

(71) Hoffmann-La Roche. *Tau PET Longitudinal Substudy Associated With: A Double-Blind, Placebo-Controlled Parallel-Group Study in Preclinical PSEN1 E280A Mutation Carriers Randomized to Crenezumab or Placebo, and in Non-Randomized, Placebo-Treated Non-Carriers From the Same Kindred, to Evaluate the Efficacy and Safety of Crenezumab in the Treatment of Autosomal-Dominant Alzheimer's Disease*; Clinical trial registration NCT03977584; clinicaltrials.gov, 2022. https://clinicaltrials.gov/ct2/show/NCT03977584 (accessed 2022-02-22).

(72) Tucker, S.; Möller, C.; Tegerstedt, K.; Lord, A.; Laudon, H.; Sjödahl, J.; Söderberg, L.; Spens, E.; Sahlin, C.; Waara, E. R.; Satlin, A.; Gellerfors, P.; Osswald, G.; Lannfelt, L. The

Murine Version of BAN2401 (MAb158) Selectively Reduces Amyloid-β Protofibrils in Brain and Cerebrospinal Fluid of Tg-ArcSwe Mice. *Journal of Alzheimer's Disease* **2015**, *43* (2), 575–588. https://doi.org/10.3233/JAD-140741.

(73) Plotkin, S. S.; Cashman, N. R. Passive Immunotherapies Targeting Aβ and Tau in Alzheimer's Disease. *Neurobiol Dis* **2020**, *144*, 105010. https://doi.org/10.1016/j.nbd.2020.105010.

(74) Nilsberth, C.; Westlind-Danielsson, A.; Eckman, C. B.; Condron, M. M.; Axelman, K.; Forsell, C.; Stenh, C.; Luthman, J.; Teplow, D. B.; Younkin, S. G.; Näslund, J.; Lannfelt, L. The "Arctic" APP Mutation (E693G) Causes Alzheimer's Disease by Enhanced Aβ Protofibril Formation. *Nat Neurosci* **2001**, *4* (9), 887–893. https://doi.org/10.1038/nn0901-887.

(75) Gellerfors, P. (54) ANTIBODIES SPECIFIC FOR SOLUBLE. 23.

(76) Eisai Inc. *A Placebo-Controlled, Double-Blind, Parallel-Group, Bayesian Adaptive Randomization Design and Dose Regimen-Finding Study With an Open-Label Extension Phase to Evaluate Safety, Tolerability and Efficacy of BAN2401 in Subjects With Early Alzheimer's Disease*; Clinical trial registration NCT01767311; clinicaltrials.gov, 2021. https://clinicaltrials.gov/ct2/show/NCT01767311 (accessed 2022-02-22).

(77) Swanson, C. J.; Zhang, Y.; Dhadda, S.; Wang, J.; Kaplow, J.; Lai, R. Y. K.; Lannfelt, L.; Bradley, H.; Rabe, M.; Koyama, A.; Reyderman, L.; Berry, D. A.; Berry, S.; Gordon, R.; Kramer, L. D.; Cummings, J. L. A Randomized, Double-Blind, Phase 2b Proof-of-Concept Clinical Trial in Early Alzheimer's Disease with Lecanemab, an Anti-Aβ Protofibril Antibody. *Alzheimer's Research & Therapy* **2021**, *13* (1), 80. https://doi.org/10.1186/s13195-021-00813-8.

(78) Eisai Inc. *A Placebo-Controlled, Double-Blind, Parallel-Group, 18-Month Study With an Open-Label Extension Phase to Confirm Safety and Efficacy of BAN2401 in Subjects With Early Alzheimer's Disease*; Clinical trial registration NCT03887455; clinicaltrials.gov, 2021. https://clinicaltrials.gov/ct2/show/NCT03887455 (accessed 2022-02-22).

(79) *EISAI and Biogen Inc. Announce U.S. FDA Grants Breakthrough Therapy Designation for LECANEMAB (BAN2401), an Anti-Amyloid Beta Protofibril Antibody for the Treatment of Alzheimer's Disease | Biogen*. https://investors.biogen.com/news-releases/news-release-details/eisai-and-biogen-inc-announce-us-fda-grants-breakthrough-therapy (accessed 2022-02-23).

(80) *Investigational Alzheimer's Disease Therapy Lecanemab Granted FDA Fast Track Designation | Biogen*. https://investors.biogen.com/news-releases/news-release-details/investigational-alzheimers-disease-therapy-lecanemab-granted-fda (accessed 2022-02-23).

(81) *FIRST SUBJECT ENROLLED IN PHASE II/III STUDY OF EISAI'S ANTI-MTBR TAU ANTIBODY E2814 FOR DOMINANTLY INHERITED ALZHEIMER'S DISEASE (DIAD), CONDUCTED BY DIAN-TU | News Release : 2022 | Eisai Co., Ltd.* https://www.eisai.com/news/2022/news202205.html (accessed 2022-02-24).

(82) Washington University School of Medicine. *A Phase II/III Multicenter Randomized, Double-Blind, Placebo-Controlled Platform Trial of Potential Disease Modifying Therapies Utilizing Biomarker, Cognitive, and Clinical Endpoints in Dominantly Inherited Alzheimer's Disease*; Clinical trial registration NCT05269394; clinicaltrials.gov, 2022. https://clinicaltrials.gov/ct2/show/NCT05269394 (accessed 2022-03-08).

(83) DeMattos, R. B.; Lu, J.; Tang, Y.; Racke, M. M.; DeLong, C. A.; Tzaferis, J. A.; Hole, J. T.; Forster, B. M.; McDonnell, P. C.; Liu, F.; Kinley, R. D.; Jordan, W. H.; Hutton, M. L. A Plaque-Specific Antibody Clears Existing β-Amyloid Plaques in Alzheimer's Disease Mice. *Neuron* **2012**, *76* (5), 908–920. https://doi.org/10.1016/j.neuron.2012.10.029.

(84) Eli Lilly and Company. *Assessment of Safety, Tolerability, and Efficacy of Donanemab in Early Symptomatic Alzheimer's Disease*; Clinical trial registration NCT04437511; clinicaltrials.gov, 2022. https://clinicaltrials.gov/ct2/show/NCT04437511 (accessed 2022-02-22).

(85) *Lilly Reports Robust Third-Quarter 2021 Financial Results as Pipeline Success Strengthens Future Growth Potential | Eli Lilly and Company*. https://investor.lilly.com/news-releases/news-release-details/lilly-reports-robust-third-quarter-2021-financial-results (accessed 2022-02-23).

(86) Eli Lilly and Company. *A Study of Donanemab Versus Placebo in Participants at Risk for Cognitive and Functional Decline of Alzheimer's Disease*; Clinical trial registration NCT05026866; clinicaltrials.gov, 2022. https://clinicaltrials.gov/ct2/show/NCT05026866 (accessed 2022-02-22).

(87) Eli Lilly and Company. *A Phase 3, Open-Label, Parallel-Group, 2-Arm Study to Investigate Amyloid Plaque Clearance With Donanemab Compared With Aducanumab-Avwa in Participants With Early Symptomatic Alzheimer's Disease*; Clinical trial registration NCT05108922; clinicaltrials.gov, 2022. https://clinicaltrials.gov/ct2/show/NCT05108922 (accessed 2022-02-22).

(88) Ayalon, G.; Lee, S.-H.; Adolfsson, O.; Foo-Atkins, C.; Atwal, J. K.; Blendstrup, M.; Booler, H.; Bravo, J.; Brendza, R.; Brunstein, F.; Chan, R.; Chandra, P.; Couch, J. A.;

Datwani, A.; Demeule, B.; DiCara, D.; Erickson, R.; Ernst, J. A.; Foreman, O.; He, D.; Hötzel, I.; Keeley, M.; Kwok, M. C. M.; Lafrance-Vanasse, J.; Lin, H.; Lu, Y.; Luk, W.; Manser, P.; Muhs, A.; Ngu, H.; Pfeifer, A.; Pihlgren, M.; Rao, G. K.; Scearce-Levie, K.; Schauer, S. P.; Smith, W. B.; Solanoy, H.; Teng, E.; Wildsmith, K. R.; Bumbaca Yadav, D.; Ying, Y.; Fuji, R. N.; Kerchner, G. A. Antibody Semorinemab Reduces Tau Pathology in a Transgenic Mouse Model and Engages Tau in Patients with Alzheimer's Disease. *Science Translational Medicine* **2021**, *13* (593), eabb2639. https://doi.org/10.1126/scitranslmed.abb2639.

(89) *US20210122811 ANTI-TAU ANTIBODIES AND METHODS OF USE*. https://patentscope.wipo.int/search/en/detail.jsf?docId=US322910423&_fid=US281655580 (accessed 2022-03-14).

(90) Genentech, Inc. *A Phase II, Multicenter, Randomized, Double-Blind, Placebo-Controlled, Parallel-Group, Efficacy, and Safety Study of MTAU9937A in Patients With Prodromal to Mild Alzheimer's Disease*; Clinical trial registration NCT03289143; clinicaltrials.gov, 2021. https://clinicaltrials.gov/ct2/show/NCT03289143 (accessed 2022-02-23).

(91) *N-Terminal Tau Antibodies Fade, Mid-Domain Ones Push to the Fore | ALZFORUM*. https://www.alzforum.org/news/conference-coverage/n-terminal-tau-antibodies-fade-mid-domain-ones-push-fore (accessed 2022-02-24).

(92) Genentech, Inc. *A Phase II, Multicenter, Randomized, Double-Blind, Placebo-Controlled, Parallel-Group, Efficacy, and Safety Study of MTAU9937A in Patients With Moderate Alzheimer's Disease*; Clinical trial registration NCT03828747; clinicaltrials.gov, 2022. https://clinicaltrials.gov/ct2/show/NCT03828747 (accessed 2022-02-23).

(93) Mercken, M.; Malia, T.; BORGERS, M.; KOLEN, K. V. Anti-Phf-Tau Antibodies and Uses Thereof. WO2018170351A1, September 20, 2018. https://patents.google.com/patent/WO2018170351A1/en (accessed 2022-02-24).

(94) Galpern, W. R.; Mercken, M.; Van Kolen, K.; Timmers, M.; Haeverans, K.; Janssens, L.; Triana-Baltzer, G.; Kolb, H. C.; Jacobs, T.; Nandy, P.; Malia, T.; Sun, H.; Van Nueten, L. P1-052: A Single Ascending Dose Study to Evaluate the Safety, Tolerability, Pharmacokinetics, and Pharmacodynamics of the Anti-Phospho-Tau Antibody Jnj-63733657 in Healthy Subjects. *Alzheimer's & Dementia* **2019**, *15* (7S_Part_5), P252–P253. https://doi.org/10.1016/j.jalz.2019.06.077.

(95) Janssen Research & Development, LLC. *A Randomized, Double-Blind, Placebo-Controlled, Parallel-Group, Multicenter Study to Assess the Efficacy and Safety of JNJ-63733657, an Anti-Tau Monoclonal Antibody, in Participants With Early Alzheimer's Disease*; Clinical trial registration NCT04619420; clinicaltrials.gov, 2022. https://clinicaltrials.gov/ct2/show/NCT04619420 (accessed 2022-02-23).

(96) Roberts, M.; Sevastou, I.; Imaizumi, Y.; Mistry, K.; Talma, S.; Dey, M.; Gartlon, J.; Ochiai, H.; Zhou, Z.; Akasofu, S.; Tokuhara, N.; Ogo, M.; Aoyama, M.; Aoyagi, H.; Strand, K.; Sajedi, E.; Agarwala, K. L.; Spidel, J.; Albone, E.; Horie, K.; Staddon, J. M.; de Silva, R. Pre-Clinical Characterisation of E2814, a High-Affinity Antibody Targeting the Microtubule-Binding Repeat Domain of Tau for Passive Immunotherapy in Alzheimer's Disease. *Acta Neuropathologica Communications* **2020**, *8* (1), 13. https://doi.org/10.1186/s40478-020-0884-2.

(97) Eisai Inc. *A Randomized, Double-Blind, Placebo-Controlled, Combined Single Ascending Dose and Multiple Ascending Dose Study to Assess Safety, Tolerability, Pharmacokinetics,*

Immunogenicity, and Pharmacodynamics of Intravenous Infusions of E2814 in Healthy Subjects; Clinical trial registration NCT04231513; clinicaltrials.gov, 2022. https://clinicaltrials.gov/ct2/show/NCT04231513 (accessed 2022-02-23).

(98) Eisai Inc. *An Open-Label Phase 1b/2 Study to Assess Safety and Target Engagement of E2814 in Subjects With Mild to Moderate Cognitive Impairment Due to Dominantly Inherited Alzheimer's Disease*; Clinical trial registration NCT04971733; clinicaltrials.gov, 2021. https://clinicaltrials.gov/ct2/show/NCT04971733 (accessed 2022-02-23).

(99) Courade, J.-P.; Angers, R.; Mairet-Coello, G.; Pacico, N.; Tyson, K.; Lightwood, D.; Munro, R.; McMillan, D.; Griffin, R.; Baker, T.; Starkie, D.; Nan, R.; Westwood, M.; Mushikiwabo, M.-L.; Jung, S.; Odede, G.; Sweeney, B.; Popplewell, A.; Burgess, G.; Downey, P.; Citron, M. Epitope Determines Efficacy of Therapeutic Anti-Tau Antibodies in a Functional Assay with Human Alzheimer Tau. *Acta Neuropathol* **2018**, *136* (5), 729–745. https://doi.org/10.1007/s00401-018-1911-2.

(100) UCB Biopharma SRL. *An Open-Label Extension Study to Evaluate the Safety and Tolerability of Long-Term UCB0107 Administration in Study Participants With Progressive Supranuclear Palsy*; Clinical trial registration NCT04658199; clinicaltrials.gov, 2021. https://clinicaltrials.gov/ct2/show/NCT04658199 (accessed 2022-02-23).

(101) UCB Biopharma SRL. *A Participant-Blind, Investigator-Blind, Placebo-Controlled, Phase 1b Study to Evaluate the Safety, Tolerability, and Pharmacokinetics of UCB0107 in Study Participants With Progressive Supranuclear Palsy (PSP)*; Clinical trial registration NCT04185415; clinicaltrials.gov, 2021. https://clinicaltrials.gov/ct2/show/NCT04185415 (accessed 2022-02-23).

(102) UCB Biopharma SRL. *A Patient- and Investigator-Blind, Placebo-Controlled Study to Evaluate the Efficacy, Safety, and Tolerability of Bepranemab (UCB0107) in Study Participants With Prodromal to Mild Alzheimer's Disease (AD), Followed by an Open-Label Extension Period*; Clinical trial registration NCT04867616; clinicaltrials.gov, 2022. https://clinicaltrials.gov/ct2/show/NCT04867616 (accessed 2022-02-23).

(103) Research, C. for D. E. and. Aducanumab (Marketed as Aduhelm) Information. *FDA* **2021**.

(104) Gauthier, S.; Ng, K. P.; Pascoal, T. A.; Zhang, H.; Rosa-Neto, P. Targeting Alzheimer's Disease at the Right Time and the Right Place: Validation of a Personalized Approach to Diagnosis and Treatment. *Journal of Alzheimer's Disease* **2018**, *64* (s1), S23–S31. https://doi.org/10.3233/JAD-179924.

(105) Kariolis, M. S.; Wells, R. C.; Getz, J. A.; Kwan, W.; Mahon, C. S.; Tong, R.; Kim, D. J.; Srivastava, A.; Bedard, C.; Henne, K. R.; Giese, T.; Assimon, V. A.; Chen, X.; Zhang, Y.; Solanoy, H.; Jenkins, K.; Sanchez, P. E.; Kane, L.; Miyamoto, T.; Chew, K. S.; Pizzo, M. E.; Liang, N.; Calvert, M. E. K.; DeVos, S. L.; Baskaran, S.; Hall, S.; Sweeney, Z. K.; Thorne, R. G.; Watts, R. J.; Dennis, M. S.; Silverman, A. P.; Zuchero, Y. J. Y. Brain Delivery of Therapeutic Proteins Using an Fc Fragment Blood-Brain Barrier Transport Vehicle in Mice and Monkeys. *Science Translational Medicine* **2020**, *12* (545), eaay1359. https://doi.org/10.1126/scitranslmed.aay1359.

(106) *Shuttle Unloads More Gantenerumab Into the Brain | ALZFORUM*. https://www.alzforum.org/news/conference-coverage/shuttle-unloads-more-gantenerumab-brain (accessed 2022-02-24).

(107) Hoffmann-La Roche. *A Phase Ib/IIa, Randomized, Double Blind, Placebo-Controlled, Multiple Ascending Dose, Parallel-Group Study to Investigate the Safety, Tolerability,*

Pharmacokinetics, and Pharmacodynamics of RO7126209 Following Intravenous Infusion in Patients With Prodromal or Mild to Moderate Alzheimer's Disease; Clinical trial registration NCT04639050; clinicaltrials.gov, 2022. https://clinicaltrials.gov/ct2/show/NCT04639050 (accessed 2022-02-23).

(108) *Apolipoprotein E and Alzheimer disease: pathobiology and targeting strategies | Nature Reviews Neurology*. https://www.nature.com/articles/s41582-019-0228-7 (accessed 2022-02-24).

(109) *JCI - Targeting of nonlipidated, aggregated apoE with antibodies inhibits amyloid accumulation*. https://www.jci.org/articles/view/96429 (accessed 2022-02-24).

(110) Xiong, M.; Jiang, H.; Serrano, J. R.; Gonzales, E. R.; Wang, C.; Gratuze, M.; Hoyle, R.; Bien-Ly, N.; Silverman, A. P.; Sullivan, P. M.; Watts, R. J.; Ulrich, J. D.; Zipfel, G. J.; Holtzman, D. M. APOE Immunotherapy Reduces Cerebral Amyloid Angiopathy and Amyloid Plaques While Improving Cerebrovascular Function. *Science Translational Medicine* **2021**, *13* (581), eabd7522. https://doi.org/10.1126/scitranslmed.abd7522.

(111) Cummings, J. L.; Tong, G.; Ballard, C. Treatment Combinations for Alzheimer's Disease: Current and Future Pharmacotherapy Options. *J Alzheimers Dis 67* (3), 779–794. https://doi.org/10.3233/JAD-180766.

(112) Samdin, T. D.; Kreutzer, A. G.; Nowick, J. S. Exploring Amyloid Oligomers with Peptide Model Systems. *Current Opinion in Chemical Biology* **2021**, *64*, 106–115. https://doi.org/10.1016/j.cbpa.2021.05.004.

(113) Kreutzer, A. G.; Nowick, J. S. Elucidating the Structures of Amyloid Oligomers with Macrocyclic β-Hairpin Peptides: Insights into Alzheimer's Disease and Other Amyloid

Diseases. *Acc. Chem. Res.* **2018**, *51* (3), 706–718. https://doi.org/10.1021/acs.accounts.7b00554.

(114) Ciudad, S.; Puig, E.; Botzanowski, T.; Meigooni, M.; Arango, A. S.; Do, J.; Mayzel, M.; Bayoumi, M.; Chaignepain, S.; Maglia, G.; Cianferani, S.; Orekhov, V.; Tajkhorshid, E.; Bardiaux, B.; Carulla, N. Aβ(1-42) Tetramer and Octamer Structures Reveal Edge Conductivity Pores as a Mechanism for Membrane Damage. *Nat Commun* **2020**, *11* (1), 3014. https://doi.org/10.1038/s41467-020-16566-1.

(115) Bakrania, P.; Hall, G.; Bouter, Y.; Bouter, C.; Beindorff, N.; Cowan, R.; Davies, S.; Price, J.; Mpamhanga, C.; Love, E.; Matthews, D.; Carr, M. D.; Bayer, T. A. Discovery of a Novel Pseudo β-Hairpin Structure of N-Truncated Amyloid-β for Use as a Vaccine against Alzheimer's Disease. *Mol Psychiatry* **2021**, 1–9. https://doi.org/10.1038/s41380-021-01385-7.

Supplementary Table S3.1.

Summary of Aβ peptide vaccines.

Vaccine	Sponsor	Antigen	Adjuvant	Carrier Molecules and Crosslinker	Immune Response by adjuvant	Phase in Clinical Research
Amilomotide (CAD 106)	Novartis Pharmaceuticals	Aβ 1–6	Alum or MF59	Bacteriophage Qbeta (VLP Qβ phage) Malamide	Th2	Phase II/III Discontinued
ACI-24 (Pal 1–15 acetate salt)	AC Immune, Roche, and Genentech	Aβ 1–15	MPLA	Liposomes with tetra-palmitoylated lysines	Th1/Th2	Phase II Withdrawn
ABvac40	Axon Neuroscience SE	Aβ40 33–40	Alum	Keyhole Limpet Hemocyanin	Th2	Phase II Active, not recruiting
UB-311	United Biomedical (Vaxxinity)	Aβ 1–14	Alum + CpG	Measles virus fusion protein (288–302) Hepatitis B virus surface antigen (19–33) UBITh platform technology	Th1/Th2	Phase II Terminated
Affiris AD02 (AffitopeAD02)	AFFiRiS and GlaxoSmithKline	Aβ 1–6	Alum	Keyhole Limpet Hemocyanin Malmaide	Th2	Phase II Recruiting
Vanutide cridificar (ACC-001, PF-05236806)	Jansen, Pfizer	Aβ 1–7	QS-21	Diphtheria Toxin, Thioether (CRM197)	Th1/Th2	Phase II 2 Terminated and 7 Completed between 2013–2014
V950	Merk	Aβ 1–15	Quil A	ISCOMATRIX	Th1/Th2	Phase I Completed
Mimovax (Affitope AD03)	AFFiRiS GlaxoSmithKline	Pyroglutamate modified N-terminal Aβ	Alum	Keyhole Limpet Hemocyanin	(Assumption) Th2	Phase I Completed
Lu AF20513	Lundbeck/Otsuka	Aβ 1–12	Alum	Th epitopes (P2P2 & P30 from Tetanus)	Th2	Phase I Terminated 2019
ALZ-101	Alzinova	Proprietary formulation of cross-linked Aβ	N/A	N/A	N/A	Phase I Recruiting

Supplementary Table S3.2

Summary of Aβ immunotherapies.

Antibody	Sponsor	Epitope Recognition	Derivation	Phase in Clinical Research
Aducanumab (BIIB037, Aduhelm)	Biogen, Eisai, and Neurimmune	Aβ 3–7	B cell library from health elderly patients	Phase III Active, not recruiting
Gantenerumab (RO4909832, RG1450)	Chugai Pharmaceutical and Roche	Aβ 2–11 and 18-27	Human antibody phage display library	Phase III Recruiting
Solanezumab (LY2062430)	Eli Lilly	Aβ 16–26	Aβ 13–28	Phase III Active, not recruiting
Crenezumab (MABT5102A, RG7412)	Genentech and Roche	Aβ 13–24	Liposome anchored peptides	Phase II Recruiting
Lecanemab (BAN2401, mAb158)	Biogen, Eisai, and BioArctic	Aβ 1–16	Fibrils of E22G mutant of Aβ	Phase III Recruiting
Donanemab (N3pG-Aβ, LY3002813, mE8)	Eli Lilly	Aβ p3–7	Aβ pE3-42 peptide	Phase III Recruiting
Bapineuzumab (AAB-001, 3D6)	Janssen, Pfizer	Aβ 1–5	Aβ 1–5 conjugated to an antibody	Phase III Terminated
MEDI1814	AstraZeneca, Eli Lilly	Aβ42 29-42	Human antibody phage display library	Phase I Completed
Ponezumab (PF-04360365)	Janssen, Pfizer	Aβ 30-40	Aβ40	Phase II Completed
RO7126209 (RG6102, Brain shuttle gantenerumab)	Roche	N/A	Gantenerumab conjugated to a Fc region that binds to the transferrin receptor	Phase I/II Recruiting
SAR228810 (SAR255952, 13C3)	Sanofi	4–20	Synthetic oligomers	Phase I Complete
AAB-003 (PF-05236812)	Janssen, Pfizer	1–8 and 1–28	Bapineuzumab with modified Fc region	Phase 1 Completed
GSK933776	GlaxoSmithKline	N-terminus of Aβ	Modified Fc region of an IgG1 antibody	Phase II Completed
LY2599666	Eli Lilly	Mid-region of Aβ	anti-Aβ Antigen-binding fragment linked to modified Fc region with polyethylene glycol	Phase I Terminated
LY3372993	Eli Lilly	N/A	N/A	Phase I Recruiting

Supplementary Table S5.3

Summary of Tau immunotherapies.

Antibody	Sponsor	Epitope Recognition	Derivation	Phase in Clinical Research
Semorinemab (RO7105705, MTAU9937A, RG6100)	AC Immune SA, Genentech, and Roche	Tau 2–24	Recombinant oligomers	Phase II Active, not recruiting
JNJ-63733657 (B296, PT3)	Janssen	Tau 204–225 (pT212–pT217)	Tau fibrils from patients	Phase II Recruiting
E2814	Eisai	HVPGG sequence and 299–303, and 362–366	Tau fragments G273–C291 and N296–D314 with an N-terminal cysteine	Phase II/III Recruiting
Bepranemab (UCB0107, Antibody D, D IgG4)	Roche, UCB S.A.	Tau 235–246	Tau recombinant fibrils	Phase II Recruiting
Tilavonemab (ABBV-8E12, C2N 8E12, HJ9.3)	AbbVie, C2N Diagnostics	Tau 25–30 and 22–34	Recombinant full length tau	Phase II Terminated
Gosuranemab (BIIB092, BMS-986168, IPN007/IPN002)	iPerian, Biogen, Bristol-Myers Squibb	Tau 15–24 and 8–19	*in vitro* aggregated full length tau	Phase II Terminated
Zagotenemab (LY3303560, MC-1 IgG1)	Eli Lilly & Co.	Tau 7–9 and 312–322	Immunopurified paired helical filaments	Phase II Completed
Lu AF87908	H. Lundbeck A/S	pS396	Tau 386–408 with pS390 and 404	Phase I Recruiting
BIIB076 (NI-105, 6C5 huIgG1/l)	Biogen, Eisai, and Neurimmune	Mid-region	Proprietary platform	Phase I Completed
RG7345 (RO6926496)	Roche	416–430, pS422	416–430, pS422 peptide	Phase I Completed

Chapter 4[a]

Pilot study in 5xFAD mice of vaccines against Alzheimer's disease using structurally defined oligomers derived from the β-amyloid peptide

Abstract

Peptide vaccines designed with causative peptides associated with Alzheimer's disease (AD), such as the β-amyloid (Aβ) peptide, hold the promise as an effective prophylactic against AD. Although there are efforts towards developing Aβ peptide vaccines, these antigens are structurally undefined fragments of Aβ. Vaccines that are generated against toxic species or conformations of Aβ are likely to be more efficacious than vaccines against structurally undefined Aβ fragments. This manuscript provides a pilot study with formulations of vaccines of two related structurally defined Aβ-derived peptides, 2AT-L and 4AT-L. The generation of antibodies against biologically relevant conformations of Aβ may provide antibodies with greater efficacy by blocking the damaging actions of toxic oligomers compared to a vaccine generated against an unstructured or generic Aβ species. 5xFAD mice received five immunizations of optimized vaccine formulations followed by an antibody titer assessment by ELISA. Treated mice then performed a battery of behavior assays which included elevated plus maze, contextual fear conditioning, and Barnes maze. To measure for vaccine efficacy and safety, histopathological analysis assessed the presence of Aβ plaques, upregulation of glial cells, and

[a] Manuscript in preparation for ACS Chemical Neuroscience

microhemorrhages. Between the two Aβ-derived peptides, mice treated with the 2AT-L peptide produced a better immune response, and although not statistically significant, showed subtle reversal of impulsive behavior and fear-based memory. Histopathological analysis showed no prevention of Aβ and glial disposition and microhemorrhages. This pilot study establishes the 2AT-L trimer as a candidate for further investigation on the therapeutic potential of this structurally defined Aβ-derived peptide.

Introduction

Alzheimer's disease (AD) is a neurological proteinopathy and the most common form of dementia that is characterized by the accumulation of the β-amyloid (Aβ) peptide.[1,2,3] In the last two decades, immunotherapies against Aβ have been a promising therapy to slow down the progression of AD.[4,5] Although the FDA approval of Biogen's Aduhelm (Aducanumab) was controversial, this led to a surge of fast-track designation among other immunotherapies such as Eisai's Leqembi (Lecanemab).[6] In a 18 month clinical trial, Leqembi slowed the rate of cognitive decline by 27% and is expected to be approved by the FDA for treating AD July 2023.[7,8] In a 12 month clinical trial, Lilly's Donanemab slowed clinical decline by 35% making it the second Aβ immunotherapy to slow cognitive decline.[9] While passive immunotherapies have provided promising results, peptide vaccines can equally contribute to slowing down the progression of AD.

In contrast to passive immunotherapies, which are infusions of a monoclonal antibody generated against Aβ, active immunotherapies, are peptide vaccines that stimulates the production of antibodies against a peptide antigen. To date, ALZ-101,[10] ABvac40,[11] and UB-311[12] are the lead Aβ peptide vaccines against AD in clinical trials. Of the three Aβ peptide

vaccines, UB-311 is the only candidate that has been granted FDA fast track designation as a treatment for AD.[12] While the significance of Aβ peptide vaccines are acknowledged as a promising therapy, a common theme among current peptide vaccines against Aβ is the antigen. More specifically, all peptide vaccines are made of a contiguous sequence of Aβ that are not structurally defined[13]. Because of the propensity for the Aβ peptide to aggregate, the structure or conformation of the antigen is unknown which could explain the failed clinical trials of peptide vaccines against AD. Vaccines that are generated against toxic species or conformations of Aβ are likely to be more efficacious than vaccines against Aβ fragments.

To address this issue, the Nowick Group has generated a library of structurally defined Aβ-derived peptide model systems to understand the biophysical characteristics of Aβ.[14] These structurally defined Aβ-derived peptide models are derived from residues 17–36 of Aβ consisting of three covalently linked $A\beta_{17-36}$ β-hairpin peptides that are constrained in a triangular arrangement. Through SDS-PAGE, SEC, X-ray crystallography, and cytotoxicity assays, the triangular trimers from Aβ (2AT-L and 4AT-L) self-assemble and are toxic to SHSY-5Y human neuronal blastoma cells in a similar fashion as Aβ oligomers.[15] In this study, we test triangular trimers and monomers of Aβ that contain either the wild type Phe_{20} (2AT-L trimer and 2AM-L monomer) or the mutated Cha_{20} (cyclohexylalanine) (4AT-L trimer and 4AM-L monomer).

To determine if these Aβ peptide models share similar structures with Aβ plaques, we generated the polyclonal antibodies pAb_{4AT-L} and pAb_{2AT-L} against the 4AT-L and 2AT-L trimer, respectively to perform immunostaining on transgenic mice and human brain slices. Immunofluorescent staining revealed that these antibodies recognize plaques in people who lived

with AD[16,17]. Because $pAb_{4AT\text{-}L}$ and $pAb_{2AT\text{-}L}$ recognize Aβ pathology through tissue staining, we turned to assess the therapeutic efficacy of the Aβ-derived trimers as antigens in peptide vaccines.

We hypothesized that by using a stable Aβ-derived peptide model in a peptide vaccine, we can prevent the onset of AD-like phenotypes in the 5xFAD transgenic AD mouse model. As a comparable comparison to the Aβ fragments used in current peptide antigens, we also tested the structurally defined monomers, 2AM-L and 4AM-L. In this current investigation, we report the results of a pilot study assessing whether the Aβ trimers, 2AT-L and 4AT-L, or Aβ monomers serve as an efficacious antigen in a peptide vaccine. Of the four Aβ-derived peptide models, we observed that mice treated with the 2AT-L trimer had the strongest immune response compared to the other Aβ-derived peptide models. Although not statistically significant, we also observe that mice treated with the 2AT-L trimer reverses AD-associated with impulsivity (primary metrics of this behavior assay include percent entries in open arms ($F(5, 51) = 1.974$, $p=0.0984$), percent time spent in open arms ($F(5, 51) = 3.767$, $p=0.0056$), percent entries in closed arms ($F(5, 51) = 1.974$, $p=0.0984$) and percent time spent in closed arms ($F(5, 51) = 3.767$, $p=0.0056$)) and fear-based memory ($F(5, 48) = 2.211$, $p=0.0685$). This pilot study establishes the 2AT-L trimer as a candidate for further investigation on the therapeutic potential of this structurally defined Aβ-derived peptide.

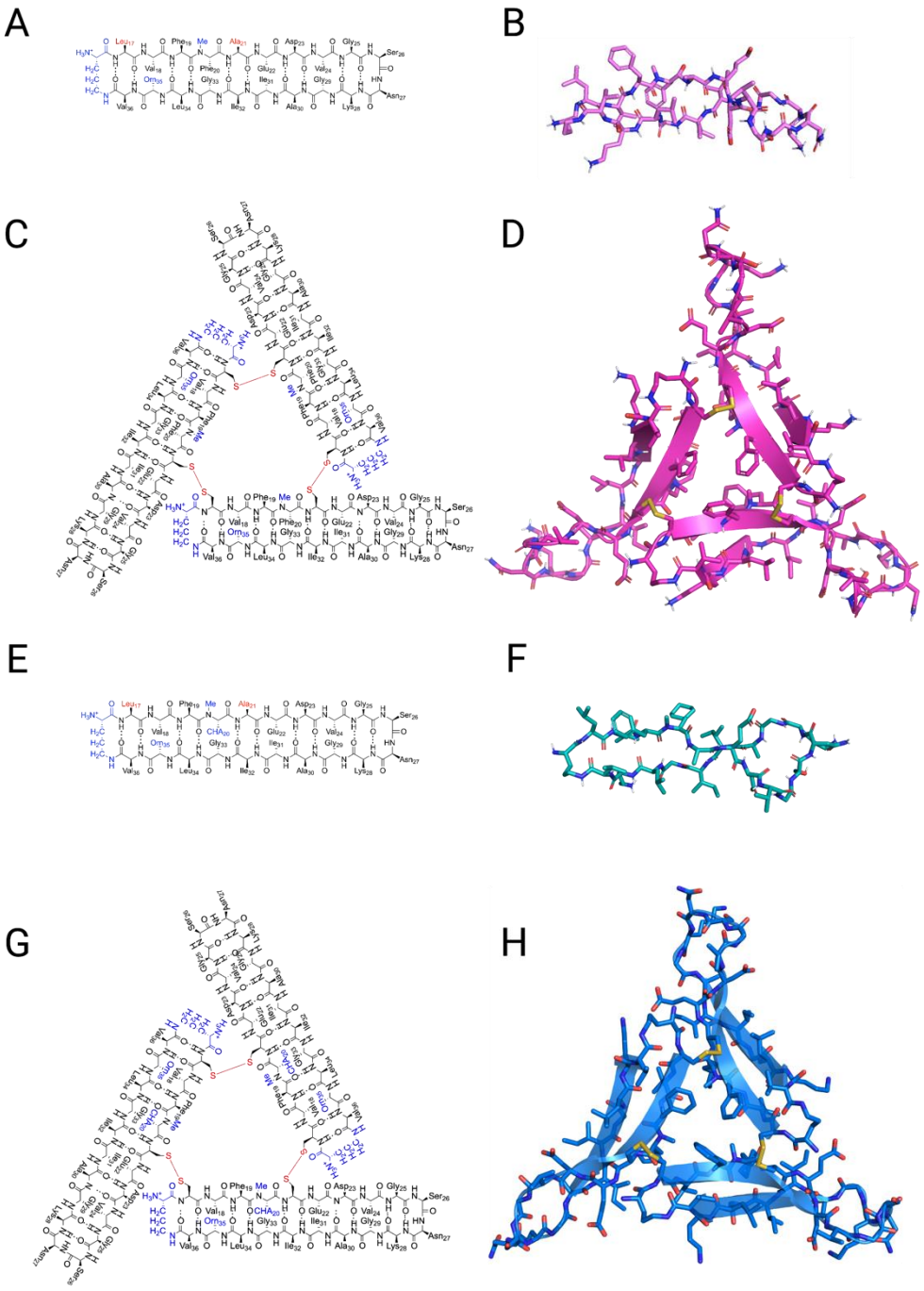

Figure 4.1. Chemical structures and X-ray crystallographic structure of the Aβ-derived peptides used in this investigation. **(A,B)** Chemical structure and X-ray crystallographic structure of 2AM-L monomer (generated from PDB 7U4P). **(C,D)** Chemical structure and X-ray crystallographic structure of 2AT-L trimer (PDB 7U4P). **(E,F)** Chemical structure and X-ray crystallographic structure of 4AM-L monomer (PDB 7JXN). **(G,H)** Chemical structure and X-ray crystallographic structure of 4AT-L trimer (PDB 7JXO).

Results

Vaccine Formulation

We optimized the formulation of vaccines using wild-type, C57BL/6 mice. To ensure that the Aβ-derived peptides elicit an immune response in mice, we used 1-Ethyl-3-(3-dimethylaminopropyl) carbodiimide (EDC) to conjugate the Aβ-derived peptides to the carrier protein, Keyhole Limpet Hemocyanin (KLH) (**Scheme 4.1**).The commercially available ThermoFisher's Imject™ EDC mcKLH Spin Kit was used to perform the conjugation. To create the final vaccine and enhance the immune response against the Aβ-derived peptides, the conjugate was immediately emulsified AddaVax (Invivogen)—an adjuvant previously used in a preclinical Aβ peptide vaccine.[18]

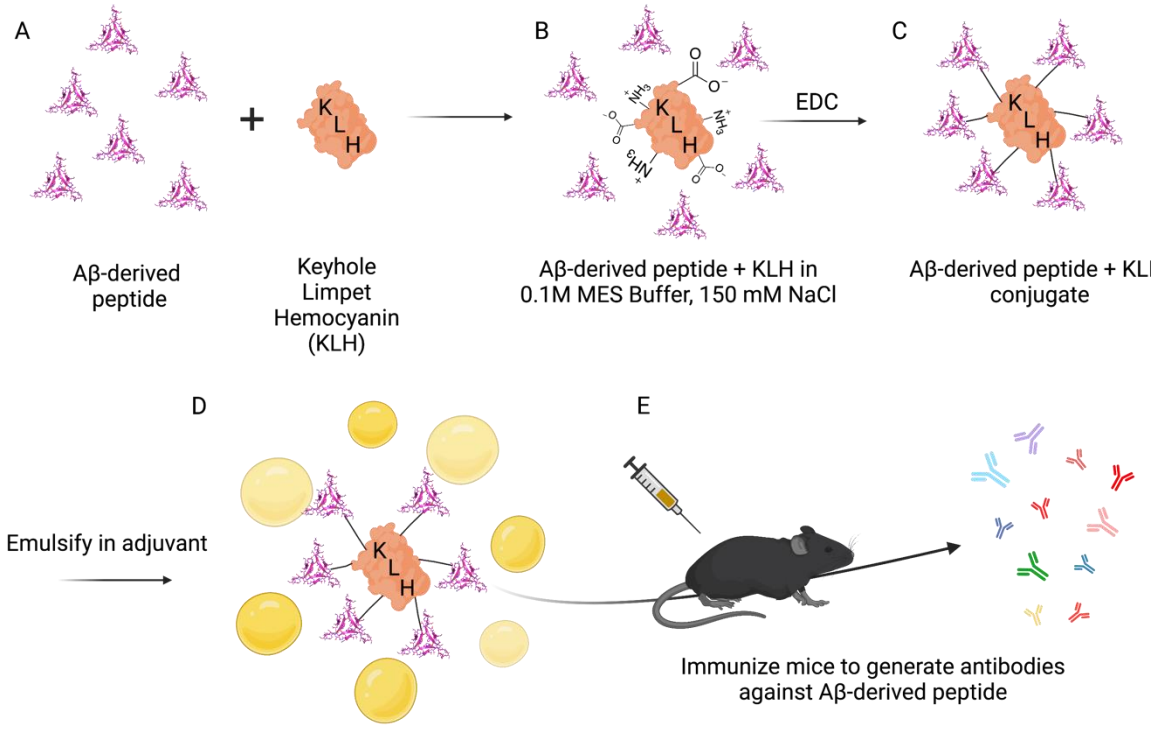

Scheme 4.1. Schematic representation of vaccine formulation. (**A**) Shows the starting material of the vaccine conjugation including the Aβ-derived peptide (red) and Keyhole Limpet

Hemocyanin (KLH, green). (**B)** The Aβ-derived peptide is then conjugated to the KLH by EDC conjugation **(C**). (**D**) The Aβ-derived peptide + KLH conjugate is then emulsified in adjuvant (yellow circles). (**E**) The mice are then immunized with the emulsified Aβ-derived peptide + KLH conjugate and generate antibodies against the Aβ-derived peptide. The figure was designed by Chelsea Marie T. Parrocha and created with BioRender.com.

When conjugating the Aβ-derived peptides to KLH in 0.1 M MES buffer with 900 mM NaCl, per manufacturer's instructions, the Aβ-derived peptides precipitated due to high salt concentrations used in KLH conjugations (**Supplemental Figure S4.1**).[19] When adding an Aβ-derived peptide to KLH in 0.1 M MES buffer with 900 mM of NaCl versus KLH in 0.1 M MES buffer with 0 mM of NaCl, the conjugation with 900 mM NaCl was cloudy compared to the clear conjugation with 0 mM NaCl (**Supplemental Figure S4.1 A**). When adding an Aβ-derived peptide to KLH in 0.1 M MES buffer with 150 mM of NaCl, the conjugation appeared similar in clarity as the conjugation with 0 mM NaCl (**Supplemental Figure S4.1 B**). To determine which of the vaccine formulations with varying salt concentrations produced the strongest immune response, we immunized mice with these formulations, and then performed ELISAs on the serum of immunized mice. Mice immunized with the vaccine formulated with 150 mM NaCl demonstrated the strongest immune response (**Supplemental Figure S4.1 C**). We thus proceeded to determine which of the Aβ-derived peptides can serve as an antigen in a vaccine to ameliorate AD-like phenotypes in the transgenic AD mouse model, 5xFAD. **Table S4.1** summarizes the outcomes of the mice that have participated in this study. No mice were injured or died due to immunizations throughout the investigation.

Experimental design and timeline of vaccine administration

Once we had a vaccine formulation that demonstrated the best immune response in wild-type mice, we applied this formulation to the transgenic AD mouse model, 5xFAD. The 5xFAD mouse model contains five familial AD mutations on APP including the Swedish (K670N/M671L), Florida (I716V), and London mutations (V717I), and two mutations on presenilin I (M146L and L286V).[20] The 5xFAD mouse model is a thoroughly characterized mouse model that possesses strong AD-like phenotypic pathology and behavior[20,21] and that has been used in preclinical Aβ peptide vaccine and immunotherapy research.[18]

5xFAD mice and wild-type littermates immunized with vehicle (adjuvant with 1 X PBS) were the control groups for this pilot study. Treatment groups for this pilot study included 5xFAD immunized with one of the four peptide vaccines each named by their respective antigen: 2AM-L, 2AT-L, 4AM-L, and 4AT-L. Each mouse received one prime and four boosts of vehicle or vaccine over the course of 112 days (**Figure 4.2**). Each immunization was about 28 days apart. After the last boost was administered, the mice were undisturbed for 81 days to test if the antibodies generated against the vaccine generated a therapeutic immune response to prevent the onset of AD-like phenotypes. Starting Day 193 post-first immunization, the mice underwent a battery of behavior assays assessing for locomotor function, working memory, impulsivity-like behavior, fear-based memory, as well as spatial and navigation memory. At the end of testing, all mice were euthanized to collect brain tissue and blood samples assess for vaccine safety and efficacy through histology and ELISAs.

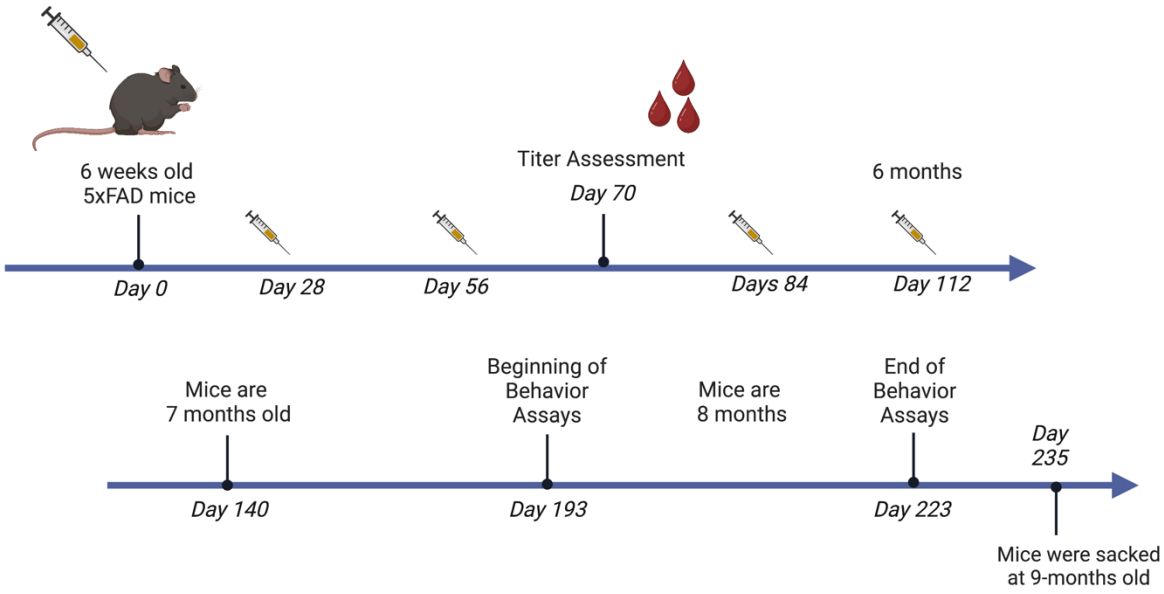

Figure 4.2. Timeline of experimental design. The figure was designed by Chelsea Marie T. Parrocha and created with BioRender.com.

5xFAD mice immunized with the 2AT-L peptide vaccine produced the strongest immune response.

To determine if treated mice were generating antibodies against their antigen, we measured the serum titers of treated mice halfway through the immunization schedule (Day 70). We performed an ELISA by plating one of the four antigens used to generate the vaccine, then added the serum of the mouse immunized with the respective antigen to the same plate. One-way ANOVA determined that there were differences between all treatment groups ($F(5, 42) = 5.518$, $p=0.0005$). Tukey *post hoc* showed that of the mice immunized with one of the four Aβ-derived peptides, mice immunized with 2AT-L had higher antibody titers against wild-type ($p = 0.0117$) and 5xFAD mice ($p = 0.0030$) immunized with vehicle (**Figure 4.3**). Antibody titers between wild type and 5xFAD mice treated with vehicle appeared to be lower than mice treated with 2AT-L. Mice immunized with 2AT-L produced the highest titers against their antigen followed

by mice immunized with 2AM-L, 4AT-L and 4AM-L. Terminal bleeds assessed by ELISA showed that 123 days after receiving an immunization with one of the four Aβ-derived peptides, all treated mice sustained antibody titers against their respective antigen (**Supplemental Figure S4.2**).

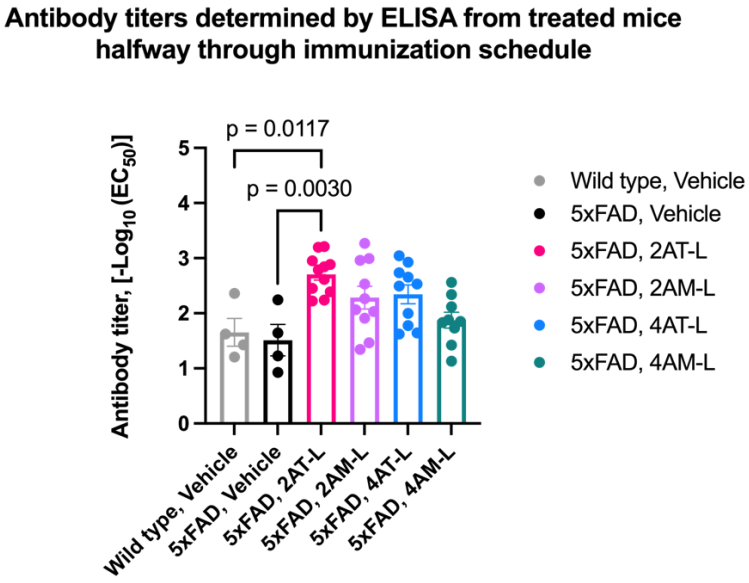

Figure 4.3. Bar graph showing normalized and inverse EC_{50} values determined by ELISAs from serum of 5xFAD mice vaccinated with 2AT-L (n=11), 2AM-L (n=10), 4AT-L (n=10), and 4AM-L (n=9). Treated mice were compared to wild-type mice (n=4) and 5xFAD mice (n=4) treated with vehicle. One-way ANOVA (F (5, 42) = 5.518, p=0.0005), followed by Tukey *post hoc* (p = 0.0117, wildtype vehicle versus 5xFAD, 2AT-L and p = 0.0030, 5xFAD, vehicle versus 5xFAD, 2AT-L). Error bars are standard error of the mean.

5xFAD mice treated with 2AT-L showed a decrease of anxiety-like behavior.

To assess the potential differences in motor function between genotypes, we performed open field, rotarod, and grip strength. All three behavior assays demonstrated that all treatment groups of mice did not have impaired locomotor behavior or motor function (**Supplemental**

Figure S4.3). This data provides confidence in the results produced by the behavior assays measuring memory and learning.[b]

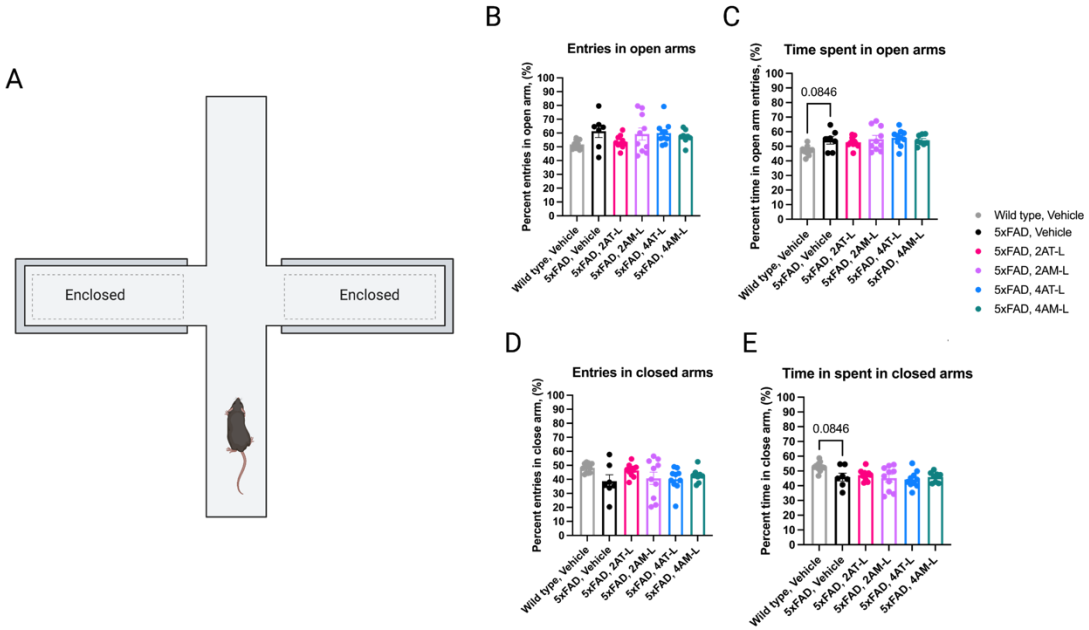

Figure 4.4. Elevated plus maze assessing for impulsivity as measured by anxiety-like behavior in 5xFAD mice vaccinated with 2AT-L (n=10), 2AM-L (n=10), 4AT-L (n=10), and 4AM-L (n=9). Treated mice were compared to wild-type mice (n=12) and 5xFAD mice (n=7) treated with vehicle. One-way ANOVA measured for statistical differences between treatment groups. (**A**) Shows a schematic representation of a mouse in the elevated plus maze. (**B**) Bar graph showing percent entries in the open arms ($F(5, 51) = 1.974$, $p=0.0984$). (**C**) Bar graph showing percent time spent in the open arms ($F(5, 51) = 3.767$, $p=0.0056$). (**D**) Bar graph showing percent entries in the closed arms ($F(5, 51) = 1.974$, $p=0.0984$). (**E**) Bar graph showing time spent in the closed arms ($F(5, 51) = 3.767$, $p=0.0056$). Tukey *post hoc* demonstrated wildtype mice immunized with vehicle spent 7.04% less time in open arms and 7.04% more closed arms compared to 5xFAD mice immunized with vehicle ($p = 0.0846$). Error bars are standard error of the mean. The figure was designed by Chelsea Marie T. Parrocha and created with BioRender.com.

Elevated plus maze (EPM) is the gold standard for assessing anxiety-like behavior.[22] However, in the 5xFAD mouse model, previous studies showed lower anxiety-like behavior

[b] When performing grip strength and rotarod, the mice were noted of having difficulty gripping due to the finger clipping ID used to differentiate mice genotypes. Although this may have been a factor influencing the outcomes of grip strength and rotarod, all treated mice appeared to have an intact locomotor function.

mirrors impulsivity or recklessness that is observed in AD.[21,23] One-way ANOVA determined subtle differences between all treatment groups in all primary metrics of EPM (**Figure 4.4**). Primary metrics of this behavior assay include percent entries in open arms ($F(5, 51) = 1.974$, $p=0.0984$), percent time spent in open arms ($F(5, 51) = 3.767$, $p=0.0056$), percent entries in closed arms ($F(5, 51) = 1.974$, $p=0.0984$) and percent time spent in closed arms ($F(5, 51) = 3.767$, $p=0.0056$).

Tukey *post hoc* demonstrated that 5xFAD mice immunized with vehicle recapitulated previously reported results. The 5xFAD mice immunized with vehicle were slightly more impulsive than wild-type immunized with vehicle as measured by percent entries in open arms (9.52%, p=0.1899) (**Figure 4.4 A**), and percent time spent in open arms (7.04%, p=0.0846) (**Figure 4.4 B**), percent entries in closed arms (9.52%, p=0.1899) (**Figure 4.4 C**), and percent time spent in closed arms (7.04%, p=0.0846) (**Figure 4.4 D**). Tukey *post hoc* demonstrated subtle differences in therapeutic effect of an Aβ-derived peptide vaccine in reversing impulsive behavior between mice immunized with 2AT-L and wild-type and 5xFAD mice immunized with vehicle. 5xFAD mice immunized with vehicle entered the open arms 7.67% more than mice treated with the 2AT-L antigen ($p = 0.4355$) and spend 1.33% more time in the open arms ($p = 0.0056$). Wild-type mice immunized with vehicle had 1.82% less entries in open arms than mice immunized with 2AT-L ($p = 0.9956$). Wild-type mice immunized with vehicle spent 5.71% less time in open arms than mice immunized with 2AT-L ($p = 0.1523$).). Although the differences are subtle, we observe a trend that mice immunized with 2AT-L appear to behave in a similar fashion to wild-type mice immunized with vehicle. The rescued impulsive-like behavior observed in 2AT-L treated mice prompted us to assess the effects of the vaccine on fear-based memory.

5xFAD mice treated with 2AT-L showed improvement of fear-based memory.

Fear-based memory is measured in contextual fear conditioning with the defensive mechanism of freezing as the primary metric.[c,24] Although not significant, one-way ANOVA suggests differences in fear-based memory between treatment groups ($F(5, 48) = 2.211$, $p=0.0685$) (**Figure 4.5**). Among the mice immunized with an Aβ-derived peptide vaccine, mice treated with 2AT-L remembered the original environment more than mice treated with the other Aβ-derived peptide vaccine.

Tukey *post hoc* demonstrated that 5xFAD mice immunized with vehicle recapitulated previously reported results.[21] The 5xFAD mice immunized with vehicle had 25.05% lower change from baseline, therefore remembered less of the original environment compared to wild-type immunized with vehicle ($p=0.1167$). Tukey *post hoc* demonstrated subtle differences in therapeutic effect of an Aβ-derived peptide vaccine in reversing fear-based memory between mice immunized with 2AT-L, wild-type and 5xFAD mice immunized with vehicle. 5xFAD mice immunized with vehicle had 16.41% lower change from baseline than mice treated with the 2AT-L antigen ($p = 0.5589$). Wild-type mice immunized with vehicle had 8.61% higher change

[c] All mice in every treatment group exhibited higher than normal baseline measurements during the initial training period assessment. The normal baseline for mice is 10%-20% freezing while mice in this study were freezing 50% while in the environment without exposure to stimuli. This behavior may be due to previous experiences in ear punches, blood draws, transferring from facilities, and administration of vaccines. Because of this, we switched from Cued Fear Conditioning (which involves a tone precedes the foot shock with tone for stimuli) to Contextual Fear Conditioning. All mice had high baseline and there was a lot of variability to normalize it by percent change to control for differences in baseline behavior. To account for high baseline and variability among treatment groups, the data was normalized by percent change between the baseline and the test post shock.

from baseline than mice immunized with 2AT-L (p = 0.9281). Although the differences are subtle, of the Aβ-derived peptide vaccines, mice immunized with 2AT-L demonstrated subtle improvement in fear-based memory. To further characterize the Aβ-derived peptide vaccines ability to prevent the onset of AD-like phenotypes in 5xFAD mice, we turned to behavior assays assessing additional forms of memory.

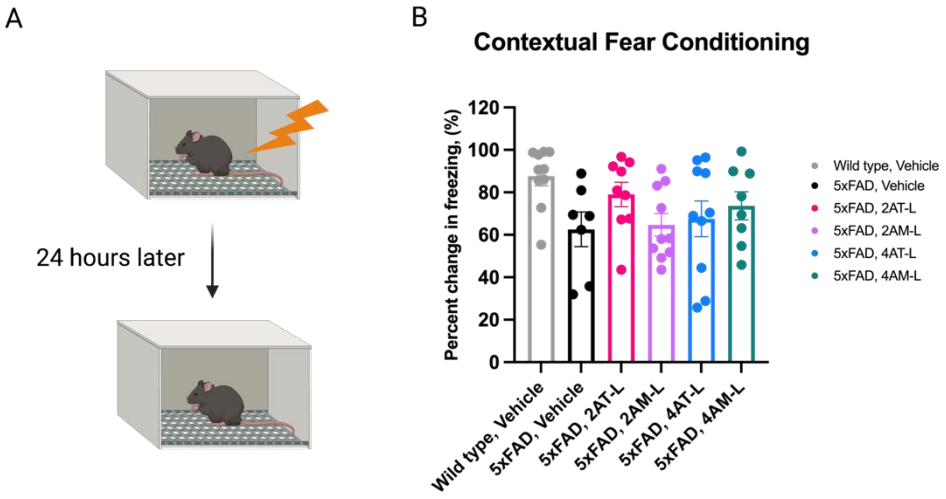

Figure 4.5. Contextual fear conditioning assesses for fear-based in 5xFAD mice vaccinated with 2AT-L (n=9), 2AM-L (n=10), 4AT-L (n=10), and 4AM-L (n=8). Treated mice were compared to wild-type mice (n=10) and 5xFAD mice (n=7) treated with vehicle One-way ANOVA measured for statistical differences between treatment groups (F (5, 48) = 2.211, p=0.0685). (**A**) Schematic representation of a mouse in the conditioning chamber with stimuli and being placed in the same chamber 24 hours later. (**B**) Bar graph showing percent change in freezing. Error bars are standard error of the mean. The figure was designed by Chelsea Marie T. Parrocha and created with BioRender.com.

5xFAD mice treated with an Aβ-derived peptide vaccine did not show improvement of working, spatial and navigational memory.

For a full evaluation of memory rescue in mice immunized with an Aβ-derived peptide vaccine, Y-Maze was used to assess working memory while Barnes Maze was performed to access spatial and navigational memory. In Y-Maze, the 5xFAD mice immunized with vehicle

should have lower percent alternations than wild-type mice immunized with vehicle which was not observed when performing this assay (**Supplemental Figure S4.4**). While this assay has been used to characterize the 5xFAD mouse model[23] and therefore could be used in assessing therapeutic intervention, the behavior assay may not be reliable or sensitive enough to measure working memory.[25]

We also observed no improvement of spatial, and navigational memory in mice treated with any of the four Aβ-derived peptide vaccines. Throughout the training period of Barnes maze, wild-type and 5xFAD mice immunized with vehicle performed as expected (**Supplemental Figure S4.5 and S4.6**). Wild-type mice immunized with vehicle displayed improved learning and memory over the training period and final testing while 5xFAD controls did not. We did not observe improvements in spatial and navigational memory in mice treated with an Aβ-derived peptide vaccine. Barnes Maze or Morris Water Maze have been the gold standard assays measuring for assessing Aβ vaccine efficacy and have been reproduced in previous studies.[26,27] However, in a recent comprehensive study of the 5xFAD mouse model, researchers suggested that these assays may not be appropriate due to potential confounding phenotypes such as hyperactivity and additional stressors.[25] After the mice completed this last behavior assay, they were euthanized according to approved procedures by the University of California, Irvine University Laboratory Animal Resources.

5xFAD mice treated with an Aβ-derived peptide vaccine did not reduce Aβ and glial pathology.

To investigate whether an Aβ-derived peptide vaccine can generate anti-Aβ antibodies to prevent the development of Aβ pathology in mice, immunostaining was performed on brain

sections of treated mice to assess plaque deposition. Because mice were treated with an Aβ-derived peptide vaccine starting at 6 weeks old, we hypothesize that treated mice would generate protective antibodies against the onset of Aβ. Thioflavin-S is a standard stain used to detect Aβ plaques in peptide vaccine and immunotherapy studies. One-way ANOVA determined that there were differences in the amount of plaque pathology between treatment groups ($F(5, 34) = 13.90$, $p<0.0001$) however, Tukey *post hoc* showed that these significant differences were between wild-type mice that were immunized with vehicle and all 5xFAD mice regardless of vaccination. Compared to 5xFAD mice immunized with vehicle, wild-type mice immunized with vehicle had virtually no Aβ plaques (Tukey *post hoc*, $p = 0.0002$, **Figures 4.6 A**). All 5xFAD mice treated with an Aβ-derived peptide vaccine had plaque depositions similar to 5xFAD mice immunized with vehicle (**Figures 4.6 D**).

Reactive astrocytes and microglia contribute to inflammation in the brains of people who live with AD.[28–30] To determine if antibodies generated from the Aβ-derived peptide vaccines can reduce the proliferation of glial cells, we performed immunostaining on the brains of treated mice using the GFAP antibody for recognizing astrocytes and IBA-1 antibody for recognizing microglia. One-way ANOVA determined that there were differences in the amount of astrocyte pathology ($F(5, 18) = 15.41$, $p<0.0001$) and microglia pathology ($F(5, 18) = 10.40$, $p <0.0001$) between treatment groups. However, Tukey *post hoc* showed that these significant differences were between wild-type mice that were immunized with vehicle and all 5xFAD mice regardless of vaccination. When comparing the wild-type control with the 5xFAD control, we observed an expected upregulation of astrocytes and microglia in 5xFAD controls (Tukey *post hoc*, $p <0.0001$, and $p = 0.1933$, respectively, **Figures 4.6 B** and **4.6C**). Mice treated with an Aβ-derived peptide vaccine had similar loads of astrocytes and microglia as the control 5xFAD mice

(**Figures 4.6 E and 4.6 F**). Since the formulation of the first Aβ peptide vaccine, (AN1792) induced a Th-1 inflammatory immune response that lead to failed clinical trials, researchers investigate if the vaccine candidate induces ARIA.[13,27,31] Because of the hypothesized upregulation of glial activity we were prompt to inquire about microhemorrhages in the brains of mice immunized with the Aβ-derived peptide vaccines.

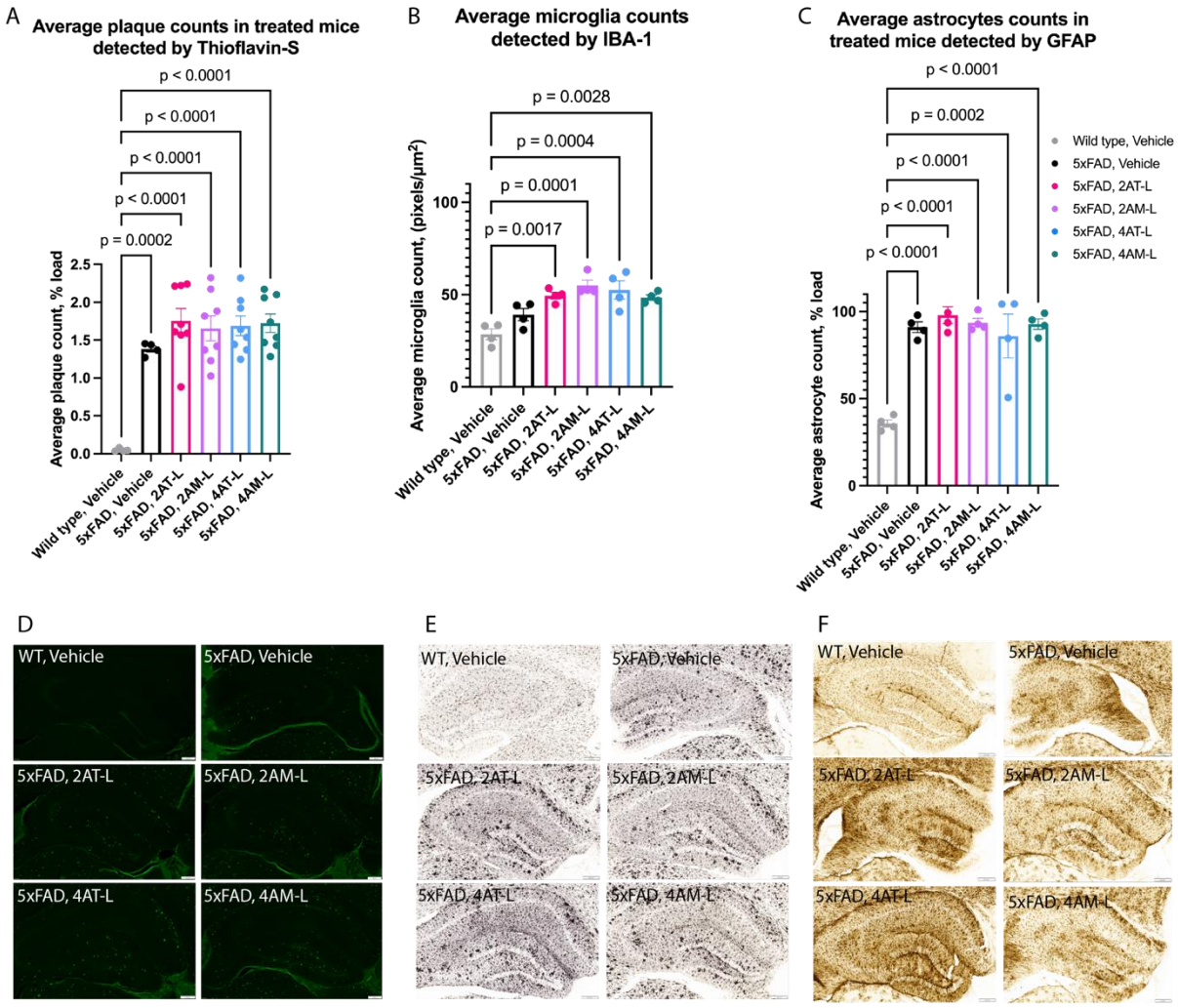

Figure 4.6. Aβ plaque pathology and glial response was not decreased in mice treated with any of the Aβ-derived peptide vaccines. (**A**) Bar graph showing average plaque counts detected by Thioflavin-S (n = 8 per group). (**B**) Bar graph showing average microglia loads detected by IBA-1 (n = 4 per group). (**C**) Bar graph showing average astrocyte loads detected by GFAP (n = 4 per group). All error bars are standard error of the mean. (**D**) Micrographs of representative

hippocampus stained with Thioflavin-S from each treatment group. (**E**) Micrographs of representative hippocampus stained with IBA-1 from each treatment group. (**F**) Micrographs of representative hippocampus stained with GFAP from each treatment group. All micrographs of Thioflavin-S stains were acquired at 20X, then zoomed in on Olympus OlyVIa at 6.6x. The scale bar is 200μm. All micrographs of IBA-1 and GFAP stains were acquired at 20X, then zoomed in on Olympus OlyVia at 0.5X. The scale bar is 500 pixels.

5xFAD mice treated with an Aβ-derived peptide vaccine may induce microhemorrhages in the brain.

To assess for the safety of the vaccine, we used Perl's Prussian blue staining to determine if the vaccine-induced microhemorrhages. We performed qualitative assessment of the hippocampus from wild-type control with the 5xFAD control, and observed more hemorrhages in the 5xFAD control (**Figures 4.7 A** and **4.7 B**). Mice treated with an Aβ-derived peptide vaccine had exacerbated microhemorrhages than the control 5xFAD mice (**Figure 4.7 C-F**). Because of the onset of glial activity at 2-4 months, we suspect that 5xFAD mice naturally obtain microhemorrhages in the brain which mimics the phenotypes observed in people.[21,32,33] Without a fully factorial design that includes wild-type mice immunized with the Aβ-derived peptide vaccines we can, we can only assume that the increase in microhemorrhages in mice treated with an Aβ-derived peptide vaccine.

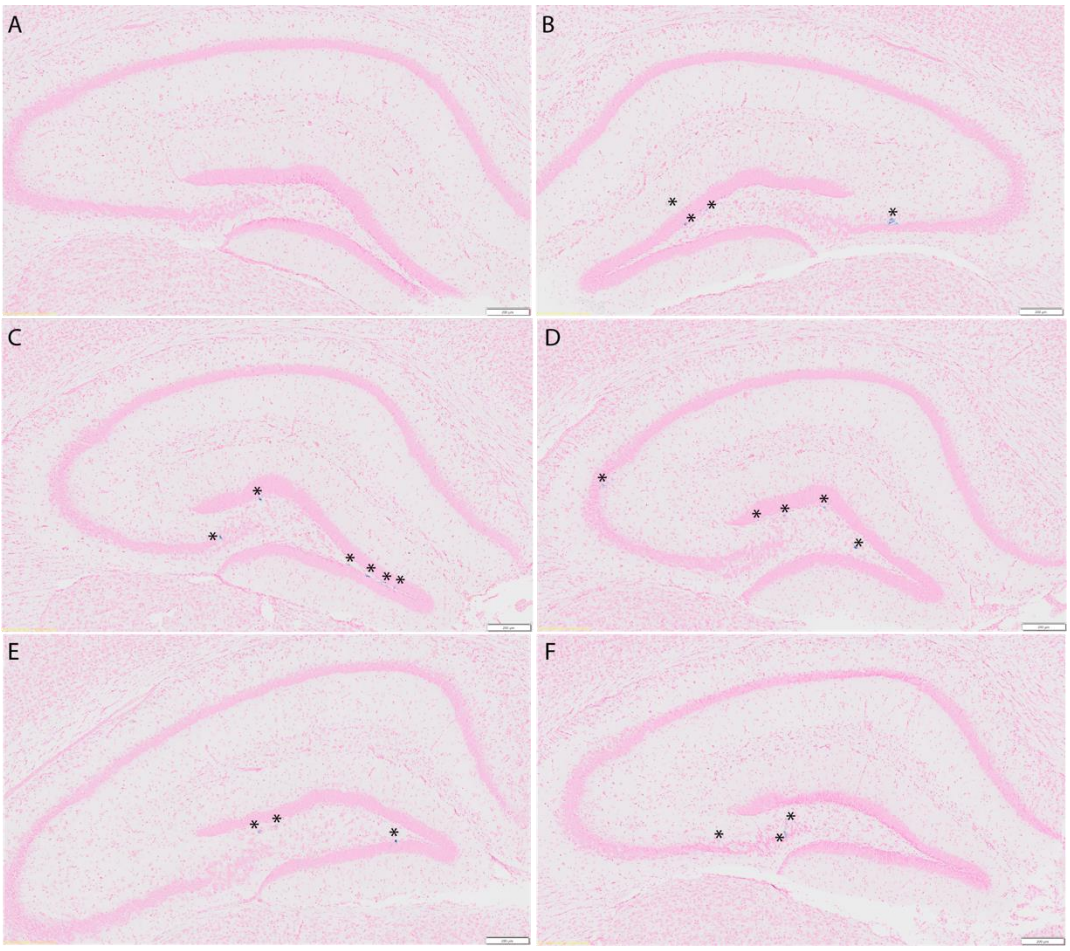

Figure 4.7. Micrographs of Perl's stained hippocampus of mice treated with either vehicle or one of the four Aβ-derived peptide vaccines. All microhemorrhages are depicted next to a *. (**A**) Micrograph of a hippocampus from a wild-type mouse treated with vehicle, (**B**) 5xFAD mouse treated with vehicle, and mice treated with (**C**) 2AT-L peptide vaccine, (**D**) 2AM-L, (**E**) 4AT-L and (**F**) 4AM-L. All images were acquired at 20X, then zoomed in on Olympus OlyVia at 6.6x. The scale bar is 200µm.

Discussion

Peptide vaccines are an opportunity to connect the structural biology of contributing peptides of AD, such as Aβ, to AD symptoms. In the design of current Aβ peptide vaccines, the antigens are made with structurally undefined fragments the *N*-terminus of Aβ, which was influenced by the results of the first Aβ peptide vaccine, AN1792. Since the discovery of

AN1792 of ARIA in ~6% of phase II clinical trial patients[34–36], subsequent studies determined that the central region of Aβ contributed to the onset of ARIA; thus researchers have limited designing antigens of Aβ peptide vaccine antigens to $A\beta_{1-15}$ to and avoid ARIA and induce a Th-2 B-cell response.[37] However, the antigens of current Aβ peptide vaccines are made with structurally undefined fragments of Aβ. The Aβ peptide has the propensity to aggregate which could occur during vaccine formulation thus leaving the conformation of the antigen unknown. This lack of understanding the structure of the antigen could lead to a lack of therapeutic precision and explain the failed clinical trials of peptide vaccines against AD. Thus, it is imperative to have structurally defined antigens that may lead to efficacious peptide vaccines against AD.

The central region of Aβ presents epitopes that form loop-like conformations and form β-hairpins; this conformation is thought to be the building blocks of toxic Aβ oligomers associated with the pathogenesis and progression of AD.[14,38,39] Although this region has been avoided due to concerns of inducing ARIA, incorporating antigens with the central region of Aβ may lead to a new generation of peptide vaccines. More specifically, these novel Aβ peptide vaccines may develop conformation-specific antibodies against toxic Aβ oligomers and thus connect the structural biology of Aβ to AD symptoms.

In this pilot study, Aβ peptide vaccines using four Aβ-derived peptide models containing the central region of Aβ were used to determine if we can prevent the onset of AD-like symptoms in 5xFAD mice. Although 5xFAD mice treated with 2AT-L showed a decrease of anxiety-like behavior and improvement of fear-based memory, albeit not statistically significant, we did not observe a reduction in pathology. Inconsistent results in preclinical studies with $A\beta_{1-}$

$_{42}$ peptide vaccines designed with demonstrate variable results in vaccine efficacy. In PDAPP transgenic AD mice with the peptide vaccine, pre-existing plaque formation was reduced,[4] however, in Tg2576 transgenic AD mice, reduction in pre-existing plaque formation was not as effective.[40] APPPS1 transgenic AD mice vaccines also did not exhibit plaque clearance or decreased glial deposition.[41] In immunized 3xTG transgenic AD mice, preexisting plaques were not reduced, but soluble Aβ was reduced along with improvement in behavioral performance.[42] The authors of these studies suggest that may target specific forms of Aβ which may not target all AD pathology and symptoms. In a similar fashion to these previously reported studies, we propose that the 2AT-L peptide vaccine may generate antibodies targeting soluble Aβ that influence anxiety-like behavior and fear-based memory. Along with the findings of this pilot study, we envision the use of the 2AT-L antigen being used in a combination vaccine with other structurally defined antigens to enhance the therapeutic efficacy of this vaccine.

Peptide vaccines can serve as a practical prophylactic to slow down the diagnosis of 13.8 million Americans by 2060.[43,44] Although Aβ passive immunotherapies have shown promise of slowing down cognitive decline, these therapies require not only fiduciary resources but also infusion centers that already serve people with other terminal diseases. Biogen's Aduhelm (Aducanumab) was originally priced at $56,000 per year with 10 mg/kg infusions every 4 weeks and has since reduced the price to $28,200.[45,46] Eisai's Leqembi (Lecanemab) is expected to be priced at $26,500 per year with 10 mg/kg infusions every 2 weeks.[47,48] Even if a person can afford these passive immunotherapies, there is still the risk of marginal efficacy and ARIA.[48,49]

Peptide vaccines are a universal, practical approach to slowing down the progression of AD that are without the limitations and challenges presented with passive immunotherapies.

Peptide vaccines are comparably less cost-effective to generate and have a stable shelf life which will allow international accessibility without taking additional resources from terminal diseases that need infusion centers. The incorporation of peptide vaccines against diseases like AD could be administered to people 20 years old and younger and is the future therapeutic to preventing the onset of AD.

Conclusion

This pilot study investigates the therapeutic potential of structurally defined models of Aβ monomers and oligomers by using them as antigens for novel Aβ peptide vaccines in mice. Halfway through the immunization schedule, 5xFAD immunized with one of the four peptide vaccines developed an immune response against the respective antigen of the vaccine. Through behavior assays, locomotor behavior was not impaired and therefore was not a confounding variable in the memory and learning behavior assays. Spatial and long-term memory was not rescued in mice treated by either of the four peptide vaccines. Nonetheless, albeit not statistically significant, impulsive behavior and fear-based memory shows promise of recovery in mice treated with the 2AT-L peptide vaccine. Histopathology demonstrated that AD pathology, including Aβ plaques and upregulation of glial cells, was not rescued in treated mice. Mice treated with the peptide vaccine also displayed an increase in microhemorrhages. We conclude that among the four peptide vaccines (2AM-L, 2AT-L, 4AM-L, and 4AT-L), 2AT-L demonstrated potential therapeutic results. The results from this pilot study suggest that a fully factorial experimental design with larger group sizes should be pursued with a peptide with the 2AT-L trimer.

Experimental Section

Synthesis of peptide antigens

The peptides 2AM-L, 2AT-L and 4AT-L in this study were sourced and prepared according to Kreutzer et al.[17] and Parrocha et al.[16] (Chapter 2), respectively. Please see manuscripts for characterization data. The peptide 4AM-L was prepared according to Haerianardakani et al. 2020.[15] Please see supplemental information for characterization data.

Curation of 5xFAD mice and wild type littermates

Information for the curation of 5xFAD mice and wild type littermates was taken verbatim from Parrocha et al.[16] (Chapter 2)All animal experiments were approved by the UC Irvine Institutional Animal Care and Use Committee (UCI IACUC). All animals were bred by the Transgenic Mouse Facility at UC Irvine. The process of breeding, genotyping, raising, and aging of 5xFAD hemizygous mice (B6.Cg Tg(APPSwFlLon, PSEN1*M146L*L286V)6799Vas/Mmjax, Stock number 34848-JAX, MMRRC) and wild type littermates for the purposes of tissue harvesting were followed as described in Forner et. al. 2021.[21]

Mice were toe clipped for identification which proved to be a relevant parameter in behavior testing. The experiment started with n=12, 5xFAD mice per treatment group followed by n=11, wild-type littermate controls. No mice were terminated due to the vaccines during the immunization schedule.

Preparation of the antigen-KLH/adjuvant and the antigen/adjuvant emulsions

Peptide conjugation to carrier protein to KLH. To prepare conjugates of 2AM-L, 2AT-L, 4AM-L, or 4AT-L peptides with keyhole limpet hemocyanin (KLH) the Thermo Fisher Imject mcKLH EDC conjugation protocol was followed according to the manufacturer's instructions with minor adjustments. 1.5 mg of the peptide was dissolved in 100% DMSO and was brought to the final concentration of 25% DMSO in the conjugation reaction. After the purification of the conjugate over the desalting column, the volume of the eluent is ~400 uL. This 400 uL was added back to the pellet from the conjugation reaction and the volume was brought to ~750 uL by adding 300 uL of PBS. This resulted in a final antigen concentration of ~1.33 mg/mL. Please note, the concentrations reflect the concentrations of the antigen only, not the carrier protein.

Emulsifying of peptide conjugates in adjuvant and vaccine administration. Using a syringe adapter (18g), 900 uL of the 1.33 mg/mL conjugate with 750 uL of Addavax to create a 0.66 μg/μL emulsion of the conjugate. 150 uL of emulsified peptide conjugate was aliquoted in 1 mL insulin syringes. After vaccines were aliquoted, mice were immediately intraperitoneally injected with 150 uL of the 0.66 μg/μL emulsion to achieve injection with 100 ug of antigen.

Saphenous Blood Draw

All animal handling was approved by the University of California, Irvine University Laboratory Animal Resources. The upper body of the mouse was restrained in a 50 mL conical vial with multiple breathing holes drilled into the tube. After the outer thigh hair of the mouse was shave, the exposed skin was cleaned with 70% EtOH. Lubricant (Optixcare) was rubbed on the saphenous vein. Using a 20g needle, the vein was pricked at a 30-degree angle, and the blood was

collected by a capillary needle. The blood was then transferred to an Eppendorf tube. After enough blood was collected (~100 uL), a gauze and light pressure were applied to the punctured vein followed by additional lubricant. Post-procedure, the mice were monitored to ensure blood clotting and locomotor function. Blood samples clotted for up to 4 hours before being centrifuged at 1500 rpm for 15 minutes. The supernatants were then transferred to another Eppendorf tube and used in ELISAs. Samples were stored at 4 ºC for long term storage.

Enzyme-linked immunosorbent assays (ELISAs)

Information for the curation of 5xFAD mice and wild-type littermates was adopted or taken verbatim from Parrocha et al. 2023[16] (Chapter 2). All procedures for this assay were performed at ambient temperature (25 ºC). 96-well flat bottom MaxiSorp immunoplate (Thermo Scientific Clear Flat-Bottom Immuno Nonsterile 96-Well Plates, Cat. No.442404) was coated with 50 µL of 1 µg/µL in triplicate of either 2AT-M, 2AT-L, 4AT-L, or 4AT-M in 1 X carbonate buffer (pH = 9.0), sealed with Axygen AxySeal Sealing Film (REF PCR-SP), and placed on a plate shaker overnight. The next day, plates were aspirated, washed, rinsed, and aspirated once using Fisherbrand accuWash and accuWash Versa plate washer (Cat. No.14-377-577) with 100 µL of 1 X PBS with 0.05% Tween 20 followed by 18 MΩ deionized water. Plates were coated with 75 µL of blocking solution, 1% BSA (Bovine Serum Albumin, Fraction V, Heat Shock Treated, Fisher BioReagents, Cat. No. BP1600-100) in 1 X PBS, sealed, and then placed on plate shaker for at least 1 hour. The collected supernatants from blood draw (serum from treated mice), were diluted 1:100 in 250 µL blocking solution. Plates were aspirated, washed, rinsed, and aspirated once, then primary antibodies were plated in triplicates in the top row of the 96-well plate, followed by a 1:3 dilution down the plate. Plates were sealed and incubated on the

plate shaker for 2 hours. After incubation, plates were aspirated, washed, rinsed, and aspirated three times. Plates were coated with 50 µL of 1:5,000 diluted goat-anti-mouse HRP (Jackson ImmunoResearch Cat No. 111-035-144) in blocking solution, sealed, and incubated on the plate shaker for 1 hour. After incubation, plates were aspirated, washed, rinsed, and aspirated three times and developed with 1:1 TMB/E substrate followed by 1 M HCl and read at 450 nm using Skant It 5.0 Software and Thermofisher Multiskan Go (Cat. No. N10588) plate reader.

Generation and affinity purification of rabbit $pAb_{4AT\text{-}L}$ and $pAb_{2AT\text{-}L}$

Please refer to Parrocha et al.[16] (Chapter 2) and Kreutzer et al.[17] for the development and application of for $pAb_{4AT\text{-}L}$ and $pAb_{2AT\text{-}L}$, respectively.

Behavior Assays

All behavior assays were performed at the University of California, Los Angeles Behavior Core Testing Facility (UCLA BTC). No mice were excluded from behavior assays. The procedures described were adapted from the researchers at UCLA BTC. Videos and data collected from mice performing behavior assays were tracked using AnyMaze Software (version v7.15). The data acquired from AnyMaze was further processed using GraphPad Prism (version 9.0).

Open Field

Open field is an assay that measures locomotor behavior in an open arena. The animal was placed in an field engineered in house (internal dimensions of the field: 40cm x 40cm with 30 cm high walls) and was allowed to explore freely for a period of 30 min. Locomotor behavior was measured for distance traveled during the first 5 minutes of the test.

Y-Maze Spontaneous Alterations

Y-Maze Spontaneous Alterations is an assay that measures working memory. This task measures the ability of the mouse to explore novel arms of the Y-maze (model 89000, Lafayette instruments). In this task, the animal was allowed to openly traverse a Y-maze undisturbed for 8 minutes. An alternation was defined as the mouse entering 3 different arms consecutively. Percent alternation was calculated to measure for short term-memory during the duration of the test.

Elevated Plus Maze

Elevated Plus Maze is an assay that measures anxiety-like behavior. This task measures preference for enclosed places and overexposed places. The maze was engineered in house with 2 open arms and 2 closed arms measuring 29 cm L x 7.5 cm W, with high walls at 14.5 cm high wall. The maze was ~45 cm off ground). The animal is placed in the center of the apparatus and observed freely exploring for 5 minutes. Recorded measures include total time spent in the open and closed arms (and central platform) as well as entries into the open and closed arms. Percent entries and time in arms throughout the tests were calculated to assess for anxiety-like behavior.

Contextual Fear Conditioning

Contextual Fear Conditioning is an assay that measures fear-based memory. This task measures the ability of an animal to learn about aversive events related to predictive stimuli and recall the aversive event when exposed to the stimuli. Defensive behavior, seen as freezing, is used to measure the animal recalling the event.

For the training trial, all animals were placed in the conditioning chamber for a total of 7.5 minutes. After 3 the initial minutes, the mice received a 30 sec, 80dB tone at 2800 Hz immediately followed by a 2-second long 0.75 mA foot-shock. This time shock pairing was repeated another two times with a 1-minute intertrial interval. After the three pairings, the subjects remain in the conditioning chamber for another 60 seconds and then are returned to their home cages.

The test trial (24 h later) assesses contextual fear conditioning by measuring freezing in the training context. Freezing was defined as a defensive posture characterized by a lack of all movement except that required for respiration. For measurements of context conditioning, the subjects are returned to the training chamber for an 8 min session. MedAssociates VideoFreeze software was used to assess this freezing with a threshold set to 18 pixel changes per frame (a threshold set based on previous research where hand-scoring of the videos was done to equate it to software results). The percent freezing was calculated for the entire session as well as broken into 1-minute bins for further assessment.

Due to high baseline freezing during the training which can make subsequent results difficult to interpret, it was decided not to test the tone conditioning memory as was originally planned. Training and testing procedures are recorded for later analysis of behavior in the pre-shock and post-shock periods of the training session as well as more detailed analyses of behavior during the tests.

Barnes maze

Barnes maze is a dry land maze that assesses spatial memory and navigation skills in mice. In this assay, a mouse is placed on a large circular arena (91 cm wide table with 20 evenly spaced, 5 cm wide holes around perimeter; Stoelting) that has 20 evenly spaced escape holes around the perimeter of the maze. Only one of the holes, the "target hole", contains a dark, enclosed goal box below the table for the mouse to escape, and the remaining 19 holes, are the "non-target holes," with no route of escape. Extra-maze cues are placed around the room for orientation and navigational cues. To encourage mice to find the goal box, the maze is brightly lit, and when necessary, loud white noise (~80-90 db) is played from the time the mouse is released until the escape is made. Please refer to the SI for a more elaborate description of Barnes maze protocol.

Rotarod

Rotarod measures for locomotor coordination. In this assay, mice are placed onto a cylinder that rotates at an accelerating speed, until the mice fall from the cylinder to the platform below (RotaRod 3375-5; TSE Technical & Scientific Equipment GmbH). The cylinder is divided into 4 compartments which allows four mice to perform the tests simultaneously. Below each compartment, there is an infrared sensor that automatically signals when the mouse fall. The apparatus is designed such that the mouse only drops a short distance (10 cm). The latency to fall from the cylinder is recorded by the apparatus and displayed on the screen to be recorded by the experimenter for later analysis. Mice have tested 3 trials per day over the course of 3 days.

Grip Strength

Grip Strength assesses motor function. In this assay, the strength of the fore- and hind-limb strength of the mouse is measured using the Chatillon (Grip Meter); Ametek; 10LBF; DFE-01. A mouse-sized metal grip bar is attached to the force meter. The mouse is scuffed and allowed to grasp the grip bar firmly in both front or back paws. The mouse is gently pulled away from the meter by the base of the tail in a horizontal motion until they release the bar. The maximum force exerted by the mouse until release is recorded. The angle of the grip bar can be adjusted for a hind-limb grip. Five grip trials are repeated in each subject with an intertrial interval of 5 minutes to prevent muscle fatigue.

Sectioning and staining of mouse brain tissue

Mouse brains were sent to Neuroscience Associates for sectioning and staining of treated mouse brains.

Quantitative Histopathology

Images of histology slides were scanned at 20X magnification from Neuroscience associates and were transferred using Proscia concentriq and TransferXL. After images were downloaded, they were viewed using the Olympus Viewer (v.3.1.) and using the Aperio ImageScope (v.12.4.6.5003). Aperio ImageScope was also used to quantify pathology identified by GFAP, and IBA-1. Qupath (Version) and protocols to analyze Thioflavin-S positive pathology were from Bankhead et al. 2015.[50]

Statistics

Raw data were acquired, exported, and processed on Microsoft Excel (v.9.0). GraphPad Prism (v.9.0) was used to perform all statistics and related figures. Unless otherwise stated, all statistical analysis were performed using a one-way ANOVA followed by Tukey, *post hoc*.

Acknowledgments

We thank the National Institutes of Health (NIH) National Institute on Aging (NIA) for funding (AG062296) for funding support. We acknowledge the support of the Chao Family Comprehensive Cancer Center Transgenic Mouse Facility Shared Resource, supported by the National Cancer Institute of the National Institutes of Health under award number P30CA062203. The content is solely the responsibility of the authors and does not necessarily represent the official views of the National Institutes of Health. Thank you to Dr. Shimako Kawauchi and UCI Transgenic Mouse Facility for providing mice for these studies. Dr. Chunni Zhu from the UCLA Brain Research Institute for allowing me to use the facilities. Dr. Stacy Kang and the team at the UCI ULAR (University Laboratory Animal Resources) for training and ensuring the health and wellbeing of the mice in this project. Figures were created with Biorender.com.

References

(1) Marciani, D. J. A Retrospective Analysis of the Alzheimer's Disease Vaccine Progress – The Critical Need for New Development Strategies. *Journal of Neurochemistry* **2016**, *137* (5), 687–700. https://doi.org/10.1111/jnc.13608.

(2) Masters, C. L.; Bateman, R.; Blennow, K.; Rowe, C. C.; Sperling, R. A.; Cummings, J. L. Alzheimer's Disease. *Nat Rev Dis Primers* **2015**, *1* (1), 1–18. https://doi.org/10.1038/nrdp.2015.56.

(3) Chen, G.-F.; Xu, T.-H.; Yan, Y.; Zhou, Y.-R.; Jiang, Y.; Melcher, K.; Xu, H. E. Amyloid Beta: Structure, Biology and Structure-Based Therapeutic Development. *Acta Pharmacol Sin* **2017**, *38* (9), 1205–1235. https://doi.org/10.1038/aps.2017.28.

(4) Schenk, D.; Barbour, R.; Dunn, W.; Gordon, G.; Grajeda, H.; Guido, T.; Hu, K.; Huang, J.; Johnson-Wood, K.; Khan, K.; Kholodenko, D.; Lee, M.; Liao, Z.; Lieberburg, I.; Motter, R.; Mutter, L.; Soriano, F.; Shopp, G.; Vasquez, N.; Vandevert, C.; Walker, S.; Wogulis, M.; Yednock, T.; Games, D.; Seubert, P. Immunization with Amyloid-β Attenuates Alzheimer-Disease-like Pathology in the PDAPP Mouse. *Nature* **1999**, *400* (6740), 173–177. https://doi.org/10.1038/22124.

(5) Marciani, D. J. Promising Results from Alzheimer's Disease Passive Immunotherapy Support the Development of a Preventive Vaccine. *Research* **2019**, *2019*. https://doi.org/10.34133/2019/5341375.

(6) *Investigational Alzheimer's Disease Therapy Lecanemab Granted FDA Fast Track Designation | Biogen*. https://investors.biogen.com/news-releases/news-release-details/investigational-alzheimers-disease-therapy-lecanemab-granted-fda (accessed 2022-02-23).

(7) *FDA Accepts Eisai's Filing of a Supplemental Biologics License Application and Grants Priority Review for Traditional Approval of LEQEMBI™ (lecanemab-irmb) for the Treatment of Alzheimer's Disease | News Release : 2023*. Eisai Co., Ltd. https://www.eisai.com/news/2023/news202316.html (accessed 2023-05-09).

(8) van Dyck, C. H.; Swanson, C. J.; Aisen, P.; Bateman, R. J.; Chen, C.; Gee, M.; Kanekiyo, M.; Li, D.; Reyderman, L.; Cohen, S.; Froelich, L.; Katayama, S.; Sabbagh, M.; Vellas, B.; Watson, D.; Dhadda, S.; Irizarry, M.; Kramer, L. D.; Iwatsubo, T. Lecanemab in Early Alzheimer's Disease. *New England Journal of Medicine* **2023**, *388* (1), 9–21. https://doi.org/10.1056/NEJMoa2212948.

(9) *Lilly's Donanemab Significantly Slowed Cognitive and Functional Decline in Phase 3 Study of Early Alzheimer's Disease | Eli Lilly and Company*. https://investor.lilly.com/news-releases/news-release-details/lillys-donanemab-significantly-slowed-cognitive-and-functional (accessed 2023-05-09).

(10) Alzinova AB. *A Double-Blind, Randomized, Parallel-Group Multiple Dose Study on the Safety, Tolerability and Immunogenicity of ALZ-101 in Participants With Early Alzheimer's Disease*; Clinical trial registration NCT05328115; clinicaltrials.gov, 2023. https://clinicaltrials.gov/ct2/show/NCT05328115 (accessed 2023-04-27).

(11) Araclon Biotech S.L. *A Multi-Center, Randomized, Double-Blind, Placebo-Controlled, 24 Months Study in Patients With Amnestic Mild Cognitive Impairment or Very Mild Alzheimer's Disease to Investigate the Safety, Tolerability and Immune Response of Repeated Subcutaneous Injections of ABvac40*; Clinical trial registration NCT03461276; clinicaltrials.gov, 2021. https://clinicaltrials.gov/ct2/show/NCT03461276 (accessed 2022-02-22).

(12) *Vaxxinity Receives FDA Fast Track Designation for UB-311 for Treatment of Alzheimer's Disease | Vaxxinity*. https://ir.vaxxinity.com/news-releases/news-release-details/vaxxinity-receives-fda-fast-track-designation-ub-311-treatment/ (accessed 2023-04-29).

(13) Parrocha, C. M. T.; Nowick, J. S. Current Peptide Vaccine and Immunotherapy Approaches against Alzheimer's Disease. *Peptide Science* **2023**, *115* (1), e24289. https://doi.org/10.1002/pep2.24289.

(14) Samdin, T. D.; Kreutzer, A. G.; Nowick, J. S. Exploring Amyloid Oligomers with Peptide Model Systems. *Current Opinion in Chemical Biology* **2021**, *64*, 106–115. https://doi.org/10.1016/j.cbpa.2021.05.004.

(15) Haerianardakani, S.; Kreutzer, A. G.; Salveson, P. J.; Samdin, T. D.; Guaglianone, G. E.; Nowick, J. S. Phenylalanine Mutation to Cyclohexylalanine Facilitates Triangular Trimer Formation by β-Hairpins Derived from Aβ. *J. Am. Chem. Soc.* **2020**, *142* (49), 20708–20716. https://doi.org/10.1021/jacs.0c09281.

(16) Parrocha, C. M. T.; Kreutzer, A. G.; Pascual, J.; Stringer, C.; Silva, J.; Nguyen, J. T.; Ith, A. L.; Ngo, P.; Andrews, E.; Head, E.; Nowick, J. S. Antibodies Generated from a Triangular Trimer from Aβ Recognize Cored and Neuritic Plaques in Brain Sections of People Who Lived with Late-Onset Alzheimer's Disease. Manuscript to be submitted to Acta Neuropathologica.

(17) Kreutzer, A. G.; Parrocha, C. M. T.; Haerianardakani, S.; Guaglianone, G.; Nguyen, J. T.; Diab, M. N.; Yong, W.; Perez-Rosendahl, M.; Head, E.; Nowick, J. S. Antibodies Raised Against an Aβ Oligomer Mimic Recognize Pathological Features in Alzheimer's Disease and Associated Amyloid-Disease Brain Tissue. bioRxiv May 12, 2023, p 2023.05.11.540404. https://doi.org/10.1101/2023.05.11.540404.

(18) Bakrania, P.; Hall, G.; Bouter, Y.; Bouter, C.; Beindorff, N.; Cowan, R.; Davies, S.; Price, J.; Mpamhanga, C.; Love, E.; Matthews, D.; Carr, M. D.; Bayer, T. A. Discovery of a Novel Pseudo β-Hairpin Structure of N-Truncated Amyloid-β for Use as a Vaccine against Alzheimer's Disease. *Mol Psychiatry* **2021**, 1–9. https://doi.org/10.1038/s41380-021-01385-7.

(19) Vuong, J. Case ID 01261857: Salt Conjugation Conditions for Hapten and Imject KLH [Ref:_00D1U19ofE._5001UtiVTS:Ref], 2022.

(20) Oakley, H.; Cole, S. L.; Logan, S.; Maus, E.; Shao, P.; Craft, J.; Guillozet-Bongaarts, A.; Ohno, M.; Disterhoft, J.; Eldik, L. V.; Berry, R.; Vassar, R. Intraneuronal β-Amyloid Aggregates, Neurodegeneration, and Neuron Loss in Transgenic Mice with Five Familial Alzheimer's Disease Mutations: Potential Factors in Amyloid Plaque Formation. *J. Neurosci.* **2006**, *26* (40), 10129–10140. https://doi.org/10.1523/JNEUROSCI.1202-06.2006.

(21) Forner, S.; Kawauchi, S.; Balderrama-Gutierrez, G.; Kramár, E. A.; Matheos, D. P.; Phan, J.; Javonillo, D. I.; Tran, K. M.; Hingco, E.; da Cunha, C.; Rezaie, N.; Alcantara, J. A.; Baglietto-Vargas, D.; Jansen, C.; Neumann, J.; Wood, M. A.; MacGregor, G. R.; Mortazavi, A.; Tenner, A. J.; LaFerla, F. M.; Green, K. N. Systematic Phenotyping and Characterization of the 5xFAD Mouse Model of Alzheimer's Disease. *Sci Data* **2021**, *8* (1), 270. https://doi.org/10.1038/s41597-021-01054-y.

(22) Walf, A. A.; Frye, C. A. The Use of the Elevated plus Maze as an Assay of Anxiety-Related Behavior in Rodents. *Nat Protoc* **2007**, *2* (2), 322–328. https://doi.org/10.1038/nprot.2007.44.

(23) Jawhar, S.; Trawicka, A.; Jenneckens, C.; Bayer, T. A.; Wirths, O. Motor Deficits, Neuron Loss, and Reduced Anxiety Coinciding with Axonal Degeneration and Intraneuronal Aβ Aggregation in the 5XFAD Mouse Model of Alzheimer's Disease. *Neurobiol Aging* **2012**, *33* (1), 196.e29-40. https://doi.org/10.1016/j.neurobiolaging.2010.05.027.

(24) Curzon, P.; Rustay, N. R.; Browman, K. E. Cued and Contextual Fear Conditioning for Rodents. In *Methods of Behavior Analysis in Neuroscience*; Buccafusco, J. J., Ed.; Frontiers in Neuroscience; CRC Press/Taylor & Francis: Boca Raton (FL), 2009.

(25) Oblak, A. L.; Lin, P. B.; Kotredes, K. P.; Pandey, R. S.; Garceau, D.; Williams, H. M.; Uyar, A.; O'Rourke, R.; O'Rourke, S.; Ingraham, C.; Bednarczyk, D.; Belanger, M.; Cope, Z. A.; Little, G. J.; Williams, S.-P. G.; Ash, C.; Bleckert, A.; Ragan, T.; Logsdon, B. A.; Mangravite, L. M.; Sukoff Rizzo, S. J.; Territo, P. R.; Carter, G. W.; Howell, G. R.; Sasner, M.; Lamb, B. T. Comprehensive Evaluation of the 5XFAD Mouse Model for Preclinical Testing Applications: A MODEL-AD Study. *Frontiers in Aging Neuroscience* **2021**, *13*.

(26) Wang, J.-C.; Zhu, K.; Zhang, H.-Y.; Wang, G.-Q.; Liu, H.-Y.; Cao, Y.-P. Early Active Immunization with Aβ3–10-KLH Vaccine Reduces Tau Phosphorylation in the Hippocampus and Protects Cognition of Mice. *Neural Regen Res* **2019**, *15* (3), 519–527. https://doi.org/10.4103/1673-5374.266061.

(27) *Prophylactic Vaccine Based on Pyroglutamate-3 Amyloid β Generates Strong Antibody Response and Rescues Cognitive Decline in Alzheimer's Disease Model Mice | ACS Chemical Neuroscience*. https://pubs.acs.org/doi/full/10.1021/acschemneuro.6b00336 (accessed 2023-04-12).

(28) Meier-Stephenson, F. S.; Meier-Stephenson, V. C.; Carter, M. D.; Meek, A. R.; Wang, Y.; Pan, L.; Chen, Q.; Jacobo, S.; Wu, F.; Lu, E.; Simms, G. A.; Fisher, L.; McGrath, A. J.;

Fermo, V.; Barden, C. J.; Clair, H. D. S.; Galloway, T. N.; Yadav, A.; Campágna-Slater, V.; Hadden, M.; Reed, M.; Taylor, M.; Kelly, B.; Diez-Cecilia, E.; Kolaj, I.; Santos, C.; Liyanage, I.; Sweeting, B.; Stafford, P.; Boudreau, R.; Reid, G. A.; Noyce, R. S.; Stevens, L.; Staniszewski, A.; Zhang, H.; Murty, M. R. V. S.; Lemaire, P.; Chardonnet, S.; Richardson, C. D.; Gabelica, V.; DePauw, E.; Brown, R.; Darvesh, S.; Arancio, O.; Weaver, D. F. Alzheimer's Disease as an Autoimmune Disorder of Innate Immunity Endogenously Modulated by Tryptophan Metabolites. *Alzheimer's & Dementia: Translational Research & Clinical Interventions* **2022**, *8* (1), e12283. https://doi.org/10.1002/trc2.12283.

(29) Weaver, D. F. Alzheimer's Disease as an Innate Autoimmune Disease (AD2): A New Molecular Paradigm. *Alzheimers Dement* **2022**. https://doi.org/10.1002/alz.12789.

(30) Xie, J.; Van Hoecke, L.; Vandenbroucke, R. E. The Impact of Systemic Inflammation on Alzheimer's Disease Pathology. *Frontiers in Immunology* **2022**, *12*.

(31) Xiong, M.; Jiang, H.; Serrano, J. R.; Gonzales, E. R.; Wang, C.; Gratuze, M.; Hoyle, R.; Bien-Ly, N.; Silverman, A. P.; Sullivan, P. M.; Watts, R. J.; Ulrich, J. D.; Zipfel, G. J.; Holtzman, D. M. APOE Immunotherapy Reduces Cerebral Amyloid Angiopathy and Amyloid Plaques While Improving Cerebrovascular Function. *Science Translational Medicine* **2021**, *13* (581), eabd7522. https://doi.org/10.1126/scitranslmed.abd7522.

(32) Biffi, A.; Greenberg, S. M. Cerebral Amyloid Angiopathy: A Systematic Review. *J Clin Neurol* **2011**, *7* (1), 1–9. https://doi.org/10.3988/jcn.2011.7.1.1.

(33) Giannoni, P.; Arango-Lievano, M.; Neves, I. D.; Rousset, M.-C.; Baranger, K.; Rivera, S.; Jeanneteau, F.; Claeysen, S.; Marchi, N. Cerebrovascular Pathology during the Progression

of Experimental Alzheimer's Disease. *Neurobiology of Disease* **2016**, *88*, 107–117. https://doi.org/10.1016/j.nbd.2016.01.001.

(34) Gilman, S.; Koller, M.; Black, R. S.; Jenkins, L.; Griffith, S. G.; Fox, N. C.; Eisner, L.; Kirby, L.; Rovira, M. B.; Forette, F.; Orgogozo, J.-M.; AN1792(QS-21)-201 Study Team. Clinical Effects of Abeta Immunization (AN1792) in Patients with AD in an Interrupted Trial. *Neurology* **2005**, *64* (9), 1553–1562. https://doi.org/10.1212/01.WNL.0000159740.16984.3C.

(35) Orgogozo, J.-M.; Gilman, S.; Dartigues, J.-F.; Laurent, B.; Puel, M.; Kirby, L. C.; Jouanny, P.; Dubois, B.; Eisner, L.; Flitman, S.; Michel, B. F.; Boada, M.; Frank, A.; Hock, C. Subacute Meningoencephalitis in a Subset of Patients with AD after Abeta42 Immunization. *Neurology* **2003**, *61* (1), 46–54. https://doi.org/10.1212/01.wnl.0000073623.84147.a8.

(36) Nicoll, J. A. R.; Buckland, G. R.; Harrison, C. H.; Page, A.; Harris, S.; Love, S.; Neal, J. W.; Holmes, C.; Boche, D. Persistent Neuropathological Effects 14 Years Following Amyloid-β Immunization in Alzheimer's Disease. *Brain* **2019**, *142* (7), 2113–2126. https://doi.org/10.1093/brain/awz142.

(37) Lemere, C. A.; Masliah, E. Can Alzheimer Disease Be Prevented by Amyloid-β Immunotherapy? *Nat Rev Neurol* **2010**, *6* (2), 108–119. https://doi.org/10.1038/nrneurol.2009.219.

(38) Kreutzer, A. G.; Nowick, J. S. Elucidating the Structures of Amyloid Oligomers with Macrocyclic β-Hairpin Peptides: Insights into Alzheimer's Disease and Other Amyloid Diseases. *Acc. Chem. Res.* **2018**, *51* (3), 706–718. https://doi.org/10.1021/acs.accounts.7b00554.

(39) Ciudad, S.; Puig, E.; Botzanowski, T.; Meigooni, M.; Arango, A. S.; Do, J.; Mayzel, M.; Bayoumi, M.; Chaignepain, S.; Maglia, G.; Cianferani, S.; Orekhov, V.; Tajkhorshid, E.; Bardiaux, B.; Carulla, N. Aβ(1-42) Tetramer and Octamer Structures Reveal Edge Conductivity Pores as a Mechanism for Membrane Damage. *Nat Commun* **2020**, *11* (1), 3014. https://doi.org/10.1038/s41467-020-16566-1.

(40) Das, P.; Murphy, M. P.; Younkin, L. H.; Younkin, S. G.; Golde, T. E. Reduced Effectiveness of Abeta1-42 Immunization in APP Transgenic Mice with Significant Amyloid Deposition. *Neurobiol Aging* **2001**, *22* (5), 721–727. https://doi.org/10.1016/s0197-4580(01)00245-7.

(41) Nemirovsky, A.; Shapiro, J.; Baron, R.; Kompaniets, A.; Monsonego, A. Active Aβ Vaccination Fails to Enhance Amyloid Clearance in a Mouse Model of Alzheimer's Disease with Aβ42-Driven Pathology. *Journal of Neuroimmunology* **2012**, *247* (1), 95–99. https://doi.org/10.1016/j.jneuroim.2012.03.017.

(42) Oddo, S.; Vasilevko, V.; Caccamo, A.; Kitazawa, M.; Cribbs, D. H.; LaFerla, F. M. Reduction of Soluble Aβ and Tau, but Not Soluble Aβ Alone, Ameliorates Cognitive Decline in Transgenic Mice with Plaques and Tangles *. *Journal of Biological Chemistry* **2006**, *281* (51), 39413–39423. https://doi.org/10.1074/jbc.M608485200.

(43) Rajan, K. B.; Weuve, J.; Barnes, L. L.; McAninch, E. A.; Wilson, R. S.; Evans, D. A. Population Estimate of People with Clinical Alzheimer's Disease and Mild Cognitive Impairment in the United States (2020-2060). *Alzheimers Dement* **2021**, *17* (12), 1966–1975. https://doi.org/10.1002/alz.12362.

(44) 2022 Alzheimer's Disease Facts and Figures. *Alzheimers Dement* **2022**, *18* (4), 700–789. https://doi.org/10.1002/alz.12638.

(45) *Biogen's $56K price on Aduhelm "simply unacceptable," Alzheimer's Association says after vouching for FDA approval | Fierce Pharma*. https://www.fiercepharma.com/pharma/biogen-s-56k-price-tag-for-aduhelm-simply-unacceptable-and-needs-fixed-alzheimer-s (accessed 2023-05-01).

(46) *Biogen Announces Reduced Price for ADUHELM® to Improve Access for Patients with Early Alzheimer's Disease | Biogen*. https://investors.biogen.com/news-releases/news-release-details/biogen-announces-reduced-price-aduhelmr-improve-access-patients (accessed 2023-05-01).

(47) Inc, E. *EISAI'S APPROACH TO U.S. PRICING FOR LEQEMBI™ (LECANEMAB), A TREATMENT FOR EARLY ALZHEIMER'S DISEASE, SETS FORTH OUR CONCEPT OF "SOCIETAL VALUE OF MEDICINE" IN RELATION TO "PRICE OF MEDICINE."* https://www.prnewswire.com/news-releases/eisais-approach-to-us-pricing-for-leqembi-lecanemab-a-treatment-for-early-alzheimers-disease-sets-forth-our-concept-of-societal-value-of-medicine-in-relation-to-price-of-medicine-301715694.html (accessed 2023-05-01).

(48) *LEQEMBI (lecanemab-irmb) Eisai Patient Support*. https://www.eisaireimbursement.com/patient/leqembi (accessed 2023-05-01).

(49) *ADUHELM® (aducanumab-avwa) | Official Patient Site*. https://www.aduhelm.com/en-us/home.html (accessed 2023-05-01).

(50) Bankhead, P.; Loughrey, M. B.; Fernández, J. A.; Dombrowski, Y.; McArt, D. G.; Dunne, P. D.; McQuaid, S.; Gray, R. T.; Murray, L. J.; Coleman, H. G.; James, J. A.; Salto-Tellez, M.; Hamilton, P. W. QuPath: Open Source Software for Digital Pathology Image Analysis. *Sci Rep* **2017**, *7* (1), 16878. https://doi.org/10.1038/s41598-017-17204-5.

Supplemental Information for

Pilot study in 5xFAD mice of vaccines against Alzheimer's disease using structurally defined oligomers derived from the β-amyloid peptide

Synthesis of peptide monomer 4AT-L_{cc} and cross-linked trimer 4AT-L

Information for the synthesis of peptide monomers 4AM-L, and 4AT-L_{cc} and cross-linked trimer 4AT-L was adopted or taken verbatim from Haerianardakani et al. 2020,[15] Kreutzer et al. 2017,[17] and Parrocha et al. 2023.[16] 2AM-L monomer and 2AT-L trimer used in this manuscript was also used in another manuscript in the Nowick Group. Characterization data for 2AM-L monomer and 2AT-L trimer can be found in the SI of Kreutzer et al. 2023.[17]

Curation of 5xFAD mice and wild type littermates

Information for the curation of 5xFAD mice and wild type littermates and preparation of mouse brain tissue can be found in Parrocha et al. 2023.[16]

Barnes Maze Protocol

The Barnes maze is a less stressful alternative to the Morris Water Maze for the assessment of spatial learning and memory in mice. When properly executed, the test can provide valuable information for acquisition/learning, as well as working memory, and long and short-term memory.

Habituation/exploration. One day prior to training, habituation is performed by allowing each subject to freely explore the table (without escape box) under modest light for 5 minutes, in order to become accustomed to the room, table, and extra- and intra-maze layout.

Pre-training. Pre-training, designed to allow subjects to learn of the presence of the escape hole, is performed under bright light prior to the start of training by placing each subject in a clear box (upside down) in the middle of the table. After one minute, the box is lifted up and the subject is gently guided near the escape hole selected randomly on the table, allowing it to enter the hole and remain inside for 1 minute. If necessary, bedding may be added to the goal box in order to make it more attractive to the mice.

Initial training. All training and test trials begin with the subject in an opaque box in the center of the table. The trial starts when the box is lifted up. If the subject locates and enters the escape box within 90s, it will be left in the box for 1 minute. If the subject fails to find the escape box within 90s, it will be gently guided to the escape hole by the tail, and allowed to stay in the box for 1 minute. Mice received 3 daily trials with a 15-20 min inter-trial interval. All trials were recorded by an overhead camera and scored for latency to find escape box and number of incorrect holes visited first.

Probe test. Twenty-four hours after the last day of training, animals are tested for 90s without the escape box. Time spent in the different quadrants is recorded.

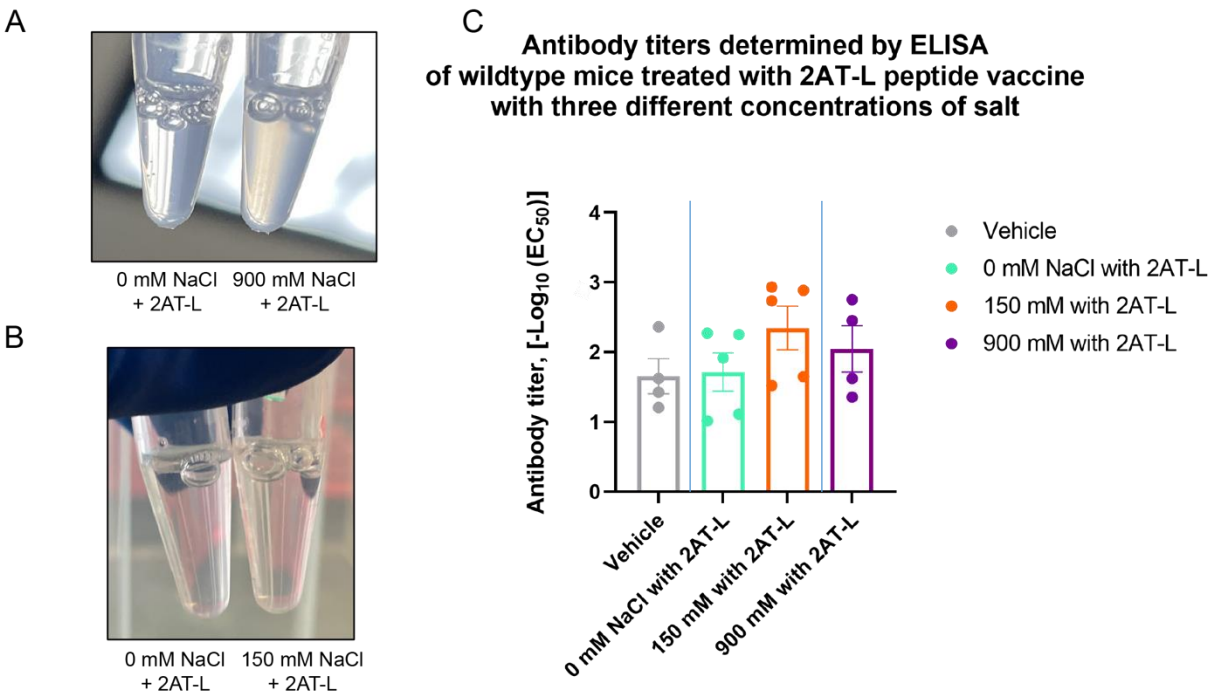

Supplemental Figure S4.1. Optimizing NaCl concentrations in the conjugation of 2AT-L to KLH by antibody titers in C57/Bl6 mice. (**A**) images of conjugation reactions with 0 mM or 900 mM NaCl with 2AT-L trimer or (**B**) 0 mM or 150 mM NaCl with 2AT-L trimer. (**C**) is a bar graph showing normalized and inverse EC_{50} values determined by ELISAs from serum of C57BL/6 mice immunized with different KLH + 2AT-L conjugations in different concentrations of NaCl (n = 4 – 5 per group). The thin blue lines represents data pooled from two different cohorts of mice from similar experiments. Error bars are standard error of the mean.

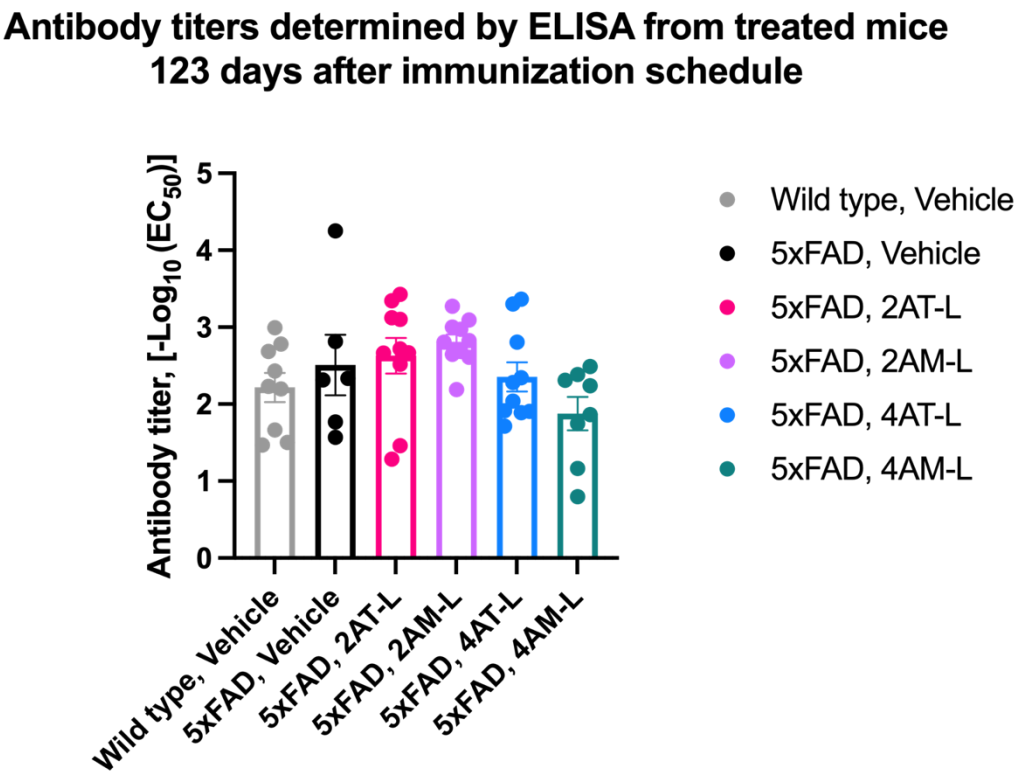

Supplemental Figure S4.2. Bar graph showing normalized and inverse EC_{50} values determined by ELISAs from serum of 5xFAD mice vaccinated 123 days after immunization schedule with 2AT-L (n=10), 2AM-L (n=10), 4AT-L (n=10), and 4AM-L (n=9). Treated mice were compared to wild-type mice (n=9) and 5xFAD mice (n=6) treated with vehicle. One-way ANOVA F (5, 47) = 2.409, p = 0.0503. Error bars are standard error of the mean.

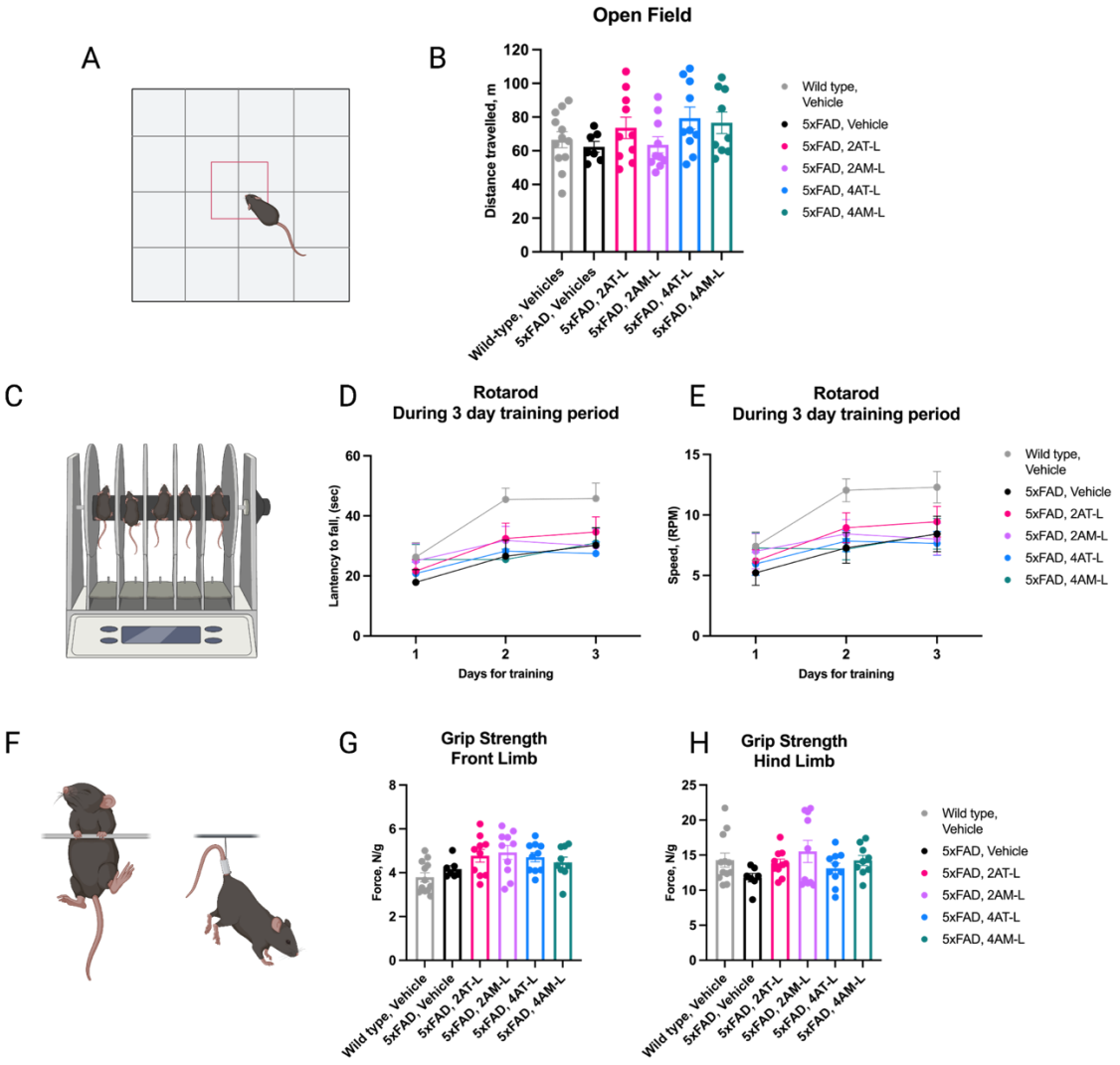

Supplemental Figure S4.3. Behavior assays assessing for locomotor behavior. (**A**) shows a schematic representation of a mouse in open field (). (**B**) bar graph showing the distance traveled by the mice during the first 5 minutes of the test (one-way ANOVA, F (5, 52) = 1.538, p=0.1943). (**C**) shows a schematic representation of a mice on a rotarod. **(D**) shows line graphs of how long the mice stayed on the rotarod (one-way ANOVA, F (5, 12) = 1.927, p=0.1632) while (**E**) shows the speed of the rotarod when the mice fell over the three day training period (one-way ANOVA , F (5, 12) = 2.019, p=0.1479). (**F**) shows a schematic representation of a mouse performing grip strength. (**G**) bar graph showing the amount of force the front limb of a mouse can exert on a scale (one-way ANOVA, F (5, 52) = 3.189, p=0.0138) while (**H**) is a bar graph showing the amount of force the hind limb of a mouse can exert on a scale (one-way ANOVA , F (5, 52) = 1.416, p=0.2340). (Wild type, vehicle n=12 , 5xFAD, vehicle, n= 7, 5xFAD, 2AT-L n=10, 5xFAD, 2AM-L n= 10, 5xFAD, 4AM-L n=10,5xFAD, 4AT-L n=10). Error bars are standard error of the mean.

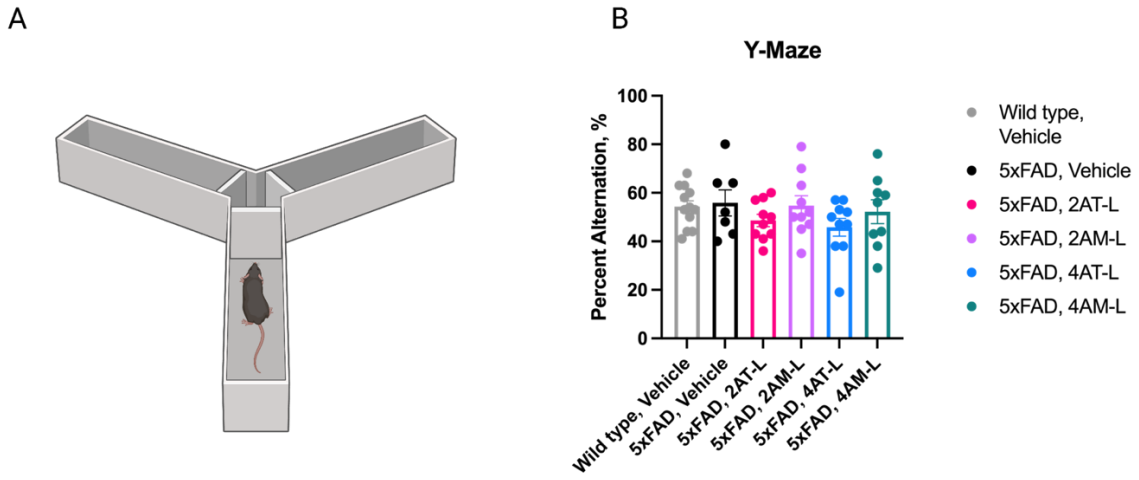

Supplemental Figure S4.4. Y-maze assesses for working memory which is not reverse in 5xFAD mice vaccinated with 2AT-L (n=10), 2AM-L (n=10), 4AT-L (n=10), and 4AM-L (n=9). Treated mice were compared to wild-type mice (n=12) and 5xFAD mice (n=7) treated with vehicle. One-way ANOVA (F (5, 52) = 1.090l, p=0.3771). (**A**) Shows a schematic representation of a mouse in the Y-maze. (**B**) Bar graph showing percent alternations of mice in during the entirety of the test. Error bars are standard error of the mean.

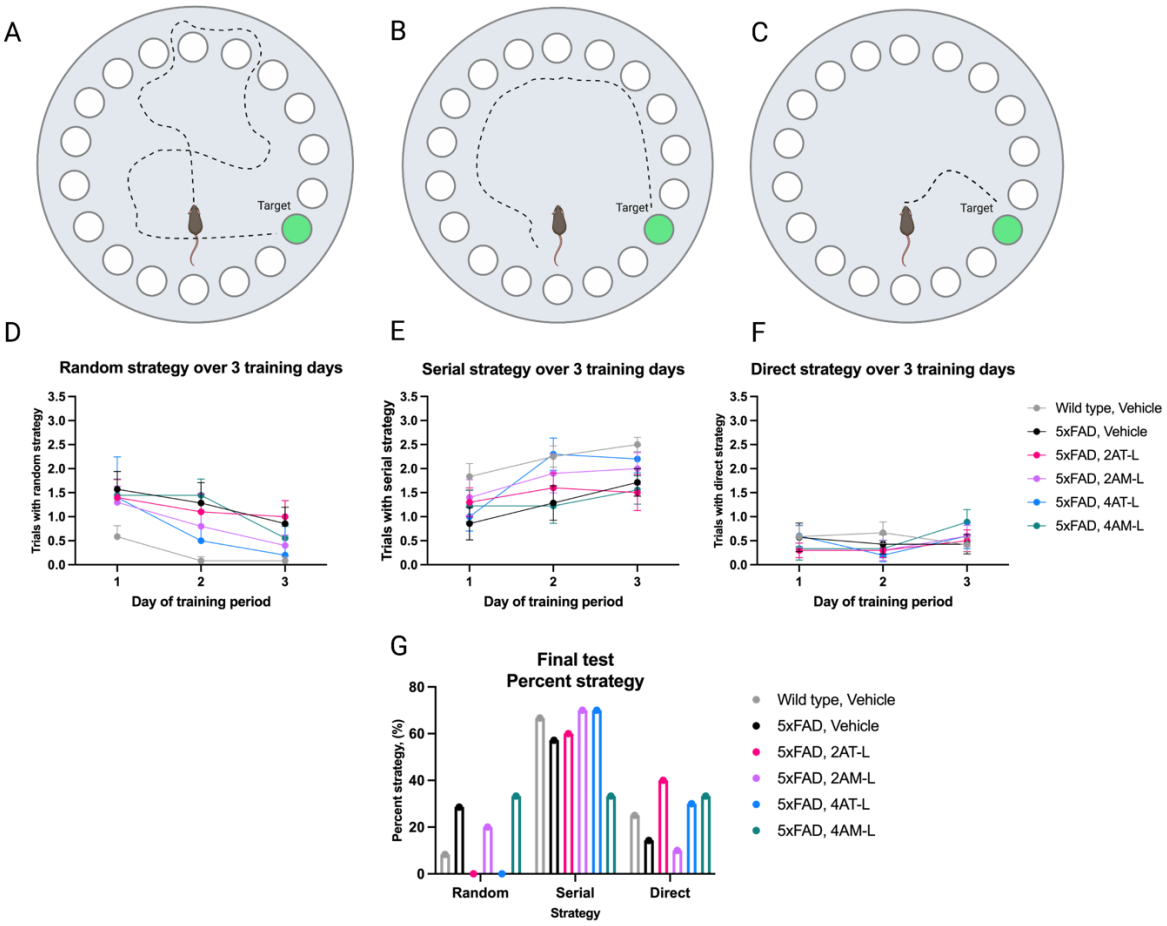

Supplemental Figure S4.5. Barnes maze accessing for navigation skills in treated mice which is not reversed in 5xFAD mice vaccinated with 2AT-L (n=10), 2AM-L (n=10), 4AT-L (n=10), and 4AM-L (n=9). Treated mice were compared to wild-type mice (n=12) and 5xFAD mice (n=7) treated with vehicle. One-way ANOVA (F (5, 52) = 1.090l, p=0.3771). (**A-C**) shows a schematic representation of a mouse in the Barnes maze demonstrating a random (**A**), serial (**B**), or (**C**) direct navigation strategy. (**D-F)** line graphs showing the average strategy each mouse performed during three days of training which was either (**D**) random (one-way ANOVA, F (5, 12) = 2.308, p=0.1092), (**E**) serial (one-way ANOVA, F (5, 12) = 2.232, p=0.1182), or (**F**) direct (one-way ANOVA, F (5, 12) = 0.4057, p=0.8358) navigation strategy. (**G**) bar graph for the final testing showing average percent strategy each mouse performed (one-way ANOVA, F (5, 12) = 8.808e-019, p>0.9999).

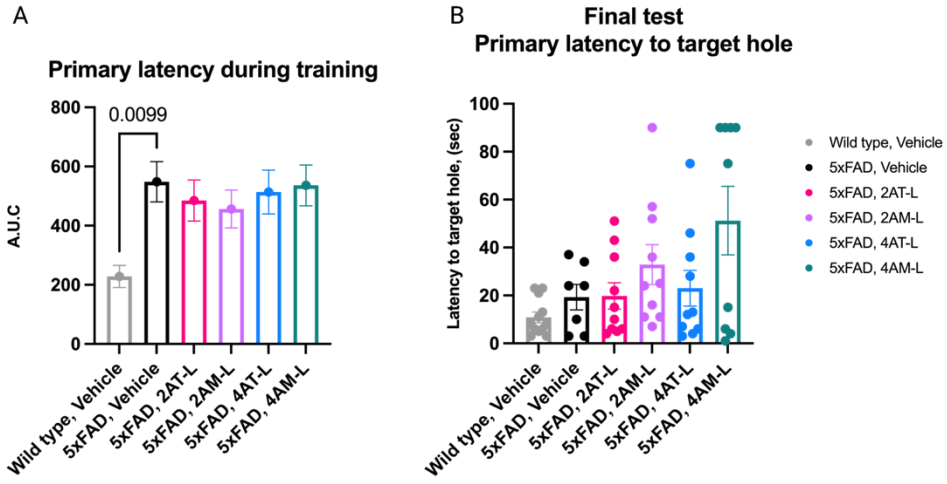

Supplemental Figure S4.6. Barnes maze accessing for spatial memory in treated mice which is not reversed in 5xFAD mice vaccinated with 2AT-L (n=10), 2AM-L (n=10), 4AT-L (n=10), and 4AM-L (n=9). Treated mice were compared to wild-type mice (n=12) and 5xFAD mice (n=7) treated with vehicle. (**A**) is a bar graph generated by calculating the area under the curve from the average time it took for mice in each treatment group to find the target hole across a total of 12 training sessions (one-way ANOVA, F (5, 624) = 4.05, p=0.0013). (**B**) shows a bar graph for the final testing showing primary latency for mice in each treatment group to get to the target hole (one-way ANOVA, F (5, 52) = 3.324, p=0.0111).).

Supplemental Table S4.1. Reagents Used in Paper

Item	Supplier	Cat No	Lot No	Storage	Dilution/ Concentration for IF and IHC
Materials for ELISA					
Peroxidase AffiniPure Goat Anti-Mouse IgG (H+L)	Jackson ImmunoResearch	115-035-003	N/A	-80 degrees	1: 5000
500 ml TMB/E Single Reagent, Blue color, Horseradish Peroxidase Substrate	Millipore	ES001-500ML	4 degrees	50 uL per well	500 ml TMB/E Single Reagent, Blue color, Horseradish Peroxidase Substrate
Materials for Immunofluorescent Staining (IF)					
Thioflavine S (Practical Grade)	Sigma-Aldrich	T1892-25G	MKCH4108	RT	0.5% in 50% EtOH
TrueBlack™ Lipofuscin Autofluorescence Quencher	GoldBiotechnology	TB-250-1	N/A	RT	50 uL per 1 mL of 70% EtOH
Materials for Immunohistochemistry Staining (IHC)					
DPX Mounting Media	Sigma-Aldrich	SKU 06522	N/A	RT	N/A
Vectastain Elite ABC-HRP Kit Peroxidase	Vector Laboratories	Cat. No. PK-6100	N/A	4 degrees	Manufacturer's instructions
DAB Substrate Kit, Peroxidase (HRP), with Nickel	Vector Laboratories	Cat. No. SK-4100	N/A	4 degrees	Manufacturer's instructions

88% formic acid (Certified ACS)	Fisher Chemical	Cat. No. A118P-100	RT	88%	88% formic acid (Certified ACS)
Normal goat serum	Vector laboratories	REF S-1000	4 degrees	5% (v/v)	Normal goat serum
Mouse IgG Blocking Reagent	Vector Laboratories	Cat. No. MKB-2213	N/A	4 degrees	Manufacturer's instructions
Normal Horse Serum	Vector Laboratories	REF S-2000	N/A	4 degrees	5% (v/v)
Horse Anti-Rabbit IgG Antibody (H+L), Biotinylated	Vector Laboratories	BA-1100-1.5	N/A	4 degrees	1:1000
Horse Anti-Mouse IgG Antibody (H+L), Biotinylated	Vector Laboratories	BA-2000-1.5			
0.1% Cresyl Violet	Abcam	ab246817	N/A	4 degrees	
Horse Anti-Mouse IgG Antibody (H+L), Biotinylated	Vector Laboratories	BA-2000-1.5			

Characterization data for monomer 4AM-L

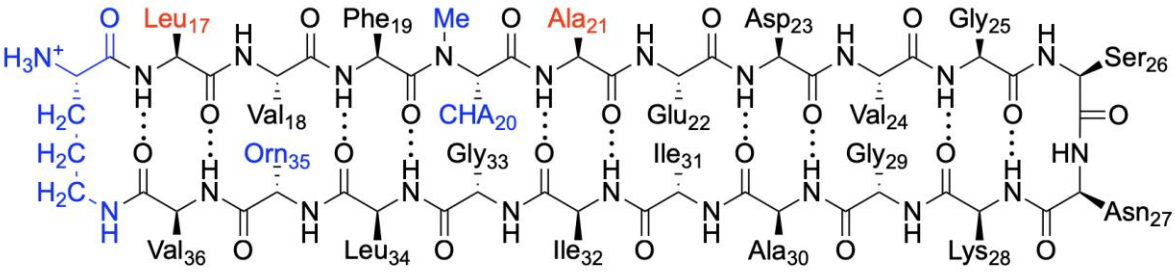

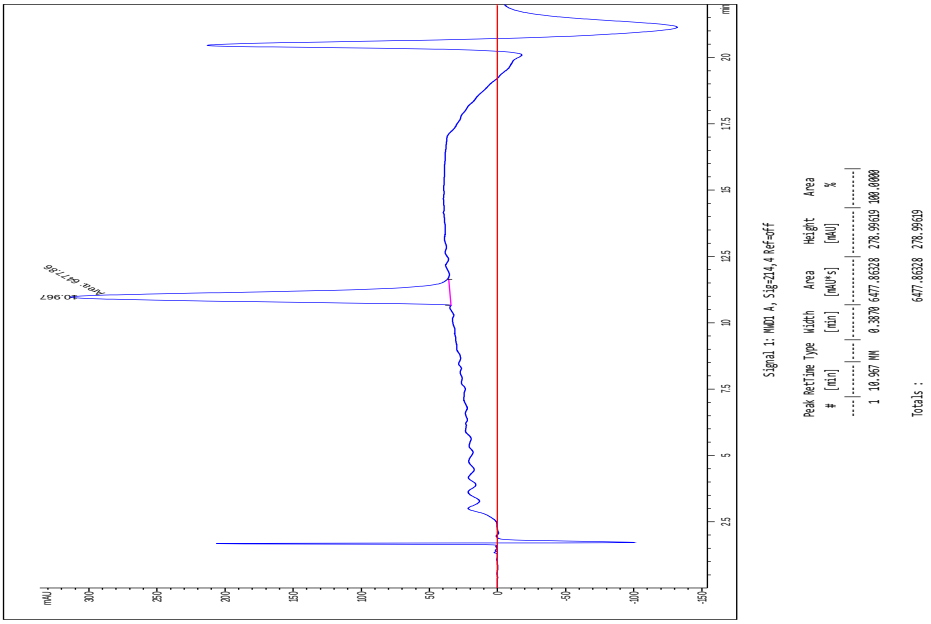

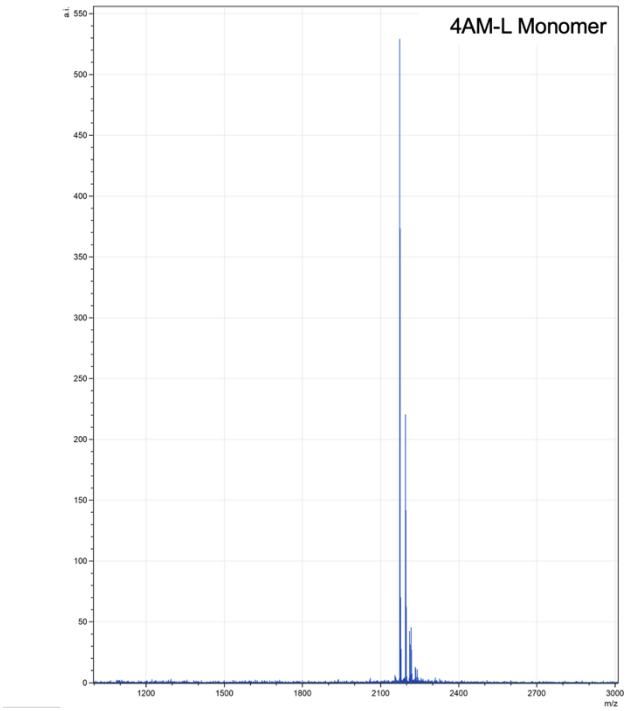
4AM-L Monomer
a.i.
m/z

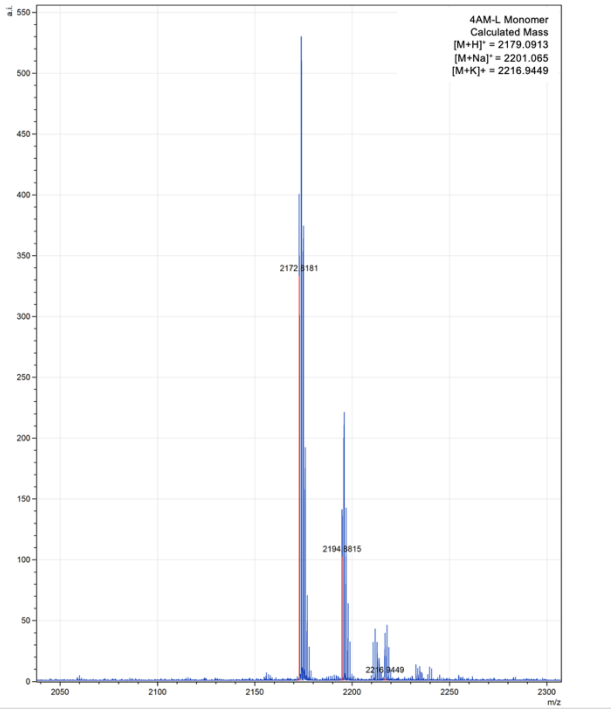
4AM-L Monomer
Calculated Mass
[M+H]+ = 2179.0913
[M+Na]+ = 2201.065
[M+K]+ = 2216.9449
2172.8181
2194.8815
2216.9449
a.i.
m/z

Chapter 5

Preliminary results on antibodies generated from a triangular trimer from Aβ recognizing Aβ pathology exclusive to people who lived with Down Syndrome and Alzheimer's disease (DSAD): an epilogue

Preface

In this epilogue, I discuss preliminary data and the motivation behind performing immunofluorescence studies with the antibody described in Chapter 2 ($pAb_{4AT\text{-}L}$) on people who lived with Down Syndrome and Alzheimer's disease (DSAD). AD can be considered a genetically inherited disease as risk factors can impact the onset of AD from as early as 40 years old. A unique case of genetically inherited AD is DSAD. DSAD is the early onset of AD in people who are carriers of an extra chromosome 21 (hence, Trisomy 21). The amyloid precursor protein (*APP*) is located in Chromosome 21.

Introduction

Alzheimer's disease (AD) is a neurological proteinopathy that is the 7th leading cause of death in the United States alone.[1,2] Risk factors associated with AD can be genetically inherited and are used to better understand the cause of AD. The apolipoprotein gene (*APOE*) is a genetic risk factor associated with early-onset AD (EOAD), and includes the APOE ε2, APOE ε3, and APOE ε4 allele.[3,4] Although genetic testing is not routinely used in the clinic, the results of

clinical studies may influence routine neurological health screenings especially to identify candidates for novel AD therapies. In a phase II study of Eisai's Lecanemab, severe cases of ARIA (Amyloid Related Imaging Abnormalities) associated with hemorrhages and inflammation (ARIA-H, and ARIA-E, respectively) correlated with people who were homozygous carriers for APOE ε4.[5] Therefore, as a precaution, it is recommended that people are genetically screened before taking this immunotherapy. This is one of the many genetic AD-associated outcomes in clinical trials influencing medical practices and research associated with a better understanding of AD.

Familial Alzheimer's disease (FAD) mutations are another form of genetically inherited AD that has allowed researchers to understand the molecular bases of the disease. These autosomal dominant mutations are also associated with EOAD and are named by the mutations in the genes of the amyloid precursor protein (*APP*) and presenilin 1 and 2 (*PSEN1*, *PSEN*2) which are involved in the production of the Aβ peptide.[3,6] FAD mutations have been used to generate AD transgenic mouse models to better understand the molecular basis of AD. The development of AD transgenic mice has enhanced the understanding of the disease and the development of therapies. However, these models lack predictive and construct validity which has been seen as therapies transition from preclinical research in mice to clinical trials in people.[7–9] Another form of genetically inherited AD is developed by people who live with Down Syndrome (DS).

People who live with DS can provide a wealth of knowledge in understanding the onset of AD in the general population. DS is a genetic disease that is caused by an extra chromatid in chromosome 21 (hence, Trisomy 21). The *APP* gene is located in chromosome 21, accelerating

the deposition of AD in people with DS (DSAD).[10] By 40 years old, people living with DS dramatically accumulate Aβ, resulting in a deposition of Aβ that is higher in the general AD population.[11] People with DSAD also have elevated levels of toxic soluble Aβ and incidences of cerebral amyloid angiopathy (CAA).[12,13] Immunostaining studies revealed new pathology present in people who live with DSAD that is also present in people who live with EOAD.[14,15] This unique pathology, namely coarse-grained plaques and bird's nest plaques, demonstrates the unique plaque pathogenesis of people who live with DSAD and EOAD.[14,15]

Coarse-grained plaques and bird's nest plaques were found in the sulcal depths and associated with CAA. Coarse-grained plaques are defined as ranging from 30-100 μm, have coarse-grainy deposits with multiple cores, and lack a border as well as Aβ pores.[16] Bird's-nest plaques are described as containing thick and dense amyloid fibrils and having a definite border that is formed by reactive astrocytes.[15] The presence of these plaques suggests unique plaque pathogenesis in people who live with DSAD and EOAD. Because people living with DS have a set temporal progression and the onset of AD, this provides construct and predictive validity that is lacking in transgenic mouse models or animals who naturally obtain AD-like phenotypes with aging. The genetic mutations in people who live with DS can allow researchers to investigate the onset of AD in a more relevant model that can be applied to the general AD population.

In this preliminary study, we explore the forms of pathology that the $pAb_{4AT\text{-}L}$ recognizes in people who live with DSAD. Chapter 2 established that the $pAb_{4AT\text{-}L}$ antibody recognizes cored and neuritic plaques along with cerebral amyloid angiopathy (CAA) that share a conformation or arrangement similar to the 4AT-L trimer. We further speculate that $pAb_{4AT\text{-}L}$ recognizes Aβ oligomers in these pathologies. Findings from this study support the hypothesis

that $pAb_{4AT\text{-}L}$ recognizes specific conformations of Aβ that differ from those recognized by a non-conformation-specific Aβ dye (Amytracker-680). We hypothesize that $pAb_{4AT\text{-}L}$ will recognize similar pathology as people who lived with LOAD. More specifically, we investigate whether $pAb_{4AT\text{-}L}$ recognizes unique pathology that is exclusive to people who lived with DSAD and EOAD. Results from this study may provide additional insight into the composition of Aβ plaques and the role arrangements of conformations of the 4AT-L trimer may be involved in the pathogenesis and progression of AD.

Results and Discussion

To perform initial characterization of pathology recognized by $pAb_{4AT\text{-}L}$ in sections of frontal cortex from two males with DSAD (~50 years old), we co-stained $pAb_{4AT\text{-}L}$ with an Aβ dye (Amytracker-680). Amytracker-680 is a modern bright fluorescence stain used for labeling protein aggregates with repetitive β-sheet arrangements.[17] Traditionally, Thioflavin-S is used to stain for similar aggregates that is identified with Amytracker-680 however, unlike Thioflavin-S, Amytracker-680 can be used in immunofluorescent staining. By observing the colocalization of pathology or lack thereof on the same tissue between Amytracker-680 with $pAb_{4AT\text{-}L}$, we gain additional insight on the molecular entities recognized by either Amytracker-680 with $pAb_{4AT\text{-}L}$.

In DSAD brain sections stained with $pAb_{4AT\text{-}L}$ and Amytracker-680, there was a striking lack of colocation on similar pathology (**Figure 5.1**). Unlike $pAb_{4AT\text{-}L,}$ Amytracker-680 stains more plaques on the same area of tissue than $pAb_{4AT\text{-}L}$ (**Figure 5.1 B**). Observed differences are noted by the * symbol. $pAb_{4AT\text{-}L}$ recognizes CAA which appears to not be colocalized with Amytracker-680 which is noted by the ^ signal (**Figure 5.1 A and B**). Although very minor

$pAb_{4AT\text{-}L}$ and Amytracker-680 have some colocalization on the tissue which is denoted in the # symbol (**Figure 5.1 C**).

$pAb_{4AT\text{-}L}$ recognition of plaques and CAA in brain tissue from people who lived with DSAD are consistent with the patterns observed on brain tissue from people who lived with LOAD.[d] The lack of colocalization suggests $pAb_{4AT\text{-}L}$ recognizes different conformations of Aβ that differ from Amytracker-680 with some exceptions of overlap as seen in the # signal of (**Figure 5.1 C**). Together, the lack of colocalization between $pAb_{4AT\text{-}L}$ and Amytracker-680 suggest that $pAb_{4AT\text{-}L}$ is more conformation-specific than Amytracker-680.

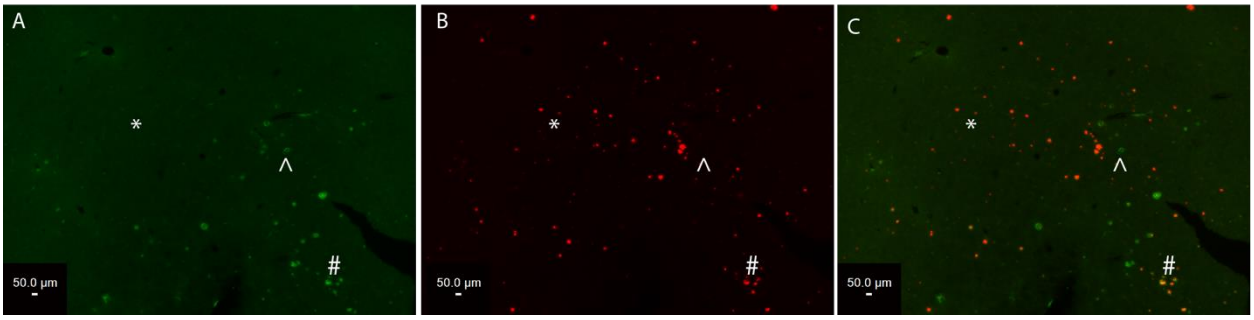

Figure 5.1. Fluorescent micrographs of occipital cortex brain slices from two individuals who lived with DSAD. The * symbol showing area on the tissue where there is a lack of colocalization between $pAb_{4AT\text{-}L}$ and Amytracker-680. The ^ symbol shows CAA that is recognized with $pAb_{4AT\text{-}L}$. The # symbol shows colocalization between $pAb_{4AT\text{-}L}$ and Amytracker-680. (**A**) is a micrograph showing $pAb_{4AT\text{-}L}$ recognizing Aβ pathology (green). (**B**) is a micrograph showing Amytracker-680 recognizing insoluble dense Aβ pathology (red). (**C**) are overlays of $pAb_{4AT\text{-}L}$ and Amytracker-680. All images were taken at 20X magnification; the scale bar is 50 µm.

To better understand the distinct differences between $pAb_{4AT\text{-}L}$ and Amytracker-680, we observed the kind of plaques based solely on plaques morphology. $pAb_{4AT\text{-}L}$ appears to identify

[d] Staining experiments used to characterize $pAb_{4AT\text{-}L}$ (as explained in Chapter 2) was performed on the occipital cortex of people who lived with LOAD. Staining experiments used to characterize $pAb_{4AT\text{-}L}$ in this preliminary study was performed on the *frontal cortex* of people who lived with DSAD. To make more meaningful comparisons, future studies should stain the *occipital cortex* of people who live with DSAD.

cored plaques that are not recognized by Amytracker-680 (**Figure 5.2 A and B**). These plaques are denoted with a * symbol. These observations suggest that suggest $pAb_{4AT\text{-}L}$ may recognize coarse-grained plaques or bird's nest plaques that are exclusive in people who live with DSAD or EOAD. These plaques are denoted with the ^ symbol. If these plaques are indeed cored plaques, coarse-grained plaques or bird's nest plaques, the preliminary results may suggest that these specific plaques may have an arrangement of conformation similar to the 4AT-L trimer. Additional immunostaining studies (such as co-staining with IBA-1 and GFAP) should be performed to confirm the plaque phenotypes.

In another form of plaque morphology, we observed Aβ pathology recognized by $pAb_{4AT\text{-}L}$ wrap around other forms of Aβ pathology that is distinctly recognized by Amytracker-680 which is denoted with the & symbol in **Figure 5.2 C-E**. We also observe this difference in recognition of similar pathology in (presumably) cored plaques (**Figures 5.2F-H**). $pAb_{4AT\text{-}L}$ is more selective in recognizing the cores and halos of the cored plaques (**Figure 5.2 F**) whereas Amytracker-680 recognition appears to be more central and less specific on the cored plaque which is denoted by the % symbol in (**Figure 5.2 G**).

The difference of recognition between Amytracker-680 and $pAb_{4AT\text{-}L}$ may provide insight on the composition of plaques in people who lived with DSAD and EOAD. Amytracker-680 recognizes β-sheet formation, and therefore fibril species of Aβ. As established in Chapter 2, $pAb_{4AT\text{-}L}$ recognizes Aβ oligomers that surround the cores of cored plaques in people who live with LOAD. Immunofluorescent staining of $pAb_{4AT\text{-}L}$ in people who live with DSAD supports that $pAb_{4AT\text{-}L}$ recognizes soluble Aβ (and perhaps Aβ oligomers) in plaques. These preliminary

studies provide an opportunity to further investigate the recognition of $pAb_{4AT\text{-}L}$ in people who live with DSAD.

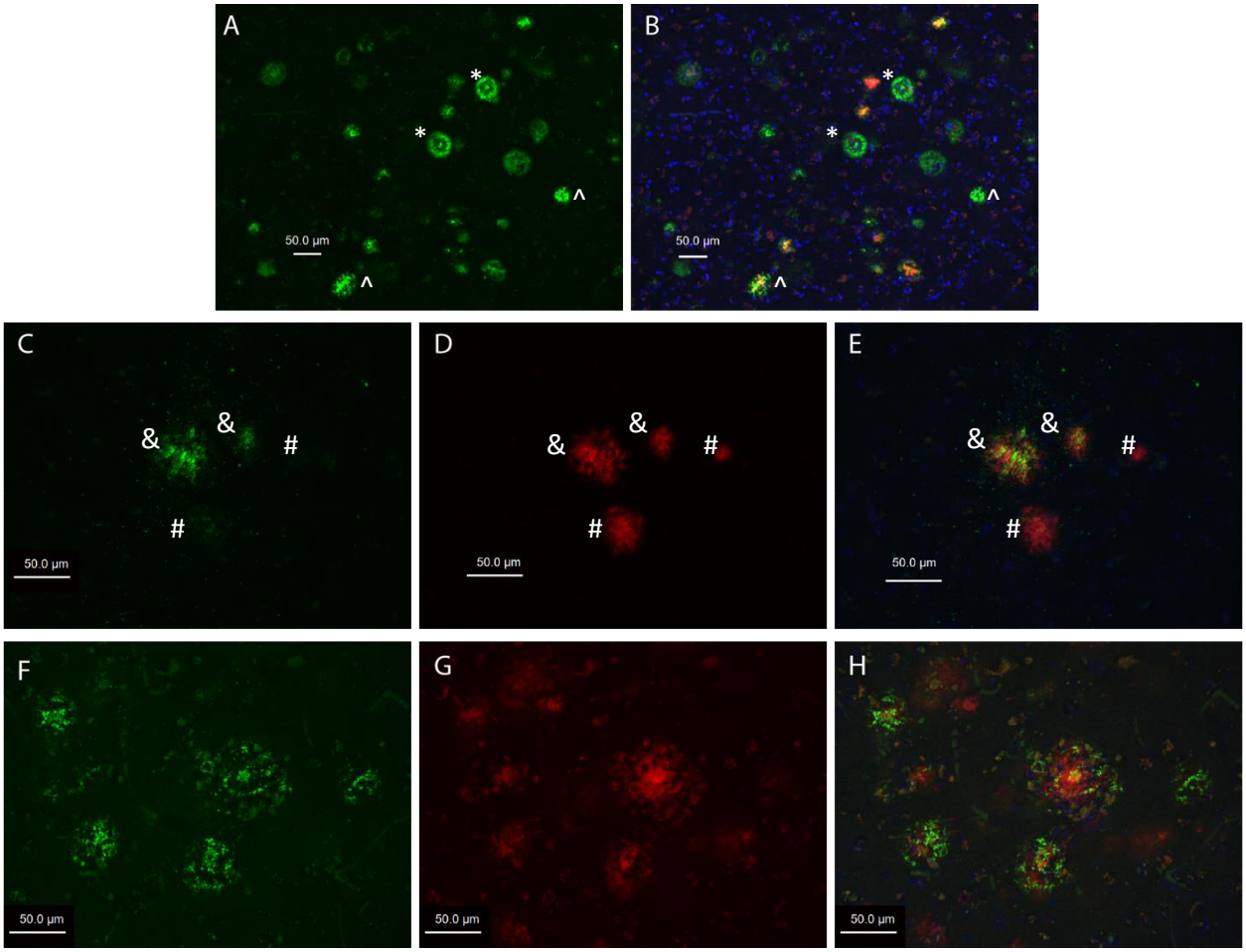

Figure 5.2. Fluorescent micrographs of frontal cortex brain slices from two individuals who lived with DSAD stained with $pAb_{4AT\text{-}L}$ and Amytracker-680. (**A** and **B**) are images showing DAPI nuclear stain (blue), $pAb_{4AT\text{-}L}$ recognizing Aβ pathology (green) with minor colocalization to Amytracker-680 (red). The * symbols denote possible pathology unique to people who live with DSAD and EOAS that are recognized by $pAb_{4AT\text{-}L}$. (**C** and **D**) are images showing lack of recognition between $pAb_{4AT\text{-}L}$ (**C**) Amytracker-680 with $pAb_{4AT\text{-}L}$ appearing to wrap around the insoluble Aβ pathology recognized by Amytracker-680 (**D**). (**E**) is an overlay of (**C** and **D**) with DAPI (blue). (**F-H**) are images of are images showing DAPI nuclear stain (blue), $pAb_{4AT\text{-}L}$ potentially recognizing regions of cored plaques (green) that do not appear to colocalize with Amytracker-680 (red). All images were taken at 20X magnification; the scale bar is 50 µm.

Future directions

The presented preliminary data has the potential to grow into a comprehensive assessment showing how pathology recognized by the $pAb_{4AT\text{-}L}$ would correlate with the onset of DSAD. The onset of AD in people with DSAD is temporal, meaning that the onset of AD symptoms can be relatively predictable. By the age of 40, virtually all people living with DS present AD pathology with the onset of cognitive symptoms occurring ca. 20 years later.[11] Future directions of this preliminary investigation may include performing tissue staining with a range of ages starting from a people who lived until their 20s to people who lived until their 60s. More specifically, tissue staining with $pAb_{4AT\text{-}L}$ starting with a population of people where changes in pathology may be detectable (around the age of 20 years old) to where the onset of cognitive impairment is apparent (around the age of 60 years old). Ultimately the data set could be quantified and build what is commonly referred to as a "Jack curve" in the AD community, which graphically demonstrates the onset of certain AD pathologies in people as they age in years.[18] *If pursued, this body of work should be executed as a collaboration with the Head Lab as they are spearheading efforts to detect the onset of multiple pathologies in people who live with DSAD.*

While these preliminary studies are informative, I recommended that they are repeated in with monoclonal antibodies generated from $pAb_{4AT\text{-}L}$. While $pAb_{4AT\text{-}L}$ is a robust tool for better understanding plaque morphology, monoclonal antibodies would be better in identifying regions of pathology because each monoclonal antibody recognizes a specific epitope. Because coarse-grained plaques and bird's-nest plaques are so novel, it is imperative to have the defining immunostaining experiments on these plaques performed in conjunction with staining

experiments with $pAb_{4AT\text{-}L}$ and associated monoclonal antibodies.[15,16] Characterizing $pAb_{4AT\text{-}L}$ and associated monoclonal antibodies in a diverse population of people who live with AD will enrich the understanding of the kind of pathology recognized by $pAb_{4AT\text{-}L}$. From these studies, additional hypotheses about the role the 4AT-L trimer in the pathogenesis and progression of AD can be formed, thus further establishing a connection between the structural biology of peptides and proteins in proteinopathies like AD.

Materials and Methods

All procedures and materials used in these experiments including the source of occipital cortex from people who lived with DSAD, immunofluorescence staining, sectioning of tissue from humans, and image acquisition can be seen in Chapter 2. The only difference in immunofluorescent staining procedures was that at the very end of the staining procedures, 1:1000 dilution of Amytracker-680 (Ebba Biotech AB) in 1 X TBS was added to the tissue for 5 minutes before being washed in three, 5-minute washes of 1 X TBS followed by DAPI staining. Samples for immunofluorescent staining were spare tissue from the Head lab which are typically used as pilot studies. It is also important to note that all brain tissue sections in this study were extra sections obtained during the sectioning process and therefore may not be the same thickness throughout the section.

Acknowledgments

We thank the National Institutes of Health (NIH) National Institute on Aging (NIA) for funding (AG072587) support. We acknowledge the support of the Chao Family Comprehensive Cancer Center Transgenic Mouse Facility Shared Resource, supported by the National Cancer Institute of the National Institutes of Health under award number P30CA062203. Tissue from cases with DSAD and nondemented controls were from the UCI Alzheimer disease research center (NIH/NIA P30AG066519). The content is solely the responsibility of the authors and does not necessarily represent the official views of the National Institutes of Health. Special thank you to Prof. Elizabeth Head and the entire Head Lab for guidance and for allowing me to learn techniques in neuropathology, especially in people who lived with DSAD. Thank you as well Justine Silva, Sierra Wright, Briana Gawronski, and the University of California, Irvine Alzheimer's Disease Research Center (UCI ADRC) for providing human tissue samples and relevant information essential for these experiments.

References

(1) Alzheimer's & Dementia **2022**, *18*, 700–789.

(2) K. B. Rajan, J. Weuve, L. L. Barnes, E. A. McAninch, R. S. Wilson, D. A. Evans, Alzheimers Dement **2021**, *17*, 1966–1975.

(3) C. L. Masters, R. Bateman, K. Blennow, C. C. Rowe, R. A. Sperling, J. L. Cummings, Nat Rev Dis Primers **2015**, *1*, 1–18.

(4) https://www.facebook.com/NIHAging, Alzheimer's Disease Genetics Fact Sheet https://www.nia.nih.gov/health/alzheimers-disease-genetics-fact-sheet (accessed 2023 -05 -02).

(5) L. S. Honig, J. Barakos, S. Dhadda, M. Kanekiyo, L. Reyderman, M. Irizarry, L. D. Kramer, C. J. Swanson, M. Sabbagh, Alzheimers Dement (N Y) **2023**, *9*, e12377.

(6) G.-F. Chen, T.-H. Xu, Y. Yan, Y.-R. Zhou, Y. Jiang, K. Melcher, H. E. Xu, Acta Pharmacol Sin **2017**, *38*, 1205–1235.

(7) M. Yokoyama, H. Kobayashi, L. Tatsumi, T. Tomita, Frontiers in Molecular Neuroscience **2022**, *15*.

(8) M. P. Vitek, J. A. Araujo, M. Fossel, B. D. Greenberg, G. R. Howell, S. J. S. Rizzo, N. T. Seyfried, A. J. Tenner, P. R. Territo, M. Windisch, L. J. Bain, A. Ross, M. C. Carrillo, B. T. Lamb, R. M. Edelmayer, Alzheimer's & Dementia: Translational Research & Clinical Interventions **2020**, *6*, e12114.

(9) B. Laurijssens, F. Aujard, A. Rahman, Drug Discovery Today: Technologies **2013**, *10*, e319–e327.

(10) D. J. Selkoe, J. Hardy, EMBO Molecular Medicine **2016**, *8*, 595–608.

(11) I. T. Lott, E. Head, Nat Rev Neurol **2019**, *15*, 135–147.

(12) M. Johannesson, C. Sahlin, L. Söderberg, H. Basun, J. Fälting, C. Möller, O. Zachrisson, D. Sunnemark, A. Svensson, T. Odergren, L. Lannfelt, Molecular and Cellular Neuroscience **2021**, *114*, 103641.

(13) A. M. Helman, M. Siever, K. L. McCarty, I. T. Lott, E. Doran, E. L. Abner, F. A. Schmitt, E. Head, J Alzheimers Dis **2019**, *67*, 103–112.

(14) C. Duyckaerts, B. Delatour, M.-C. Potier, Acta Neuropathol **2009**, *118*, 5–36.

(15) S. Ichimata, I. Martinez-Valbuena, S. L. Forrest, G. G. Kovacs, Acta Neuropathol **2022**, *144*, 1171–1174.

(16) B. D. C. Boon, M. Bulk, A. J. Jonker, T. H. J. Morrema, E. van den Berg, M. Popovic, J. Walter, S. Kumar, S. J. van der Lee, H. Holstege, X. Zhu, W. E. Van Nostrand, R. Natté, L. van der Weerd, F. H. Bouwman, W. D. J. van de Berg, A. J. M. Rozemuller, J. J. M. Hoozemans, Acta Neuropathol **2020**, *140*, 811–830.

(17) Amytracker 680 https://www.ebbabiotech.com/products/amytracker-680 (accessed 2023 -05 -05).

(18) C. R. Jack, D. S. Knopman, W. J. Jagust, R. C. Petersen, M. W. Weiner, P. S. Aisen, L. M. Shaw, P. Vemuri, H. J. Wiste, S. D. Weigand, T. G. Lesnick, V. S. Pankratz, M. C. Donohue, J. Q. Trojanowski, Lancet Neurol **2013**, *12*, 207–216.

Chapter 6

Conclusion and Future Directions

The application of triangular trimers derived from Aβ to create antibodies for immunohistochemical studies and as vaccines against Alzheimer's disease (AD) addresses the need to understand the structures of the Aβ peptide aggregates that cause neurodegeneration. Studies that connect the structures of causative peptides such as Aβ in AD will expand the molecular understanding of the disease and ultimately the development of therapies to slow down disease progression.

Chapter 2 demonstrates the generation of $pAb_{4AT\text{-}L}$, a conformation-specific antibody generated from a readily synthesized, conformationally defined Aβ-derived peptide (4AT-L trimer). Immunofluorescent staining experiments revealed that $pAb_{4AT\text{-}L}$ recognizes neuritic plaques, cerebral amyloid angiopathy (CAA), and strongly recognizes the cores of cored plaques. The staining of the cores of cored plaques by $pAb_{4AT\text{-}L}$ supports the previously proposed model in which the cores of cored plaques are surrounded by and attract Aβ oligomers to induce dystrophic neurons and ultimately cognitive decline in AD. The features of plaques recognized by $pAb_{4AT\text{-}L}$ and unique conformationally defined antigen 4AT-L make $pAb_{4AT\text{-}L}$ a valuable tool for identifying Aβ plaque composition and providing functional insights into Aβ plaque morphology.

Preliminary results described in chapter 5 suggests that $pAb_{4AT\text{-}L}$ selectively recognizes pathology in people who lived with Down Syndrome and Alzheimer's disease (DSAD). This body of work has the potential to grow into a comprehensive investigation showing how

pathology recognized by $pAb_{4AT\text{-}L}$ would correlate with the temporal onset of AD pathology and phenotypes. While $pAb_{4AT\text{-}L}$ is a robust tool for better understanding plaque morphology, monoclonal antibodies would be better in identifying regions of pathology because each monoclonal antibody recognizes a specific epitope. Because coarse-grained plaques and bird's-nest plaques are recently characterized, it is important to have the defining immunostaining experiments on these plaques performed in conjunction with staining experiments with $pAb_{4AT\text{-}L}$ and associated monoclonal antibodies.[1,7]

Characterizing $pAb_{4AT\text{-}L}$ and associated monoclonal antibodies in AD pathology in different groups of people who live with LOAD, DSAD, or EOAD will enrich the understanding of the kind of pathology recognized by $pAb_{4AT\text{-}L}$. From these studies, additional hypotheses about the role the 4AT-L trimer in the pathogenesis and progression of AD can be formed, thus further establishing a connection between the structural biology of peptides and proteins in proteinopathies like AD. The work outlined in chapters 2 and 5, can be repeated or even further explored with the monoclonal antibodies isolated in $pAb_{4AT\text{-}L}$. Isolating and characterizing a monoclonal antibody could help better understand the antibody binding to species of Aβ through immunoassays and even structural biology tools such as X-ray crystallography. Isolating a well characterized monoclonal antibody could also serve as a potential preclinical passive immunotherapy candidate in transgenic AD mice which would expand the work outlined in chapter 3 and 4.

Chapter 3 discusses the current landscape of current peptide vaccines and immunotherapies against AD while chapter 4 discusses the therapeutic potential of structurally defined models of Aβ monomers and oligomers by using them as antigens for novel Aβ peptide

vaccines for mice. Current peptide vaccine and immunotherapies against AD are typically immunized with the *N*-terminus of Aβ to proliferate antibody production and not the onset of ARIA (Amyloid Related Imaging Abnormalities). Although the middle region of Aβ (residues 16-32) have been avoided out of concerns to induce ARIA, this region of Aβ can present unique peptide epitopes in loop-like conformations when folded into β-hairpins, which are thought to make up the Aβ oligomers associated with neurodegeneration.[8] Chapter 4 demonstrates our attempt to create an efficacious vaccine in transgenic AD mice using structurally defined Aβ-derived trimers and monomers.

In chapter 4, we conclude that among the four peptide vaccines (2AM-L, 2AT-L, 4AM-L, and 4AT-L), a fully factorial experimental design with larger group sizes (n=18) should be pursued with a peptide with the 2AT-L trimer. Vaccine formulations with 2AT-L that are biased towards a B-cell (Th-2) response may prevent the onset of microhemorrhages (ARIA) which is an important safety concern with both peptide vaccines and immunotherapies. On the occasion that a monoclonal antibody generated from $pAb_{4AT\text{-}L}$, I recommend comparing the efficacy of this potential preclinical monoclonal antibody candidate to be compared with the clinical candidate, Acumen's "AβO-selective therapeutic antibody," ACU193.[8]

This body of work is one of earliest collection of studies in the Nowick Group which provides a biological and therapeutic application to structurally defined triangular trimers derived from Aβ. As this collection of studies continue to grow, it is important that these studies be shared outside of the peptide research community and into the AD community. Suggested spaces for presentation would include more biologically affiliated conferences such as the Association of Alzheimer's Disease International Conference (AAIC). Future expansion of this

body of work and scientific exchange in the AD conferences will continue to connect structures of the Aβ peptide aggregates to neurodegeneration in the hopes of better understanding the molecular basis of AD, and develop therapies to slow down the progression of AD.

References

(1) Boon, B. D. C.; Bulk, M.; Jonker, A. J.; Morrema, T. H. J.; van den Berg, E.; Popovic, M.; Walter, J.; Kumar, S.; van der Lee, S. J.; Holstege, H.; Zhu, X.; Van Nostrand, W. E.; Natté, R.; van der Weerd, L.; Bouwman, F. H.; van de Berg, W. D. J.; Rozemuller, A. J. M.; Hoozemans, J. J. M. The Coarse-Grained Plaque: A Divergent Aβ Plaque-Type in Early-Onset Alzheimer's Disease. *Acta Neuropathol* **2020**, *140* (6), 811–830. https://doi.org/10.1007/s00401-020-02198-8.

(2) Thal, D. R.; Capetillo-Zarate, E.; Del Tredici, K.; Braak, H. The Development of Amyloid β Protein Deposits in the Aged Brain. *Science of Aging Knowledge Environment* **2006**, *2006* (6), re1–re1. https://doi.org/10.1126/sageke.2006.6.re1.

(3) Jellinger, K. A. Understanding Conflicting Neuropathological Findings. *JAMA Neurology* **2016**, *73* (4), 479–480. https://doi.org/10.1001/jamaneurol.2015.4879.

(4) De Felice, F. G.; Wu, D.; Lambert, M. P.; Fernandez, S. J.; Velasco, P. T.; Lacor, P. N.; Bigio, E. H.; Jerecic, J.; Acton, P. J.; Shughrue, P. J.; Chen-Dodson, E.; Kinney, G. G.; Klein, W. L. Alzheimer's Disease-Type Neuronal Tau Hyperphosphorylation Induced by A Beta Oligomers. *Neurobiol Aging* **2008**, *29* (9), 1334–1347. https://doi.org/10.1016/j.neurobiolaging.2007.02.029.

(5) Choi, S. H.; Kim, Y. H.; D'Avanzo, C.; Aronson, J.; Tanzi, R. E.; Kim, D. Y. Recapitulating Amyloid β and Tau Pathology in Human Neural Cell Culture Models: Clinical Implications. *US Neurol* **2015**, *11* (2), 102–105. https://doi.org/10.17925/USN.2015.11.02.102.

(6) Ayalon, G.; Lee, S.-H.; Adolfsson, O.; Foo-Atkins, C.; Atwal, J. K.; Blendstrup, M.; Booler, H.; Bravo, J.; Brendza, R.; Brunstein, F.; Chan, R.; Chandra, P.; Couch, J. A.; Datwani, A.;

Demeule, B.; DiCara, D.; Erickson, R.; Ernst, J. A.; Foreman, O.; He, D.; Hötzel, I.; Keeley, M.; Kwok, M. C. M.; Lafrance-Vanasse, J.; Lin, H.; Lu, Y.; Luk, W.; Manser, P.; Muhs, A.; Ngu, H.; Pfeifer, A.; Pihlgren, M.; Rao, G. K.; Scearce-Levie, K.; Schauer, S. P.; Smith, W. B.; Solanoy, H.; Teng, E.; Wildsmith, K. R.; Bumbaca Yadav, D.; Ying, Y.; Fuji, R. N.; Kerchner, G. A. Antibody Semorinemab Reduces Tau Pathology in a Transgenic Mouse Model and Engages Tau in Patients with Alzheimer's Disease. *Science Translational Medicine* **2021**, *13* (593), eabb2639. https://doi.org/10.1126/scitranslmed.abb2639.

(7) Ichimata, S.; Martinez-Valbuena, I.; Forrest, S. L.; Kovacs, G. G. Expanding the Spectrum of Amyloid-β Plaque Pathology: The Down Syndrome Associated 'Bird-Nest Plaque.' *Acta Neuropathol* **2022**, *144* (6), 1171–1174. https://doi.org/10.1007/s00401-022-02500-w.

(8) Krafft, G. A.; Jerecic, J.; Siemers, E.; Cline, E. N. ACU193: An Immunotherapeutic Poised to Test the Amyloid β Oligomer Hypothesis of Alzheimer's Disease. *Front Neurosci* **2022**, *16*, 848215. https://doi.org/10.3389/fnins.2022.848215.